TRACE ANALYSIS OF LANTHANIDES AND ACTINIDES USING LIQUID CHROMATOGRAPHY

By

P.G. Jaison

CHEM01200604030

Bhabha Atomic Research Centre, Mumbai

A thesis submitted to the

Board of Studies in Chemical Sciences

In partial fulfilment of requirements

For the Degree of

DOCTOR OF PHILOSOPHY

of

HOMI BHABHA NATIONAL INSTITUTE

July 2013

HomiBhabha National Institute

Recommendations of the Viva Voce Board

As members of the Viva Voce Board, we certify that we have read the dissertation prepared by P.G. Jaison entitled "Trace Analysis of Lanthanides and Actinides using Liquid Chromatography" and recommend that it may be accepted as fulfilling the dissertation requirement for the Degree of Doctor of Philosophy.

V. Venugopal — **Date:** 2/9/14

Chairman - (Prof. V. Venugopal)

S.K. Aggarwal — **Date:** 25/8/14

Guide / Convener -(Prof. S.K. Aggarwal)

K K Verma — **Date:** 25-8-2014

External Examiner – (Prof. Krishna K. Verma)

Date:

Member 1 - (Prof. K.L. Ramakumar)

K. Ram — **Date:** 25/8/2014

Member 2 - (Dr. S.K. Mukerjee) 28-8-2014

Final approval and acceptance of this dissertation is contingent upon the candidate's submission of the final copies of the dissertation to HBNI.

I hereby certify that I have read this dissertation prepared under my direction and recommend that it may be accepted as fulfilling the dissertation requirement.

Date: 25/8/14

Place: Mumbai.

S.K. Aggarwal

STATEMENT BY AUTHOR

This dissertation has been submitted in partial fulfilment of requirements for an advanced degree at Homi Bhabha National Institute (HBNI) and is deposited in the Library to be made available to borrowers under rules of the HBNI.

Brief quotations from this dissertation are allowable without special permission, provided that accurate acknowledgement of source is made. Requests for permission for extended quotation from or reproduction of this manuscript in whole or in part may be granted by the Competent Authority of HBNI when in his or her judgment the proposed use of the material is in the interests of scholarship. In all other instances, however, permission must be obtained from the author.

(P.G. Jaison)

DECLARATION

I, hereby declare that the investigation presented in the thesis has been carried out by me. The work is original and has not been submitted earlier as a whole or in part for a degree / diploma at this or any other Institution / University.

(P.G. Jaison)

List of Publications arising from the thesis

Referred Journals

1. Direct determination of lanthanides in simulated irradiated thoria fuels using reversed phase high-performance liquid chromatography
   P.G. Jaison, Narendra M. Raut, Suresh K. Aggarwal
   Journal of Chromatography A, 1122 (2006) 47–53.

2. Reversed-phase liquid chromatography using mandelic acid as an eluent for the determination of uranium in presence of large amounts of thorium
   P.G. Jaison, Vijay M. Telmore, Pranaw Kumar, Suresh K. Aggarwal
   Journal of Chromatography A, 1216 (2009) 1383–1389.

3. Comparative Study of Ion Interaction Reagents for the Separation of Lanthanides by Reversed-Phase High Performance Liquid Chromatography (RP-HPLC)
   P. G. Jaison, Pranaw Kumar, Vijay M. Telmore, and Suresh K. Aggarwal
   Journal of Liquid Chromatography & Related Technologies,32 (2009) 2146–2163.

4. A RP-HPLC Method using α-Hydroxy Isobutyric Acid for Preconcentration and Determination of Uranium in Seawater
   P.G. Jaison, Vijay M. Telmore, Pranaw Kumar, and Suresh K. Aggarwal
   Journal of Chromatographic Science, 49 (2011) 72-78.

5. Determination of Uranium in Seawater Samples by Liquid Chromatography using Mandelic Acid as a Complexing Agent
   P.G. Jaison, Vijay M. Telmore, Pranaw Kumar and Suresh K. Aggarwal
   Journal of Chromatographic Science, 49(2011) 657-664.

6. Electrospray ionization mass spectrometric studies on uranyl complex with α-hydroxyisobutyric acid in water methanol medium
   P.G. Jaison, Pranaw Kumar, Vijay Telmore and Suresh K. Aggarwal
   Rapid Communications in Mass Spectrometry, 27(2013) 1105 -1118.

DEDICATIONS

This thesis is dedicated to my parents who have supported me since the beginning of my studies. Also this thesis is dedicated to my family, who offered unconditional love and support throughout the course of this work.

ACKNOWLEDGEMENTS

I was guided, supported and encouraged by many persons who deserve my gratitude. First of all I want to sincerely thank my guide, Prof. S.K. Aggarwal, for his guidance, support, his exquisite attention to detail and for his demand for excellence throughout this work. From the formative stages of this thesis to the final draft, I owe an immense debt of gratitude to my supervisor.

I am most grateful to the members of my Committee, Prof. K.L. Ramakumar and Dr. S.K. Mukerjee for their time, encouragement, and expertise throughout this work. Special thanks to the chairman of my Committee, Prof. V. Vengopal for all the support and encouragement. Their comments and questions were quite helpful in shaping up my research work. I am grateful to Dr. S. Kannan and Dr. N. Sivaraman for the discussion and interpretation of some results presented in the thesis.

I would be remiss without mentioning Shri Pranaw Kumar and Shri Vijay Temore, who have extended their wholehearted co-operation and provided fruitful suggestions during the entire course of the work. It is also a great pleasure to express my gratitude to Dr. (Ms.) D. Alamelu for her encouragements. My special thanks are to Dr. Arnab Sarkar and Ms. Sumana Paul for their kind cooperation and valuable suggestions. I would like to thank all the members of the Fuel Chemistry Division, BARC in particular to Shri A. R. Parab, Mrs. Radhika Rao, Sh. Raju V. Shah, Sh. K. Sasi Bhushan, Sh. S. Jagadish Kumar, Sh. G.K. Prasad, Dr. Manoj K. Sharma and Sh. Sourv K. Guin for their support and help at all stages of my work. Thanks are due to Mr. T.L. Prasad of Desalination Division, BARC for providing the seawater samples. I would like to acknowledge Dr. Narendra Raut with whom I have learnt the basics of chromatography during the formative years. Special thanks are due to Sh. R. Shivaram of FCD office for the unfailing help and consistent support.

Jaison

CONTENTS

	Synopsis	i
	List of Figures	xviii
	List of Tables	xxiv
Chapter 1	**Introduction**	1
1.1	Introduction	2
1.1.1	Relevance of Trace Determination of Lanthanides, Thorium and Uranium	2
1.1.2	Nomenclature	3
1.1.3	Occurrence	4
1.1.3	Electronic Configuration	5
1.1.4	Oxidation State	7
1.1.5	Chemistry of Lanthanides and Actinides	8
1.1.6	Importance of Lanthanides, Th and U	10
1.1.7	Analytical Methods for the Determination of Lanthanides	12
1.1.8	Separation of Lanthanides and Actinides	14
1.1.9	Methods for the Separation of Lanthanides and Actinides	15
1.1.10	Classifications of Chromatography	17
1.1.11	Historic Perspective of Liquid Chromatography	21
1.1.12	Milestones in Chromatography	22
1.1.13	Advantages and Limitations of LC	23
1.1.14	Concepts in Liquid Chromatography	25
1.1.14.1	Eddy Diffusion	25
1.1.14.2	Longitudinal Diffusion	26
1.1.14.3	Mass Transfer Effects	27

1.1.14.3.1	Mobile-phase Mass Transfer	27
1.1.14.3.2	Stagnant Mobile-phase Mass Transfer	27
1.1.14.3.3	Stationary-phase mass transfer	28
1.1.14.4	Van Deemter Model of Band Broadening	29
1.1.15	Chromatographic Parameters	32
1.1.16	Need for HPLC	37
1.2	Instrumentation	39
1.2.1	HPLC	39
1.2.1.1	Solvent Delivery System (Pump)	39
1.2.1.2	Sample Injector	43
1.2.1.3	Solvents for HPLC	45
1.2.1.4	HPLC Column	46
1.2.1.4.1	Silica	46
1.2.1.4.2	Modified Silica	48
1.2.1.4.3	Styrene Divenylbenzene	48
1.2.1.5	Detectors	49
1.2.1.5.1	UV-Vis Detector	53
1.2.1.5.1.1	Fixed Wavelength Detector	54
1.2.1.5.1.2	Dispersion Detector	54
1.2.1.5.1.3	Diode Array Detector	55
1.2.1.5.2	Derivatisation Reaction in Chromatography	56
1.2.2	Mass Spectrometer	58
1.2.2.1	Ionisation Techniques	58
1.2.2.2	Mass Analyzers	60
1.2.2.2.1	Time-of-Flight Analyzer	60
1.2.2.2.2	Quadrupole Mass Analyzer	62

1.2.2.2.3	Magnetic Sector Analyzers	63
1.2.2.2.4	Ion Trap Analyzers	63
1.2.2.2.5	Fourier Transform Ion Cyclotron Mass Analyzer	64
1.2.2.2.6	Hybrid Analyzers	65
1.2.2.3	Detectors	66
1.2.2.4	Vacuum System	67
1.2.3	Electrospray Ionisation Tandem Mass Spectrometer	68
1.2.3.1	Electrospray Ionisation	68
1.2.3.1.1	Mechanism of Ion formation	69
1.2.3.2	Mass Analyser	71
1.2.3.3	Detector System	73
1.2.4	Thermal Ionisation Mass Spectrometer	73
1.3	Scope of the Present Work	76
Chapter 2	**Separation of Lanthanides Using Ion Interaction Chromatography**	79
2.1	Introduction	80
2.2	Comparative Study of Ion Interaction Reagents for the Separation of Lanthanides	83
2.2.1	Background	83
2.2.2	Experimental	84
2.2.2.1	Instrumentation	84
2.2.2.2	Reagents	84
2.2.2.3	Procedure	85
2.2.3	Results and Discussion	86
2.2.3.1	Optimization of IIR Composition	87
2.2.3.2	Optimization of the IIR Volume	88

2.2.3.3	Optimisation of Washings with Water	90
2.2.3.4	Optimization of Washings with Mobile Phase	92
2.2.3.5	Comparison of Resolution Data using Different IIRs	93
2.2.3.6	Application of the Method for Geological Sample	97
2.2.3.7	Long-term Adsorption and Reproducibility of Coating	99
2.3	Direct Determination of Lanthanides in Thoria Matrix	101
2.3.1	Background	101
2.3.2	Experimental	102
2.3.2.1	HPLC System	102
2.3.2.2	Reagents	102
2.3.2.3	Procedure	103
2.3.3	Results and Discussion	103
2.3.3.1	Effect of Ion Interaction Reagent (IIR) Concentration on Retention of Lanthanides, Th and U	103
2.3.3.2	Th Holding Capacity of RP Column	105
2.3.3.2.1	Effect of Concentration of IIR on Th Holding Capacity of RP Column	106
2.3.3.2.2	Effect of pH of Eluent on the Th Capacity	107
2.3.3.3	Separation of Fission Products from Thorium	108
2.3.3.4	Quantification of La and Nd	112
2.3.3.5	Application of the Method for Irradiated Fuel Sample	113
2.4	Ligand exchange and Coupled Column Liquid Chromatography using Mandelic Acid for the Determination of Lanthanides in Thorium Matrix	115
2.4.1	Background	115
2.4.2	Experimental	116
2.4.2.1	Instrumentation	116

2.4.2.3	Reagents	116
2.4.2.2	Procedure	117
2.4.3	Results and Discussion	117
2.4.3.1	Effect of Concentration and pH of Mandelic Acid	117
2.4.3.2	Mechanism of Retention of Metal Mandelates	119
2.4.4	Conclusions	124
Chapter 3	**Separation of Thorium and Uranium by HPLC**	126
3.1.	Introduction	127
3.2	Separation of Similar Proportions of Th and U	128
3.2.1	Background	128
3.2.2	Experimental	129
3.2.2.1	Instrumentation	129
3.2.2.2	Reagents	129
3.2.2.3	Procedure	129
3.2.3	Results and Discussion	130
3.2.3.1	Effect of Concentration of HIBA	130
3.2.3.2	Effect of pH of Mobile Phase	131
3.2.3.3	Effect of Methanol	132
3.3	Determination of U in Presence of Large Amounts of Th	134
3.3.1	Background	134
3.3.2	Experimental	135
3.3.2.1	Instrumentation	135
3.3.2.2	Reagents	136
3.3.2.3	Procedure	136
3.3.3	Results and Discussion	136
3.3.3.1	Effect of pH of Mandelic Acid	136

3.3.3.2	Effect of Concentration of Mandelic Acid	138
3.3.3.3	Effect of Methanol Content	139
3.3.3.4	Separation of Th and U by Monolith Column	140
3.3.3.5	Determination of Small Amounts of U in Presence of Large Amounts of Th	141
3.3.3.5.1	Effect of Methanol Content on the Th Retention Capacity	141
3.3.3.5.2	Effect of pH of Mobile Phase on the Th Retention Capacity	142
3.3.3.5.3	Calibration Curves for U and Th	143
3.3.3.5.4	Separation of Th and U by Particulate Column	145
3.4	Mechanism of Separation of Th and U using Mandelic Acid Eluent	149
3.4.1	Background	149
3.4.2	Experimental	149
3.4.3	Results and Discussion	150
3.4.3.1	Effect of Sodium n-Octane Sulphonate IIR	150
3.4.3.2	Effect of Tetra-n-butyl Ammonium Bromide IIR	151
3.4.4	Conclusions	154
Chapter 4	**HPLC Methods for the Determination of Uranium in Seawater**	155
4.1	Introduction	156
4.2	HPLC Method Using HIBA as the Chelating Agent for Pre-concentration and Determination of Uranium in Seawater	158
4.2.1	Background	158
4.2.2	Experimental	159
4.2.2.1	Instrumentation	159
4.2.2.2	Reagents	159
4.2.2.3	Procedure	160

4.2.3	Results and Discussion	162
4.2.3.1	Optimization of Parameters for U Pre-concentration	162
4.2.3.2	Optimization of Parameters for U Separation	164
4.2.3.3	Pre-concentration Studies	166
4.2.3.4	Studies with Simulated Samples	168
4.2.3.5	Analysis of Seawater Samples	169
4.3	Liquid Chromatographic Method for the Determination of Uranium in Seawater and Process Samples using Mandelic Acid as a Complexing Agent	172
4.3.1	Background	172
4.3.2	Experimental	173
4.3.2.1	Instrumentation	173
4.3.2.2	Reagents	173
4.3.2.3	Procedure	174
4.3.3	Results and Discussion	176
4.3.3.1	Fe(III) and U(VI) Separation study	176
4.3.3.1.1	Separation of Fe(III) and U(VI) on a Modified RP Column	176
4.3.3.1.2	Effect of Concentration of Mandelic Acid on the Retention of Fe(III) and U(VI)	177
4.3.3.1.3	Effect of Methanol Content on the Retention of Fe(III) and U(VI)	178
4.3.3.2	Preconcentration Study	179
4.3.3.2.1	Suitability of Eluent	180
4.3.3.2.2	Effect of Concentration of Mandelic acid on the Recovery of U	181
4.3.3.2.3	Effect of pH of Mandelic acid on the Recovery of U	182
4.3.3.2.4	Effect of Amount of the Sample Solution	183

4.3.3.2.5	Effect of Sample Loading Flow Rate on the Recovery of U	185
4.3.3.3	Linearity and Reproducibility of the Method	187
4.3.3.4	Effect of Fe (III) on the Recovery of U (VI)	189
4.3.3.5	Analysis of Seawater Samples	190
4.4	Conclusions	192
Chapter 5	**ESI-MS Studies on Uranyl Complex with α-Hydroxyisobutyric Acid and Mandelic Acid**	194
5.1	Introduction	195
5.2	Experimental	198
5.2.1	Instrumentation	198
5.2.2	Reagents	198
5.2.3	Procedure	199
5.3	Results and Discussion	199
5.3.1	ESI-MS Studies on UncomplexedUranyl Ion	199
5.3.1.1	Need of Electrolyte	199
5.3.1.2	Effect of Solution Composition	203
5.3.1.3	Effect of Solute Concentration	206
5.3.2	Complexation of Uranyl Ion with α-HydroxyisobutyricAcid	209
5.3.2.1	Positive Ion Mode	210
5.3.2.2	Negative Ion Mode	213
5.3.2.3	Selection of ESI Parameters	214
5.3.2.3.1	Capillary Voltage	215
5.3.2.3.2	Dry Gas Temperature	217
5.3.2.3.3	In-source CID Energy	219
5.3.2.3.4	Quadrupole Ion Energy	220
5.3.2.3.5	Collision Cell Energy	221

5.3.2.3.6	End-plate Offset Voltage	222
5.3.2.4	Effect of Ligand to Metal Ratio	224
5.3.3	Complexation of Uranyl Ion with Mandelic Acid	227
5.3.3.1	Effect of Electrospray Ionisation and Transfer Parameters	231
5.4	Conclusions	232
	References	234

Synopsis

Chromatography is an analytical method that separates the components in a mixture based on the differences in their partitioning between a mobile phase and a stationary phase.When the mobile phase used is a liquid, the method is known as liquid chromatography (LC)which is useful for separation, identification and determination of ions or molecules that are present in a solution.The interaction of the solute between mobile and stationary phases can be controlled through different choices of solvents and stationary phases. As a result, LC acquires a high degree of versatility as compared to other chromatographic systems and it also has the ability to adapt to a wide variety of mixtures by proper selection of solvents.The understanding that the use of small particles and high pressures is mandatory to improve the separation efficiency in LC, led to the development of high performance liquid chromatography (HPLC).Improvements in instrumentation, column technology and theory paved the way to rapid and high resolution LC separations. Application of HPLC with on-line detection has reduced the analysis time from days to a few minutes because of its speed, high sensitivity and multi-elemental analysis capability using single injection. However, LC system using on-line spectrophotometric detection has a limitation for co-eluting species having similar or no absorption in the UV-VIS range.

Separation and determination of lanthanides, Th and U is of great importance in geochemistry, environmental sciences, material science, nuclear technology etc. In nuclear technology, separation of individual lanthanides, Th and U is required to minimize the isobaric / spectral interferences during the quantitation or atom ratio measurements by mass spectrometry.Individual separation of lanthanides is a challenging task in view of their similar electronic configuration and nearly same ionic radii. The use of complexing agents as eluents in the ion exchange chromatography helps to amplify the slight differences in the stability constants of the Ln-eluent complexes and leads to better separations. In the present work, reversed phase (RP) chromatography was used for the separation of Th and U as they form hydrophobic complexes with ligands used as eluents.Effects of different parameters

such as concentration of eluent and ion interaction reagent (IIR), pH of mobile phase etc. were studied systematically for the optimization of separation procedure for a given type of sample. The aim of the present thesis was to develop the LC based methods for the trace level determination of lanthanides, U and Th. Several HPLC techniques have been reported for the determination of lanthanides and actinides in a variety of samples relevant to nuclear industry and geological studies. In view of its high efficiency, ion interaction chromatography was preferred over bonded phase ion exchangers for the individual separation of lanthanides. The IIRs employed are not easily destroyed by chemical treatments and their presence in the separated lanthanide fractions lowers the ionisation efficiency during subsequent isotope ratio measurements by thermal ionisation mass spectrometry (TIMS). An IIR which would remain sorbed on the column for a considerably long time and thus subsequently, need not be added to the mobile phase when running the samples is desired. Also better resolution would imply higher decontamination factor and more accurate atom ratio measurements for the separated fractions. The reported HPLC methods for the determination of burn-up involve preliminary separation of lanthanides or fission products from the bulk of the fuel matrix elements. The separation steps to isolate the fission product(s) pose the risk of contamination of the sample and also make the process cumbersome. Direct HPLC methodology for the determination of burn-up of irradiated thoria-based fuels, without involving any pre-separation of matrix elements U and Th is, therefore, needed. Though a number of HPLC methods have been reported for the separation of U and Th, majority of thesedeal with samples containing similar amounts of U and Th. Hence, it is required to develop LC method for determination of U in samples containing large amounts of Th in view of its importance to thorium based nuclear fuel cycle.The determination of U in natural water systems is of interest since seawater is considered as an alternative potential source of uranium. Reported LC methods were performed using spiked samples containing large amounts of U added externally compared to the amount present in seawater. LC methods for the selective pre-concentration

and determination of U in seawater and process water were, therefore,developed in the present work. LC separation me can be easily elucidated if the species responsible for the adsorption / elution from a given stationary phase are understood. Hence, an attempt was made to studythe solution equilibrium between $UO_2^{2+}$and hydroxyl carboxylic acid ligands typically used for the separations. Speciation studies of actinide elements are also important from the point of their migration under the waste immobilization conditions. Due to the soft nature of ionization, Electrospray ionization mass spectrometry (ESI-MS) is suitable for studying the solution equilibria of metal-ligand system.

Hence, the objectives of the present thesis were:

- Individual separation of lanthanides with a high degree of resolution
- Separation and determination of lanthanides in presence of large amounts of Th or U
- Quantification of small amounts of U in bulk of Th
- LC method for the determination of U in seawater and process samples
- Study the speciation of UO_2^{2+}-α-HIBA and UO_2^{2+}-mandelate systems

The work described in this thesis is divided into five Chapters.

Chapter 1

This Chapter gives an introduction to lanthanides and actinides, particularly Th and U with respect to their role in nuclear science and technology. Brief review is presented on the various analytical methods for the separation and determination of lanthanides and actinides. Broad classifications of liquid chromatography and the relevance of reversed phase chromatography and ion interaction chromatography which are used in the present work are also described. LC coupled with a diode-array UV-Vis absorption spectrometer was employed for major part of the work presented.Isotope dilution-thermal ionisation mass spectrometry (ID-TIMS), a well-recognised analytical methodology, was employed for validating the HPLC methodology developed for the determination of U in seawater samples

and process samples. An ESI system coupled to tandem mass spectrometer system was employed for studying the complexation of UO_2^{2+} withhydroxyl carboxylic acids. Analytical techniques such as high performance liquid chromatography (HPLC), thermal ionisation mass spectrometry (TIMS) and electrospray ionization mass spectrometry (ESI-MS) used in the present work are described in this Chapter. Finally, the scope of the present work is described.

Chapter 2

This Chapter deals with the studies carried out for the separation of lanthanides using HPLC based on ion interaction chromatography. High resolution separation of lanthanides is important in nuclear technology for the burn-up determination of irradiated fuels and for the characterization of nuclear fuels with respect to trace constituents.

Mobile phase parameters such as nature of the complexing agents, pH, solvent strength etc. play significant role in deciding the interaction of a given lanthanide ion with the stationary phase. In the present work, the objective was to bring out the influence of ion interaction reagent on the resolution of lanthanide separations. Another objective was to identify a suitable IIR offering long term adsorption onto the reversed phase (RP) column, thereby obviating the need to introduce the IIR in the mobile phase during the separation of lanthanides. This avoids the rigorous treatment of purified fractions before their mass spectrometric analyses. Hence, comparative study of ion interaction reagents (IIRs) was carried out under identical experimental conditions.

IIRs viz. n-octane sulphonate, n-octane sulphate, n-octadecane sulphonate and eicosyl sulphate were selected for the study. Separation efficiency was assessed on the basis of resolution, which is related to the number of theoretical plates. The resolution between two adjacent peaks of lanthanides was calculated using the equation: $R = 1.18\frac{R_{t2} - R_{t1}}{(W_{(1/2)1} + W_{(1/2)2})}$;

where, R_{t1} and R_{t2} are the retention times of the two adjacent peaks 1 and 2, respectively and W's denote their peak widths at half maximum heights. Volume and composition of the IIR and volumes of washings with water and mobile phase etc. for the proper equilibration of the column were optimized for each IIR. Separation of lanthanide mixtures was carried out using a concentration gradient of α-hydroxy isobutyricacid solution of pH 5.0. The long term adsorption of these IIRs onto the stationary phase was also studied. Among different IIRs studied, n-octadecyl sulphonate showed the highest resolution for the 14 lanthanides (Fig. 1) and provided good long term adsorption stability.

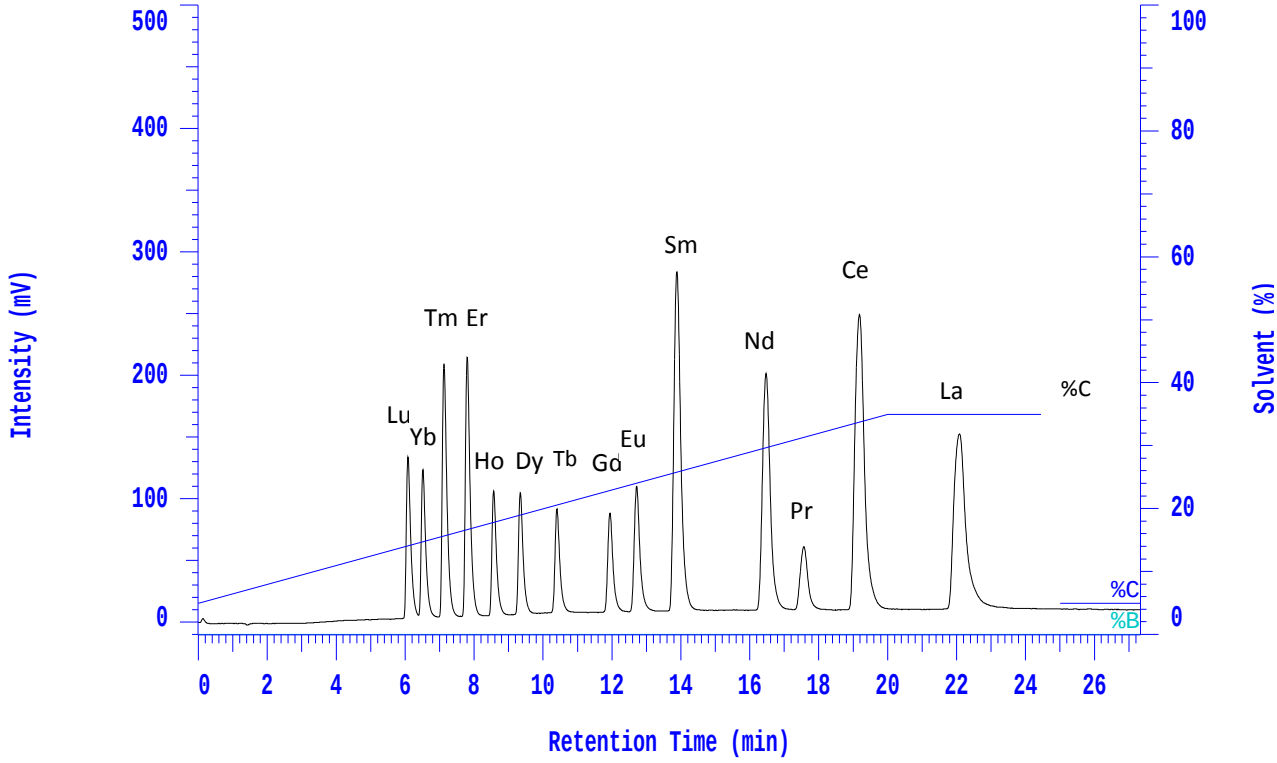

Fig. 1: Separation of 14 lanthanides on a C18 column coated with C18-sulphonate

The coating of n-octadecyl sulphonate over the stationary phase was found to be quite stable as indicated by the reproducibility (RSD 2-8%) of resolution data among lanthanide peaks over a period of two months. Applicability of the method for the real life samples was demonstrated by analyzing lanthanides in a geological reference material viz. SY-3.Under the dynamic cation exchange conditions employed for the individual separation of lanthanides, presence of Th and U can cause interference in the separation. The problem becomes more

severe when Th or U is present in large amounts as the matrix element peaks can mask some of the lanthanides. The possibility of separating the lanthanides without involving any pre-separation of the matrix elements, U and Th was explored.

The pH of the eluent and concentration of ion interaction reagent were found to play a vital role in deciding the capacity of the column to retain Th. A dual gradient elution condition was employed for the direct determination of lanthanides in presence of large amounts of Th using single column. This was achieved by employing concentration gradient of α-HIBA (pH 6 or above) for separating individual lanthanides and for retaining Th and U onto the stationary phase. After their separation, low pH α-HIBA was introduced for the elution of Th and U. Since the elution of matrix elements takes place after the elution all the lanthanides, the method allows the use of a minor fission product (Tb) as an internal standard for the precise quantification of fission monitors, La and Nd, along with other lanthanide fission products (Fig. 2).

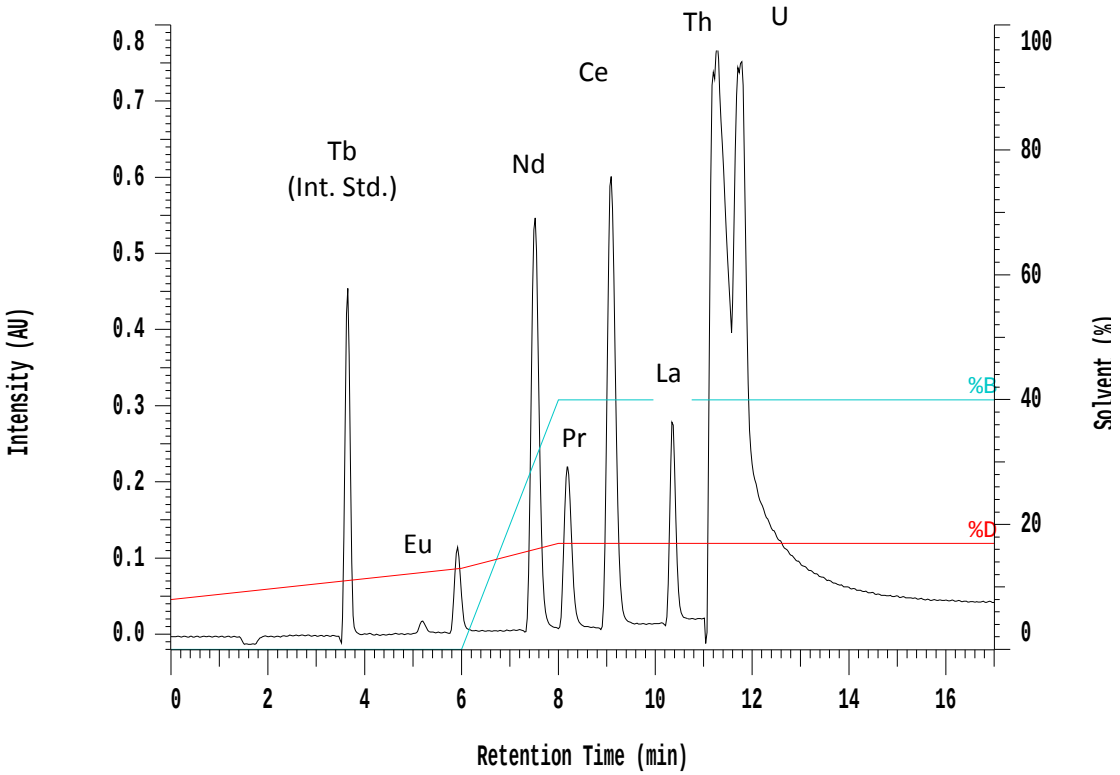

Fig.2: Separation of lanthanides, Th and U in simulated 1 atom% burn-up solution using dual (concentration and pH) gradient elution.

The simulated samples of thoria with burn-up of 0.5, 1 & 2 atom% fissions were repeatedly analysed over a period of two weeks and the overall precision for the determination of La and Nd concentrations by internalstandard method was found to be ~2%.

The methodology exploits the advantages of the internal standard approach as well as direct injection method.Since no preliminary separation is involved, analysis is faster and is less prone to contamination. Since internal standard was used for quantification, it takes care of majority of the fluctuations and uncertainties during the sample handling. The method can be used as a quick substitute for mass spectrometric analysis of the burn-up determination with reasonable precision and accuracy using Tb as an internal standard. Coupled column LC method was also explored for the determination of lanthanides in bulk of thorium. The method employed a RP column and a cation exchange column, connected in series. Mandelic acid was used as the eluent for the on-line matrix removal as well as for the separation of individual lanthanides. Under the optimized conditions, thorium-mandelate was retained in the RP column whereas less retaining lanthanide ions were transferred into the cation exchange column for their individual separation. The method was used for the separation of synthetic samples with Th/Ln amount ratios up to 10,000.

Chapter 3

This Chapter discusses the separation of thorium and uranium by HPLC. Due to similar chemistry, the separation and accurate determination of U in presence of a large excess of Th is difficult. Th based nuclear fuel cycle demands quantification of small amounts of U in presence of large amounts of Th. Objective of the present work was to develop an HPLC method for the determination of U in samples with Th/U amount ratios as high as 100,000 without involving any pre-separation of the matrix element. When mandelic acid was used as the elunt, elution of U occurred prior to Th contrary to that observed with α-HIBA as the eluent. Hence, it was also of interest to understand the mechanism of adsorption of metal-mandelate complexes onto the stationary phase.

Since both Th and U form hydrophobic complexes with the eluting ligands, the separation was carried out on unmodified RPcolumn. The parameters such as pH& methanol content of the mobile phase and concentration of the eluentwere studied to optimise separation between Th and U on the RP column.The parameters controlling the Th retention capacity were taken into consideration while optimizing the gradient conditions. Synthetic samples were introduced in multiple injections since the amount of U per injection (100 µL) would be below the quantification level. Concentration of Th in the synthetic mixture solution was restricted to ~ 3,000 ppmw as it shows turbidity on standing over a period of time (1 hr to overnight) due to the precipitation of $Th(OH)_4$.

The developed method allowed reliable determination of small amounts of U in the presence of large amounts of Th. Monolith columns could be used for samples with Th/U amount ratios up to 3,000 whereas for samples with higher Th/U ratios, i.e., up to 100,000, particulate column could be used. Fig. 3 shows the chromatogram obtained for a mixturewith Th/U amount ratio >100,000 on a particulate column.

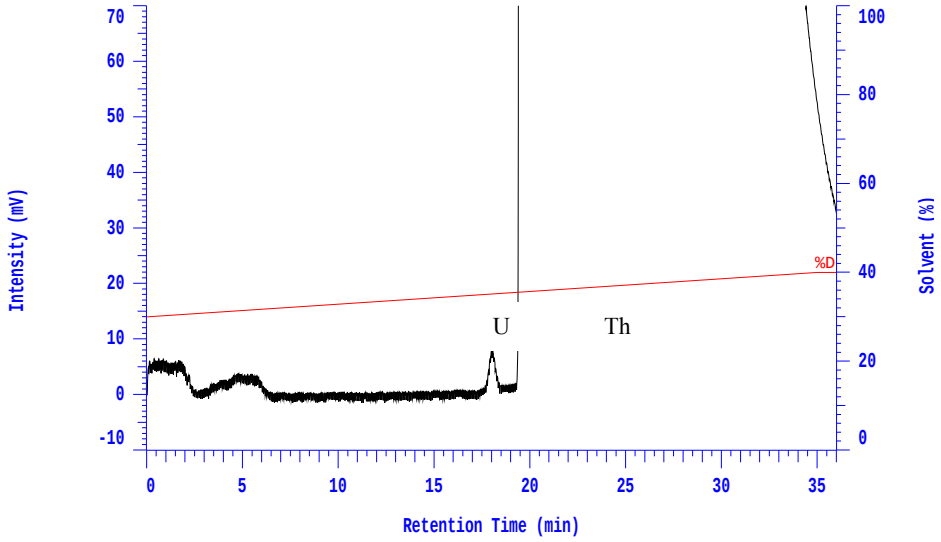

Fig 3: Separation of U and Th in a mixture with Th/U amount ratio of 106,479 on a particulate RP column

To understand the mechanism of adsorption of mandelate complexes of Th and U onto the RP stationary phase, two different IIRs viz. sodium n-octane sulphonate and tetra-n-

butyl ammonium bromide were introduced into the mobile phase at varying concentrations and the corresponding changes in the retention times of Th and UO_2 were monitored.Results from the experiments support the charge neutrality of thorium mandelate complex and the anionic nature of uranyl-mandelate complex. The difference in nature of the major species of Th and Uexplained distinct elution pattern observed when mandelic acid was used as the eluent.

Chapter 4

This Chapter deals with the development of HPLC methods for the determination of U at ultra trace levels from seawater and process samples.Recovery of U from seawater is an option for increasing its availability to meet the future energy requirements. A method for the determination of U at different stages of pre-concentration and separationwas required for assessing the feasibility of recovering U from seawater. In addition, determining the fate of U in natural water systems including seawater is important for environmental monitoring. However, U determination in seawater is a challenging task because of the high salt content, presence of bio-fouling agents and low concentrationsat ppb levels of U.

Low Uconcentrations and largeamounts of other dissolvedspecies in seawater necessitate chemical separation of U prior to its determination. In the first approach, α-HIBAwas used as a chelating agent for the separation of U on a monolith RP column. The same column was employed for the pre-concentration and separation of U. The acid treated seawater sample was mixed with 0.025 M α-HIBA and the pH of the solution was adjusted to 6 – 7. This solution was pumped through the column for the pre-concentration. The adsorbed Uwas eluted from the column by using (α-HIBA+MeOH) gradient and was detected spectrophotometrically after post-column reaction. Under the optimized conditions, metal ions viz. V, Ni, Ti, Mo were not retained on the column and hence showed no interference during the elution of U.

However, during the determination of U in processed samples containing high levels of Fe(III), the method was found to be unsuitable due to the clogging of the pre-concentration column by the precipitate formed in the feed solution. Hence further studies were carried out with the objectives to obtain: (i) good separation between U (VI) and Fe (III) (ii) possibility to introduce the samples at pH ≤ 4to avoid the formation of turbidity and (iii) quantitative recovery of U during the pre-concentration procedure.Use of mandelic acid (pH ~4) as a chelating agent allowed the pre-concentration of U without hydrolysis of other metal ions like Fe (III). Two separate columns were employed for pre-concentration and separation. Elution conditions were optimized by studying the effect of concentration of mandelic acid, MeOH content in the mobile phase etc. for separation of U(VI) from Fe(III) and other impurities. The method offered quantitative pre-concentration of U(VI) and linear response was obtained for U concentration in the range of 0.5 to 500 ppb. The methodology was applied for the determination of uranium in seawater and process samples from different stages of the recovery process of uranium from seawater. This method was found to be robust as the U peak area was not affected by the presence of Fe (III) in the sample upto Fe/U amount ratio of 3000. Figs. 4(a) &(b) show the chromatograms obtained for the separation of U from seawater sample and process sample, respectively. Both the methods were applied to seawater samples and the precision was in the range 5 - 9%. In both the cases, the developed methodologies were validated by comparing the results with those from internationally accepted technique of isotope dilution-thermal ionization mass spectrometry.

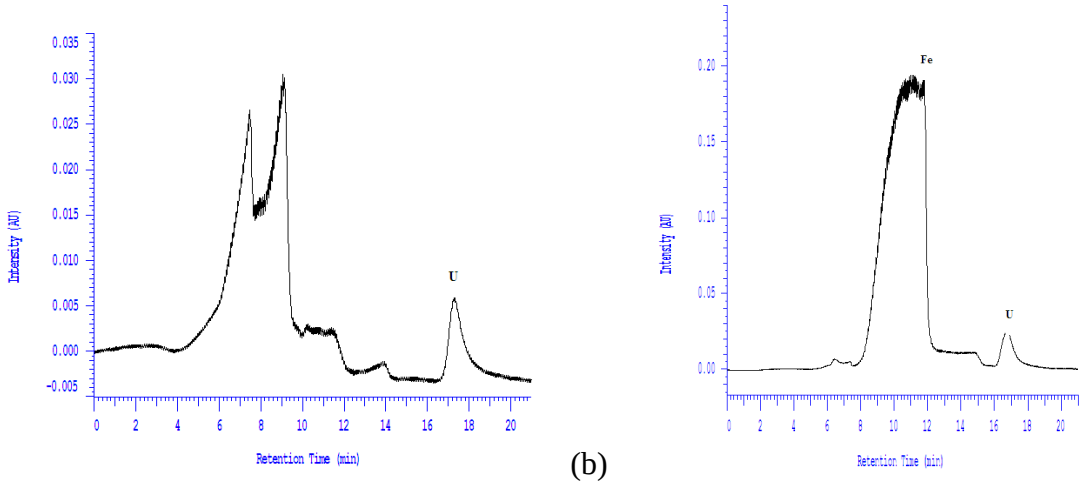

(a) (b)

Fig. 4: Chromatograms obtained for U separation from (a) seawater sample and(b) processed sample

Chapter 5

This Chapter discusses about the electrospray ionization mass spectrometric studies on the complexation of UO_2^{2+} with α-hyydroxy carboxylic acids.These chelating agents are extensively used as the eluents in the LC separation of lanthanides and actinides. Studying the nature of different species of the metal-ligand complexes would provide an insight to the various mechanisms responsible for the chromatographic separations.

ESI-MS was used to follow the complexation of uranyl ion with two hydroxy carboxylic acids viz. α-hyydroxy isobutyric acid and mandelic acid. The different peaks corresponding to the free UO_2^{2+} as well as complexed uranyl-ligand $[UO_2^{2+}\text{-}(L)_n]$ species were identified by comparing the theoretically calculated isotopic pattern or by MS/MS analysis. Appropriate experimental parameters were chosen by monitoring the effect of capillary voltage and dry gas temperature on the intensities of the important species. Calibration curve was obtained for the ESI response of uncomplexed UO_2^{2+} ions in the concentration range of $1x10^{-6}$ M to $2x10^{-5}$ M. Fig. 5 shows the typical ESI-MS spectrum in positive ionization mode obtained for uranylnitrate dissolved in methanol. For monitoring the overall trend in complexation, the reaction was studied as a function of ligand-to-metal ratios ranging from 1 to 10. Uranyl nitrate and ligand solutions prepared in methanol were mixed on volume basis to give the complex solution with the required M/L ratios. In order to follow

the equilibrium using ESI-MS, uncomplexed UO_2^{2+} ions and UO_2^{2+}-ligand complex ions were monitored in the positive mode. Concentrations of complex species, $[UO_2^{2+}\text{-}(L)_n]$, were determined based on the intensity of the free UO^{2+}. Distribution of 'free metal' (M) and metal-ligand complex species (ML_1, ML_2 and ML_3) as a function of L/M molar ratio was determined. Stability constant of the UO_2^{2+}-ligand reaction was determined based on the distribution data as well as the ESI calibration curve of the free UO^{2+}.

The studies helped in the identification of different species of uranyl-α-HIBA and uranyl-mandelate complexes in methanol medium. In the case of uranyl-α-HIBA system, the stability constant data obtained ($\log\beta_1 = 3.5$) were comparable to those reported in literature (3.2) for the ML_1 type complexes. However, for ML_2 and ML_3, the stability constant values obtained were higher than the reported data. This could be attributed to the fact that most of the associated species of ML_2 and ML_3 exist as negative ions, which could not be taken into account in the present study. In the case of uranyl-mandelate system, stability constant data obtained for the uranyl-mandelic acid system ($\log\beta_1 = 2.9$ and $\log\beta_2 = 4.0$) were comparable to the literature data (2.6 and 4.1, respectively).

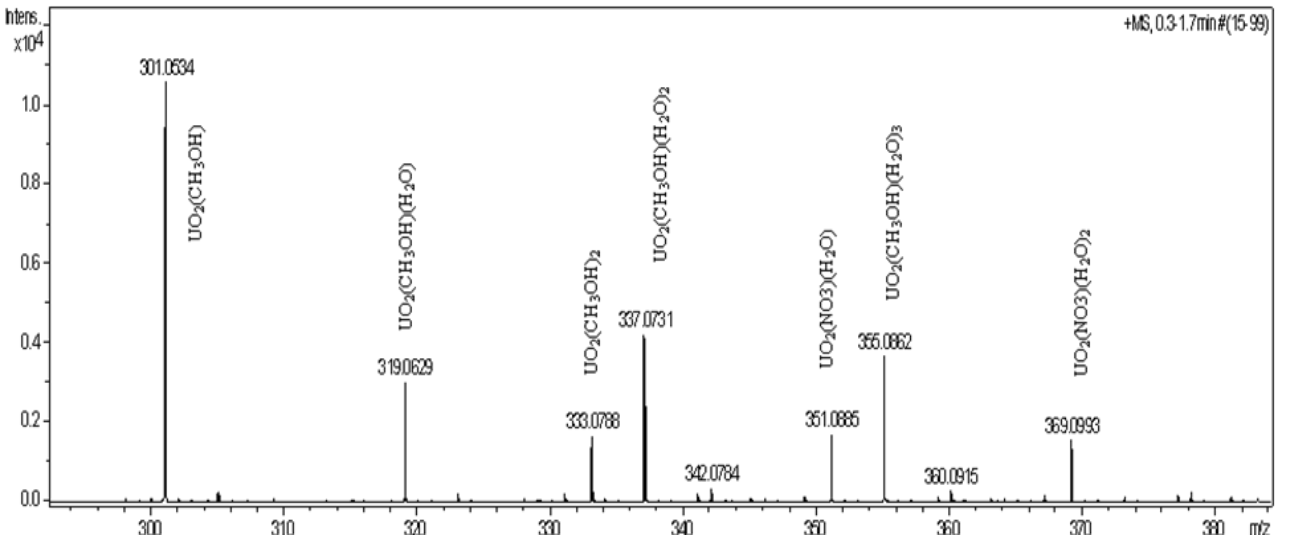

Fig. 5: ESI-MS spectrum for uranylnitrate in methanol in positive ionization mode.

In summary, the important highlights of the work are as follows:

1. LC method based on the use of n-octadecyl sulphonate as ion interaction reagent provided efficient separation of lanthanides. The IIR offers good long term adsorption onto the RP column, thereby obviating the need to introduce the IIR in the mobile phase during the separation of lanthanides.
2. A novel dual gradient elution was developed for the determination of lanthanides without involving any pre-separation of matrix elements U and Th. The method was used for the quantification of La and Nd in simulated irradiated thoria samples.
3. A method was developed for the trace level determination of U in samples containing large amounts of Th using mandelic acid as the eluent. The studies were extended to understand the mechanism of adsorption of mandelate complexes of Th and U onto the RP stationary phase.
4. HPLC methods for the determination of ppb levels of uranium in seawater and process samples were developed.The method offers determination of U in the concentration range of 0.5 to 500 ppb and could tolerate the presence of Fe (III) in the process sample up to Fe/U amount ratio of 3000.
5. Electrospray ionization mass spectrometric studies on the UO_2^{2+}-α-hyydroxy carboxylic acid systems were carried out with an objective to determine the distribution of different species of the metal-ligand complexes. The data on the stability constants for uranyl-α-HIBA system and uranyl-mandelic acid system were obtained.

Part of the work being submitted for the award of the degree of Doctor of Philosophy hasbeen published in the following International Journals:

1. Direct determination of lanthanides in simulated irradiated thoria fuels using reversed phase high-performance liquid chromatography

   P.G. Jaison, Narendra M. Raut, Suresh K. Aggarwal

   Journal of Chromatography A, **1122** (2006) 47–53.

2. Reversed-phase liquid chromatography using mandelic acid as an eluent for the determination of uranium in presence of large amounts of thorium

   P.G. Jaison, Vijay M. Telmore, Pranaw Kumar, Suresh K. Aggarwal

   Journal of Chromatography A, **1216** (2009) 1383–1389.

3. Comparative Study of Ion Interaction Reagents for the Separation of Lanthanides by Reversed-Phase High Performance Liquid Chromatography (RP-HPLC)

   P. G. Jaison, Pranaw Kumar, Vijay M. Telmore, and Suresh K. Aggarwal

   Journal of Liquid Chromatography & Related Technologies, **32** (2009) 2146–2163.

4. A RP-HPLC Method using α-Hydroxy Isobutyric Acidfor Preconcentration and Determination ofUranium in Seawater

   P.G. Jaison, Vijay M. Telmore, Pranaw Kumar, and Suresh K. Aggarwal

   Journal of Chromatographic Science, **49** (2011)72-78.

5. Determination of Uranium in Seawater Samplesby Liquid Chromatography using Mandelic Acidas a Complexing Agent

   P.G. Jaison, Vijay M. Telmore, Pranaw Kumar and Suresh K. Aggarwal

   Journal of Chromatographic Science, **49** (2011) 657-664.

6. Electrospray ionization mass spectrometric studies onuranyl complex with α-hydroxyisobutyric acid in watermethanolmedium

   P.G. Jaison,Pranaw Kumar, Vijay Telmore and Suresh K. Aggarwal

   Rapid Communications in Mass Spectrometry, **27** (2013) 1105 -1118.

In addition to these journal publications, eight contributed papers in various Symposia / Conferences werepresented:

International

1. Determination of Uranium in Seawater by Liquid Chromatography Using Mandelic Acid as a Complexing Agent

   P.G. Jaison, V.M. Telmore, Pranaw Kumar and S.K. Aggarwal

   34th International Symposium on High-Performance Liquid Phase Separations and Related Techniques (HPLC2009) held in Dresden, Germany during June 28 – July 2,2009, Paper No. ENV10, p. 324.

2. Coupled Column Liquid Chromatography Using Mandelic Acid for the Determination of Lanthanides in Thorium Matrix

   P.G. Jaison, Pranaw Kumar, V.M. Telmore and S.K. Aggarwal

   Ibid, Paper No. MCS09, p. 558.

National

3. Chromatographic Studies for the Separation of Uranium and Thorium using Mandelic Acid

   P.G. Jaison, V.M.Telmore and S.K. Aggarwal

   DAE–BRNS Biennial Symposium on "Emerging Trends in Separation Science and Technology (SESTEC–2008)" held at University of Delhi, Delhi during March 12-14, 2008, Paper No. D-4, p. 281.

4. Reverse Phase-High Performance Liquid Chromatographic Separation of Lighter Lanthanides using Salicylic acid as eluent

   Pranaw Kumar, **P. G. Jaison** and S. K. Aggarwal

   Ibid, Paper No. D-5, p. 283.

5. Separation of Th, U and Pu from Irradiated Thoria by RP-HPLC

   P.G. Jaison, Vijay M. Telmore, Pranaw Kumar and Suresh K. Aggarwal

   Tenth biennial symposium on Nuclear and Radiochemistry (NUCAR-2011) held at GITAM Institute of Science, Visakhapatnam during February 22-26, 2011, Paper No. B-48, p. 268.

6. Separation and determination of lanthanides and actinides by HPLC

   P.G. Jaison and S.K. Aggarwal

   22nd Research Scholars' Meet-2010 (RSM-2010) held at Sathaye Collage, Mumbai during February 19-20, 2010, Abstract No. 35, p. 35.

7. Electrospray Ionization Mass Spectrometric Studies on Uranyl-α-Hydroxy Isobutyric Acid Complex

   P.G. Jaison, Pranaw Kumar, V.M. Telmore and S.K. Aggarwal

   14th ISMAS Symposium cum Workshop on Mass Spectrometry (14th ISMAS-WS 2011) held in Munnar during November 7 - 11, 2011, Paper No. CP – 37, p.237.

8. Electrospay Ionization Mass Spectrometric Studies on Uranyl-Mandelic Acid Complex

   P.G. Jaison, Pranaw Kumar, V.M. Telmore, D. Alamelu and S.K. Aggarwal

   12th ISMAS Triennial International Conference on Mass Spectrometry (12th ISMAS-TRICON-2013) held in Cidade-de-Goa, Dona Paula, Goa during March 3-8, 2013, Paper No. CP - 27, page 230.

List of Figures

Figure No	Figure Caption	Page No.
Figure 1.1	Atomic and ionic radii of lanthanides as a function of atomic number	8
Figure 1.2	Illustration of eddy diffusion	26
Figures 1.3	Illustrations of longitudinal diffusion of a solute band and change in the pattern of solute band as a function of time spent in the mobile phase	26
Figure 1.4	Band broadening due to flow distribution	27
Figure 1.5	Mass transfer in the stagnant mobile phase	28
Figure 1.6	Mass transfer in the stationary phase	28
Figure 1.7	Representation of theoretical plates in a chromatographic column	29
Figure 1.8	Van Deemter plot showing the dependence of eddy diffusion, longitudinal mass transfer, mass transfers effect and the cumulative factor on the linear velocity of the mobile phase	31
Figure 1.9	Comparison of Van Deemter curves of columns packed with particles of different sizes	32
Figure 1.10	Representation of retention time in a chromatogram.	32
Figure 1.11	Illustration of baseline peak width and peak width at half maximum	34
Figure 1.12	Illustration of measurement of resolution	35
Figure 1.13	Dependence of resolution on retention factor, k; number of theoretical plates, N; and separation factor	37
Figure 1.14	Schematic diagram of an HPLC system with post-column derivatisation detection	39
Figure 1.15	Block diagram of a low pressure quarternary gradient solvent delivery system	40
Figure 1.16	Schematic diagram of a single piston reciprocating pump	42

Figure 1.17	Comparison of flow profiles obtained by reciprocating pumps with different pump heads	43
Figures 1.18	Schematic diagram of injectors in load position and inject position	44
Figure 1.19	Representation of different silanol groups present in silica	47
Figure 1.20	Representation of figures of merits in chromatographic analysis	53
Figure 1.21	Schematic diagram of a diode array detector	55
Figure 1.22	Schematic of electrospray ionisation system	69
Figure 1.23	Schematic diagram of a quadrupole-ToF hybrid mass spectrometer	71
Figure 1.24	Schematic diagram of a magnetic sector mass spectrometer	75
Figure 2.1	Separation of 14 lanthanides on a C_{18} column coated with C18-sulphonate	97
Figure 2.2	Sequential separation of Fe, lanthanides, Th and U from a geological reference material (SY-3) on C18-sulphonate coated C_{18} column	98
Figure 2.3	Effect of concentration of IIR on the retention of Lu, La, Th and U	104
Figures 2.4	Elution of Th under different conditions	105
Figure 2.5	Effect of concentration of IIR on the amount of Th retained on RP column	106
Figure 2.6	Effect of pH of α-HIBA on the amount of Th retained on RP column	108
Figure 2.7	Separation of lanthanides, Th and U in simulated 1 atom% burn-up solution using dual (concentration and pH) gradient	110
Figure 2.8	Separation of lanthanides from the dissolved $(Th,Pu)O_2$ sample using dual gradient elution	114
Figure 2.9	Schematic diagram of the coupled column chromatographic set-up	116

Figure 2.10	Effect of concentration of mandelic acid on the retention of La, Lu and Th on a RP stationary phase	118
Figure 2.11	Change in the retention of La, Lu and Th on RP stationary phase as a function of pH of the mobile phase	119
Figure 2.12	Effect of concentration of $NaNO_3$ in mobile phase on the retention times of La, Lu and Th	120
Figures 2.13	Separation of individual lanthnides using bonded cation exchanger column and RP column modified with C-18 sulphonate	121
Figure 2.14	Chromatograms for the separation of lanthanides (1 ppm each) and Th (10,000 ppm) under identical elution conditions	123
Figure 3.1	Changes in the retention time of Th and U as a function of concentration of eluent	130
Figure 3.2	Effect of pH of mobile phase on retention of Th and U	131
Figure 3.3	Effect of methanol in the mobile phase on U peak response	132
Figure 3.4	Separation of Th and using concentration gradient of HIBA and MeOH in the mobile phase	133
Figure 3.5	Effect of pH of mandelic acid eluent on the retention time of Th and U	137
Figure 3.6	Effect of concentration of mandelic acid on the retention of Th and U	138
Figure 3.7	Effect of methanol content on the retention behaviour of Th and U	139
Figure 3.8	Separation of Th and U (Th/U amount ratio = 1) on an RP column using mandelic acid as the eluent	140
Figure 3.9	Th retention capacity of stationary phase as a function of methanol content in the mobile phase	141
Figure 3.10	Th retention capacity of monolith column as a function of pH of mobile phase	142
Figure 3.11	Calibration curve for U in presence of Th	143

Figure 3.12	Calibration curve for Th in presence of U	144
Figure 3.13	Separation of U and Th in a mixture with Th/U amount ratio of 3000on a monolith RP column	144
Figure 3.14	Peak area response of U as a function of number of injections	146
Figure 3.15	Separation of U and Th in a mixture with Th/U amount ratio of 106479, on a particulate C_{18} RP column	147
Figure 3.16	Retention times of Th and U as a function of concentration of n-octane sulphonate	151
Figure 4.1	Schematic diagram of the preconcentration set-up	161
Figure 4.2	Effect of concentration HIBA on the retention of U	163
Figure 4.3	Effect of pH of HIBA on the retention of U and La	164
Figure 4.4 a	Chromatogram of isocratic separation of U	165
Figure 4.4 b	Separation of U under the optimized gradient condition	166
Figure 4.5	Chromatogram of elution of U adsorbed onto the PTFE tubing	167
Figure 4.6	Recovery of U as function of loading flow rate	169
Figure 4.7	Peak area of U as function of its concentration in simulated seawater	169
Figure 4.8	Chromatogram obtained for a seawater sample	170
Figure 4.9	Effect of concentration of tetrabutyl ammonium bromide on the retention of Fe(III) and U(VI)	177
Figure 4.10	Effect of concentration of mandelic acid on the retention of Fe(III) and U(VI)	178
Figure 4.11	Effect of methanol content on the retention of Fe(III) and U(VI)	178
Figure 4.12	Effect of concentration of mandelic acid on the recovery of U	181
Figure 4.13	Effect of pH of mandelic acid on the recovery of U	182
Figures 4.14	Chromatograms obtained by the elution of concentrator column in the forward and in the reverse directions	185
Figure 4.15	Effect sample loading flow rate on the recovery of U	187

Figure 4.16	Peak area/gm of U as function of its concentration in simulated seawater	188
Figure 4.17	Chromatogram of a simulated seawater sample containing Fe(III) and U(VI) in the proportion 1:3000	190
Figures 4.18	Chromatograms obtained for seawater sample and processed sample	191
Figure 5.1 (a)	ESI MS spectrum of $5x10^{-6}$ M $UO_2(NO_3)_2$ in MeOH	200
Figure 5.1(b)	ESI MS spectrum of $5x10^{-6}$ M $UO_2(NO_3)_2$ in MeOH and 10^{-5} M $NaClO_4$ added as electrolyte	202
Figures 5.2	Positive mode ESI-MS spectra of uranyl nitrate solution prepared in mobile phase containing 10^{-5} M $NaClO_4$ and 1:1 methanol-water	208
Figures 5.3	ESI-MS spectra of UO_2 – HIBA system in positive mode and negative mode	210
Figures 5.4	Changes in the fractional intensities of uranyl species as a function of capillary voltage in the positive ion mode and in the negative ion mode	216
Figure 5.5	Changes in the fractional intensity of uranyl species as a function of dry gas temperature in the positive mode	218
Figure 5.6	Changes in the relative intensities of uranyl species as a function of in-source collision induced dissociation energy in the positive ion mode	219
Figure 5.7	Distribution of uranyl species as a function of quadrupole ion energy in the positive ion mode	220
Figure 5.8	Distribution of uranyl species as a function of collision cell energy in the positive ion mode	222
Figure 5.9	Effect of end-plate offset voltage on the distribution of uranyl species in the positive mode	223
Figure 5.10 (a)	Distribution of uranyl-HIBA complex species as a function of ligand-to-metal ratio in positive ion mode	224

Figure 5.10(b)	Distribution of uranyl-HIBA complex species as a function of ligand-to-metal ratio in the negative ion mode	226
Figure 5.11(a)	ESI-MS spectrum of uranyl-mandelic acid system in the positive ion mode	227
Figure 5.11(b)	ESI-MS spectrum of uranyl-mandelic acid system in the negative ion mode	229
Figure 5.12 (a)	ESI-MS spectrum of the dimeric uranyl-mandelic acid species $[(UO_2)_2(C_8H_8O_3)_4]^{2+}$	230
Figure 5.12(b)	ESI-MS spectrum of the monomeric uranyl-mandelic acid species $[(UO_2)(C_8H_8O_3)_2]^{+}$	230
Figure 5.13	Changes in the intensities of uranyl-mandelate species as a function of dry gas temperature in the positive ion mode	231
Figure 5.14	Changes in the intensities of uranyl-mandelate species as a function of in-source collision induced dissociation energy in the positive ion mode	232

List of Tables

Table No	Table Caption	Page No.
Table 1.1	Electronic configuration and oxidation states of lanthanides	5
Table 1.2	Electronic configuration and oxidation states of Actinides	6
Table 1.3	Comparison of different separation methods	15
Table 1.4	Classification of liquid chromatography based on the nature of equilibrium	19
Table 1.5	Comparison between GC and LC	24
Table 1.6	Comparison of pre-column and post-column derivatisations in liquid chromatography	57
Table 1.7:	Comparison of important features of mass analyzers	65
Table 2.1	Effect of composition of C20-sulphate solution used as IIR for the separation of lanthanides	88
Table 2.2	Effect of volume of C18-sulphonate IIR solution on the separation of lanthanides	89
Table 2.3	Effect of volume of C20-sulphate solution on the separation of lanthanides	90
Table 2.4	Effect of volume of water passed through C18-sulphonate coated column on the separation of lanthanides	91
Table 2.5	Effect of mobile phase conditioning of C18-sulphonate coated column on the separation of lanthanides	93
Table 2.6	Comparison of resolution for the separation of lanthanides using column modified with different IIRs	94
Table 2.7	Comparison of resolution for the separation of lanthanides using C_8 and C_{18} columns modified with C8-sulphonate and C9-sulphonate	96

Table 2.8	Gradient conditions for separation of Fe, lanthanides, Th and U	98
Table 2.9	Determination of lanthanides in SY-3 sample	99
Table 2.10	Long-term performance of C_{18} monolith column coated with C18-sulphonate	100
Table 2.11	Optimized conditions for separation of lanthanides in presence of large amounts of Th	109
Table 2.12	Chemical composition of dissolver solution of irradiated thoria sample	111
Table 2.13	Concentrations of lanthanides, U &Th in simulated samples	111
Table 2.14	Quantification of La and Nd determined (in ppm) using internal standard	112
Table 2.15	Optimized gradient conditions for the coupled column separation	122
Table 2.16	Recovery of lanthanides added to Th	124
Table 3.1	Determination of U in synthetic mixtures with different Th/U amount ratios	148
Table 3.2	Effect of concentration of tetra-n-butylammonium bromide on the retention time of Th and U on the RP column	153
Table 4.1	Composition of simulated seawater sample	160
Table 4.2	Optimized gradient condition for the elution of U	161
Table 4.3:	Concentration of U in seawater determined by HPLC and ID-TIMS	171
Table 4.4	Sequence of operations involved in the HPLC analysis of seawater/processed samples	175
Table 4.5	Optimised gradient condition for the separation of U(VI)	179
Table 4.6	Comparison of elution of U from RP column using different eluents	180
Table 4.7	Comparison of the data on the response of U using two different stationary phases for concentration and separation	184

Table 4.8	Comparison of peak area/mL obtained for U under different injection/loading conditions	189
Table 4.9	Concentration of U in seawater and processed samples obtained by HPLC and ID-TIMS	191
Table 5.1	Effect of electrolyte on the ESI response of UO_2 species	201
Table 5.2	Distribution of uranyl species in methanol-water system in positive ion mode	204
Table 5.3	Distribution of species at different concentrations of uranyl nitrate in mobile phase	207
Table 5.4 (a)	Uranyl-HIBA species observed in the positive ion mode	211
Table 5.4 (b)	Uranyl-HIBA species observed in the negative ion mode	212
Table 5.5(a)	Uranyl-mandelic acid species observed in the positive ion mode	228
Table 5.5(b)	Uranyl-mandelic acid species observed in the negative ion mode	229

Chapter 1

Introduction

1.1 Introduction

1.1.1 Relevance of Trace Determination of Lanthanides, Thorium and Uranium

Recent years have seen a growing importance in the role of trace elemental determination in different domains such as energy sector, environmental monitoring, material science, geochemical characterization etc. Thorium (Th) and uranium (U) are used as fertile and fissile elements, respectively, in nuclear reactors and these are also of great technological value. In view of the radiation protection also, determination of natural radionuclides such as Th and U in the environmental samples is important. During the nuclear fission of the fissile nuclides like ^{235}U or ^{239}Pu, different lanthanide elements are produced along with different fission products. Because the fission yields of selected lanthanides are known, analysis of dissolved irradiated fuel elements for their lanthanide content can be used to determine the extent to which the fuel was 'burned' in the reactor [1-3]. In view of the analogy with actinides, concentrations of lanthanides in ground water is considered as an indicator for modeling the leaching of actinides from nuclear waste repositories [4]. The geochemical behavior of lanthanides, Th and U are relatively close to one another when compared to other elements in the geological environment. Lanthanide abundance has proven to be extremely useful to understand and to improve knowledge on the composition, structure and evolution of earth's upper mantle [5]. Similarity in their chemical properties and low solubility make these elements useful as geochemical indicators in sediments. Thus lanthanides profiles are extensively used as a signature of water-rock interactions in various aquatic systems [6]. Suitable methods for accurate and rapid determination of lanthanides, Th and U in geological and nuclear samples are, therefore, required [7]. However, the complex nature of the matrices makes the trace determination of lanthanides and actinides complicated. Challenges posed by the above samples include matrix effect, spectroscopic interference, high salt concentration, relatively low levels of analyte concentrations in the sample etc. Liquid chromatography

(LC)is a powerful and cost effective tool for trace analysis. In combination with element selective detection techniques, LC provides low limits of detection and overcomes spectral interferences and matrix effects. The application of chromatographic techniques to highly radioactive samples offers several unique challenges. Hyphenation of LC with selective and sensitive techniques like mass spectrometry is important for identifying and characterizing different species in complex samples [2,3]. In this thesis, studies were carried out for developing LC methods for the separation and determination of lanthanides, Th and U in different types of samples.

1.1.2 Nomenclature

Lanthanides consist of fourteen elements following La (Z = 57) to Lu (Z = 71) and occupy a special location in the Periodic Table. The ending 'ide' normally indicates a negative ion, and therefore according to IUPAC, the name ‘Lanthanoid’ (meaning 'like lanthanum') is preferred for this class of elements [8]. However, lanthanide and actinide are still allowed owing to wide current use. Together with the elements scandium and yttrium, the lanthanoids are known also as rare-earth elements (REEs). All the REEs have similar outer electronic configuration and their oxides are collectively termed as rare earths. The actinide elements are a group of chemically similar elements with atomic numbers 90 to 103 and are placed below lanthanides in the Periodic Table.

The discovery of the lanthanides began in 1788 when B. Geijer reported the analysis of a stone found near Ytterby, Sweden. This mineral was called yttria and its composition was analyzed by Gadolin and Arrhenius. The word lanthanum is originated from the Greek word *lanthanein* which means “to lie hidden” as it hid in cerium ore and was difficult to separate from the mineral. The term lanthanide is aptly given as it took over a century to discover all the 15 elements belonging to this family. In 1804, J. J. Berzelius and W. Hisinger discovered

Ce and in 1947 Marinsky *et al.* discovered Pm [9]. Thorium was discovered in 1828 by J. J. Berzelius and later, he named his discovery after Thor, who is the ancient Scandinavian God of thunder and weather. In 1898, G. Carl Schmidt and Marie Curie independently established the radioactive nature of Th. Uranium was first isolated from pitchblende in 1789 by M. Klaproth who named it after 'Uranus' which was a newly discovered planet at that time. In 1896, H. Becquerel discovered the phenomenon of radioactivity while studying the spontaneous emission of a uranium-bearing crystal.

1.1.3 Occurrence

REEs occur in more than 100 minerals and are widely distributed in low concentrations throughout the earth's crust. Except for Promethium (Z = 61), all rare-earth elements have at least one stable nuclide and occur naturally. The term 'rare-earth' may not be correct as some of the Lanthanides are present in the earth's crust in greater quantities than lead. Cerium, the most abundant REE, is also the 25^{th} most abundant element, similar to copper. The particular chemical properties of rare earth elements make them difficult to extract and these elements are rarely found at concentrations that allow them to be processed in economically viable manner and hence are named rare earth elements. The principal source of rare earth elements includes the minerals known as monazite, bastnaesite and xenotime.

Actinides, on the other hand, have only three naturally occurring elements out of 14. Only actinium, thorium and uranium occur naturally. The most common ore of thorium is monazite which contains up to 12% of thorium oxide and is also the primary source of rare earth elements. The principal uranium minerals are uraninite, pitchblende etc. U also occurs in significant amounts in oceans though at very low concentration levels. Protoactinium, Neptunium and Plutonium are found in uranium ores at very low concentrations. All of the

elements beyond Pu do not occur naturally. Each of these elements has a number of isotopes, mostly synthetic in origin, and all are radioactive.

1.1.4 Electronic Configuration

Table 1.1: Electronic configuration and oxidation states of lanthanides

Atomic number	Element	Electronic configuration	Oxidation state
57	La	$5d^1\ 6s^2$	+3
58	Ce	$4f^1\ 5d^1\ 6s^2$	+3, +4
59	Pr	$4f^3\ 6s^2$	+3
60	Nd	$4f^4\ 6s^2$	+3
61	Pm	$4f^5\ 6s^2$	+3
62	Sm	$4f^6\ 6s^2$	+3
63	Eu	$4f^7\ 6s^2$	+2, +3
64	Gd	$4f^7\ 5d^1\ 6s^2$	+3
65	Tb	$4f^9\ 6s^2$	+3, +4
66	Dy	$4f^{10}\ 6s^2$	+3
67	Ho	$4f^{11}\ 6s^2$	+3
68	Er	$4f^{12}\ 6s^2$	+3
69	Tm	$4f^{13}\ 6s^2$	+3
70	Yb	$4f^{14}\ 6s^2$	+2, +3
71	Lu	$4f^{14}\ 5d^1\ 6s^2$	+3

In the lanthanide series, fourteen 4f electrons are added beginning formally with cerium (Z = 58) and ending with lutetium (Z = 71). The first member of the lanthanides series (La) does not have any 4f electron, and has electronic configuration, $6s^2\ 5d^1$. In the case of lanthanides, the 4f orbital becomes appreciably lower in energy compared to 5d orbital immediately after La. Consequently the electrons fill the 4f orbitals in a regular manner

among the lanthanides (except in the case of half filled 4f shell). The electronic configuration of lanthanides is presented in Table 1.1.

In the actinide series, successive electrons are added to the inner 5f shell beginning with Thorium and ending with Lawrencium. In the case of actinides, the difference between energies of 5f and 6d orbitals is very small for the first four elements viz. Th, Pa, U and Np. Consequently, electron may occupy either 5f or 6d or both. Only in the latter actinides, the 5f orbital gets appreciably lower in energy than 6d and hence from Pu onwards, 5f shell is filled regularly. Table 1.2 shows the electronic configuration and oxidation states of actinides.

Table 1.2: Electronic configuration and oxidation states of actinides

Atomic number	Element	Electronic configuration	Oxidation state
89	Ac	$6d^1\ 7s^2$	+3*
90	Th	$6d^2\ 7s^2$	+4
91	Pa	$5\ f^2\ 6d^1\ 7s^2$	+4, +5*
92	U	$5f^3\ 6d^1\ 7s^2$	+3, +4, +5, +6*
93	Np	$5f^4\ 6d^1\ 7s^2$	+3, +4, +5*, +6, +7
94	Pu	$5f^6\ 7s^2$	+3, +4*, +5, +6, +7
95	Am	$5f^7\ 7s^2$	+3*, +4, +5, +6
96	Cm	$5f^7\ 6d^1\ 7s^2$	+3*, +4
97	Bk	$5f^9\ 7s^2$	+3*, +4
98	Cf	$5f^{10}\ 7s^2$	+3
99	Es	$5f^{11}\ 7s^2$	+3
100	Fm	$5f^{12}\ 7s^2$	+3
101	Md	$5f^{13}\ 7s^2$	+3
102	No	$5f^{14}\ 7s^2$	+3
103	Lr	$5f^{14}\ 6d^1 7s^2$	+3

** Most stable oxidation state*

1.1.5 Oxidation State

In solution, +3 is the most common oxidation state exhibited by all the lanthanides. In the lanthanide series, while moving from La^{3+} to Lu^{3+}, the 4f orbital situated inside the 5sand 5porbitals, is being filled from 0 to 14 electrons. The 4f electrons do not play a role in chemical bonding as they are shielded by the 5s and 5pelectrons. The chemical properties of the lanthanides are, therefore, very similar. The $4f^0$ (empty f orbital), $4f^7$ (half–filled f orbital) and $4f^{14}$ (filled f orbital) configurations are the most stable. Therefore, besides the trivalent state, some ions also occur in the divalent and the tetravalent states under favourable conditions. Examples are Ce^{4+} ($4f^0$), Eu^{2+} and Tb^{4+} ($4f^7$) and Yb^{2+} ($4f^{14}$). Cerium is referred to as cerous in the +3 oxidation state and ceric, in the +4 oxidation state. The common oxidation states exhibited by lanthanides in solution are also listed in Table 1.1.

Due to the low and comparable binding energies of 5f, 6d, 7s and 7p electrons in early actinides, these elements show variable oxidation states. With progressive filling of electrons, the 5f orbitals become more stable and their energy is lowered compared to that of 6d and 7s orbitals. Hence elements from Americium onwards exhibit +3 as the most stable oxidation state and their behavior is similar to that of lanthanides. The most common oxidation states of actinides are also included in the Table 1.2.

U is usually present in the form of UO_2^{2+} ion in its compounds. A similarity between the lanthanide and actinide elements was recognized in 1944 on the basis of chemical studies of Np and Pu [10]. There is a strong correlation between properties of the elements in the pairs: Eu - Am, Gd - Cm, Tb - Bk [11]. Because of their high similarity in electronic structure, valence and ionic radii, REEs have been used to predict the behavior of actinide-series elements in solutions [12].

1.1.6 Chemistry of Lanthanides and Actinides

Both lanthanides and actinides are called 'f' block elements' because the differentiating electron or extra electron enters (n-2)f orbitals. Since the (n-2)f orbitals lie inside the penultimate shell, these elements are also called inner-transition elements. Since the f orbitals are not spherically symmetric, the nuclear charge is not effectively screened by the additional electron. As a result, each successive element exhibits a slightly greater nuclear attraction over the electrons, leading to the contraction of the outer valence orbitals. Thus, atomic/ionic radius should gradually decrease as one move through the lanthanide series and is known as lanthanide contraction. The change in the ionic and atomic radii of lanthanides as a function of atomic number is presented in Fig. 1.1. Such a contraction is also observed for the actinides and is termed as actinide contraction. It amounts to approximately 0.2 Angstrom over the entire lanthanide series or an average of about 0.014 Angstrom between elements [13].

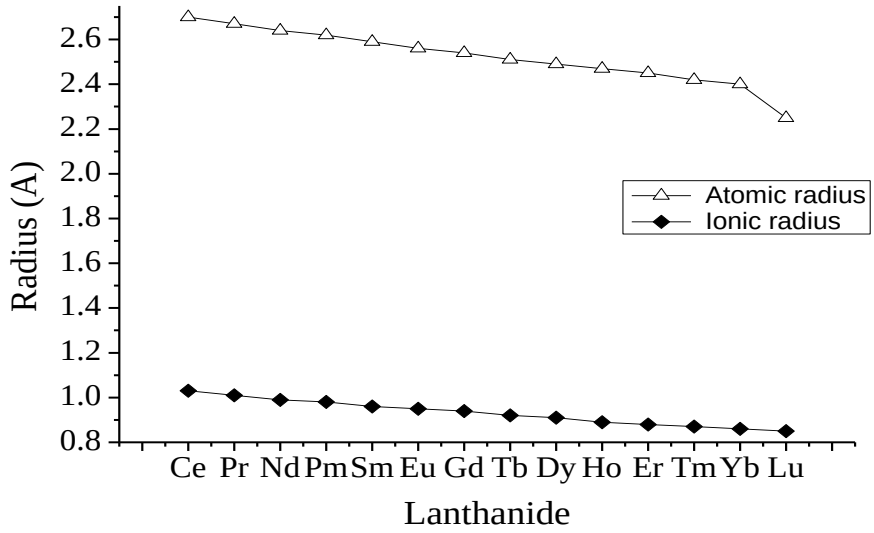

Figure 1.1: *Atomic and ionic radii of lanthanides as a function of atomic number.*

The chemical homogeneity of the lanthanides results from the relatively small radial extension of the 4f valence orbitals, which are buried beneath the spatially more extended 5d and 6s orbitals. Since 4f electrons are buried so deep within the atom, they have little

opportunity to participate in chemical bonding. Hence the addition of another f electron to the valence shell has little effect on the overall bonding character or reactivity of the element. Thus, all the lanthanides tend to behave chemically the same [13].

In the case of actinides, the 5f orbitals are very close in energy to the 6d's. The ground-state configuration of the thorium atom is $6d^2 7s^2$, indicating that the 6d orbital is lower in energy than the 5f orbital. With the progressive filling up of the electrons, 5f becomes lower in energy than the 6d, and the gap between the 5f and 6d orbitals begins to widen [14]. This leads to the split in behavior between light and heavy actinide elements. While lighter actinides exhibit rich and varied chemistry, the heavy actinides exhibit fewer oxidation states and simpler behavior. The differences between the light actinides and light lanthanides are due to the greater radial extension and diffused nature of 5f orbitals compared with 4f orbitals. Thus in the early part of the actinide series, electrons find relatively easy to switch between 5f and 6d configurations. Hence, these elements exhibit multiple and higher oxidation states similar to transition elements.

Generally the size of atom increases down a group in the Periodic Table. A consequence of lanthanide contraction is the similarity in the size of the elements in the second and third transition series. For example, radii of Zr (Z = 40) 1.59 A^o and Hf (Z = 72) 1.56 $A^o$are nearly the same, though they belong to the 5^{th} and 6^{th} periods of the Periodic Table, respectively. The increase in mass and the unchanged radii lead to a sharp increase in the density of elements from period5 to 6 in the transition elements [15].

According to Pierson, the metal ions are classified into hard and soft acids based on their polarisability [16]. Generally both lanthanides and actinides are considered as hard acids and show preference for bonding with oxygen donor ligands. However, actinides show relatively more soft character due to the diffused nature of the 5f orbitals and this difference is

being used in their selective separation known as actinide partitioning. Thus the properties of lanthanides and actinides are quite distinct and this has resulted in their increasing use in technologically important applications. REE are often used for their highly specific properties and wherever substitutes are unknown [17].

1.1.7 Importance of Lanthanides, Th and U

The chemical, physical and nuclear properties of the lanthanides make them ideal for a number of high technology applications. Importance of lanthanides was significantly enhanced after the discovery of the high-temperature superconductors with rare earth and cupric oxide as major constituents [18]. Due to their paramagnetic and ferromagnetic nature, they are extensively used in magnetic and electronic devices. Moreover, in many of these key applications, no substitute exists for lanthanide elements. Lanthanides, in pure form, or in mixtures, are key components of magnets used in hybrid cars, catalysts used for petroleum cracking, batteries, plasma television sets, mobile phones, wind turbines, computer memories, defense applications like propulsion system and radars used in warships etc. High-purity individual lanthanides are used increasingly as major components in lasers, phosphors, refractive index lenses, medical imaging, fiber optics, and superconductors etc. In view of their high thermal neutron absorption cross-sections, Gd and Dy are used as burnable poisons in nuclear fuels [19,20]. Radioactive isotopes of lanthanides are finding growing applications in nuclear medicine. e.g. ^{149}Tb ($T_{(1/2)}$ = 4.2 hrs) is used in radioimmunotherapy. These key applications of lanthanides have made them strategically important materials for many nations across the world.

Though the existence of lanthanides was known for a long time, the difficulty associated with their processing and separation limited their usage. Separating REE from one another is challenging and requires sophisticated methods because of similarities among REE.

In recent years, however, due to the development of efficient separation methods, the applications of lanthanide elements have grown immensely. In 2010, the world demand for REE was ~136,100 tons and it is predicted that by 2015 the global demand for REE may rise to 210,000 tons per year [21].

In India, instead of depleted uranium, thorium is being used for flux flattening during the initial start up of a nuclear power reactor. In view of the large scale availability of Th, India has planned utilisation of thorium for large-scale energy production as a major goal in its nuclear power program [22].Uranium is commonly used in nuclear power plants to generate energy. Apart from its nuclear related applications, U also finds use in material for armor and armor-piercing projectiles, as shielding material (depleted uranium) etc.

Other than their direct use in industry, lanthanides, Th and U are of importance to many branches of science e.g. the abundance of REE is used as a tool for elucidating the origin of rocks. The geochemical behavior of thorium, uranium and rare earth elements is relatively close to one another while compared to other elements in a geological environment [23]. Rare earth elements (REEs) are important indicators in many geochemical cycles. The lanthanides show characteristic behaviour as a group during geochemical processes. The ability to distinguish between geochemical and cosmochemical processes based on REE abundances has proven to be extremely useful for understanding the physico-chemical processes involved in the formation of early solar system solids [5]. REE concentration in waters was studied quite extensively in the last decade. Investigations were done utilizing REE patterns as signatures of water-rock interactions in various aquatic systems [24]. Similar chemistry of REE and low solubility make these elements useful as geochemical indicators in sediments and sedimentary rocks.

In view of their appreciable neutron absorption cross-sections, there are specified limits on the impurity content of different lanthanide elements (Gd, Sm, Eu, Dy etc.) in

different nuclear materials. For instance, the specifications on some of the lanthanides concentrations in nuclear grade uranium is as low as 0.1 ppm [25]. In the destructive method for the determination of atom percent fission or 'burn-up' of irradiated nuclear fuels, stable fission product ^{148}Nd is used as a burn-up monitor in view of the possibility to determine burn-up with high accuracy and reliability[2,26-28]. Elemental concentrations of La and Nd are also being used as markers for determining the extent of fissions in the nuclear fuels [29]. The fact that these elements are finding increasing importance in specific applications demands availability of different analytical methods for their accurate characterization and meaningful interpretation of the data.

1.1.8 Analytical Methods for the Determination of Lanthanides

Though element-specific detection techniques are sometimes adequate for lanthanides analysis, they are prone to suppression of the trace elements signal by high concentration of the matrix elements. Further, various isobaric/spectral overlaps restrict the direct determination of trace levels of lanthanides. All lanthanides have similar absorption spectra when they are reacted with a chromogenic agent. Hence, it is difficult to determine the individual lanthanides by spectrophotometry, unless a proper separation technique is employed. The most common techniques used in the determination of REE are atomic absorption spectroscopy (AAS), isotope dilution-thermal ionisation mass spectrometry(ID-TIMS), inductively coupled plasma-mass spectrometry (ICP-MS), inductively coupled plasma emission spectrometry (ICP-OES), X-ray fluorescence (XRF) and neutron activation analysis (NAA). NAA is a very sensitive and multi-elemental analysis technique; but depends upon the availability of a nuclear reactor and sometimes involves chemical separations [24,30,31]. If a more accurate determination is required, ID-TIMS can be employed but a chemical separation is mandatory as the technique is prone to isobaric interferences in the case of certain

lanthanides. Further, the technique cannot be used for mono-isotopic lanthanides viz. Pr, Tb, Ho & Tm. Though AAS allows accurate and precise determination, the technique suffers from poor sensitivity and is a single element analysis technique. ICP-OES has the capability of multi-element determination over a wide concentration range. However, the concentrations of REE in environmental samples are usually much lower than detection limits of this technique, and major constituents, such as organic compounds and inorganic salts, can cause some matrix effects [32].XRF offers the possibility of direct analysis of solid materials and provides multi-elemental capability. In view of the serious spectral interference problems in XRF, wave length dispersive (WDXRF) spectrometers are applied for REE determination rather than energy dispersive (EDXRF) instruments. However, the typical detection limits for REE are in the ppm range, which may not be useful for the analysis of environmental or biological samples. ICP-MS is one of the most powerful techniques for the trace determination of lanthanides due to its high sensitivity, large dynamic range, multi-element capability and possibility to perform isotopic measurements. Compared to ICP-OES, ICP-MS provides simpler spectra and lower detection limits which are beneficial to bypass extensive sample preparations in certain cases. Nevertheless, isobaric interferences are still a major constrain in ICP-MS analysis [24]. The different approaches to solve the interference in various detection techniques are high resolution or chemical separation [33].Often, high resolution is obtained at the expense of sensitivity and mathematical corrections cannot be easily applied to samples which have seen the nuclear reactor as the true isotopic composition of the analyte element may not be known.

Most of the limitations of the elemental specific techniques can be overcome by the judicious selection of separation methods [3]. Separation methods are useful to remove the matrix elements, minimize spectral interferences and improve the overall sensitivity by their ability to pre-concentrate. Thus improvements in separations of lanthanides led to the

development of analytical methods for their rapid and sensitive determination in different matrices [34].

1.1.9 Separation of Lanthanides and Actinides

Lanthanides exhibit similarity in their properties due to common oxidation of +3 and the small differences in the sizes of their hydrated ions. The similarity in properties makes the separation of individual lanthanide elements one of the most challenging tasks in separation science. The mutual separation of actinide elements also poses similar challenge especially if they are present in their most common trivalent state. On the other hand, U and Th exhibit rather different chemical properties and offer relatively lesser difficulty from the separation point of view. Procedures for mutual and group separation are widely used in mineral exploration, geochemistry, material science, environmental science and in the nuclear industry[35].Separation of lanthanides is important in different fields of science. The lanthanides are obtained industrially by treating their ores monazite and bastnastite with sodium hydroxide and hydrochloric acid. The resulting aqueous solutions of chlorides of the lanthanide ions are then subjected to column chromatography or solvent extraction to separate them according to decreasing atomic number. In the ID-TIMS method for the experimental determination of burn-up, separation procedure is employed to minimize the potential isobaric interferences by ^{142}Ce, ^{148}Sm, ^{150}Sm at ^{142}Nd, ^{148}Nd and ^{150}Nd, respectively [26,27]. Separation of individual lanthanides is also essential in the production of carrier free radionuclides for their use in medicinal applications. In this case, the radioactive species must be separated from excess amounts of its nearest neighboring stable Ln [36].In nuclear technology, separation and quantification of individual lanthanides is a challenging task, since it should be done in a short time and in a simple way.

Though the elemental specific detector like ICP-MS offers good sensitivity and multi-elemental capability, in the case of rare earths, there are problems associated such as signal suppression, the formation of polyatomic ions (MO^+, MOH^+) and doubly charge ions (M^{2+}) generated in the plasma, which interfere in the quantification of the isotopes of interest. Such problems can be overcome by using separation procedures, such as ion-exchange, liquid chromatography and solvent extraction [37].Interfacing the separation procedure with ICP-MS would enhance the accuracy for the determination of lanthanides by employing isotope dilution methodology.

The development of lanthanide and actinide chemistry is strongly dependent on the status of separation science at any given time. The isolation of these elements and investigation of their properties, not only required sophisticated separation methods, but often inspired the introduction of new separation methods, resulting in further advances [38].

1.1.10 Methods for the Separation of Lanthanides and Actinides

The key factors responsible for different separation methods are given in Table: 1.3.

Table 1.3: Comparison of different separation methods

Sr. No.	Method	Basis
1.	Masking	Making interferent as a nonreactive complex
2.	Mechanical phase separation	
a.	Precipitation	Difference in solubility
b.	Distillation	Difference in volatility
c.	Extraction	Difference in solubility in two immiscible solvents
3.	Chromatography	Difference in the rate of movement of a solute through stationary phase
4.	Electrophoresis	Difference in the migration rate in an electrical field gradient

A number of methods were employed in the past for the separation of lanthanides but these methods required long separation times or gave only partial resolution between the neighboring lanthanides. Before 1940s, the task of separating lanthanides was accomplished using laborious fractional procedures like fluoride, oxalate, phosphate and hydroxide precipitations, partial decomposition, dissolution etc. These classical processes were time consuming, required significant sample size and suffered from the possibility of lanthanides losses [39,40]. Onset of World War II imposed an urgent need for the development of more effective separation procedures. Several groups were engaged to develop faster methods for separating lanthanides due to their analogy with actinides and also due to the fact that these elements are produced in the nuclear fission. Liquid chromatography, solvent extraction, capillary electrophoresis etc. are the commonly employed analytical scale separation methods for lanthanides. Though ion exchange was the originally developed method for the separation of lanthanides in 1940s, the selectivity was not satisfactory. Later the selectivity was improved with the introduction of complexing agents like citrates. Subsequently, the use of ethylene diamine tetra acetic acid (EDTA) and α-hydroxyisobutyric acid (HIBA) resulted in better separation efficiency among the lanthanides. However, large scale applicability of ion exchange methods at those times was limited by the low solubility of lanthanide-carboxylates in aqueous solutions [41].Solvent extraction is more often applied for the pre-concentration of rare earths as a group from the matrix elements or in the treatment of a large amount of rare earth ore. Solvent extraction process requires large volumes of solvent and the separations are not clean[42].

Capillary electrophoresis (CE) separations rely on differences in the electrophoretic mobility of analyte species under the influence of an applied electric field. CE offers unparallel resolution for the separation of cationic, anionic and neutral species covering both the small and the large molecules. The separation efficiencies are sometimes an order-of-

magnitude better than the competing HPLC methods. However, the differences in the mobilities of the aqua cation alone are not sufficient enough to bring about the individual separation of lanthanides by CE. Introduction of chelating agents forming complexes with the ions leads to improved separation [38,43]. Though competitive chelation strategy achieved individual separation in CE, in many cases, quantitation of a few lanthanides was affected adversely e.g. Eu–Gd pair [44].Now it has been fairly established that LC and CE are complementary techniques especially with respect to their separation selectivity and the type of applications.

Neither gas chromatography nor supercritical fluid chromatography has influenced the separation of lanthanides in a significant manner [45]. Fluorinated β-diketones and their derivatives were investigated for the GC separation of lanthanides but their success was restricted by the non-volatility and thermal lability of the complexes in addition to the poor resolutions and absorption [46].Among the analytical-scale separations techniques for lanthanides, the most widely used methods are based on liquid chromatography[46,47]. For the better appreciation of the various liquid chromatographic methods used for the separation of lanthanides and actinides, a brief introduction is given about the classifications of chromatography and further sub-grouping of liquid chromatography.

1.1.11 Classifications of Chromatography

Chromatography refers to a group of techniques in which the components of a mixture are separated based on the differences in the distributions of components between a stationary phase and a mobile phase. As a result, the components would elute out from the stationary phase in the reverse order of their preference (distribution coefficient) with respect to the stationary phase. Based on the state of the mobile phase employed, chromatographic technique can be broadly categorized as gas chromatography (GC), super critical fluid

chromatography (SFC) and liquid chromatography (LC). The first criterion for any type of chromatography is that the sample must be soluble in the mobile phase employed. Due to the limited volatility and thermal labile nature, only a limited number of compounds are amenable to GC and SFC. Thus LC has been widely recognized as a powerful method for the separation of different compounds – inorganic, organic and bio-molecules. The stationary phase in chromatography can be a solid or a liquid adsorbed or chemically bonded to a solid support. Thus liquid chromatography can be further divided into liquid-solid chromatography and liquid-liquid chromatography. Depending upon the physical means by which the stationary phase and mobile phase are brought into contact i.e. geometry, liquid chromatography can by categorized as column chromatography or planar chromatography.

Column Chromatography: The stationary phase is held in a narrow tube through which the mobile phase is passed either by gravity or by the application of pressure. Examples are classical column chromatography, high pressure liquid chromatography (HPLC).

Planar Chromatography: The stationary phase is supported on a flat plate or in the fibers of a paper. Here the mobile phase moves through the stationary phase by capillary action. e.g. paper chromatography, thin layer chromatography (TLC).

Liquid chromatography using column can be further differentiated based on the types of equilibrium involved in solute transfer between the phases, as shown in Table 1.4.

Table 1.4: Classification of liquid chromatography based on the nature of equilibrium

Specific method	Stationary phase	Type of equilibrium
Liquid-solid (adsorption)	Solid	Adsorption
Liquid-Liquid (Partition)	Liquid sorbed on a solid	Partition between two immiscible liquids
Liquid-bonded phase (Reversed Phase)	Organic species covalently bonded to solid surfaces	Partition between liquid and bonded surface
Ion exchange	Stationary phase contains ionic groups ($-N^+R_3$, $-SO_3^-$)	Ion exchange
Ion-pair	Reversed phase (Ionic sample molecules are masked by a counter ion)	Partition
Size exclusion	Liquid in interstitials of a polymeric solid	Sieving
Affinity	Stationary phase contains group or molecules with specific orientation	Specific biochemical interactions

Reference [48]

The most useful column chromatographic techniques that have been applied for lanthanides are the following:

Adsorption Chromatography: Separation is based mainly on the differences between the adsorption affinities of the sample components for the surface of an active solid. The stationary phase used in this type of chromatography is generally more polar than the mobile phase and was termed as normal phase (NP) chromatography.

Partition Chromatography: The stationary phase consists of a liquid either adsorbed or chemically bonded onto the solid support. Separation is based mainly on the differences between the solubilities of the components in the mobile and stationary phases. When organic liquids covalently bonded to solid surfaces are used as the stationery phase and its polarity is less than the mobile phase employed, then it is termed as reversed phase (RP)

chromatography. Adsorption chromatography relies on the uptake of lanthanide ions by silica or alumina as a solid phase transfer medium whereas aqueous chelating agents are employed as mobile phase in partition chromatography.

Extraction Chromatography: It involves the application of conventional solvent extraction chemistry in chromatographic mode. The lipophilic extractant immobilized on a solid support is used as a stationary phase to achieve separation without the addition of water-soluble chelating agents. Adaptation of solvent extraction reagents to chromatographic applications resulted in significant improvements in the analytical chemistry of the REEs [49,50].

Ion-Exchange Chromatography: Separation is based on the differences in the ion exchange affinities of the sample components. Ion exchange resin is used as a stationary phase and aqueous chelating agent is used as the eluent. Mainly sulfonated polystyrene-divinylbenzene copolymers have been used as the stationary phase. Anion exchange chromatography is also employed for lanthanides but with less frequency. A variation of ion-exchange chromatography employing limited capacity columns is known as ion chromatography (IC). It employs techniques for suppressing the background conductivity of the mobile phase and is based on conductivity detection [51].

Exclusion Chromatography: Separation is based on exclusion effects, such as differences in molecular size, shape or charge. The terms Gel filtration and Gel-permeation Chromatography were used earlier to describe this process when the stationary phase is a swollen gel. The term Ion-Exclusion Chromatography is specifically used for the separation of ions in an aqueous phase.

Affinity Chromatography: This method refers to the particular variant of chromatography in which the unique biological specificity of the analyte and ligand interaction is utilized for the

separation. The stationary phase must contain specific group or molecules which can absorb the analyte species only if certain steric and charge conditions are satisfied [52].

Ion Interaction Chromatography: It uses long-chain alkyl groups covalently bonded to silica as the stationary phase. An aqueous solution containing a mixture of chelating agent and an ion interaction reagent is used as a mobile phase. Because of the excellent resolution, this method is one of the most successful methods for lanthanide quantitation [53-55].The ion-exchange method using complexing agent as an eluent is the best known method, but it is time consuming with respect to elution and quantitation. Use of high performance liquid chromatography (HPLC) along with on-stream detection methods has shortened the analysis time from several days to a few minutes [56]. The progressive development of different chromatographic techniques is discussed below with special emphasis on HPLC.

1.1.12 Historic Perspective of Liquid Chromatography

Liquid chromatography (LC) was the first type of chromatography to be discovered and was originally used in the late 1903 by the Russian botanist, Tswett [58] to separate and isolate various plant pigments. The colored bands produced on the adsorbent bed evoked the term ‘chromatography’ (meaning ‘color writing’) for this type of separation. In the late 1930s and early 1940s,A. J. P. Martin and R. L. M. Synge introduced a form of chromatography by using silica gel as the stationary phase for the separation of some amino acids [59]. They suggested the replacement of the liquid mobile phase with a suitable gas for improving the mass transfer between the two phases and for efficient separations. Thus, the concept of gas chromatography was born. They also proposed the use of small particles and high pressures in LC to improve the separation which later led to the development of high performance liquid chromatography (HPLC).

Developments in different areas of science and technology have prompted scientists to develop efficient methods for the separation of lanthanides. The introduction of the use of complexing eluents in the ion exchanger has made possible the repetition of the same chemical reaction many thousands of time, amplifying the slight difference in the stability constants of the Ln-eluent complexes and this has led to better separation methods. The use of complexing agents offers added advantage of minimizing the hydrolysis of metal ions in the operating pH range imposed by the stability of the bonded stationary phase. The first chromatographic separation of lanthanides was carried out using cation-exchange resin Dowex 50 under controlled pH elution with citric acid at 100 °C and this resulted in the separation of 5–6 rare earth elements in about 42 hours[60].

The conventional chromatography methods were originally applied using gravity fed columns. But these methods have poor resolution and are time consuming with respect to elution and quantification [61].Application of HPLC with on-line detection has reduced the separation time from days to a few minutes because of its high resolution [62]. Some of the important milestones in the history of LC leading to the development of HPLC are given below:

1.1.13 Milestones in Chromatography

- 1903 M. Tswett - plant pigments separated on chalk columns
- 1931 Lederer & Kuhn - LC of carotenoids (natural products) by normal phase chromatography was performed by passing a gravity-fed solvent through small glass tubes packed with pellicular adsorbent beads
- 1938 Introduction of TLC and ion exchange
- 1945 First chromatographic separation of lanthanides by Kettele and Boyd
- 1940s Gas chromatography (GC)

- 1950 Introduction of reverse phase LC
- 1950s Paper chromatography, reversed-phase partition chromatography (RPC), and hydrophobic interaction chromatography (HIC)
- 1952 HETP concept by Martin & Synge (Nobel Prize)
- 1959 Gel permeation chromatography
- 1960s Affinity chromatography
- 1965 Instrumental LC by Waters
- 1970 The acronym *HPLC*, coined by Prof. Csaba Horvath -a pressure capability of up to 35 bar
- 1973 First HPLC Conference in Switzerland
- Mid – late 1970s HPLC instruments up to 400 bar pressure, and incorporated injectors, detectors, and columns
- Late 1980s Polymeric monoliths
- 1990s 3μm particulate columns
- 2001 commercial availability of Silica monolith columns
- 2004 Columns with smaller particles [1.7 micron] and holistically developed instrumentation with pressure capabilities ~ 1,000 bar (UPLC)
- Research is being conducted with columns containing sub 1-micron-diameter particles and instrumentation capable of performing at 6,800 bar
- 2013 HPLC conference (40^{th})in Hobart, Australia

1.1.14 Advantages and Limitations of LC

Though GC was a later development, it overtook LC due to inherent advantages of fast separation and resolution. However, GC cannot be applied to a large number of compounds / elements as they are not sufficiently volatile or undergo decomposition upon heating to temperatures at which the separation occurs. It has been estimated that about only 20% of the

known compounds can be successfully used in GC. Thus LC is capable of separating a wide variety of ionic, organic, polymeric compounds and labile natural products. The development of column technology and instrumentation has made LC the preferred choice for many separation problems. Further, the option for selection of stationary phase and mobile phase and use of relatively lower temperatures in LC has made it easier to solve a given separation problem as compared to GC. Table 1.5 presents the comparison between GC and LC.

Table 1.5: Comparison between GC and LC

Parameter	GC	LC	Significance
Viscosity of mobile phase	Less	More	Less viscosity leads to less resistance in the mobile phase flow
Diffusion coefficient of the solute in the mobile phase	Large	Small	Faster mass transfer helps in fast separation
Number of theoretical plates	Very high	High	Faster and/or better separations are possible
Separation temperature	High	Low	Adaptable for thermally labile compounds
Optional chromatographic phases	Stationary phase	Stationary phase and mobile phase	Amenable for complex separation problems
Type of column packing	Limited	Versatile	More possibilities for separation
Interactions possible for chromatographic separation	Sample molecule & stationary phase	Sample molecules & stationary phase as well as sample molecules & mobile phase	Additional variable for controlling and improving the separation and hence easy adaptation
Detectors	Less choice but offer more sensitivity	More choice and hence selectivity	Selection to be decided by the nature of the sample
Recovery of fractions after separation	Less convenient	Readily isolated and quantitative	Convenience for further use or analysis by supplementary techniques
Restrictions	Lack of volatility, thermal decomposition	Insolubility	Less adaptability constraints

Developments in modern LC are mainly due to the advancements in the instrumentation, column technology and understanding the principles governing the separation. Concepts of GC theory were understood first and later, these were extended to LC and this finally led to the development of HPLC. For the better appreciation of the topic, the basics of chromatography are presented in a concise form below:

1.1.15 Concepts in Liquid Chromatography

When a mixture of different components is introduced into a chromatographic system, the separation occurs by the differential migration of various components. This result in the formation of different bands corresponding to each component and leads to separation. However, differences in the migration of different molecules of the same component would lead to spreading and this can hamper the effective separation of different bands. Different processes contributing to molecular spreading in a chromatographic process are discussed below:

1.1.15.1 Eddy Diffusion

It arises from the different microscopic flow paths that the mobile phase takes while flowing between different stationary phase particles inside a column. Figure1.2 demonstrates the different flow streams taken by three different molecules of the same solute. Due to Eddy diffusion, different molecules of the same solute may travel unequal distance and thus reach the detector at different times and this leads to broadening of peak. The extent of broadening by eddy diffusion (Term A) may be represented as $A = \lambda d_P$ where, d_P indicates the diameter of the particle and λdepends on the quality of the packing and its value is less for uniform packing.

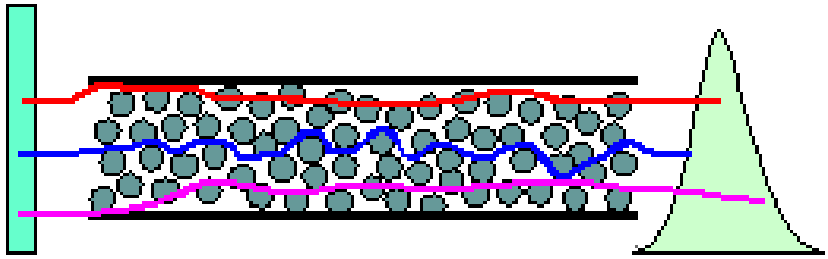

Figure 1.2: *Illustration of eddy diffusion.*

1.1.15.2 Longitudinal Diffusion

Due to the concentration gradient, the solute molecules in the mobile phase would diffuse out randomly in all the directions and cause the broadening of solute band. This effect is more prominent at low flow velocities as the solute spends more time in the mobile phase. The term has less significance in LC as compared to GC because of the relatively lower values of the diffusion coefficient of the solute in the mobile phase. Longitudinal diffusion of the solute and the resultant change in the pattern of the solute band with the progress of time spent in the column ($t_0 < t_1 < t_2$) are presented in Figures1.3(a) and (b), respectively.

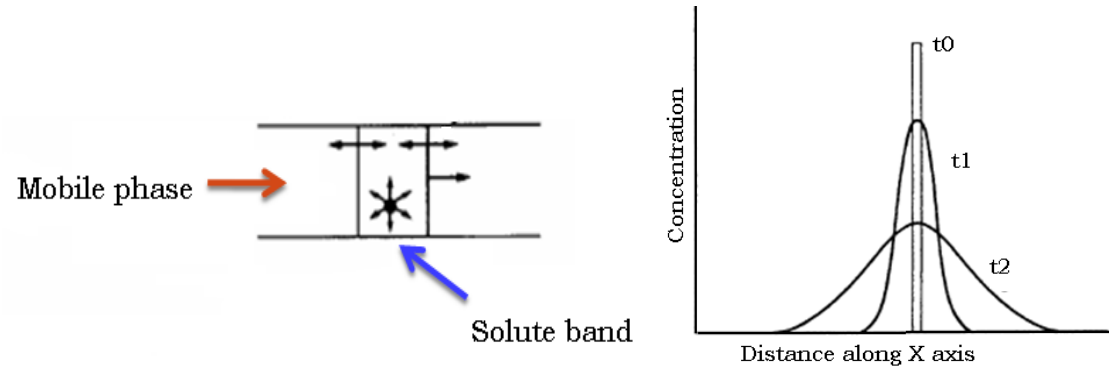

(a) **(b)**

Figures 1.3: *Illustrations of (a) longitudinal diffusion of a solute band and (b) change in the pattern of solute band as a function of time spent in the mobile phase.*

Longitudinal diffusion (term B) can be represented as $B = 2\gamma D_M$where, γ indicates the hindrance factor which depends on the quality of the packing and can take values from 0.7 for packed column to 1 for open column. D_M indicates the diffusion coefficient of the solute molecule in the mobile phase.

1.1.15.3 Mass Transfer Effects

Mass transfer effects causing band broadening can be sub-divided into three components viz. flow distribution (C_F), mass transfer in the stagnant mobile phase (C_M) and mass transfer in the stationary phase (C_S).

1.1.15.3.1 Mobile-phase Mass Transfer

This refers to differing flow rates of a single flow stream at different points between surrounding particles. Figure1.4 shows that the mobile phase layer adjacent to the particles moves very slowly, whereas the one at the centre would move fast. The intermediate layers would have a gradation of flow rates due to viscosity. Thus the solute molecule [X_3]moving along the central layer is expected to exit the column first while the molecule [X_1] of the same solute moving close to the particles would come out last and this leads to spreading of the solute band (term C_F).

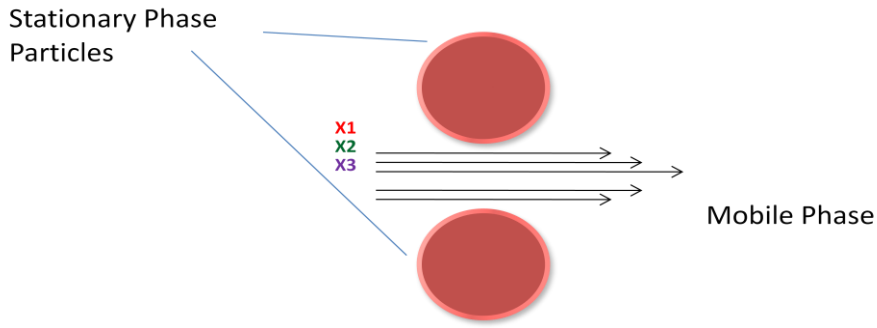

Figure 1.4: *Band broadening due to flow distribution.*

1.1.15.3.2 Stagnant Mobile-phase Mass Transfer

Irrespective of the flow rates or pressure applied externally, the mobile phase is stagnant in the pores of the stationary phase. Solute molecules move in and out of these pores by diffusion. As shown in Figure 1.5, a solute molecule (X_1)which has diffused only to a small distance into the pore and then move out into the mobile phase, would travel a longer

distance in the column compared to a solute molecule (X_2) diffused to a longer distance into the pore.

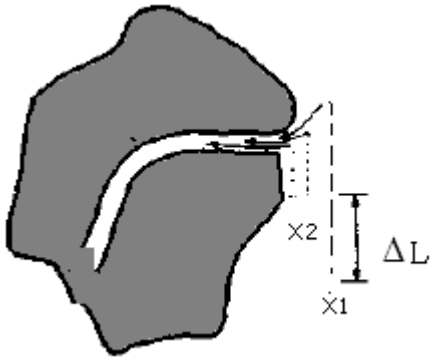

Figure 1.5: *Mass transfer in the stagnant mobile phase.*

The broadening due to mass transfer in the stagnant mobile phase can be represented as $C_M = \frac{d_P^2}{D_M}$, where, d_P is the particle diameter and D_M is the coefficient of mass transfer in the mobile phase.

1.1.15.3.3 Stationary-phase mass transfer

During diffusion into the stationary phase, a given solute molecule can attach to the periphery of the particle (X_1) or penetrate deep inside the stationary phase (X_2). The molecule which has diffused deep inside the particle would spend more time in the stationary phase and hence travel lesser distance in the column as compared to a loosely bound molecule. Figure 1.6 shows the relative movement of solute molecules X_1 and X_2 as a result of mass transfer in the stationary phase.

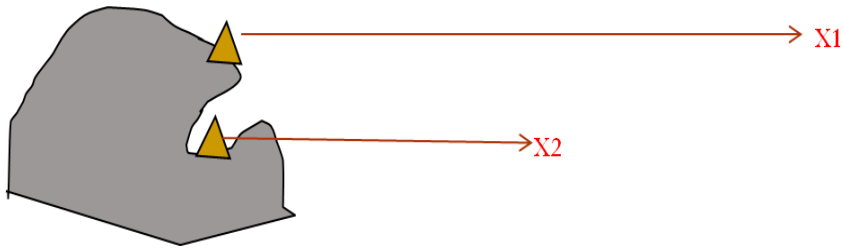

Figure 1.6: *Mass transfer in the stationary phase.*

Mass transfer in the stationary phase is expressed as $C_S = \frac{d_f^2}{D_S}$

where, C_S is the coefficient of mass transfer in stationary phase; d_f is the stationary phase film thickness and D_S is the diffusion coefficient of analyte in the stationary phase.

The combined mass transfer contribution may be represented as $C = C_F + C_M + C_S$

1.1.15.4 Van Deemter Model of Band Broadening

In this approach, the contributions of important band broadening mechanisms are combined as a function of mobile phase velocity in order to evaluate the efficiency of a given separation. The efficiency of a separation condition is represented in terms of height equivalent to a theoretical plate (HETP), H, written as: $H = A + \frac{B}{u} + Cu$

The constants A, B, and C vary from one column to another, and to some extent also depend on the sample, mobile-phase and separation temperature. A popular way of quantifying the efficiency of separation is based on 'theoretical plates'. Theoretical plate is a conceptual quantity which corresponds to that portion of a column where the solute is in equilibrium with the mobile phase and stationary phase. The chromatographic column contains a large number of such 'plates' as indicated in Fig.1.7. H is the height (or length) of one such plate and it is used as a measure of the efficiency of a given column. The solute moves down the column by transfer of equilibrated mobile phase from one plate to another.

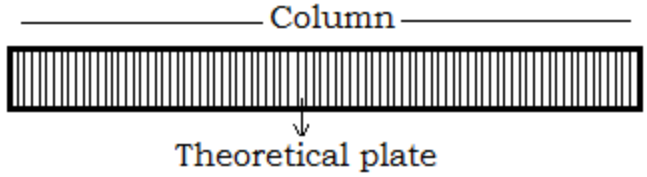

Figure 1.7: *Representation of theoretical plates in a chromatographic column.*

Lesser the height of an individual plate, more number of plates can be accommodated in a given column and more number of equilibrations would be taking place of the solute between the stationary and the mobile phases. Thus a small value of H of a given column is indicative of high efficiency of separation conditions. N, the number of theoretical plates in the column is related to the plate height, H as N = L/H where, L is the length of the column. The rate theory describes the process of peak width (band spreading) and helps to calculate the height of the theoretical plate (HETP) in terms of the mobile phase velocity and other physical and chemical properties of the solute. Different processes contributing to the peak dispersion such as eddy diffusion, longitudinal diffusion and mass transfers in the mobile phase and in the stationary phase etc. were taken into account while developing the plate theory. The rate theory has resulted in a number of different equations viz. Van Deemter Equation, Giddings Equation, Huber Equation, Horvath Equation and Knox Equation etc. All the equations predict a minimum plate height at an optimum velocity and, thus, a maximum efficiency. At normal operating velocities, it has been demonstrated that the Van Deemter equation gives the best fit to the experimental data. The plot of HETP vs. average linear velocity, known as Van Deemter plot, is shown in Fig. 1.8.

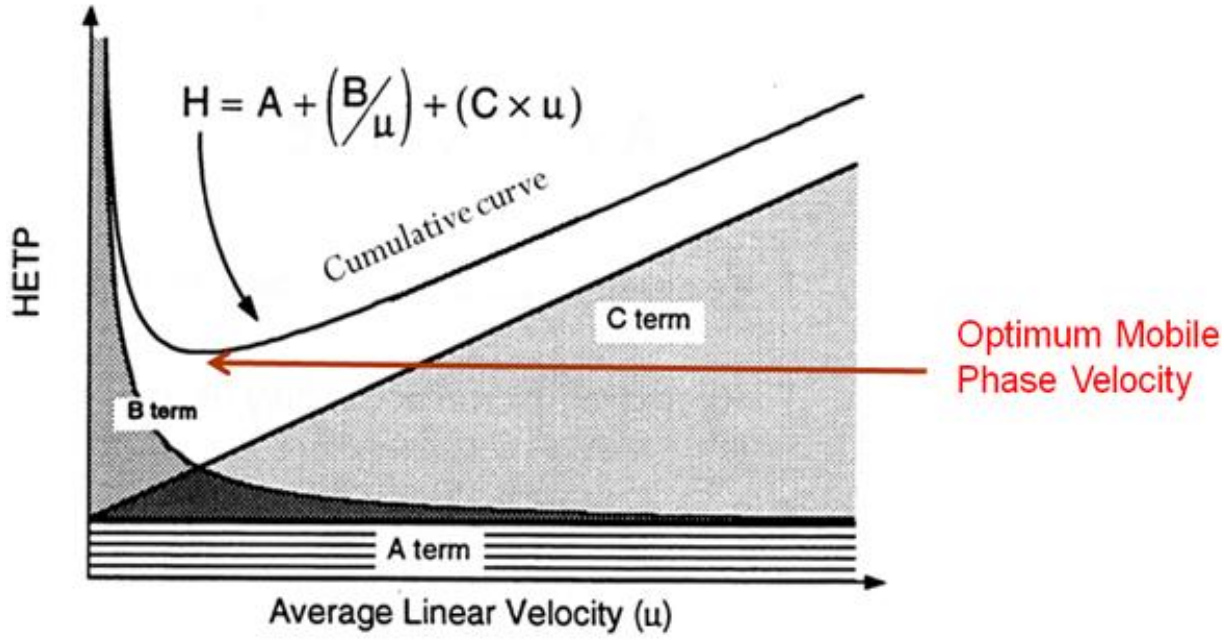

Figure 1.8*: Van Deemter plot showing the dependence of eddy diffusion (A), longitudinal mass transfer (B), mass transfers effect (C) and the cumulative factor (H) on the linear velocity of the mobile phase (U).*

Small H value means more efficient column and large N values. A central goal in LC practice is the attainment of small H values for maximum N and the highest column efficiencies. Thus separations must be carried out at the optimum flow rates of the mobile phase to achieve the best efficiency possible. From the different factors contributing to band broadening, it is clear that the value of H is small when small particle size columns (dP) are employed. Figure 1.9 shows the Van Deemter curves obtained with columns packed with three different particle sizes viz. 1.8 µm, 3 µm and 5 µm. It is seen that the lowest value of H and hence the highest column efficiency is possible for column packed with the smallest (1.8 µm) size particles. Thus separation efficiencies improve with long columns packed with small sized particles due to the increase in 'N'. Some of the benefits of using columns packed with small particles are narrow and taller peaks, better sensitivity and more peak capacity.

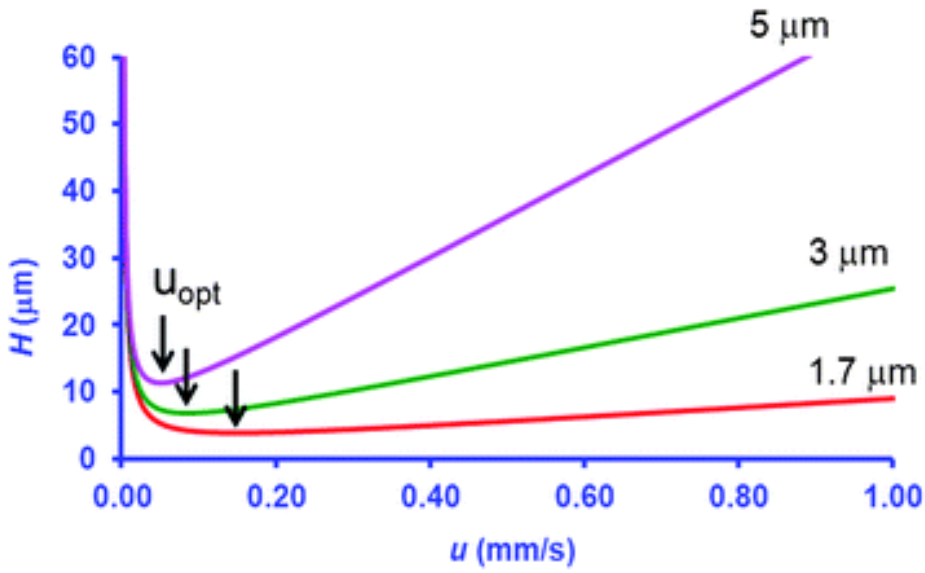

Figure 1.9: *Comparison of Van Deemter curves of columns packed with particles of different sizes.*

1.1.16 Chromatographic Parameters

Some of the common parameters used to characterize a particular chromatographic separation are discussed below:

Retention Time (t_R): This is the time taken by a solute from sample injection to the appearance of the top of the peak in the chromatogram. In Fig. 1.10, $t_R(x)$ represents the retention time of the component 'x'. In the same Figure, t_0 indicates the time taken by the non-retained species or solvent front to reach the detector and the peak is called 'solvent peak' or 'deadpoint' [63].

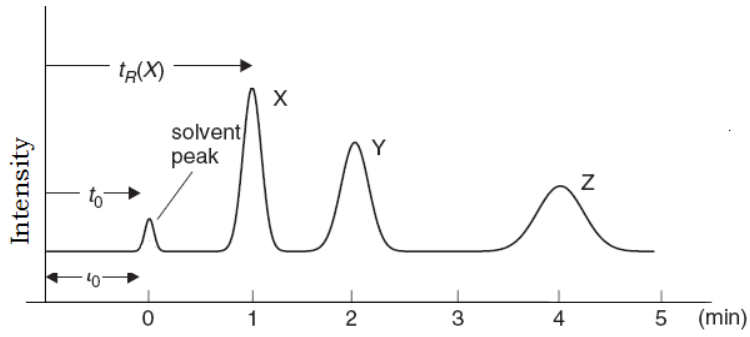

Figure 1.10: *Representation of retention time in a chromatogram.*

Retention Factor (k): It is defined as the ratio of the quantity of solute in the stationary phase (s) to its quantity in the mobile phase (m). If Cs and Cm indicate the concentrations of the solute in the stationary phase and the mobile phase, respectively, with corresponding volumes Vs and Vm then

$$k = \frac{C_S V_S}{C_m V_m} = C_S / C_m * V_S / V_m$$

k = K Ψ where, K = $\frac{C_S}{C_M}$ is the equilibrium constant and $\Psi = \frac{V_S}{V_m}$ is the phase ratio of the stationary phase to mobile phase inside the column.

The retention factor can be represented in terms of retention time as $k = \frac{t_R - t_0}{t_0}$

In other words, retention factor is the time a solute spends in stationary phase relative to that in mobile phase. In typical separations, the preferred value of k lies between 1 and 10 as prolonged separation time leads to excessive peak broadening. Retention factor helps to compare the retention times of a given component obtained by two different columns or in two LC systems with different void volumes. The retention factor can easily be controlled by changing the solvent strength of the eluent [64].

Peak Width (W): When the solute molecules migrate inside the column, they spread out due to different factors discussed earlier and this leads to peak formation. In Fig. 1.11, the first peak (i) is shown with 'baseline peakwidth'. In this case, tangents are drawn at the points of inflection on either side of the peak. The length of the segment formed by the intersection of the two tangents with the base line is the peakwidth (W). The accurate measurement of peakwidth by this approach necessitates that the peak in question must be baseline separated from adjacent peaks. However, baseline separations may not be always possible in practice. Peakwidth at half maximum can be used for measuring the width of the peaks more accurately

and conveniently. Peakwidth at half maximum is shown for the second peak (j) in the figure and is denoted as $W_{1/2}$.

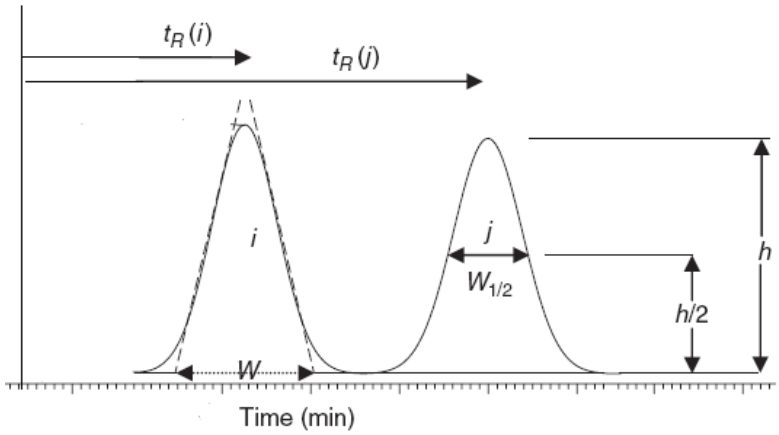

Figure1.11: *Illustration of baseline peakwidth and peakwidth at half maximum.*

Plate Number (N): Column efficiency for a given separation is usually described as the number of theoretical plates per unit length of the column or 'plate number'. Since the ability of the column to provide narrow peak is described as efficiency, plate number N can be related to peak width [65]. The ideal chromatographic peak has the shape of a Gaussian curve and hence the peakwidth (W) can be represented in terms of standard deviation (σ) as, $W = 4\sigma$

Thus plate number $N = (\frac{t_R}{\sigma})^2$

$N = 16\ (\frac{t_R}{W})^2$ where, W is the baseline peakwidth.

In terms of $W_{1/2}$, peakwidth at half maximum, N can be written as: $N = 5.545(\frac{t_R}{W_{1/2}})^2$

Separation Factor (α): For a pair of adjacent peaks A & B, separation factor is defined as the ratio of retention factor of A to that of B. Thus, $\alpha = \frac{k_A}{k_B}$. Separation factor must be > 1 to result in the separation between two adjacent peaks.

Resolution (R_S): It is the measure of separation between two components A and B and can be represented as the ratio of difference in their retention times to average peak width. Thus resolution is experimentally determined for a chromatogram shown in Fig. 1.12as

$$R_S = \frac{(t_{R(B)} - t_{R(A)})}{(W_A + W_B)/2}$$

As mentioned earlier, it may not be always possible to have a baseline separation for all the peaks. In such cases, the resolution between two adjacent peaks can be calculated using the equation: $R = 1.18\frac{R_{t2} - R_{t1}}{(W_{(1/2)1} + W_{(1/2)2})}$; where, R_{t1} and R_{t2} are the retention times of the two adjacent peaks 1 and 2, respectively, and $W_{1/2}$ denotes their peak widths at half maximum heights.

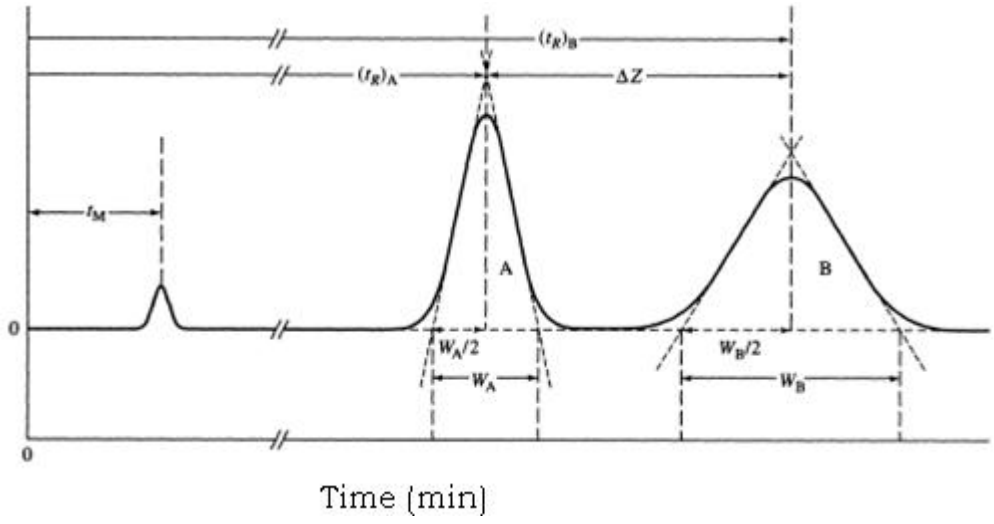

Figure 1.12: *Illustration of measurement of resolution*.

A resolution value of Rs ≥2 is adequate for quantification based on the chromatographic peak response, provided the peaks are of similar size and are symmetric [64,65]. While developing the chromatographic methods, a more convenient expression may be used for obtaining the resolution as given below:

$$R_S = \frac{1}{4}\left[\frac{k}{1+k}\right]\left[\frac{\alpha-1}{\alpha}\right]N^{0.5}$$

Where, k is the retention factor for the first peak, α is the separation factor and N is the plate number.

The required degree of resolution is achieved by the following approaches:

a) Changing the retention factor by varying the composition of the mobile phase
b) Increasing the plate number by optimizing the flow rate, increasing the length of the column and use of columns packed with smaller particles, lowering the viscosity of the mobile phase
c) Changing the separation factor by varying the mobile phase, stationary phase, pH of mobile phase etc.

In practice, changing the retention factor is the easiest but it has a little influence on the resolution. Significant improvement in the resolution is brought about by small changes in the selectivity factor. However, among the three parameters, changing the separation factor is the most difficult task. Figure 1.13 depicts the change in the resolution as a function of three independent variables viz. retention factor (k), number of theoretical plates (N) and separation factor (α)[66].

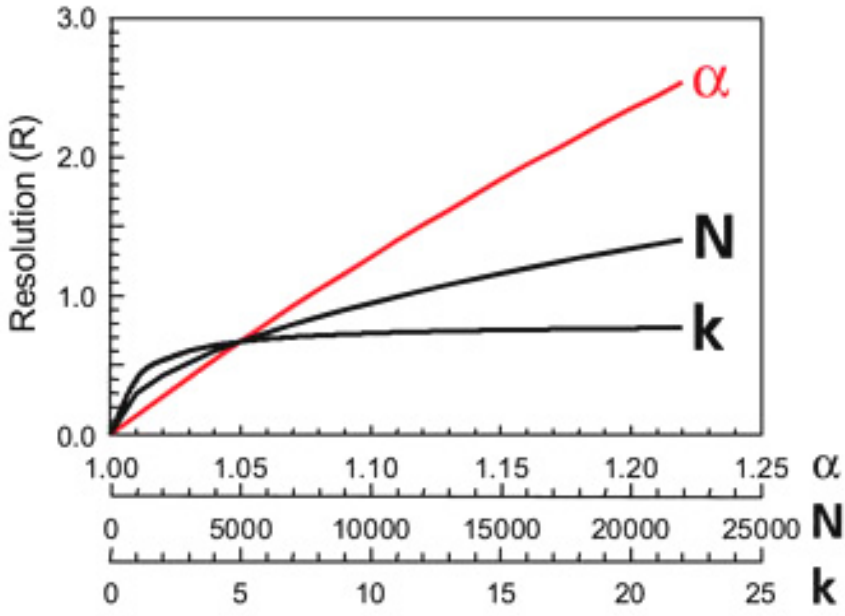

Figure 1.13: *Dependence of resolution on retention factor, k; number of theoretical plates, N; and separation factor, α[66].*

1.1.17 Need for HPLC

It is seen that the separation efficiencies can be significantly improved by using long columns packed with small sized particles. Advantages of carrying out separations on columns packed with small particles are improved resolution, narrow and taller peaks resulting in better sensitivity and more peak capacity. Thus overall efficiency of separation or performance increases by columns packed with small particles. High performance liquid chromatography (HPLC) refers to separations carried out using columns containing ≤10 µm particles. However, the pressure required to force the mobile phase through the column increases with the decrease in the particle size according to the equation, $\Delta P \alpha 1/(d_P)^3$.

Thus use of small particle filled columns requires solvent delivery systems to force the mobile phase through tightly packed column. Hence, HPLC is also known as high pressure liquid chromatography. Application of HPLC with on-line detection has reduced the analysis time from days to a few minutes because of its speed, improved sensitivity and multi-

elemental analysis capability using single injection. Technological advancements in the field of instrumentation as well as column technology have helped the technique to move ahead with time and maintain its importance in separation science. A brief description of the instrumentation of liquid chromatography and mass spectrometry is given below for the better appreciation of the technique.

1.2. Instrumentation

1.2.1 HPLC

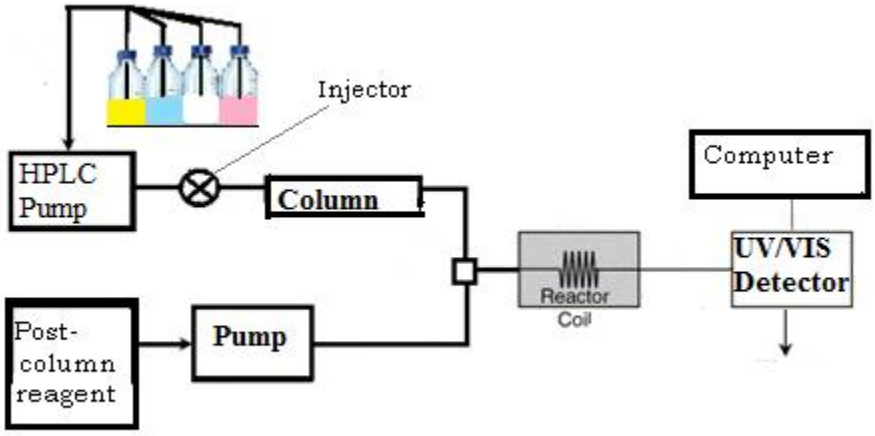

Figure 1.14: *Schematic diagram of an HPLC system with post-column derivatisation detection.*

Figure 1.14 shows the schematics of the HPLC system used in the present work. The important components are the solvent delivery system, sample injector, column, detector and data processor. A post-column reaction system was used for enhancing the detection sensitivity by reacting the ions eluted from the column with a chromogenic reagent. The resultant complex with high molar absorption coefficient is then monitored using a spectrophotometric detector. The main components are briefly discussed below:

1.2.1.1 Solvent Delivery System (Pump)

The solvent delivery system consists of 1 to 4 solvent reservoirs. The solvents are filtered through individual stainless steel filters to remove any solid particles and are then passed through a membrane to remove the dissolved air from the solvents. Air has different solubility in different solvents. When two or more solvents are mixed on-line, there will be a change in the solubility and the dissolved gas can be released in the form of bubbles. The dissolved air can form bubbles in the detector and cause ghost peaks or cause a shift in retention time[67].

The two modes of operation of the solvent delivery system in HPLC are isocratic and gradient. In the isocratic mode, the composition of the mobile phase remains the same throughout the chromatographic run whereas in the gradient mode, it can be changed continuously or in stepwise. Isocratic elutions lead to chromatograms which are reproducible and no equilibration time is needed between the successive injections. On the other hand, gradient systems are useful for rapid and efficient separation of mixtures containing a number of components with widely varying affinity for the stationary phase. There are two basic types of configurations employed for achieving the solvent delivery in the gradient mode. In the first, individual pumps are used for each solvent and solvent mixing occurs at high pressure (high pressure gradient system). In the second approach, the individual solvents are pre-mixed at low pressure and a single pump is employed for the delivery of the mixture and it is known as low pressure gradient system [64]. Block diagram of a low pressure quarternary gradient solvent delivery system is shown in Fig. 1.15. Though the low pressure gradient systems are less expensive, the involvement of mixing manifold and pump dead volume after the point of mixing contribute to the void volumes and this delays the gradient when steep compositional changes are required.

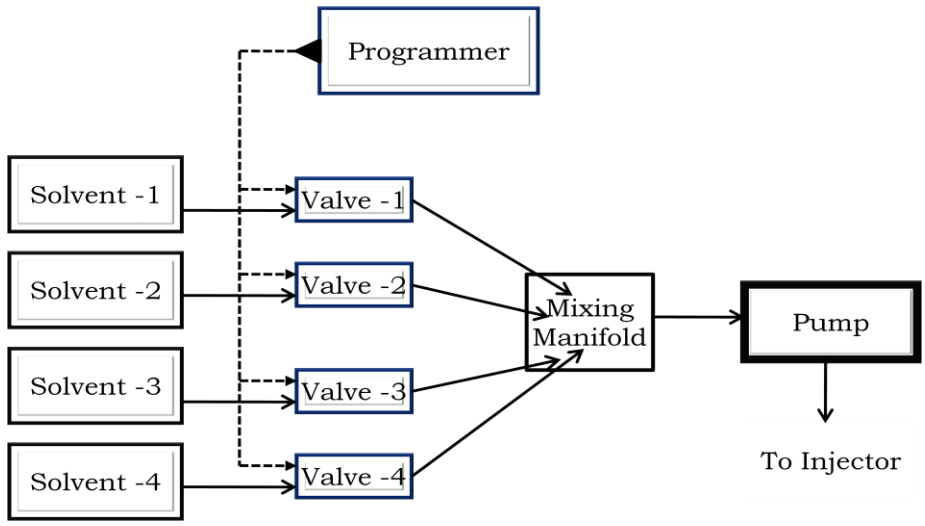

Figure 1.15: *Block diagram of a low pressure quarternary gradient solvent delivery system.*

The pump must be able to deliver the mobile phase at precise flow rates against a high pressure drop and with minimum pulse in the flow profile. The important characteristics of an HPLC pump are:

- Parts in contact with the mobile phase must be made of inert materials.
- Capability to deliver solvents at pressures>400 bar.
- Provide relatively pulse-free delivery or should have a pulse damper.
- Flow rate range 0 to 5 mL/min or more, with steps of 0.1 mL/min.
- Must provide accurate delivery (±0.1% at 1mL/min).
- Deliver mobile phase with good long term as well as short term reproducibility (< 0.1%).
- Linear and step flow profiles.
- Small holdup volume for rapid solvent changes, thus enabling sharp gradient.
- Reproducible mixing of solvents during gradient operation.

Various types of HPLC pumps used are direct gas pressure systems, syringe pump, pneumatic intensifier pump, reciprocating pump, etc. Pneumatic pumps can provide extremely high pressures and have high flow capacity and hence are mostly used for column packing rather than general analysis. In syringe pump, the piston is propelled and controlled by a stepper motor. This type of pump finds use where small volumes of mobile phase are required and for reagent delivery in post-column derivatization as it can supply reagent with extremely low pulsation. Over the years, the reciprocating piston pumps have become the most commonly employed analytical pumps by virtue of their low hold-up volume, accuracy, precision and trouble-free operation. The working of a typical single piston reciprocating pump is shown in Fig. 1.16.

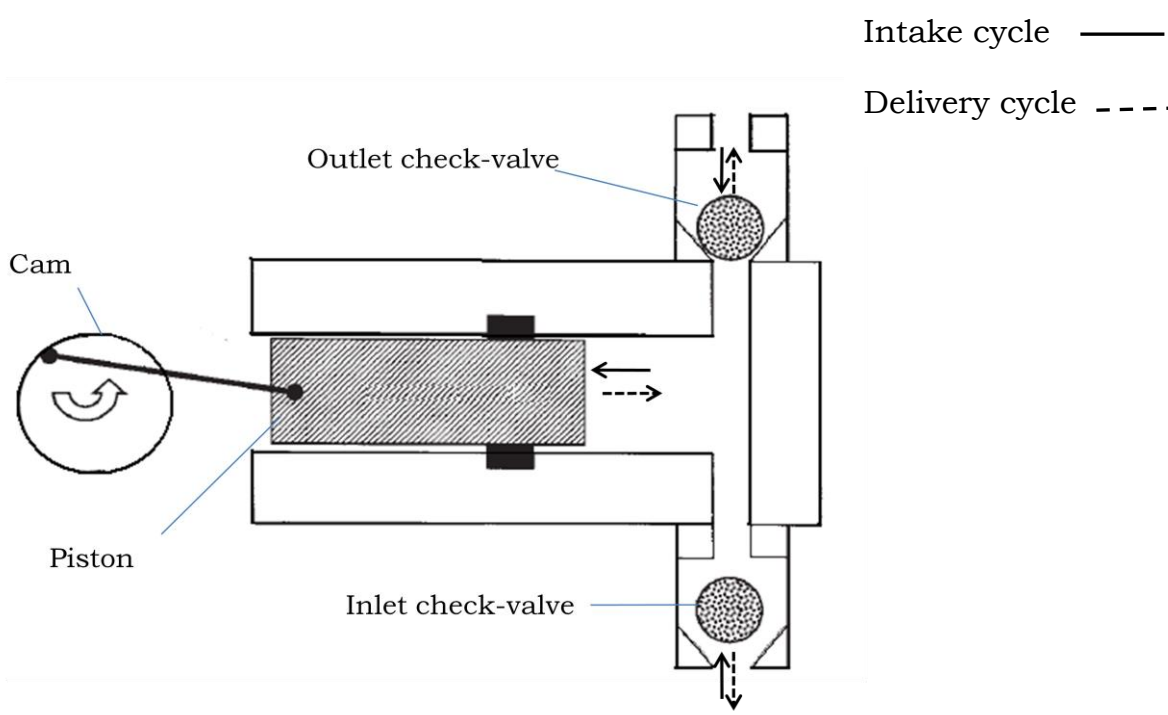

Figure 1.16: *Schematic diagram of a single piston reciprocating pump.*

Essential components of a reciprocating pump are motor, ceramic piston and check valves made of ruby ball and sapphire seat. Rotation of the motor drives a cam which in turn guides the piston to move back and forth. During the intake cycle, the piston is moved out to create a low pressure zone in the cavity. The outlet check valve closes while the inlet check valve opens and this helps in trapping a small volume of the solvent in the pump-head (cavity). During the delivery cycle, the piston moves in and this causes the inlet valve to close and the outlet valve to open. The resultant action is the purging of the small volume of the trapped solvent out of the cavity. The flow profile from a single piston reciprocating pump is irregular due to the pause during the intake cycle. Instead of a perfect circle, the cam is given an irregular shape so that the delivery stroke of the piston is slow and steady while the refill stroke is rapid to ensure a smooth flow. However, there would still be some pulsations which can be minimized by using two pistons working in tandem and this arrangement is known as double head pump. The typical flow profiles obtained using a single pump head with a

circular cam, a single pump head with an irregular cam and a double pump head are shown in Fig. 1.17.

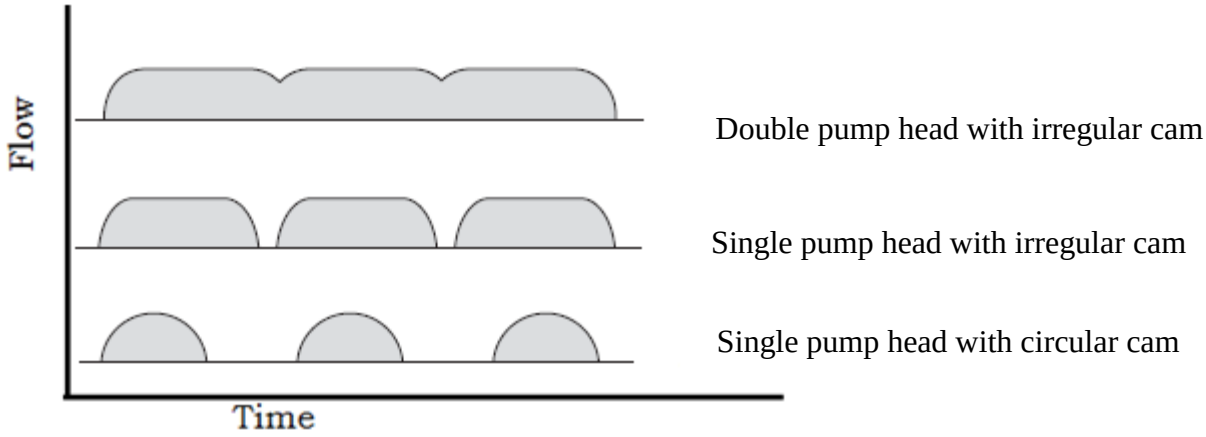

Figure 1.17: *Comparison of flow profiles obtained by reciprocating pumps with different pump heads.*

1.2.1.2 Sample Injector

The sample must be introduced as a narrow band in order to minimize the band broadening inside the column. Direct introduction of the sample into the column is not possible due to the flow of the mobile phase at very high pressure. In earlier times, stopped-flow direct injection through septum was used to introduce the sample but the precision obtained on the retention time or peak area was not satisfactory. Six port sample injection valves with fixed volume loops are, therefore, used to seamlessly inject the precise amount of the sample [65]. When analysis of a large number of samples is involved, auto-sampler is employed to carry out the precise and accurate sample injection in unattended manner. The holdup volume of the injector system must be as low as possible to minimize the possibility of band broadening. Figures 1.18(a) and 1.18(b) show the commonly used sample injector in load mode and in inject mode, respectively.

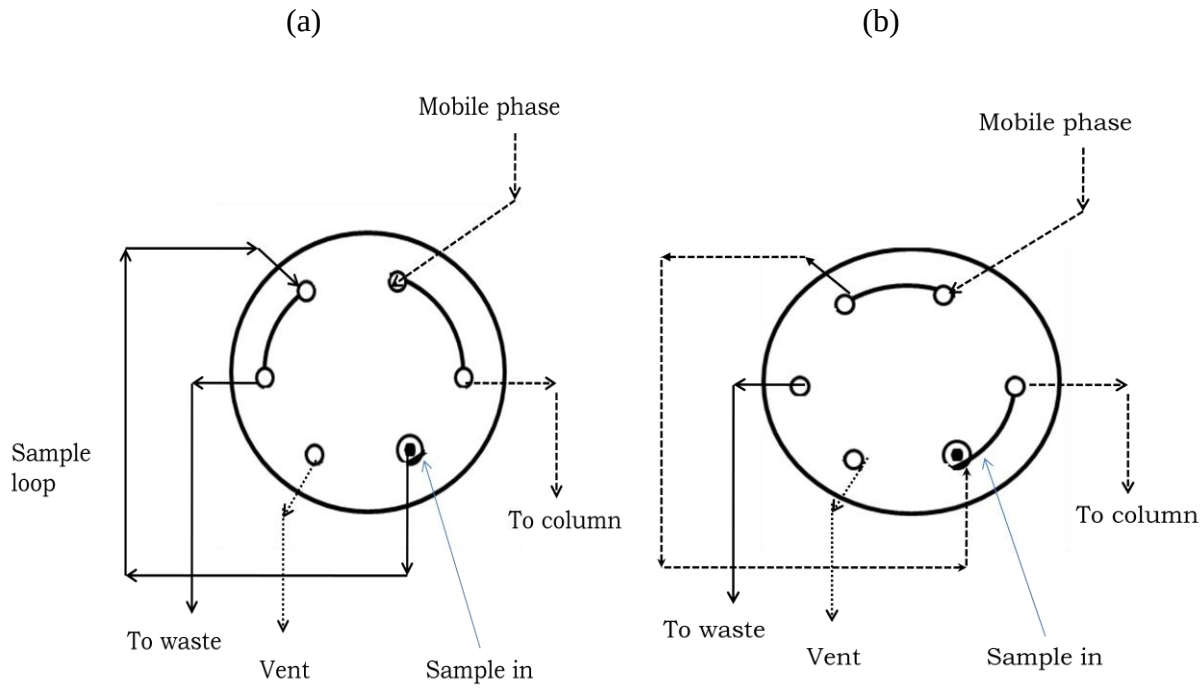

Figures 1.18: *Schematic diagram of injectors in (a) load position and (b) inject position.*

When the valve is in position (a), injection to the port (sample in) causes the sample to flow through the sample loop and the excess sample will be discharged through the vent. Once the injection is completed, the valve is rotated to position (b) and the mobile phase passes through the loop and carries the sample into the column. The sample loops are available in sizes of 5 – 100 µL and this type of injection system is ideally suited for quantitative LC. Autosamplers work in the same way as the loops and are operated electrically or by compressed air. The six port valve configuration can also be used for column switching in on-line pre-concentration or two-dimensional chromatography. In column switching, a preconcentrator column or an analytical column is connected in place of the loop and the effluent from this column can be regulated into the second analytical column or waste through the valve. This configuration allows the use of two different columns in tandem and thereby significantly improving the versatility of LC.

1.2.1.3 Solvents for HPLC

The choice of proper mobile phase in LC is very important as its interaction with the sample and stationary phase is responsible for the efficient separation of the components. Following are the guidelines followed while deciding on the mobile phase for a given separation problem:

- Solubility: the sample must be readily soluble in the mobile phase.
- Viscosity: a solvent with low viscosity produces less resistance while passing through the column. Further low viscosity leads to rapid mass transfer which leads to fast chromatographic separation.
- Detector transparency: the solvent response to the detector must be minimum as this would influence the sensitivity of analyte detection. For example, if UV detector is used, the solvent used should not absorb in the wavelength region of interest.
- Boiling point: volatile solvents show a tendency of formation of bubbles in the detector. However, such solvents are preferred if the components are to be recovered after the chromatographic run.
- Purity: presence of impurities in the solvent would lead to a significant change in the base line during gradient elutions.
- Inertness: solvents must not react with the stationary phase and the sample and should not corrode the HPLC hardware.
- Miscibility: the solvents chosen in the gradient mode must be miscible with each other and also with the sample.
- Interaction: properties like dipole character and acidity/basicity determine the interaction of the solvent with the solute.

Both methanol and acetonitrile are easily miscible with water and do not have significant absorption in the UV region. Hence, these solvents find extensive use in HPLC. When compared to methanol, acetonitrile has a lower UV cut-off (200-210 nm) and generates lower back pressure in aqueous based gradients. On the other hand, methanol is less expensive and is more stable than acetonitrile. When exposed to ambient light under dry conditions, acetonitrile produces some polymers which might clog the solvent filters or LC columns.

1.2.1.4 HPLC Column

Stationary phase is considered to be the 'heart of the LC system'. Early experiments on LC were carried out on silica column because of its high surface area, porosity, polar nature and good mechanical strength. Correspondingly, the mobile phases used with silica were non-polar in nature. This type of combination, where stationary phase is more polar than the mobile phase, is termed as 'normal phase'. Conversely, the combination in which the mobile phase is more polar than the stationary phase is called 'reversed phase'. Porous particles, pellicular particles, perfusion particles and monolithic stationary phase are employed for column packing depending upon the application. Important stationary phases are described below:

1.2.1.4.1 Silica

Reaction between sodium silicate with hydrochloric acid results in the formation of silicic acid which gradually undergoes condensation reaction to form aggregates and then polymer spheres called 'primary silica particles'. The surface silanol groups on the primary silica particles react further resulting in the growth of silica particle. The slow condensation of the surface silanol groups of the primary particles is responsible for the mechanical strength, high porosity and large surface area of silica particle. The particles produced by this route are irregular in shape. Spherical silica particles are produced by spraying the neutralized silicate

sol into fine droplets and drying in a stream of hot air. Another route for the synthesis of spherical particles is by dispersing the silicate sol into a suitable hot organic solvent to form an emulsion (sol-gel process) [68].

In silica, Si atom is bridged three dimensionally by four oxygen atoms. Surface of the silica particle contains a large number of silanol (SiOH) groups which are of different nature as depicted in Fig. 1.19.

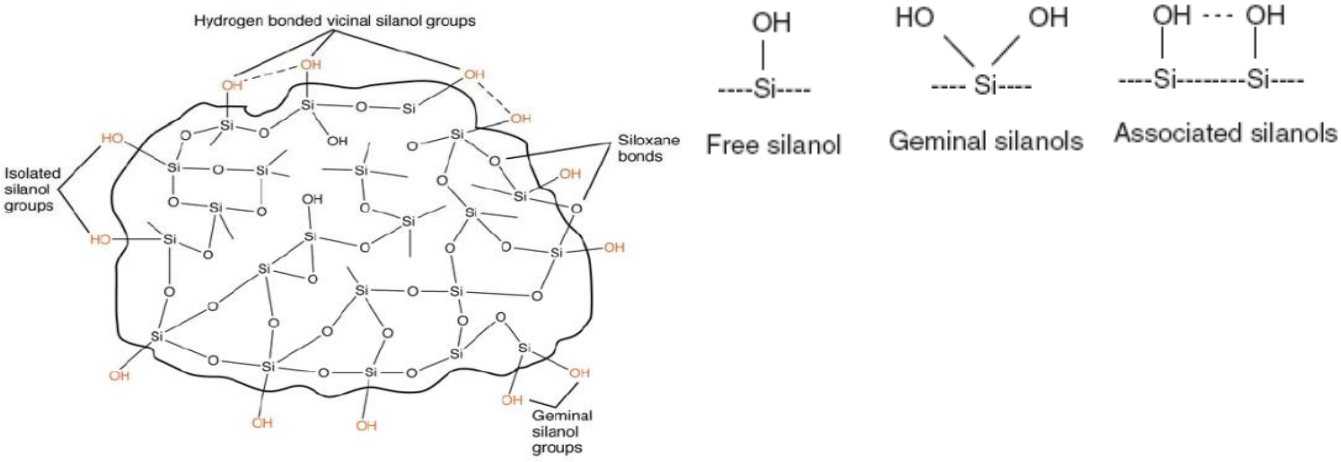

Figure 1.19: *Representation of different silanol groups present in silica.*

Free silanols are weakly acidic and hence strongly interact with solutes with basic nature. This is the reason for the appearance of a strong peak tailing of basic components when unmodified silica is used as the stationary phase. The two hydroxyl groups attached to the same silicon atom are called Geminal hydroxyl groups [69].Two hydroxyl groups from adjacent silanols which are bonded by H-bonding are called 'associated silanol groups'. Geminal silanols are not acidic similar to Associated silanol groups. Silanols near the metal cations are strongly acidic and can adversely affect the separation of basic compounds. Metals like Al and Fe can increase silica acidity by withdrawing electrons from the oxygen of the silanol, as well as interact directly with chelating solutes. Water can be hydrogen bonded to the hydroxyl groups and multi-layers of water adsorbed on the top of the silica surface. Thus unmodified silica offers a host of interaction mechanisms based on hydrogen bonding, dipole-

dipole and ion exchange, and thus the adsorption process is difficult to understand, reproduce and is less efficient. Another factor not favouring the utilization of silica is the pH restriction because silica dissolves in alkaline conditions.

1.2.1.4.2 Modified Silica

Silanol groups on the surface of the silica particles can be chemically modified to give stationary phase with specific properties. Products with Si-O-Si bond are generally preferred in view of its resistance to water and alcohol.

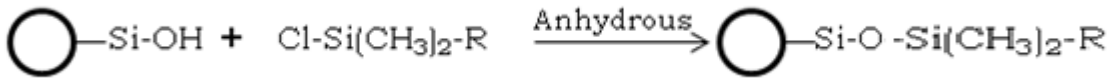

When R = $-(CH_2)_{17}-CH_3$, the product is known as octadecylsilane (ODS) which is the most widely used modified stationary phase. As it is extremely non-polar, this stationary phase is an ideal candidate for reversed phase chromatography. Chemical modification may not convert the entire silanol group into ODS. The unreacted silanol groups are subsequently reacted with trimethylchlorosilane to minimize the silanol activity. This treatment is known as 'endcaping'. Instead of $-CH_3$, bulkier side chains can be incorporated in the ODS to protect the analytes from exposing to the residual silanol groups. Modified silica has a narrow pH range for safe operation as low pH conditions lead to the cleavage of siloxane bond, Si-O-Si-R and high pH causes the silica dissolution [64].

1.2.1.4.3 Styrene Divenylbenzene

The cross-linked polymer obtained by the co-polymerization of styrene and divenylbenzene is a resourceful stationary phase for LC. The degree of cross-linking and the porosity can be controlled by the proportion of divenylbenzene in the reaction mixture. These polymers are stable over a wide range of pH conditions and can be used in reversed phase separations. Anion and cation exchange stationary phases are obtained by the incorporation of

$-N^{+}(CH_3)_3$ and $-SO_3^{-}$ groups, respectively, into the polymer matrix. Polymers obtained with controlled porosity can be used as the stationary phase for size exclusion chromatography. Polymeric stationary phases do not have the same mechanical strength as silica and they are susceptible to dimensional changes under extreme conditions of pressure[65].

Stationary phases made of alumina, hydroxylalkylmethacrylate gel, porous graphitic carbon, titania, zirconia etc. are found in special applications and are less commonly used.

1.2.1.5 Detectors

A suitable detector is required to recognize the presence of a solute in the eluent from the column. The ideal characteristics of an LC detector are as follows [70,71].

They should be compatible for all types of compounds under testing.

- Detector response should not be affected by the change in the composition of the mobile phase or temperature.
- Must be able to monitor the analyte at very low concentrations and also offer good dynamic range.
- Detector cell volume must be small so that it does not contribute to band broadening of the eluted solutes.
- Should have fast response time to detect very narrow or fast eluting peaks in a representative way.
- Should contribute to minimum noise or drift.
- Preferably non-destructive to the sample.
- Produce uniform and reproducible response.

However, there is no universal detector satisfying all the above requirements. The selection of the detector for a specific application is based on the nature of the analyte,

detection limit, affordability etc. LC detectors can be categorized based on their selective nature of response to the solute presence in the mobile phase. A non-selective detector would respond to the change in the bulk property of the mobile phase such as refractive index or conductivity. A detector which responds to a property specific to the solute is known as selective detector e.g. UV-Vis detector.

The LC detectors can also be classified into two categories: (i) concentration sensitive and (ii) mass sensitive detectors [70]. Concentration detector produces a signal (S) which is proportional to the concentration (C) of the solute in the mobile phase: $\propto C$ $(\frac{g}{mL})$. In the case of mass sensitive detector, the response is proportional to the mass flux or the number (n) of solute molecules or ions per unit time in the mobile phase: $S \propto n/t$ $(\frac{g}{s})$.The commonly employed LC detectors are:

Concentration sensitive type

- UV-Vis
- Fluorescence
- Evaporative light scattering
- Refractive index
- Mass-spectrometry
- Radioactivity

Mass sensitive type

- Electrochemical
- Conductivity

Conductivity detectors are used for the detection of inorganic ions that are electrically conducting e.g. Na^+, Cl^- and find widespread applications in ion chromatography. A suppressor, for removing the ions contributing to the background conductivity of the mobile phase, is essential for satisfactory detection sensitivity. Radiometric detectors are used for detecting components which are radioactive. Though they are less commonly employed, radioactivity detectors are often much more sensitive than many spectrophotometric and other physical procedures. UV-Vis detector is preferred if the components of interest absorb light in the wavelength range of 200 nm to 800 nm. It is one of the most widely used and robust LC detector, and will be discussed in detail in the following Section. Fluorescence detectors offer highly selective and sensitive detection (10-100 times more as compared to UV-Vis) for fluorescence active compounds. In this detector, the fluorescence rays emitted by sample, after absorbing incident light from a Xenon arc lamp, are measured after passing through grating. Electrochemical detector is useful for compounds that can be easily electrochemically reduced or oxidized, such as phenols, aromatic amines etc. Electrochemical detectors offer better selectivity and sensitivity for such compounds. Refractive index detectors are used when the analyte components (e.g. carbohydrates, polymers) do not have any specific property suiting other selective detectors. Being a bulk property detector, its sensitivity is very low (100 – 1000 times lower than that of UV-Vis detector) and are not suitable for gradient elution chromatography. Evaporative light scattering detector is also a bulk property detector but as the detection is after the complete evaporation of solvents, this detector is adoptable to gradient elutions. In view of high specificity and sensitivity, mass spectrometric detectors are gained popularity even though they are expensive. Tandem mass spectrometers offer the advantage of being a universal detector in MS mode and a highly selective detector in MS/MS mode. They complement liquid chromatography as an indispensible tool for identification and characterization of unknown species in complex samples. MS systems are in general available

in two different configurations. The single-stage detector, sometimes called an MSD (mass selective detector), is used to measure a single ionic species for each analyte, often the molecular ion. Instruments using this type of detection are referred to as LC-MS. Typically such MS system uses a quadrupole as the mass analyser and in a given run, a large number of analyte ions can be monitored by rapidly scanning the mass-to-charge ratios (*m/z*). The second type of configuration isolates the primary ionic species or parent ion, fragments it into product ions in a collision cell and monitors one or more of these product ions. This process gives added selectivity and the pattern of the fragmented ions is used as ‘‘signature’’ of a specific analyte. Such MS systems are known as tandem mass spectrometers and the associated hyphenated system is represented as LC-MS/MS.

The limit of detection for a detector can be characterized by its signal to noise ratio (S/N) for an analyte under a given set of conditions. Limit of detection (LOD) in chromatography can be defined as the amount of solute required to produce the Signal/Noise >3. LOD is the result of the whole chromatography system performance and not decided by the detector characteristics alone. Limit of quantification (LOQ) is defined as the amount of the solute required to produce Signal/Noise >10. The concepts of LOD, LOQ, linearity etc. are demonstrated in Fig. 1.20.

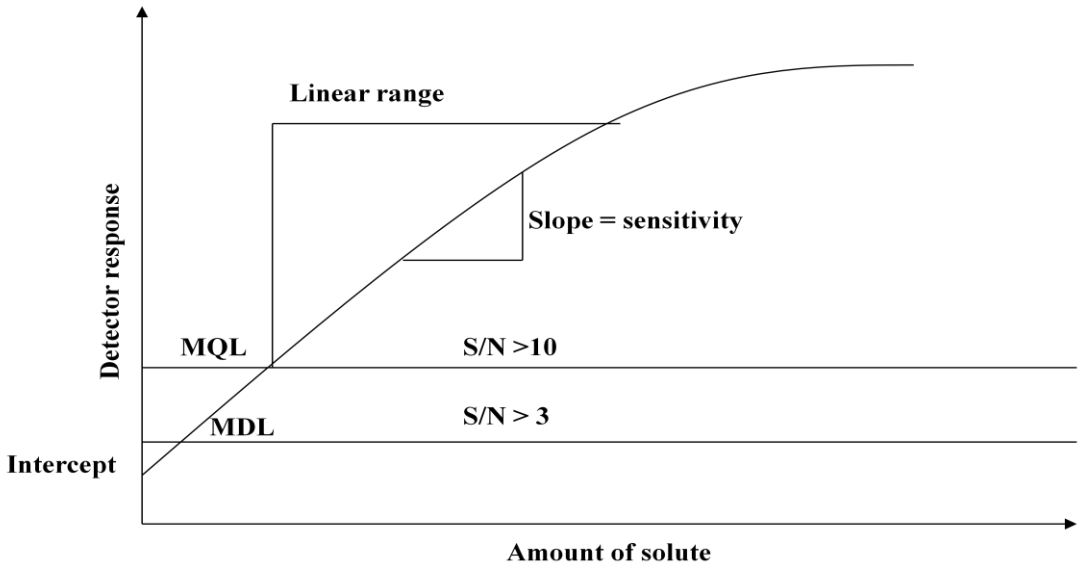

Figure 1.20: *Representation of figures of merits in chromatographic analysis [70].*

1.2.1.5.1 UV-Vis Detector

The UV-Vis detector is the most popular LC detector since it offers the best combination of sensitivity, linearity, versatility, reliability and affordability. The detector can be used for most of the solutes except for those not having a chromophore. The relationship between the light absorbed and the concentration of the solute in the detector flow cell is given by the Beer-Lambert law, $A = E\ b\ C$ where, A is the measured absorbance of a sample; E is molar absorption coefficient (at a particular wavelength λ) of the compound that is analyzed; b is the distance between the inner faces of the sample cell or optical path length; and C is the concentration of the compound in solution. Thus the two factors that control the detector sensitivity are the magnitude of the molar absorption coefficient of the solute and the path length of the light passing through the cell. The cell length cannot be increased beyond a certain limit because increase in length would lead to increase in volume as well. Large sized flow cells contribute to the broadening of the solute bands separated out of the column and thus result in poor chromatographic resolution. Small size flow cells (10 – 20 µL) are thus preferred for chromatographic detectors. A limitation of employing the small cell volume is

the increased back-pressure to the effluent flow. The different types of UV-Vis detectors in use are the fixed wavelength detector and the dispersion detector.

1.2.1.5.1.1 Fixed Wavelength Detector

As the name indicates, fixed wavelength detector allows light absorption at a specific wavelength. Depending on the type of samples, different sources are available e.g. mercury vapour lamp, cadmium vapour lamp, zinc vapour lamp. Mercury vapour lamp is the most popular as it produces emissions at 253.7 nm which can be absorbed by a wide range of compounds. Fixed wavelength detectors are the least expensive and since most of the emissions are taking place at a specific wavelength, they offer a higher intrinsic sensitivity when compared to variable wavelength detectors. But this advantage is not of much practical use if the solute has a λ_{max} widely different from the output wavelength of the source.

1.2.1.5.1.2 Dispersion Detector

The multi-wavelength detectors can be further divided as the dispersion detector (variable wavelength) which monitors the eluted solute at a particular wavelength and the diode array detector which monitors over a range of wavelengths simultaneously. In the case of dispersion detector, the light from a broad emission source (deuterium or xenon discharge lamp) is passed though a monochromator and the light with the wavelength of choice is then passed through the flow cell. Some detector versions offer the option of switching the monitoring wavelengths or to scan the wavelength during the chromatographic run so that each solute can be monitored with maximum sensitivity. Switching the wavelength can be tedious when a large number of solutes with varying λ_{max} are eluted with less time gap.

1.2.1.5.1.3 Diode Array Detector

Due to the possibility of monitoring individual solutes at its λ_{max}, diode array detector provides both sensitivity and selectivity. A diagram of a diode array detector is shown in Fig.1.21.

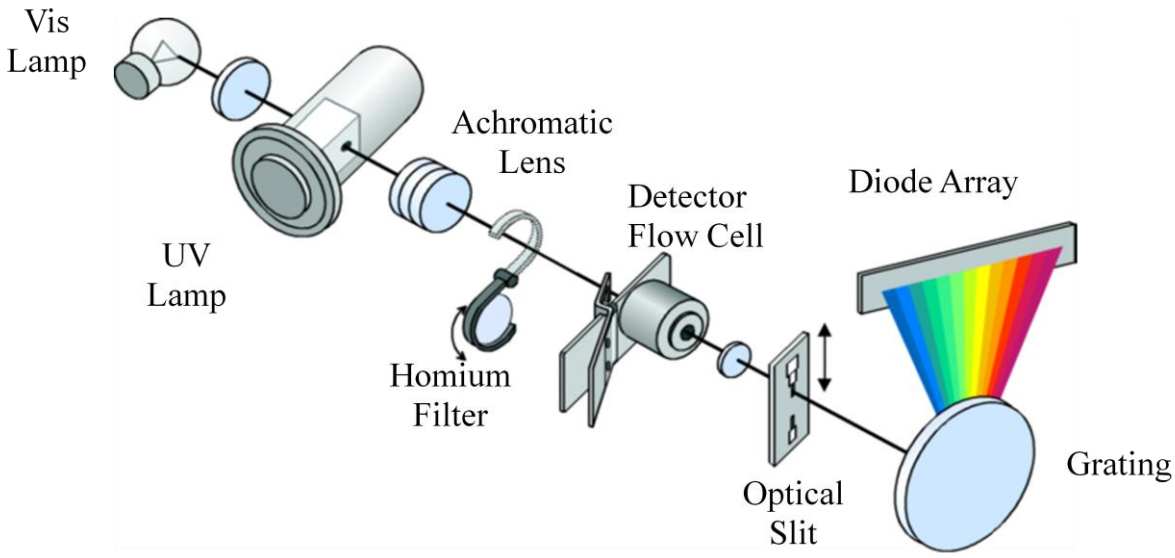

Figure 1.21: *Schematic diagram of a diode array detector.*

In diode array detector, the composite light from the broad emission source (deuterium lamp or tungsten lamp) is collimated by a lens into a flow cell. Thus the sample is exposed to all the wavelengths generated by the lamp source. The transmitted light from the flow cell is then dispersed by using a prism or grating. The dispersed light is allowed to fall on an array of large number of (512 or 1024) diodes, so that each diode can monitor the change in the intensity of a particular wavelength. A configuration of 1024 diode makes it possible to achieve wavelength resolutions better than 1 nm, provided wavelength range of the detector is 200 - 800 nm. The output from each diode is regularly sampled and stored by a computer and at the end of the run, the output from any diode can be selected to produce a chromatogram based on the wavelength that was falling on that particular diode. Most instruments permit the monitoring of the output of at least one diode in real time so that the chromatogram can be

followed as the separation progresses. A holmium oxide filter which can be moved in or out of the optical path is used for the wavelength calibration of the detector.

1.2.1.5.2 Derivatisation Reaction in Chromatography

Derivatisation is employed when the analyte of interest is non-absorbing or has a very low molar absorption coefficient. The derivatised compound would have sufficient response to conventional UV-Vis or fluorescence detectors. Pre-column and post-column derivatisations are the two general approaches for derivatisation. In pre-column derivatisation, the reaction is performed before the sample is injected into the column whereas in the post-column derivatisation, the reaction takes place after the analyte is eluted from the column. Pre-column derivatisation is usually done to modify the chromatographic characteristics and sensitivity. The reaction can be carried out manually or automated and is not constrained by the rate of the reaction. However, the reaction must be completed before the sample is injected. It also offers the option to remove the excess reagent after the completion of the reaction. In post-column derivatisation, the reaction is taking place as the solute travels between the column and the detector and hence the reaction must be quick. The possibility of band broadening due to the introduction of reaction set-up and reproducibility of the reaction is a concern. Some of the important characteristics required by pre-column and post-column derivatisation in LC are summarized in Table 1.6.

Table 1.6: Comparison of pre-column and post-column derivatisations in liquid chromatography

Requirement	Pre-column derivatisation	Post-column derivatisation
Fast reaction rate	Not necessary	Essential
Completeness of the reaction	Essential	Not essential
Reproducibility of reaction	Essential	Essential
Alteration to the chromatographic separation condition	Possible	No effect
Compromise in resolution due to band broadening	No effect	Possible

The UV-Vis detectors can be used only when the eluting solutes are capable of absorbing light in the wavelength range of the light source employed. The technique has been extended for non-absorbing species by indirect detection wherein a chromogenic substance (e.g. Creatinine at 220 nm) is added in the mobile phase [72]. Another limitation of UV-Vis detector is the inability to discriminate the co-eluting species having same absorption spectra or not absorbing at all in the wavelength range of the detector. Demand for unambiguous detection of components and identification of unknown peaks led to the hyphenation of LC with independent analytical techniques such as mass spectrometer (MS), nuclear magnetic resonance (NMR), Fourier transform infrared spectrometer (FTIR), inductively coupled plasma emission spectrometer (ICP-AES) etc. [73]. The high selectivity of these detectors helps in quick method development and sometimes compensates for the need for high resolution separation. Among the different hyphenated liquid chromatography systems, LC-MS is the most popular because of the ability of the mass spectrometer to recognize the components in an overlapped peak and to assign molecular mass or even structural information to a species (or peak). Thus MS has become the standard detector for LC analysis

of complex samples such as pharmaceutical compounds in biological systems (e.g. plasma or urine).

Development of suitable interface is the key factor for the successful coupling of liquid chromatography to mass spectrometry system. LC employs mobile phase in liquid state whereas mass spectrometer requires low pressures, typically $\leq 10^{-6}$ mbar, for its operation. The interfacing process must take care of the evaporation of the mobile phase, generation of sample ions and preferential transmission of ions into the MS system. When the mobile phase is converted from liquid to gas state, the resultant expansion in volume is about 1000 fold and this poses tremendous load to the interface. One of the most successful interfaces in LC-MS is electrospray ionization (ESI).

1.2.2 Mass Spectrometer

Mass spectrometer is an important analytical tool for the identification, characterization and determination of a wide variety of species. The important components of a mass spectrometer are ion source, mass analyser, detector, vacuum system and data acquisition system.

1.2.2.1 Ionisation Techniques

Given below are some of the commonly employed mass spectrometers based on the ionization method employed:

- Accelerator based mass spectrometer (AMS)
- Electron ionization mass spectrometer (EIMS)
- Electrospray ionization mass spectrometer (ESIMS)
- Fast atom bombardment mass spectrometer (FABMS)
- Inductively coupled plasma mass spectrometer (ICPMS)

- Matrix assisted laser desorption and ionization (MALDI)
- Secondary ion mass spectrometer (SIMS)
- Thermal ionization mass spectrometer (TIMS)

The choice of the technique used depends upon the nature the sample and the type of the information required. Electron ionization (or electron impact) and chemical ionization methods are generally employed for volatile samples and are found mostly in GC-MS hyphenated techniques. For non-volatile compounds, the preferred ionization methods are electrospray ionization (ESI), atmospheric pressure chemical ionization (APCI), matrix assisted laser desorption and ionization (MALDI), fast atom bombardment (FAB)etc[74]. Among these, ESI and MALDI are regarded as soft ionization techniques as they result in the formation of molecular ions with minimal fragmentations. In MALDI, sample is dissolved in a matrix which absorbs light from a short pulse of laser of a specific wavelength. The matrix transfers the absorbed energy to the sample and thus assists in ionization. The extracted ions are then guided to a time-of-flight system for mass analysis. MALDI is useful for the ionization of very large molecular weight samples like proteins, polymers etc. ESI is regarded as one of the softest ionisation technique and is best usable for polar non-volatile compounds (peptides, pharmaceuticals, natural products). The tendency of electrospray to produce multiply charged ions is advantageous in the determination of analytes with high molecular weight. APCI is also an ionization technique widely used in LC-MS hyphenation. Compounds with a wide range of polarity are amenable to APCI and this technique is compatible to larger flow rates of the mobile phase and higher salt contents. Usually solution phase samples are examined with ESI and APCI while MALDI is particularly appropriate for solid phase samples. Fast atom bombardment is also used for large compounds with low volatility (peptides, proteins, carbohydrates) and the sample has to be mixed with a suitable non-volatile matrix (glycerol, crown ethers, nitrobenzyl alcohol etc.).Immobilized matrix is then

bombarded with a fast beam of Argon or Xenon atoms to generate the ions. Thermal ionization and inductively coupled plasma belong to the class of inorganic mass spectrometers providing the elemental information. Thermal ionisation is widely recognized as the technique of choice where precise and accurate isotope ratios are required. Inductively coupled plasma, due to the high ionization efficiency, low detection limits and wide dynamic range finds important position in trace elemental analysis. Secondary ionization is a surface analysis technique which can provide the elemental distribution over a surface along with the isotopic data and the depth profiling. Electrospray ionisation and thermal ionisation, the two techniques used in the present study, will be discussed in detail in the following Sections.

1.2.2.2 Mass Analyzers

Mass analyzers are used to distinguish the ions based on their *m/z* values. Mass analyser can be selected depending upon the nature of the ion source, mass range and mass resolution required. Some of the commonly used mass analyzers are time-of-flight, quadrupole, ion cyclotron, magnetic sector, ion trap and hybrid [75].

1.2.2.2.1 Time-of-Flight Analyzer

Time of flight analyser consists of ion-accelerating region, flight tube and detector. Since a definite start time is required, these instruments are used in sequential mode e.g. MALDI. At the start of the flight tube, all the ions are exposed to the same potential difference and thus have the same kinetic energy. Hence, the ions migrate through the field free region with different velocities depending upon their masses. Flight time t of the ion is related to its *m/z* by the equation:

$$v = (2Vz/m)^{1/2}$$

$$t = l(m/2Vz)^{1/2}$$

where, l is the length of the flight tube traveled by an ion with mass ‘m’, charge ‘z’ and a velocity ‘v’, and V is the acceleration potential.

Mass resolutions obtained by the linear ToF instruments suffer due to the spread in the flight of the ions of the same *m/z*. This distribution in energy is contributed by the difference in the special positioning of the ions at the time of receiving the acceleration pulse. Sometimes the ionization process also adds a certain amount of initial kinetic energy to the ions before acceleration. The two methods employed to enhance mass resolution in ToF are reflectron and delayed extraction.

A reflectron is used to focus the ions of the same *m/z* into a narrow band and thereby improve the resolution significantly. Reflectron consists of a series of rings or grids placed at the other end of the drift tube. These grids create a retarding potential which increases with the penetration depth. The ions with same *m/z* but of relatively lesser kinetic energy will deflect faster into the flight tube. Ions with higher kinetic energy penetrate deeper into the reflectron and spend more time and thus manage to join together with the ions with lesser kinetic energy, after deflection.

Delayed extraction (pulsed ion extraction) technique is used to compensate for the velocity distributions of ions. Before accelerating into the flight tube, the ions are allowed to drift free of electric fields for a certain delay time. By allowing them to drift, faster ions move farther away from the acceleration target than the slower ions. Thus faster ions will experience less of the accelerating voltage than the slower ions. This procedure compensates for the initial energy distributions of ions with the same *m/z*.

ToF analyzers offer the advantage of high mass range, mass accuracy and simultaneous detection of all the ions. TOF analyzers exhibit very fast acquisition times and thus are ideal for hyphenation with fast LC. The inherent sequential nature of ToF makes it

the ideal choice for combination with MALDI, which operates in pulsing mode. One of the limitations of ToF is its limited dynamic range, making it less attractive for quantitative applications [76,77].

1.2.2.2.2 Quadrupole Mass Analyzer

Quadrupole analyzers have four parallel rods and opposite potentials are applied to the set of diagonal pair of rods. Quadrupoles are used as mass analyser, ion transfer optics, collision cells, and linear ion traps. While employed as mass analyser, a quadrupole works on the basis of electric fields generated between a set of four axial rods through which the ions are passed. The quadrupole field created by the dc and rf combination dictates the *m/z* range to pass through the quadrupole and reach the detector. Ions beyond the selected range will hit the rods and get discharged. Thus quadrupole mass analyzers are also called mass filters. The potential applied to the rods is given by $\Phi = U + V \cos\omega t$ where, U is the dc voltage and V $\cos\omega t$ is the rf potential of frequency $\omega/2\pi$. Two rf waveforms are applied to two pairs of opposing parallel rods, with 180° phase shift. Hence trajectory of the ion fluctuates constantly as it travels in the space between the rods [78].

Quadrupoles with only rf field are used as ion transfer optics and collision cells. In this case, ions passing through the quadrupole are confined in the center of the quadrupole(sometimes hexapoles or octopoles) axis at low gas pressures, thus increasing transmission efficiency. This effect is called collisional cooling or collisional focusing. By incorporating trapping electrodes at the beginning and the end of such a quadrupole, ions get stored in the device, which is the basis of linear ion traps. Quadrupoleanalysers are economical and compact and have found a wide application range in LC–MS and GC–MS. However, they have relatively lower resolution and offer less sensitivity when operated in scanning mode.

1.2.2.2.3 Magnetic Sector Analyzers

When an ion of mass m and charge z is accelerated by a potential of V, its kinetic energy is given by, $mv^2/2 = zV$ where, v is the velocity of the ion after acceleration. The accelerated ion enters a magnetic field, H, applied perpendicular to the direction of ion trajectory and then the centrifugal force acting on the ion is balanced by the magnetic force, $HeV = mv^2/R$, where R is the radius of curvature of the ion's path in the magnetic field. Therefore it is possible to write $m/z = H^2R^2/2V$

Thus ions will have different radius of curvatures depending on their *m/z* and thus separation takes place. When there is only one detector, the desired ion can be brought to the detector either by changing the magnetic field (magnetic scanning) or by changing the acceleration voltage (voltage scanning). When multiple detectors are available, it is possible to simultaneously collect the ions on specific detectors by keeping magnetic field and acceleration voltage constant. Magnetic analyser alone results in directional focusing and is adequate to provide nominal resolution (~ 500) when there is no significant spread in the energy of the ions. Combination of directional focusing and velocity focusing is required when high mass resolution is required or the relative ion energy spread is considerable. Velocity focusing is achieved by using electric field. The combination of magnetic field and electric field is known as double focusing and is used in mass spectrometers offering high resolution power (10,000 – 20,000).

1.2.2.2.4 Ion Trap Analyzers

Three hyperbolic electrodes, consisting of a ring and two endcaps, form the core of this instrument. In earlier days, the ion trap was operated in "mass-selective stability" mode of operation. In this mode, the amplitudes of rf and dc voltages applied to the ring electrode were

ramped at a constant ratio to allow the storage of a particular *m/z* value in the ion trap. Advancements in ion trap technology have made it possible to trap all the ions created over a given time period and then are sequentially ejected from the ion trap into a detector (electron multiplier). Thus all ions are stored while mass analysis is performed and hence this simplifies the use of the instrument. Filling the trap volume with a residual gas (He) at a low pressure (~1 mbar) helps in the collisional cooling of the ions which in turn contract the ion trajectories to the center of the trap. This allows ions of a given *m/z* to form a packet. The ion packet is ejected more quickly and efficiently than a diffuse cloud of ions and thus improving resolution[79].The biggest strength of the ion trap technique is its ability to perform multiple stages of mass spectrometry, unlike other tandem mass spectrometers. Possibility of performing multiple stages of tandem mass spectrometry greatly increases the amount of structural information obtainable for a given molecule. Thus ion trap MS systems are regarded as powerful tools for the structural characterization. Up to 12 stages of tandem mass spectrometry, $(MS)^{12}$, can be performed using an ion trap. The mass range obtainable with ion trap is higher than that obtained on a quadrupole instrument and lower than that achievable on TOF analyser.

1.2.2.2.5 Fourier Transform Ion Cyclotron Mass Analyzer

In view of its extremely high resolution and mass accuracy, Fourier Transform Ion Cyclotron Mass Analyzer (FT-ICR) has become an invaluable tool in drug discovery. When an ion with a certain velocity enters the homogeneous magnetic field of the ICR cell, it starts moving in a circular path. If the ion is under extremely low pressure conditions, it does not experience any collisions with residual gas molecules in the cell. Consequently, the speed of an ion in the FT-ICR cell is constant and its angular velocity is proportional to the *m/z* of the ion[80].Unlike other mass spectrometers, FT-ICR analyzer does not have a detector where ions are discharged physically. Detection is based on measuring the image current that individual

ion packages induce when they pass the detector plates repeatedly, at their cyclotron frequencies. In a typical FT-ICR experiment, the ions in the cell are excited simultaneously, and a composite image current for all ions is measured. Next, this transient signal is converted from the time domain to the frequency domain using a fast Fourier transform algorithm.

A comparison of important characteristics of different mass analysers is presented in Table 1.7.

Table 1.7: Comparison of important features of mass analyzers

Feature	Mass analyser				
	Sector magnet	**Time-of-flight**	**Ion cyclotron resonance**	**Ion trap**	**Quadrupole**
Quantity measured	Momentum to charge ratio	Flight time	Cyclotron frequency	Frequency	Filters for *m/z*
m/z range	10^4	10^6	10^5	10^4	10^3 -10^4
Resolution @ m=1000	10^4	10^4	10^6	10^3 -10^4	10^3 -10^4
Dynamic range	10^7	10^4	10^4	10^4	10^5

Reference [81]

1.2.2.2.6 Hybrid Analyzers

Combinations of different analyzers are designed to enhance the mass spectrometric capabilities such as MS/MS, novel scan modes, high mass accuracy and resolution etc. Quadrupole time-of-flight (QToF) is an example of one of the most successful hybrid mass analysers. It allows the generation of MS/MS spectrum similar to triple quadrupole along with the high resolution, accurate mass capability and simultaneous monitoring ability of the ToF analyser. ToF analysers can be placed parallel or in the perpendicular (orthogonal) direction with respect to the ion source. Orthogonal positioning of the ToF reduces the average initial

energy in ToF direction to almost zero and this significantly enhances the resolution and accuracy of the mass analyser [82].

1.2.2.3 Detectors

A detector is used to measure the analyte ions passing out of the mass analyzer after suitable amplification. Magnetic sector based MS systems generally use a Faraday cup or a secondary electron multiplier (SEM) as the detector. Faraday cup provides the detector response independent of the mass of the ions and hence is highly useful for precise isotope ratios measurements. SEM is preferred for achieving high sensitivity particularly in case of samples giving low ion currents. In SEM, when an ion strikes the conversion dynode, it causes the emission of several secondary electrons. These electrons are accelerated at different dynodes, subsequently providing an increased signal for further processing. However, one has to be careful about the additional mass discrimination in the isotope ratios data introduced by the velocity dependent response of SEM.

An electron multiplier is the most commonly used type of detectors in quadrupole based mass spectrometric systems and some MS systems use a modified type of electron multiplier known as "dual-stage discrete dynode detector". Positively charged ions exiting the mass spectrometer are attracted to the negatively charged first dynode of the detector. The impact of an ion results in the emission of a number of electrons from its surface. These electrons are attracted to the positively charged second dynode of the detector, where each of them causes the emission of further electrons. As this process continues along a series of more than 20 individual dynodes, the number of electrons generated increases rapidly. In this manner, the signal due to ions entering the detector is detected and amplified. The signal intensity is measured simultaneously at two different points in the detector and hence the term "dual-stage" detector [83].

1.2.2.4 Vacuum System

When the mean free path (the average distance between collisions) of the gas molecules exceeds the dimensions of the vacuum container, the system is under molecular flow conditions. Under such conditions, the ion moves without colliding with other ions or residual gas molecules. Vacuum system is important to maintain the mean free path in the analyser and improve its efficiency. Further, in LC to MS coupling, a large volume of the gas is produced during the solvent evaporation. Heated dry gases are employed for assisting the evaporation of solvent molecules. These gases put tremendous load in the vacuum system. Differential vacuum pumping is employed for the effective removal of neutral molecules without hampering the ion transmission efficiency.

Based on their working principle, vacuum pumps can be broadly classified into positive displacement pumps, momentum transfer pumps and entrapment pumps. A combination of different vacuum pumps is used for achieving the desired vacuum levels in different components of the mass spectrometer. Positive displacement pumps (e.g. rotary pump) use a mechanism to repeatedly expand a cavity, allow gases to flow in from the chamber, and exhaust it to the atmosphere.

Momentum transfer pumps impose a net directional motion to the residual gas molecules in the vacuum system. For example, in a turbomolecular pump, the residual gas molecules collide with the angled high speed rotating blades on a turbine shaft. The net direction imparted to the residual gas molecules is into a region of higher pressure and towards the exhaust of the high vacuum pump. The exhaust of the high vacuum pump is connected to a rotary pump that accomplishes the transport of the residual gas molecules to

the final exhaust at atmospheric pressure. Turbomolecular pumps produce vacuum levels of the order < 10^{-7} mbar.

Entrapment pumps capture gases in a solid or adsorbed state. This includes cryopumps, getters, and ion pumps. Ion getter pumps (IGP) capture and hold gases by converting them into solid compounds and binding them in the pump. Ion pumps remain the cleanest and the most efficient method of achieving ultra high vacuum (<10^{-9} mbar). These pumps require the backing of rotary pump and turbo molecular pumps. In TIMS, a cold finger is provided for adsorbing the gases evolved during heating of the filaments in the ion source[83].

The two different mass spectrometric systems employed during the course of the present work are described in detail below:

1.2.3 Electrospray Ionisation Tandem Mass Spectrometer

1.2.3.1 Electrospray Ionisation

Figure 1.22 shows the schematic of an electrospray ionisation system. A high voltage (3–5 kV) is applied between the tip of the metallic capillary and a counter electrode. The strong electric field charges the surface of the liquid emerging from the capillary and forms a fine spray of charged droplets. Nebulizer gas assists the droplet formation at higher flow rates of the mobile phase. When an analyte is dissolved in a polar solvent, it can either ionize or form a strong dipole moment. Analytes that exist in the ionized form in the solution can easily evaporate from the droplets during the electrospray and result in high sensitive response. For analytes that form strong dipole moments in solution, the ionization process is driven by the strong electrostatic fields in the spray chamber. These fields induce a charge on

the surface of the droplets. These analytes can also be ionized chemically by adduction using selected chemicals.

The charged droplets are migrated under the influence of the potential towards the counter electrode. During this process, a flow of heated nitrogen (drying gas) dries the droplets and carries away uncharged mobile phase molecules. This process results in the continuous shrinkage of the droplet size. The droplets continue to shrink until the repulsive electrostatic (Coulombic) forces exceed the surface tension, leading to droplet explosions as indicated in the inset of the Fig 1.22. The point at which this occurs is called the Rayleigh Stability Limit. This process is repeated several times as the droplets continue to evaporate in the presence of high electrical potential fields [84, 85]

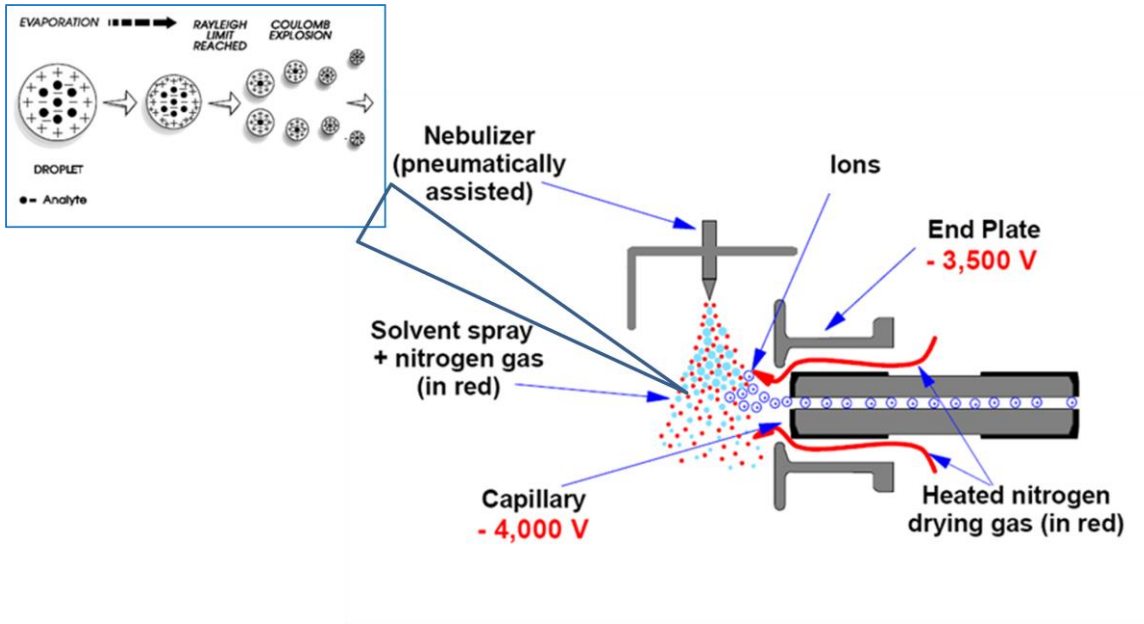

Figure 1.22: *Schematic of electrospray ionisation system.*

1.2.3.1.1 Mechanism of Ion formation

The two mechanisms recognized to be involved in the ion formation in electrospray are the ion evaporation model and the coulombic explosion model. According to the coulombic explosion model, continuous evaporation of solvent from the droplets in the

presence of the strong electric field results in the charging of the droplet surface. When the coulombic repulsion between the ions at the surface of the droplet exceeds the surface tension, the droplet undergoes a series of fissions and this finally leads to the formation of analyte ion cluster. According to the ion evaporation model, when the field created by the ions at the surface of the droplet exceeds a certain limit, bare analyte ions are emitted directly from the droplet [86]. Electrospray may be thought of as ionization followed by ion evaporation or desorption. Ion evaporation or desorption occurs when the charge density in the droplets reaches ~ 10^8 V/cm^3 [87].The emerging cluster ions are then directed into the heated glass capillary where it undergoes declustering as a result of multiple collisions onto the glass wall. A series of funnels or cones focus the ions into a beam, while at the same time, evacuating the excess drying gas and neutral molecules using differential pumping. The ions are then transferred into the mass analyser.

Advantages of ESI include 'soft' nature of the ionization process (preserves intact ions of even fragile molecules) and high sensitivity of the technique for medium to high-polarity analytes. The characteristic of ESI to produce multiply charged ions enables the analysis of proteins, peptides, oligonucleotides, and other macromolecules using conventional mass analyzers with relatively low mass range limits.

Disadvantages include the strong influence of solution chemistry on the ionization process, poor sensitivity for low polarity analytes (low degree of ionization in solution), the possibility of multiple adduct ions with some species (complicated spectral interpretation) and lowering the sensitivity at higher flow rates (due to poor nebulization, inadequate droplet charging and inadequate desolvation).

1.2.3.2 Mass Analyser

The hybrid mass analyser consists of three quadrupoles, Q_0, Q_1 and Q_2, followed by a reflecting TOF mass analyzer with orthogonal injection of ions, as shown in Fig.1.23. The rf only quadrupole (hexapole in certain cases), designated as Q_0 focuses the ion beam by collisional cooling. The quadrupole used for the isolation of the precursor ion is designated as Q_1. When the instrument is operated in MS mode, Q_1 is operated in the rf-only mode so that it serves merely as a transmission element, while the TOF analyzer is used to record spectra. The collision cell, represented as Q_2, is also a quadrupole operated in rf only mode because the rf-field creates a potential well that provides radial confinement of the precursor and/or fragment ions [88].

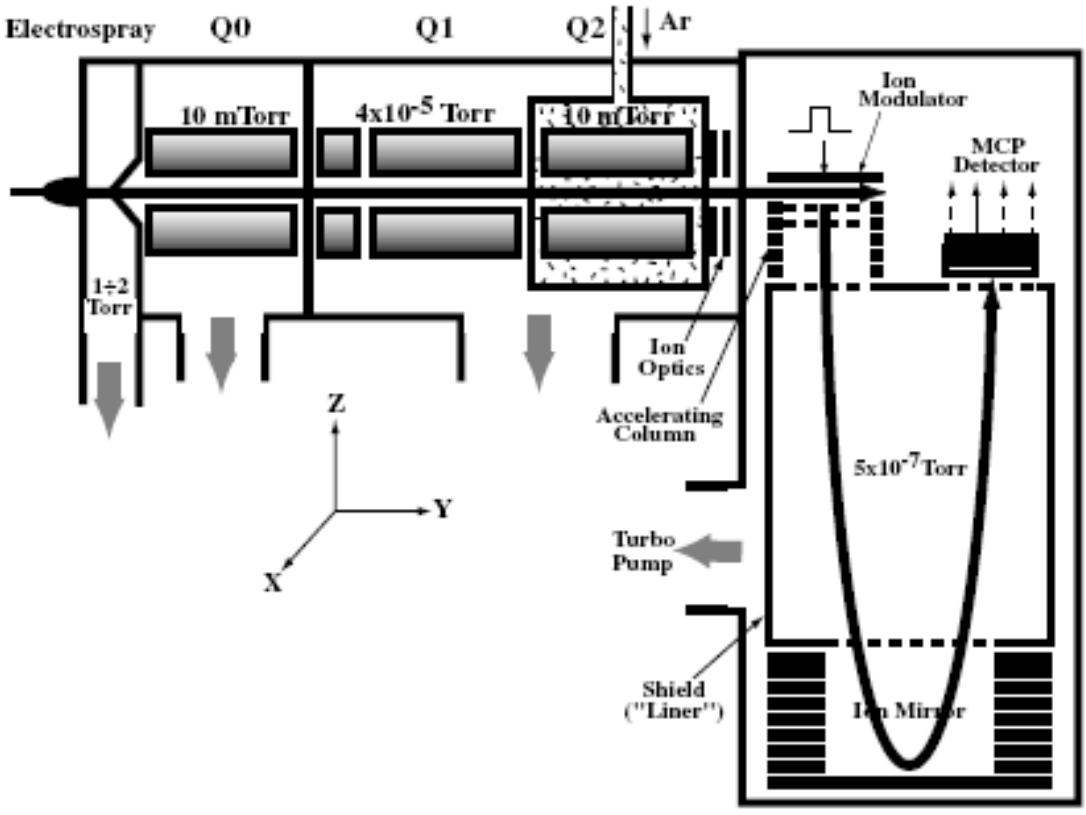

Figure 1.23: *Schematic diagram of a quadrupole-ToF hybrid mass spectrometer [88].*

Since the rf quadrupoles contain residual gas at pressures ~ 10^{-3} mbar, the transmitted ions are thermalised in collisions with gas molecules. This process reduces both the energy spread and the beam diameter, and results in better transmission. Ions emerging out of the rf

quadrupoles are again accelerated in the axial direction. When the instrument is operated in the MS/MS mode, Q_1 is operated in the mass isolation mode so that only the parent ions of interest are allowed to be transmitted. Normally, an *m/z* window of 3 – 10 is selected to allow the isotopic signature to be reflected in the MS/MS spectrum. The filtered ions are then accelerated by applying a potential of 10 – 200 V depending upon the nature of the molecule and the extent of fragmentation. The accelerated ion upon entering the collision cell undergoes collision induced dissociation (CID).

CID involves the collision of ions with neutral gas molecules (Ar or He) to cause fragmentation. Since ESI ionization is relatively "soft", CID is an important mass spectrometric capability. While the soft ionization is advantageous in providing the molecular ions information, CID can be used to obtain detailed structural information based on the fragmentation pattern. Thus molecular ion along with fragmentation pattern enhances the confidence on the confirmation of the compound identity. The extent of fragmentation can be controlled by regulating the ion energy in the collision cell. Higher ion energy leads to more energetic collisions of analyte ions with the gas molecules and hence greater fragmentation. Thus molecular ions are observed with greater abundance at low energy conditions. Ion energy can be changed by adjusting the potential difference between the two optics elements in the ion path. The resultant fragmented ions and remaining parent ions are focused by collisional cooling so that both resolution and sensitivity are improved.

Ions leaving the collision cell are again accelerated so that they enter the ion modulator. A pulsed electric field (~ 9 kV) is applied at a high frequency (a few kHz) across the modulator gap, pushing ions in a direction orthogonal to their original trajectory. The accelerated ions thus arrive in the field-free drift space, where mass separation occurs based on the difference in flight time. Reflectron compensates for the initial energy spread and

special distribution of ions and thus ions of same *m/z* but with different energies are focused on to a horizontal plane at the detector entrance.

1.2.3.3 Detector System

The detector is made of two microchannel plates (MCP) in a chevron configuration [89]. MCPs are preferred for TOF analyzers because they provide a flat conversion surface with a large area, suitable for recording flat (in Y axis in Fig. 1.23) and narrow (in Z axis) ion packets. Also they have a fast response time. All mass spectra from the TOF spectrometer are recorded with a time-to-digital converter (TDC). The instruments are capable of producing mass accuracy <5 ppm and mass resolutions > 20,000 (FWHM basis).

1.2.4 Thermal Ionisation Mass Spectrometer

Thermal ionization mass spectrometer is the instrument of choice for the precise and accurate isotopic analysis because thermal ionization produces steady ionisation with a very small energy spread. Samples in the solution form are loaded onto a single, double or triple filament followed by drying by passing current. Filaments are made of refractory non-reactive metals such as platinum, rhenium, tungsten or tantalum having high work function. When the filament is heated by passing a current, neutral species and ions of the element are emitted from the hot surface of the filament according to the Saha- Langmuir equation:

$$\frac{N^+}{N^0} = \frac{g^+}{g^0} e^{\frac{\Phi - I}{kT}}$$

where, N^+/N^0 is the ratio of number of positive ions to that of neutrals, $g^+/g^0$is the statistical weights of ion and neutral states, Φis the work function of the surface of the filament material,

I is the ionization potential of the element, k is the Boltzmann's constant and T is temperature of the filament surface [83].

For single filament configuration, the same filament acts as both the vaporization and the ionization filament. In double or triple filament configurations, one filament acts as an ionization filament and the other filaments loaded with sample act as vaporization filaments. Use of multiple filaments allows independent control over the ionization and vaporization processes and thereby achieving higher efficiency [90].

Schematic diagram of a TIMS is shown in Fig. 1.24. The ions produced from the heated filaments are accelerated across a potential (8-10 KV) and focused into a beam via a series of slits and electrostatically charged plates. This ion beam then passes through a sector magnet analyser. Ions entering a homogeneous magnetic field are deflected perpendicular to their flight direction and perpendicular to the magnetic field according to the Lorentzian rule. As a result, light ions follow a path with a smaller radii whereas heavier ions with larger radii. Because of the relatively low spread in the energy of the ions produced, single focusing is sufficient to achieve the required resolution (resolution ~ 450, based on 10% valley). Magnetic-sector analyzers produce "flat-topped" peaks for the separated ions. Since flat top peaks are not affected by the changes in the relative ion intensities if small drifts occur in the instrument during analysis, they are preferred for the high precision isotope ratio measurements.

The mass-resolved beams are then directed into detectors where the ion current is converted into voltage. Most commonly employed detectors are Faraday cups and secondary electron multipliers. Availability of multi-collector systems enables the simultaneous collection of ions of different *m/z*. Simultaneous collection of all isotopes of interest is also important for high-precision analyses, since ion beams may have small variations in

intensities due to small changes in source conditions during analysis. Fluctuations of the ion currents due to temperature changes, electron beam instability etc. cancel completely when the ratios of the detector outputs are taken.

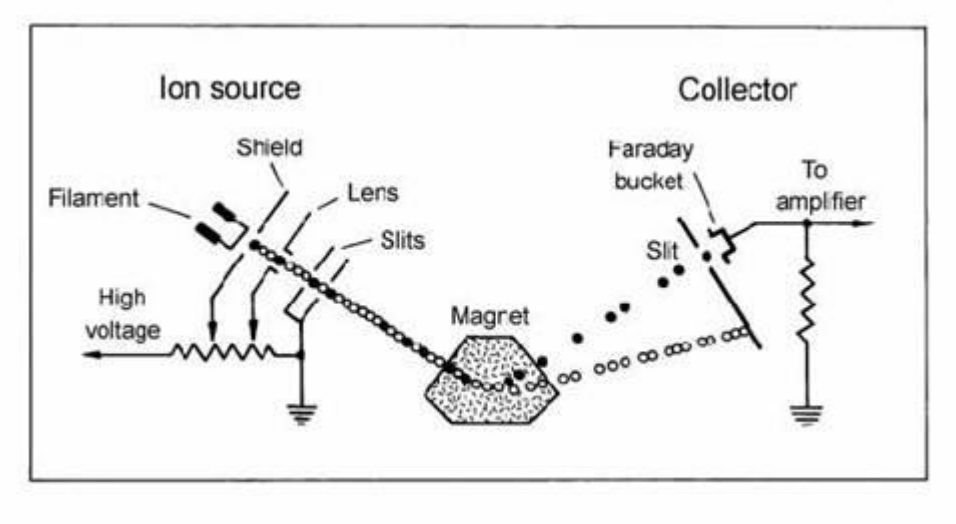

Figure 1.24: *Schematic diagram of a magnetic sector mass spectrometer.*
Solid and open circles represent the light and heavy isotopes, respectively, of an element.

Some of the advantages of TIMS are:

- Highly precise isotope ratio measurements
- Production of ions with a restricted range of energies eliminates need for energy filter

The disadvantages include:

- Not all elements are easily ionized, especially ions with high ionisation potential.
- Ionization is not equally efficient for all elements, and is generally less than 1%.
- Mass fractionation continually changes isotope ratios during analysis.
- Elementally pure solutions are required to avoid isobaric interferences, which require extensive sample preparation.

1.3 Scope of the Present Work

This thesis presents the studies carried out for developing different liquid chromatographic methods for the separation and determination of lanthanides (Ln), thorium (Th) and uranium (U). Determination of lanthanides, Th and U is of great importance in nuclear technology, geochemistry, environmental sciences etc. Individual separation of lanthanides is a difficult task due to their similar electronic configuration and nearly the same ionic radii. The use of complexing agents as eluents in the liquid chromatography helps to amplify the slight differences in the stability constants of the Ln-eluent complexes and thus leads to their separations. Effects of different parameters such as concentration of eluent, ion interaction reagent (IIR), pH of mobile phase etc. were studied systematically for the optimization of separation procedure for a given type of sample.

In view of its high efficiency, ion interaction chromatography was employed for the individual separation of lanthanides. A comparative study of different ion interaction reagents (IIRs) viz. n-octane sulphonate, n-octane sulphate, n-octadecanesulphonate and eicosylsulphate, was carried out under identical experimental conditions. Among different IIRs studied, n-octadecylsulphonate was showed the highest resolution for all the lanthanide pairs and showed good long term adsorption stability. The excellent performance exhibited by n-octadecylsulphonateis attributed to its preferential adsorption by the C_{18} bonded stationary phase. The applicability of the developed method was demonstrated by analyzing lanthanides in a geological reference material viz. Syanite-3 (SY-3). Since IIR is not required to be present during the elution, the method is beneficial for further analysis of the separated fractions by mass spectrometry.

Under the ion exchange conditions employed for the individual separation of lanthanides, presence of large amounts of Th and U causes interference as matrix element

peaks can mask some of the lanthanides. The pH of the eluent and the concentration of IIR were found to play a vital role in deciding the retention of Th and U on the stationary phase. A novel dual gradient elution was developed for the determination of lanthanides without involving any pre-separation of matrix elements U and Th. Further, the method allowed the use of Tb as an internal standard for the precise quantification of lanthanide fission products. The method was applied for the separation and determination of lanthanides in simulated as well as actual samples of irradiated thoria. Coupled column method employing a RP column and a cation exchange column was also investigated for the determination of lanthanides in bulk of Th using mandelic acid as the eluent. The method was used for the separation of synthetic samples with Th/Ln amount ratios up to 10,000.

Th based nuclear fuel cycle demands quantification of small amounts of U in presence of large amounts of Th. When mandelic acid was used as the eluent, elution of U occurred prior to Th, contrary to that observed with α-HIBA as the eluent. The parameters such as pH & methanol content of the mobile phase and concentration of the eluent were studied to optimise separation between Th and U on the RP column. The developed method allowed determination of trace amounts of U in synthetic samples with Th/U ratios up to 100,000, without involving any pre-separation. It was also of interest to understand the mechanism of adsorption of metal-mandelate complexes onto the stationary phase. The difference in nature of the major species of Th and U, charge neutrality of thorium mandelate complex and the anionic nature of uranyl-mandelate complex explained distinct elution pattern observed when mandelic acid was used as the eluent.

In view of the increasing energy demand, recovery of U from seawater is considered as an option for increasing its availability in future. A method for the determination of U at different stages of pre-concentration was developed for assessing its recovery. In the first approach, α-HIBA in combination with monolith RP column was employed for the pre-

concentration and separation of U. Under the optimized conditions, high salt content and metals viz. V, Ni, Ti and Mo showed no interference during the determination of U. However, this method was found to be unsuitable for samples containing high levels of Fe. Hence further studies were carried out with mandelic acid chelating agent and separate columns for pre-concentration and separation. By studying the effect of concentration of mandelic acid, MeOH content etc., it was possible to develop a method to give (i) good separation between U and Fe (ii) to introduce the samples at pH $\leq$ 4 to avoid the formation of turbidity and (iii) quantitative recovery of U in the range of 0.5 to 500 ppb. The methodology was applied for the determination of uranium in seawater and process samples from different stages of the recovery process. The developed methodology was validated by comparing the results with those from isotope dilution-thermal ionization mass spectrometry.

Knowledge about the nature of the metal-ligand species in solution is helpful in understanding the mechanism of adsorption on the stationary phase and also in developing separation conditions for a specific problem. Electrospray ionisation mass spectrometry being a soft ionisation technique was used for studying the complexation of UO_2^{2+} with hydroxyl carboxylic acids. Effects of solution conditions and the ESI parameters on the mass spectra of free uranyl as well as uranyl-HIBA species were studied in detail to obtain sensitive and representative ESI-MS spectra. Major uranyl-HIBA species observed in the positive and negative ion modes were identified. Solution composition and concentration of the uranyl salt were found to influence the major uncomplexed uranyl species. Though ESI parameters do not influence the species distribution of uranyl-HIBA, these are significantly affected by the transmission parameters. Overall trend in the complexation reaction between uranyl and HIBA was studied as a function of ligand-to-metal ratio. The species distribution obtained in the positive mode was found to be comparable to that obtained in the negative mode.

Chapter 2

Separation of Lanthanides using Ion Interaction Chromatography

2.1 Introduction

Separation and determination of lanthanides is of interest in geochemistry, environmental sciences, mineral exploration, material science and in nuclear industry [35,91-94]. Individual separation of lanthanides is a challenging task due to the similarities in their ionic radii and the existence of most of these elements in trivalent oxidation state [18,47]. Though different element specific analytical techniques are available for the sensitive determination of lanthanides, they suffer from spectral or isobaric interferences or matrix effects while dealing with complex geological or nuclear fuel samples. Separation of lanthanides minimizes the above problems and at the same time, caters to the pre-concentration of the analyte thereby improving the overall sensitivity of the method. Several HPLC techniques have been reported for the determination of lanthanides and actinides in a variety of samples relevant to nuclear industry and geological studies [95-97]. The widely used LC methods for individual separation of lanthanides are based on bonded phase cation exchangers [14,36,98]. Though bonded ion-exchange columns offer high capacity and stability over wider pH range, they yield poor resolution due to peak broadening and longer retention times. Ion interaction chromatography (IIC) is also known as ion-pair chromatography or dynamically modified reversed-phase chromatography [18,99-101]. IIC offers the advantages such as high resolution resulting from faster mass transfer at the surface of the stationary phase and the possibility for replenishment of damaged exchange groups due to radiolysis when dealing with radioactive samples [102]. Studies have shown that IIC also offers greater flexibility with regard to choice of separation conditions than bonded ion-exchangers [103,104]. For example, the same column hardware can be used for the separation of anionic, cationic and neutral species by selecting suitable modifiers. Further, capacity of the column can be changed as per the sample requirement by changing the concentration of

the modifier or the modifier itself. However, a major drawback of the IIC is the lower capacity which becomes a bottleneck when the matrix elements also show adsorption to the stationary phase. IIC in combination with post-column detection has been used for the determination of lanthanides in complex matrices. Studies have shown that ion interaction chromatography can be applied for routine determination of lanthanides and actinides at trace levels [103,105-106]. This Chapter highlights the potential of IIC for the separation of lanthanides relevant to different applications.

Generally, aliphatic sulphonate and sulphates are used as the ion interaction reagents (IIRs) for the separation of cations. In IIC, separation occurs based on ion-pair interaction as well as ion exchange mechanism. In the case of ion-pair interaction mechanism, the IIR would form an ion pair with the cations and then is adsorbed on to the RP stationary phase. In cation exchange mechanism, IIRs are sorbed onto the surface of the reversed phase to produce a charged layer at the surface where ion exchange can occur. When short chain IIRs are employed, the ion pair interaction is the dominating route whereas in the case of long chain IIRs, ion exchange is the major factor responsible for the separation [107]. Due to their moderate hydrophobicity, short chain IIRs require to be passed continuously through the column and hence are included in the mobile phase. Due to the same reason, they offer the advantage of changing the capacity of the column in a short time. On the other hand, presence of IIRs in the mobile phase is not desirable if the separated fractions are used for further analysis e.g. presence of IIR significantly suppresses the ionisation efficiency of the analyte during the thermal ionisation mass spectrometric (TIMS) analysis. It is also desired that the lanthanides are separated with adequate resolution among them so that quantification can be done based on their peak areas with a high degree of confidence. Hence it was of interest to understand the effect of the nature of the surfactant on the separation of lanthanides.

One of the applications demanding individual separation of lanthanides is the use of La and Nd as fission monitors for determining the burn-up of irradiated nuclear fuels [108,109]. A perennial problem need be addressed in these types of samples is the interference caused by the Th or U matrix element during the individual separation of lanthanides. Under typical cation exchange conditions, both Th and U elute in between lanthanide series. When Th and U are present in large proportions, they can mask some of the lanthanide peaks and thus restrict their determinations.

Thus the main objectives of studies presented in this Chapter can be summarized as:

1. Comparison of IIRs for the separation of lanthanides to achieve high resolution and without the need for adding IIR in the mobile phase.
2. Developing a method for the reliable determination of lanthanides without any pre-separation of matrix elements.
3. Development of a ligand exchange and column switching method for the on-line removal of Th matrix (in larger proportions) followed by the individual separation of lanthanides.

2.2 Comparative Study of Ion Interaction Reagents for the Separation of Lanthanides

2.2.1 Background

It is recognized that a resolution of $R \geq 2$ is required between the adjacent peaks for the reliable quantification based on the chromatographic peak response. Separation of lanthanides with good resolution is, therefore, required for their quantitation and also for the isotopic ratio measurements by mass spectrometric analysis of the separated fractions. The IIRs employed are not easily destroyed by chemical treatments and their presence in the separated lanthanide fractions lowers the ionisation efficiency during thermal ionisation mass spectrometric (TIMS) analysis. Elaborate treatment of the collected fractions with HNO_3 and H_2O_2 is needed for the destruction of the IIR prior to loading of solution onto the filament for analysis by TIMS [110]. The objective of the present study was to identify an IIR which would (i) separate lanthanides with good resolution and (ii) offer long term adsorption to the stationary phase so that IIR need not be added to the mobile phase when running the samples. Use of C20-sulphate prepared in 25% acetonitrile as IIR was reported for the separation of lanthanides for the determination of burn-up of irradiated nuclear fuel samples [102]. This Section of the Chapter presents the detailed studies carried out using the two IIRs viz. n-octadecanesulphonate (C18-sulphonate) and eicosylsulphate (C20-sulphate) for the separation of lanthanides. Since the two IIRs contain two different functional groups, C8-sulphate and C8-sulphonate were also included in the comparative study to find out the effect of different functional groups on the separation of lanthanides. In this work, resolution was used as a measure of column efficiency [65]. Volume and composition of the IIR and volumes of washings with water and mobile phase etc. for the proper equilibration of the column were optimized for each IIR. The long term adsorption of these IIRs onto the stationary phase was also studied. Better resolutions for the separation of lanthanides were obtained with a RP

column modified using C18-sulphonate as compared to C20-sulphate. The preference of the stationary phase for C18-sulphonate over C20-sulphate is believed to be due to the similarity in the number of carbon atoms in the carbon chain. In order to support this assumption, comparative studies have been carried using C8-sulphonate and n-nonanesulphonate (C9-sulphonate) employing C_8 and C_{18} stationary phases. The column modified with C18-sulphonate was demonstrated to be useful for the separation of lanthanides in a synthetic mixture and also in a geological reference material.

2.2.2 Experimental

2.2.2.1 Instrumentation

HPLC system with a post-column detection system as shown in Fig. 1.14 was used in this study. It consisted of an L-7100 (Hitachi) low-pressure quaternary gradient pump and an L-7420 (Hitachi) variable wavelength detector. A C_{18} 100 mm × 4.6 mm monolith RP column (Chromolith, Merck) and a C_8 150 mm x 4.6 mm, 5 μm particulate column (Purospher STAR, Merck) were used as stationary phases. Samples were injected into the column using a Rheodyne injector (Model 7725i) having 100 μL sample loop. The post-column reagent (PCR) was added with a reciprocating pump (Eldex Laboratories Inc.) into a low dead volume-mixing tee (Valco). The signal from the detector was processed by HSM software package. A microwave digestion system (Milestone, Italy) was used for carrying out the dissolution of geological sample.

2.2.2.2 Reagents

All solutions were prepared using the deionised water obtained from the Milli-Q system (Millipore). α-hydroxyisobutyric acid (α-HIBA) purchased from Lancaster was used as an eluent. The reagents used as IIRs are sodium n-octanesulphonate (Fluka), sodium n-octane

sulphate (Alfa-Aesar), sodium n-nonanesulphonate (Fluka), n-octadecylsulphonate (Alfa-Aesar) and sodium n-eicosylsulphate (Regis Technologies Inc). A mixture of 14 lanthanides was prepared from the stock solution of individual lanthanide solution. High-purity reagents such as HNO_3, HF, NH_4OH, MeOH, CH_3CN etc. used during the sample treatment and preparation of IIRs were obtained from Merck. Arsenazo(III) (Fluka) was used as a post-column reagent. Geological reference material (SY-3) of Canadian Geological Survey was used for the validation of the separation procedure.

2.2.2.3 Procedure

Stock solution of lanthanides, Th and U: The oxides of lanthanides were dissolved in nitric acid, evaporated to near dryness and stock solutions were prepared in 1 M HNO_3. Ce solution was prepared by treating cerium oxide with nitric acid and reducing Ce (IV) to Ce (III) with hydrogen peroxide. The standardization of lanthanide solutions was done by titrating against standard EDTA solution in a buffer solution of pH 5 using Arsenazo (III) as an indicator. Th solution was also standardized by complexometric titration against standard EDTA solution at pH 3 using xylenol orange as an indicator [111]. U as uranyl was standardized by biamperometric method [112].

Mobile phases for chromatography: Different IIRs viz. C8-sulphonate, C8-sulphate, C9-sulphonate, C18-sulphonate and C20-sulphate were used for the separation of lanthanides with one IIR at a time. Appropriate quantities of C8-sulphonate, C8-sulphate and C9-sulphonate were dissolved in water to prepare 0.1 M solutions. The mobile phase used for the elution of lanthanides under dynamically modified conditions consisted of 7% (v/v) (0.007M) of these IIRs. 2.5×10^{-4} M each of C18-sulphonate and C20-sulphate were prepared in 30% MeOH. All the solutions were filtered through a 0.45 µm Millipore membrane filter before use. HPLC columns were equilibrated by passing required volume of the specific IIR before

carrying out the separation studies. 0.5 M α-HIBA solution of pH 5.0 was used as the eluent. The PCR solution was prepared by dissolving $1.5x10^{-4}$ M Arsenazo (III) and 0.01 M urea in 0.1M HNO_3. All LC experiments were conducted at room temperature (25°C). Flow rates of the mobile phase and PCR solution were 1 mL/min and 0.3 mL/ min, respectively.

Rock sample treatment: SY-3 rock sample (~100 mg accurately weighed) used for the method validation was taken in a mixture of 3 mL conc. HF and 4 mL conc. HNO_3 and subjected to microwave digestion. The digested sample was evaporated to dryness on a hot plate under infra-red lamp. This was further treated repeatedly (3 times) with 5 mL of conc. HNO_3 to remove the excess of fluoride. The residue was taken in ~20 mL buffer of pH 8.5 (2M NH_4NO_3 in NH_4OH) and was warmed to ensure complete precipitation. The precipitate was filtered using 0.45 μm membrane and washed with ~40 mL of buffer solution of pH 7.5. The precipitate was further washed with ~40 mL of 1 M NaOH solution and was transferred into a beaker and dissolved in conc. HNO_3. The contents of the beaker were evaporated to near dryness to remove HNO_3 and finally, the residue was dissolved in 10 mL of mobile phase for HPLC separation.

2.2.3 Results and Discussion

Resolution was determined among various lanthanide pairs under identical chromatographic conditions to find out the effect of carbon chain length of IIRs on the efficiency of separation. The resolution between two adjacent peaks of lanthanides was calculated using the equation given in Chapter 1, Section 1.1.15; $R = 1.18\dfrac{R_{t2} - R_{t1}}{(W_{(1/2)1} + W_{(1/2)2})}$;

where, R_{t1} and R_{t2} are the retention times of the two adjacent peaks 1 and 2, respectively, and W's denote their peak widths at half maximum heights [64].

2.2.3.1 Optimization of IIR Composition

Table 2.1 shows a comparison of resolution among lanthanides separated by a C_{18} RP column (Monolith) modified with C20-sulphonate prepared in 30, 40 and 50% of MeOH with that obtained by the same column modified with C20-sulphonate prepared in 25% acetonitrile. Resolution data obtained for the column modified with C20-sulphate prepared in acetonitrile were found to be poorer as compared to those obtained by the IIR prepared in all the three compositions of MeOH-water [102]. Also, it is obvious from data in the Table that the efficiency of separation of lanthanides decreases with the increase in percentage of MeOH in the IIR loading solution. Thus passing of sufficiently large volume of the IIR solution prepared in higher percentage of MeOH through the column could result in the bleeding of IIR, rather than its adsorption onto the RP surface. The bleeding of IIR is prominent for solutions prepared in acetonitrile has more hydrophobic character than MeOH. Hence further studies were carried out by using C18-sulphonate and C20-sulphate prepared in 30% MeOH since this is the minimum percentage of MeOH required to dissolve the IIRs ($2.5x10^{-4}$ M) in aqueous solution.

Table 2.1: Effect of composition of C20-sulphate solution used as IIR for the separation of lanthanides

Ln pair	Resolution			
	50% MeOH	40% MeOH	30% MeOH	25% ACN
Lu- Yb	0.83	1.18	1.21	0.42
Yb- Tm	1.01	1.62	1.65	0.69
Tm- Er	1.12	1.47	1.59	0.81
Er-Ho	1.40	1.50	1.58	1.02
Ho-Dy	1.28	1.36	1.39	0.90
Dy-Tb	1.69	1.83	1.92	1.32
Tb-Gd	2.20	2.39	2.61	1.55
Gd-Eu	0.97	0.98	1.15	0.50
Eu-Sm	1.24	1.56	1.86	0.76
Sm-Nd	2.39	3.38	4.08	1.38
Nd-Pr	0.82	1.18	1.42	Not resolved
Pr-Ce	1.04	1.63	2.04	1.46
Ce-La	2.08	2.69	3.52	1.44

C_{18} monolith column (100 mm x 4.6 mm) modified by passing 200 mL each of $2.5x10^{-4}$ M C20-sulphate solution prepared in 50, 40 and 30% of MeOH and 25% acetonitrile.
Elution condition: HIBA of pH 5.0 concentration was changed from 0.03 to 0.18 M in 20min.

2.2.3.2 Optimization of the IIR Volume

The data on the changes in the resolution among lanthanides separated by a RP column modified with different volumes of C18-sulphonate solution ($2.5x10^{-4}$ M in 30% MeOH) are given in Table 2.2. It was found that there was a steady improvement in resolution with increase in volume of IIR solution, up to 600 mL. Beyond this volume, no appreciable improvement in the resolution was observed. Thus 600 mL was chosen as the volume of the C18-sulphonate solution to be passed for modifying the column for carrying out comparative

studies with other IIRs. A volume of the IIR solution larger than the optimised volume causes slight decrease in the resolution especially, for lighter lanthanides. This is possibly due to the removal of the adsorbed modifier by the MeOH present in the modifier solution.

Table 2.2: Effect of volume of C18-sulphonate IIR solution on the separation of lanthanides

Ln pair	Resolution obtained after passing different volumes of C18-sulphonate (mL)				
	100	**300**	**500**	**600**	**800**
Lu- Yb	1.10	1.27	1.37	1.62	1.61
Yb- Tm	1.39	1.71	1.83	2.22	2.25
Tm- Er	1.44	1.77	1.63	2.20	2.18
Er-Ho	1.70	2.10	1.73	2.33	2.33
Ho-Dy	1.66	2.10	1.82	2.27	2.32
Dy-Tb	2.23	2.74	2.57	3.09	3.09
Tb-Gd	2.75	3.57	3.80	4.08	3.95
Gd-Eu	1.16	1.63	1.95	1.91	1.82
Eu-Sm	1.39	2.01	2.68	2.30	2.23
Sm-Nd	2.14	3.68	5.29	4.20	3.79
Nd-Pr	0.51	1.27	2.26	1.81	1.73
Pr-Ce	0.70	1.56	2.79	2.11	2.05
Ce-La	0.91	2.80	4.47	3.30	3.18

RP column modified by C18-sulphonate ($2.5x10^{-4}$ M prepared in 30% of MeOH). Elution conditions were same as those given in Table 2.1.

Similarly, the effect of volume of C20-sulphate IIR solution ($2.5x10^{-4}$ M in 30% MeOH) on the resolution for the separation of lanthanides was determined and the data are given in Table 2.3. The optimum volume of the C20-sulphate IIR solution required for conditioning

the column to obtain good resolution for the separation of lanthanides was found to be 600 mL.

Table 2.3: Effect of volume of C20-sulphate solution on the separation of lanthanides

Ln pairs	Resolution obtained after passing different volumes of C20-sulphate (mL)			
	200	**400**	**600**	**800**
Lu- Yb	1.13	1.18	1.21	1.19
Yb- Tm	1.46	1.62	1.65	1.63
Tm- Er	1.35	1.47	1.59	1.42
Er-Ho	1.34	1.50	1.58	1.40
Ho-Dy	1.23	1.36	1.39	1.26
Dy-Tb	1.68	1.83	1.92	1.70
Tb-Gd	2.22	2.39	2.61	2.24
Gd-Eu	0.91	0.98	1.15	1.02
Eu-Sm	1.49	1.56	1.86	1.69
Sm-Nd	3.45	3.38	4.08	3.65
Nd-Pr	1.18	1.18	1.42	1.30
Pr-Ce	1.60	1.63	2.04	1.87
Ce-La	2.69	2.69	3.52	3.08

A RP column modified using C20-sulphate ($2.5x10^{-4}$M prepared in 30% of MeOH). Elution conditions were same as those given in Table 2.1.

2.2.3.3 Optimisation of Washings with Water

The stationary phase coated with IIR was washed with different volumes of water and the change in the resolution for the separation of lanthanides at regular intervals was noticed. Table 2.4 shows the change in the resolution among the lanthanide pairs separated by a column modified with C18-sulphonate with progressive washings with water. It is seen that

the resolution improves after washing the C18-sulphonate coated column with water. This improvement in the efficiency of the coated column with the passage of water was observed to continue up to 700 mL of water and was attributed to the increase in the available surface area resulting from better orientation of the IIR molecules on the RP surface. However, when a very large volume (>700 mL) of water was passed, the hydrophobic moiety of the IIR molecules could undergo shrinkage and this might be the reason for the slight decrease in resolution.

Table 2.4: Effect of volume of water passed through C18-sulphonate coated column on the separation of lanthanides

Ln pairs	Resolution values obtained after passing different volumes of water (mL)				
	100	**200**	**400**	**700**	**1600**
Lu- Yb	1.67	1.75	1.92	1.99	1.73
Yb- Tm	2.22	2.36	2.61	2.77	2.49
Tm- Er	2.33	2.47	2.73	3.04	2.64
Er-Ho	2.59	2.84	3.03	3.49	3.01
Ho-Dy	2.55	2.82	3.07	3.37	3.01
Dy-Tb	3.33	3.41	3.95	4.35	4.01
Tb-Gd	4.24	4.46	5.23	5.68	5.63
Gd-Eu	1.93	2.05	2.36	2.67	2.73
Eu-Sm	2.44	2.78	3.03	3.63	3.78
Sm-Nd	4.43	5.24	5.81	6.92	7.05
Nd-Pr	1.80	1.89	2.22	2.65	3.02
Pr-Ce	2.12	2.42	2.79	3.45	4.13
Ce-La	3.26	3.46	4.14	5.18	6.12

A RP column modified by passing 600 mL of C18-sulphonate ($2.5x10^{-4}$ M prepared in 30% of MeOH).

Elution conditions were same as those given in Table 2.1.

In a similar way, the volume of water required to be passed through the C20-sulphate coated column for the separation of lanthanides was optimised and was found to be 1000 mL.

While studying the effect of washings with water, it was observed that the relative change in the resolution among the lighter lanthanide (late eluting) pairs is 5-20 times higher than the corresponding change observed with heavier (early eluting) lanthanides. Since lighter lanthanides reside longer in the column, they have the opportunity for better equilibration with the mobile phase containing the eluent (0.03 M α-HIBA) resulting in an enhanced improvement in resolution as compared to heavier lanthanides. This observation indicated that there is a need for optimizing the eluent mobile phase volume required for conditioning the coated column for maximizing the resolution possible with a given IIR.

2.2.3.4 Optimization of Washings with Mobile Phase

Table 2.5 shows the changes in the resolution among the lanthanides with progressive washings using mobile phase containing α-HIBA. A RP column coated by passing 600 mL of C18-sulphonate solution and subjected to 1600 mL of water washing was employed for this study. It was found that lanthanides were separated with enhanced resolution when chromatographic runs were performed after conditioning the C18-sulphonate coated column with 30 mL and 70 mL of the mobile phase (0.03 M α-HIBA).Though conditioning of the column with 70 mL of the mobile phase gave slightly better resolution than that obtained by using 30 mL, the relative improvement in resolution for various pairs of lanthanides is less than 5%. Considering that each chromatographic run is to be taken after conditioning with the mobile phase, this improvement in resolution is not a significant gain. Thus, 30 mL of 0.03 M HIBA was chosen for the final conditioning of the C18-sulphonate coated column.

Table 2.5: Effect of mobile phase conditioning of C18-sulphonate coated column on the separation of lanthanides

Ln pair	Resolution obtained after passing different volumes of mobile phase for conditioning (in mL)		
	10	**30**	**70**
Lu- Yb	1.77	1.84 (4)*	1.84 (4) *
Yb- Tm	2.40	2.50 (4)	2.49 (4)
Tm- Er	2.52	2.73 (8)	2.74 (9)
Er-Ho	3.01	3.09 (2)	3.12 (4)
Ho-Dy	3.16	3.12 (1)	3.16 (0)
Dy-Tb	4.05	4.09 (1)	4.30 (6)
Tb-Gd	5.46	5.63 (3)	5.82 (7)
Gd-Eu	2.65	2.64 (0)	2.53 (4)
Eu-Sm	3.74	3.53 (6)	3.48 (7)
Sm-Nd	7.11	6.81 (4)	6.75 (5)
Nd-Pr	2.82	2.74 (3)	2.84 (1)
Pr-Ce	3.87	3.92 (1)	3.95 (2)
Ce-La	6.05	6.05 (0)	6.14 (2)

** Percentage change with respect to the resolution obtained by conditioning with 10 mL of the mobile phase.*
Elution conditions were same as those given in Table 2.1.

2.2.3.5 Comparison of Resolution Data using Different IIRs

Table 2.6 presents a comparison of resolution values obtained for the separation of lanthanides using C8-sulphate, C8-sulphonate, C18-sulphonate and C20-sulphate under identical chromatographic conditions. C-8 sulphate and C-8 sulphonate were included in the study for identifying the influence of the different functional groups on the resolution of lanthanides. As it is seen from the Table, both C8-sulphate and C8-sulphonate gave

comparable performances indicating that no significant improvement in separation is contributed by the functional group difference (i.e., sulphate and sulphonate).

Table 2.6: Comparison of resolution for the separation of lanthanides using column modified with different IIRs

Ln pair	Resolution			
	C8-sulphonate	C8-sulphate	C18-sulphonate	C20-sulphate
Lu- Yb	1.61	1.55	1.99	1.21
Yb- Tm	1.81	1.79	2.77	1.65
Tm- Er	1.77	1.70	3.04	1.59
Er-Ho	1.90	1.91	3.49	1.58
Ho-Dy	1.86	1.96	3.37	1.39
Dy-Tb	2.42	2.47	4.35	1.92
Tb-Gd	3.42	3.52	5.68	2.61
Gd-Eu	1.63	1.72	2.67	1.15
Eu-Sm	2.31	2.48	3.63	1.86
Sm-Nd	4.72	4.63	6.92	4.08
Nd-Pr	1.75	1.79	2.65	1.42
Pr-Ce	2.32	2.29	3.45	2.04
Ce-La	3.73	3.70	5.18	3.52

IIRs used: 0.007M each of C8-sulphate, and C8-sulphonate; $2.5x10^{-4}$ M each of C18-sulphonate and C20-sulphate (prepared in 30% MeOH).

Elution conditions were same as those given in Table 2.1.

C20-sulphate was expected to have the strongest adsorption onto the stationary phase and provided the highest resolution as compared to C18-sulphonate. However, C18-sulphonate was found to give better resolution for the separation of lanthanides compared to C20-sulphate. The chemically bonded octadecyl group in the reversed phase (C_{18}) of the

monolith column and the C18-sulphonate used for the ion exchange modification contain the same number of carbon atoms. This similarity would cause better adsorption and orientation of the modifier on the stationary phase.

In order to confirm this interpretation, RP columns based on C_8 and C_{18} were compared for the improvement in separation of lanthanides when the IIR was changed from C8-sulphonate to C9-sulphonate. Table 2.7 shows the data on the resolution of lanthanides separated on RP columns based on C_8 and C_{18} under dynamically modified conditions employing C8-sulphonate and C9-sulphonate as IIRs.

For both types of stationary phases, C9-sulphonate gave better resolution for the separation of lanthanide ions indicating the dominance of hydrophobicity. However, it is seen that for most of the adjacent lanthanide pairs, relative change in resolution obtained using C9-sulphonate with respect to C8-sulphonate (R^1_9/R^1_8) is higher for C_{18} column as compared to the corresponding values obtained for C_8 column (R_9/R_8). This observation supports our interpretation of enhancement in resolution due to increased hydrophobicity while changing from C8-sulphonate to C9-sulphonate using C_{18} column. In the case of C_8 column, the preference of the C_8 stationary phase for an IIR having equal number of carbon atoms in its chain, could be responsible for partially offsetting the expected enhancement in (R_9/R_8). When C18-sulphonate and C20-sulphate were used as the IIRs in combination with C_{18} stationary phase, the degree of hydrophobicity is comparable for these two modifiers. Hence the resolution for the separation of lanthanides is influenced more by the preference of the stationary phase for the IIR having equal number of carbon atoms in its chain.

Table 2.7: Comparison of resolution for the separation of lanthanides using C_8 and C_{18} columns modified with C8-sulphonate and C9-sulphonate

Ln pair	Resolution obtained for the C_8 column using the IIR			Resolution obtained for the C_{18} column using the IIR		
	C8-sulphonate (R_8)	C9-sulphonate (R_9)	(R_9/R_8)	C8-sulphonate (R^1_8)	C9-sulphonate (R^1_9)	(R^1_9/R^1_8)
Lu- Yb	2.4	1.94	0.81	1.61	1.71	1.06
Yb- Tm	2.88	2.87	1.00	1.81	2.4	1.33
Tm- Er	3.04	3.15	1.04	1.77	2.36	1.33
Er-Ho	2.42	3.58	1.48	1.9	2.63	1.38
Ho-Dy	2.7	3.89	1.44	1.86	2.66	1.43
Dy-Tb	4.17	4.91	1.18	2.42	3.47	1.43
Tb-Gd	5.72	6.52	1.14	3.42	4.96	1.45
Gd-Eu	2.98	3.38	1.13	1.63	2.42	1.48
Eu-Sm	3.99	4.41	1.11	2.31	3.25	1.41
Sm-Nd	7.55	8.70	1.15	4.72	6.22	1.32
Nd-Pr	2.32	3.92	1.69	1.75	2.67	1.53
Pr-Ce	3.48	5.08	1.46	2.32	3.23	1.39
Ce-La	7.93	8.00	1.01	3.73	5.16	1.38

Resolutions calculated from the chromatograms recorded under dynamically modifying condition by passing 0.007 M each of C8-sulphonate and C9-sulphonate.
Elution conditions were same as those given in Table 2.1.

In view of the high separation efficiency and stability of adsorption, C18-sulphonate was chosen as the IIR for carrying out the further separation studies. The chromatogram of separation of 14 lanthanides on a RP column modified with C18-sulphonate and conditioned as per the procedures discussed above is given in Fig. 2.1. It is seen that all the peaks are base-line separated and display good peak shapes indicative of excellent mass-transfer of lanthanide ions between the mobile phase and the coated ion-exchanger.

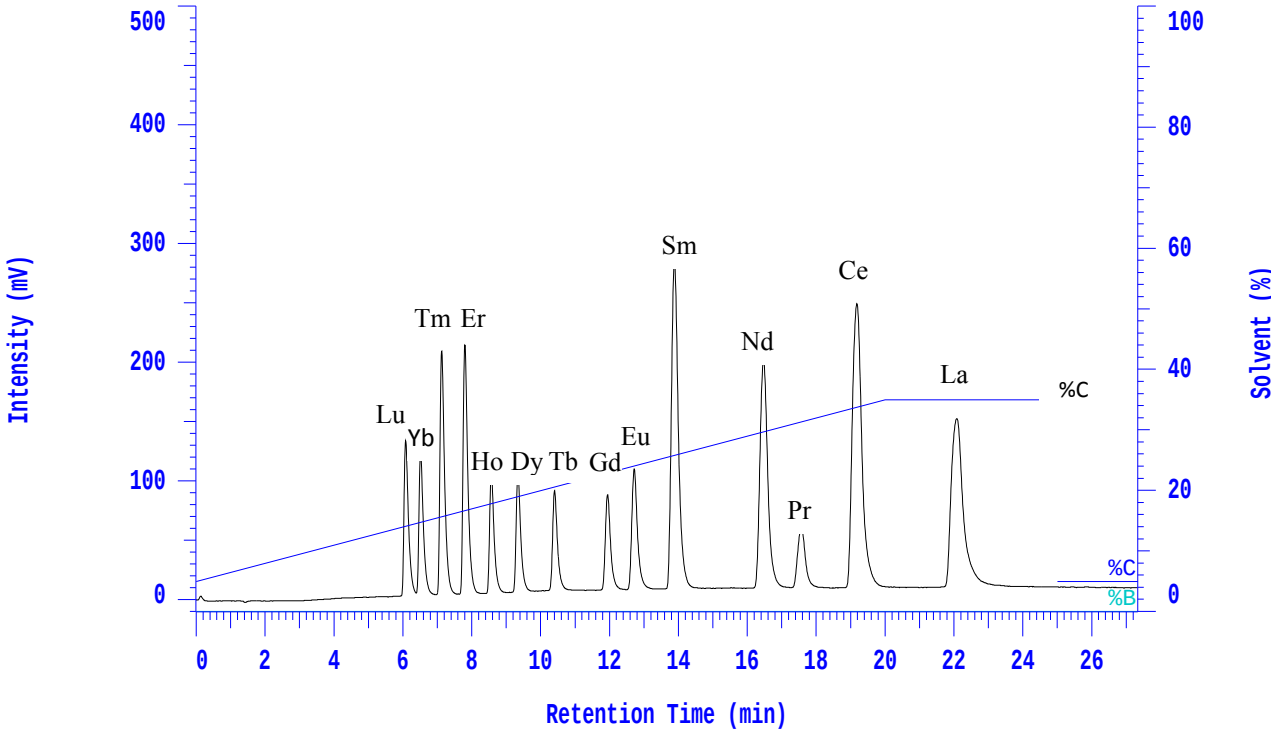

Figure 2.1: *Separation of 14 lanthanides on a C_{18} column coated with C18-sulphonate. Stationary phase: C_{18} Chromolith (100 mm x 4.6 mm) was modified by passing 600 mL of C18-sulphonate prepared in 30% MeOH followed by washing with 700 mL water and 30 mL of mobile phase. Elution conditions: HIBA of pH 6.0 [C] was changed from 0.03 to 0.35 M in 20 min.*

2.2.3.6 Application of the Method for Geological Sample

The utility of the excellent resolution obtained by the developed method was demonstrated by the separation of lanthanides in a complex matrix such as geological samples. Figure 2.2 shows the chromatogram obtained for the separation of Fe, lanthanides, Th and U on a C18-sulphonate modified column using a geological reference material (SY-3). The gradient condition was changed to dual (concentration and pH) gradient conditions as given in Table 2.8 to allow the sequential separation of Fe, lanthanides, Th and U. Table 2.9 shows the data on the concentration of lanthanides determined by this method. Dy could not be determined in this sample due to its overlapping with Y using HIBA as the complexing agent. As the digested sample was not subjected to extensive purification procedure for the isolation of rare-earth fractions, the chromatogram contains other peaks also. Good resolution

obtained by the optimised procedure allowed the separation and quantitation of lanthanides which were present in widely differing proportions.

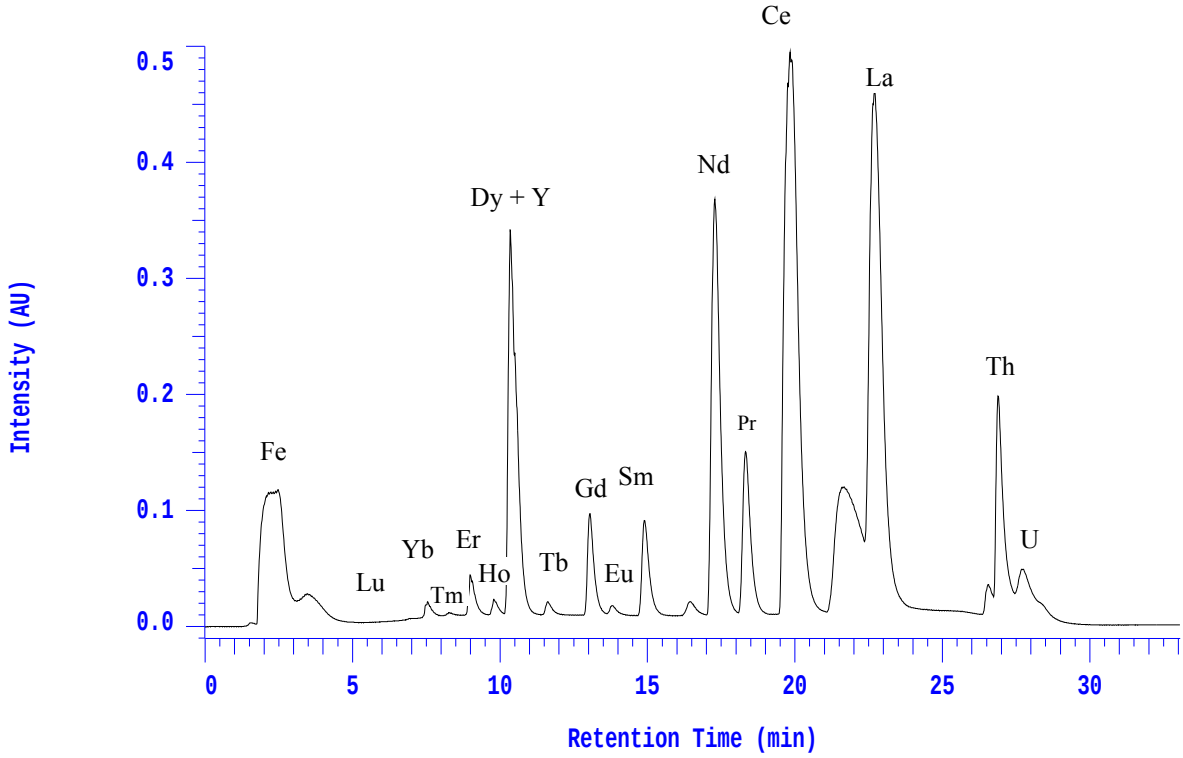

Figure 2.2: *Sequential separation of Fe, lanthanides, Th and U from a geological reference material (SY-3) on C18-sulphonate coated C_{18} column. Stationary phase modification: same as in Fig. 2.1; Elution conditions: Same as given in Table 2.8.*

Table 2.8: Gradient conditions for separation of Fe, lanthanides, Th and U

Time (min)	Concentration of α-HIBA at pH 5.5 (M)	Concentration of α-HIBA at pH 2.0 (M)
0	0.03	0
20	0.35	0
25	0	0.6
30	0	0.6

Table 2.9: Determination of lanthanides in SY-3 sample

Element	Recommended concentration (ppm)	Determined concentration (ppm)	RSD (%)*
La	1340	1432	16
Ce	2230	2195	4
Pr	223	219	10
Nd	670	661	1
Sm	109	105	7
Eu	17	18	3
Gd	105	104	3
Tb	18	20	6
Dy	118	ND	-
Ho	29.5	27	7.8
Er	68	65	3.7
Tm	11.6	10	4.6
Yb	62	58	8.1
Lu	7.9	6	10.3

ND: Not determined
** Relative standard deviation from triplicate runs.*

2.2.3.7 Long-term Adsorption and Reproducibility of Coating

Long term stability of adsorption of C-18 sulphonate modifier on to the RP stationary phase was confirmed by monitoring the separation of lanthanides under identical conditions over a period of two months. The modified column was given a conditioning with the mobile phase before each chromatographic run. The modified column showed consistent resolution for all the pairs of lanthanides indicating the efficacy of C18-sulphonate for the long term modification of reverse-phase to obtain high resolution separation of individual lanthanide.

Table 2.10 shows the average resolution for lanthanides obtained from chromatograms recorded over a period of two months. It is seen that the C18-sulphonate coating over the stationary phase is quite stable as indicated by the reproducibility (RSD 2-8%) of resolutions among lanthanide peaks. The reproducibility of the coating procedure using C18-sulphonate was verified by removing the coating completely from column by washing with methanol, re-modifying the column by passing the IIR solution, followed by water and mobile phase washings. Reproducible data *(better than 10%)* on resolution were obtained for the separation of lanthanides performed with these re-coated columns.

Table 2.10: Long-term performance of C_{18} monolith column coated with C18-sulphonate

Ln pair	Mean value of resolution	RSD (%)*
Lu- Yb	1.7	8
Yb- Tm	2.4	6
Tm- Er	2.5	8
Er-Ho	2.7	5
Ho-Dy	2.7	6
Dy-Tb	3.7	3
Tb-Gd	4.9	2
Gd-Eu	2.3	2
Eu-Sm	3.4	5
Sm-Nd	6.9	7
Nd-Pr	2.7	5
Pr-Ce	3.8	6
Ce-La	6.2	6

**Relative standard deviation (RSD) calculated from eight chromatograms recorded over a period of two months.*

2.3 Direct Determination of Lanthanides in Thoria Matrix

2.3.1 Background

The Indian nuclear energy programme aims at large-scale utilizations of thorium for the sustained production of electricity in the country and this requires development of new technologies in thorium based nuclear fuel cycle [113,114]. Burn-up is an important parameter for the irradiated nuclear fuel studies and is used to denote the atom percent fission of heavy elements (mass >225) during the life of the fuel in a nuclear reactor [29,53,115,116]. Experimental determination of burn-up provides a relevant database for the development and validation of theoretical codes [106,117]. This involves the determination of total heavy element composition after irradiation and the concentration of a suitable fission product (used as a burn-up monitor) to determine the total number of fissions in the fuel [118]. For fuels based on U and Th, stable fission product ^{139}La meets the selection criteria required for the burn-up monitor [119]. Chemical analysis techniques can be used for its determination since La is produced almost mono-isotopically during the fission [120]. Separation of Nd is also important for minimizing the isobaric interference during the burn-up determination by thermal ionisation mass spectrometry.

Most of the reported methods dealt with those types of samples where the concentrations of lanthanides, Th or U were in similar proportions [121,122]. Some of the reported HPLC methods for the determination of burn-up involve preliminary separation of lanthanides or fission products from the bulk of the fuel matrix elements [29,101]. The separation steps to isolate the fission product(s) pose the risk of contamination of the sample and also make the process cumbersome. Direct HPLC methods in which irradiated fuel dissolver sample is injected to the column, without any prior separation, have also been reported for the determination of burn-up of ThO_2-UO_2 and UO_2 fuels [53,119]. However, as Th and U are

present in large proportions compared to lanthanides, the matrix element peaks can mask some of the early eluting lanthanides [109].

Work presented in this Section explores the possibility of interference free and sequential elution of lanthanides in presence of large amounts of Th and U. The pH of the eluent and the concentration of ion interaction reagent were found to play a vital role in deciding the capacity of the column to retain Th and thus control its elution. Since the elution of matrix elements takes place after the elution all the lanthanides, the method allows the use of a minor fission product (Tb) as an internal standard for the precise quantification of fission monitors, La and Nd, along with other lanthanide fission products. The relative ratios of the detector response of fission product lanthanides to that of Tb would give the concentration of lanthanides in a single run.

2.3.2 Experimental

2.3.2.1 HPLC System

The HPLC system with the post-column detection system derivatisation used for the separation studies was described in Section 2.2.2.1. The samples were injected using a Rheodyne injector (7725i) with 100 μL loop. 150 mm x 4.6 mm C_{18} particulate column (Supelcosil, Supelco) and 100mm x 4.6 mm C_{18} monolith column (Performance, Merck) were used for carrying out the separation studies. A pH meter (PHAN, Labindia) was used for monitoring pH.

2.3.2.2 Reagents

α-Hydroxyisobutyric acid (HIBA) (Fluka) was used as the eluent. Sodium n-octane sulphonate monohydrate (Fluka) was used as the IIR. The oxides of lanthanides (La, Ce, Pr,

Nd, Sm, Eu and Tb) and the nitrate salts of Th and U were used for preparing the respective stock solutions. HNO_3 and NH_4OH (Merck) were used for adjusting the pH.

2.3.2.3 Procedure

Preparation of stock solutions of lanthanides, Th and U, the mobile phase and PCR was done as discussed in Section 2.2.2.3 of this Chapter. Throughout the experiment, flow rates of the mobile phase and PCR were kept at 1mL min^{-1} and 0.3 mL min^{-1}, respectively. Initially, the studies were carried out using simulated samples to develop and validate the method. An estimated burn-up value was used for arriving at the concentrations of lanthanides to be used for preparing simulated samples. Simulated fission product mixtures containing lanthanides (La, Ce, Pr, Nd, Sm, Eu and Gd) and Th and U were prepared for 0.5, 1 and 2 atom% burn-up using their fission yield data [124]. A dissolved solution of irradiated $(Th,Pu)O_2$ fuel sample with ~ 1.5 atom% fission was used for the analysis by optimized LC method. Quantification of lanthanides present in the synthetic mixtures as well as the dissolved fuel solution was achieved using relative response of peak areas of lanthanides to that of internal standard (Tb).

2.3.3 Results and Discussion

2.3.3.1 Effect of Ion Interaction Reagent (IIR) Concentration on Retention of Lanthanides, Th and U

La and Lu were used as representative elements for lanthanides and mixed with similar proportions of Th and U. At higher pH (>5), the peak shapes of Th and U were too broad to determine the exact retention times. Hence, a lower pH (4.0) of HIBA was chosen for carrying out this study. Figure 2.3 shows the effect of concentration of IIR on the elution of lanthanides, Th and U. The effect is represented in terms of retention factor (k) which is defined in Chapter 1, Section 1.1.15. In the absence of an IIR, the HIBA complexes of

lanthanides showed no interaction with the hydrophobic RP column and eluted together as a group near the solvent front.

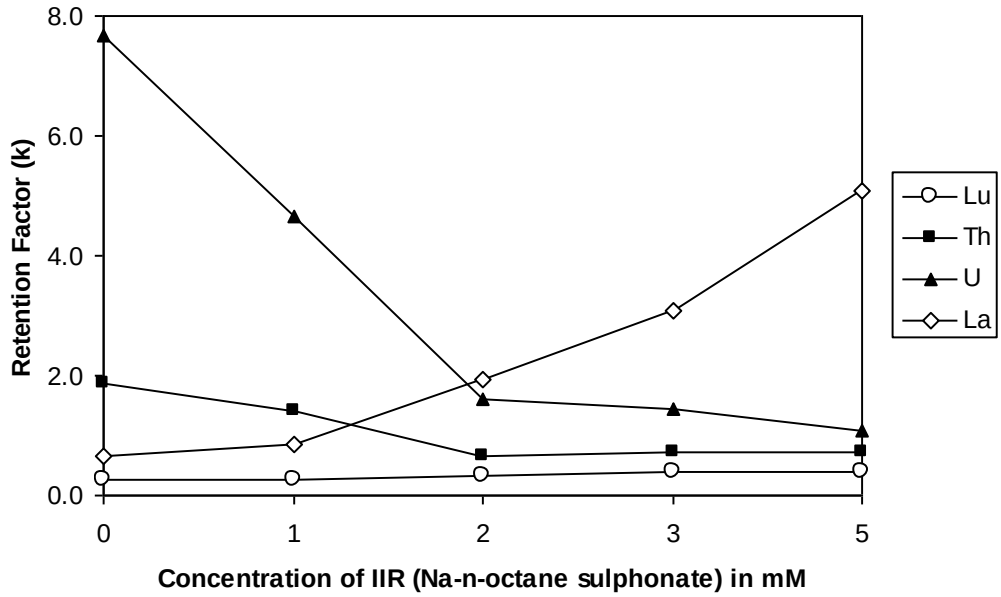

Figure 2.3: *Effect of concentration of IIR on the retention of Lu, La, Th and U. Chromatographic conditions: 0.2 M of HIBA at pH 4.0 using 10 cm monolith C_{18} column.*

HIBA complexes of Th and U displayed a hydrophobic nature as indicated by their greater retention at lower concentrations of IIR. With increase in modifier concentration, the increased sorption of hydrophobic anions on the reversed phase resulted in decreasing the retention of Th and U. On the other hand, the increase in modifier concentration increased the ion exchange capacity of reversed phase column and thereby increased the retention from Lu to La. At IIR concentrations above 0.002 M, both Th and U eluted between Lu and La and an increase of IIR concentration up to 0.05 M did not change this elution trend. Furthermore, no change in the retention time of the studied ions was observed from 0.02 to 0.05 M indicating the possibility of saturating the RP column with hydrophobic anions.

From the above studies, it was clear that a practical strategy for the determination of lanthanides in irradiated Th based fuels would be to retain Th on the stationary phase till all

the lanthanides are eluted. This suggested that the sensitivity of the method depends on the amount of Th that can be held on the column before the elution of La takes place. Hence, the studies were carried out for maximizing the Th load on stationary phase. Further studies were, therefore, carried out on the longer (Supelcosil, 150 mm x4.6 mm) column, which would offer a higher capacity.

2.3.3.2 Th Holding Capacity of RP Column

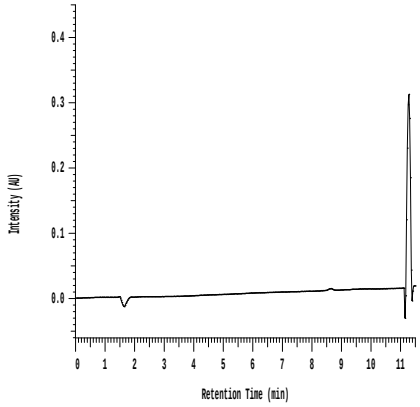

Figure 2.4a

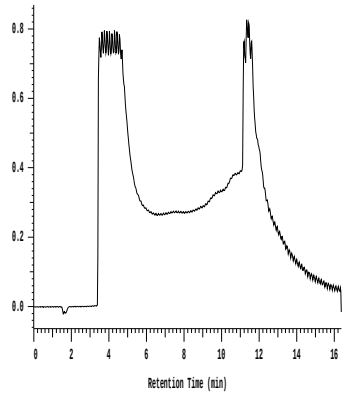

Figure 2.4b

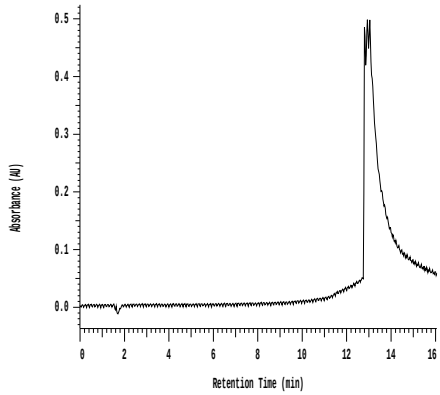

Figure 2.4c

Figures 2.4: *Elution of Th under the conditions:*
a) 1 μg of Th using gradient as mentioned in Table 2.8.
b) 200 μg of Th under same condition as given in Table 2.8.
c) 400 μg of Th using optimized gradient as given in Table 2.11.

Chromatograms obtained for Th under different conditions are represented in Fig. 2.4. Dual gradient of concentration and pH of HIBA was employed for the sequential elution of lanthanides, Th and U as given in Table 2.8. [109]. Fig. 2.4a shows the typical chromatogram obtained for Th using dual gradient of α-HIBA, when it is present in small amounts (1 μg). When the lanthanides are to be determined in irradiated thoria-based fuel samples, much larger amount of Th needs be injected as no pre-separation of matrix elements (U and Th) is involved. However, when the amount of Th loaded onto the column is high (>100 μg), it was observed to elute at two different retention times (Rt 3.5 and 11.5 min). Fig. 2.4b shows the chromatogram obtained by injecting 200 μg of Th under the same elution conditions as in Fig. 2.4a. The size of the first peak (Rt 3.5 min) was found to increase with the increase in Th

amount and would mask some of the lanthanide peaks. The reason for Th to elute out as two peaks may be due to the lack of adequate capacity of the column to quantitatively retain Th. Elution of Th at a relatively longer time as a single peak is desired, as it would not interfere with early eluting lanthanide peaks. Hence, conditions under which Th eluted as a single band with retention time greater than that of La (as in Fig. 2.4a) were considered for the capacity of Th.

2.3.3.2.1 Effect of Concentration of IIR on Th Holding Capacity of RP Column

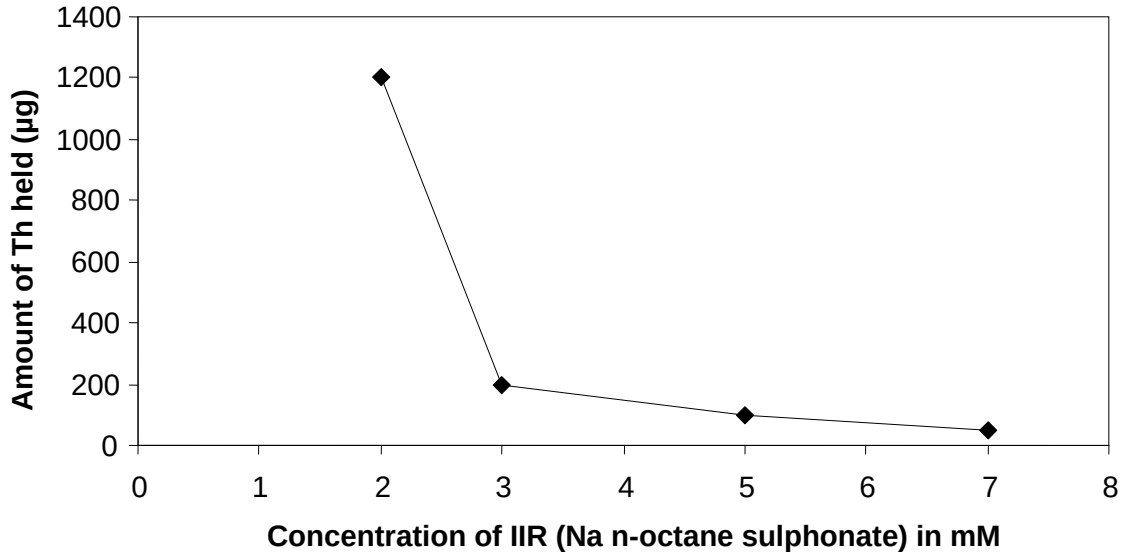

Figure 2.5: *Effect of concentration of IIR on the amount of Th retained on RP column. Conditions: 0.15 M of HIBA at pH 5.5 using 15 cm x 4.6 mm C_{18} column.*

Figure 2.5 shows the amount of Th that can be held on a RP column as a function of concentration of IIR. If the amount of Th injected at a given concentration of IIR exceeds this limiting value, then a second peak appears for Th at retention times closer to those of early eluting lanthanides. HIBA of pH 5.5 was used for carrying out the studies. The capacity for retention of Th (without the appearance of a second peak) was found to increase significantly with lowering the concentration of IIR in the mobile phase. Hence, minimum concentration of

IIR was preferred from the point of view of holding the maximum amount of Th in the column. However, a certain concentration of IIR in the mobile phase is essential to bring about the retention and hence the individual separation of lanthanides (as seen in Fig. 2.3). Considering these factors, the concentration of sodium n-octanesulphonate (IIR) was chosen as 3 mM for carrying out further studies.

2.3.3.2.2 Effect of pH of Eluent on the Th Capacity

The limiting amount of Th injected to the RP column modified with 3 mM sodium n-octanesulphonate, at different pH values of HIBA is shown in Fig. 2.6. It is seen that the pH of HIBA is a crucial factor in deciding the amount of Th retained on the modified column. The capacity for holding Th (without the appearance of a broad, early eluting peak) increased with the increase in pH and reached a plateau value at pH > 6. This can be correlated with the ionisation of HIBA having pKa of 3.77 [123]. Practically, no appreciable change occurs in the composition of ionized HIBA after pH 6 and hence, no change in the capacity for Th. In view of the maximum capacity, optimum pH of 6.2 to 6.5 was chosen. At this pH (6.2 to 6.5) condition, total of 0.4 mg of Th could be retained on the 15 cm RP column without the appearance of a second peak at optimum IIR concentration of 3 mM (Fig. 2.4c). Th was eluted as a single tight peak with retention time well beyond that of La.

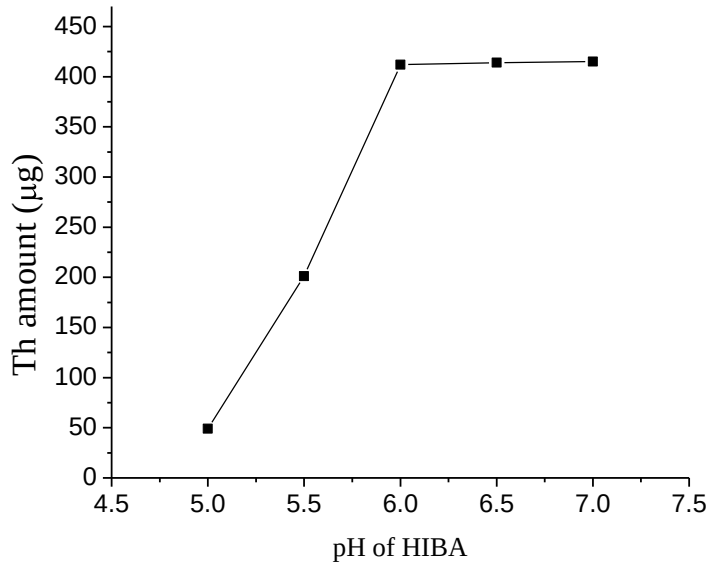

Figure 2.6:*Effect of pH of HIBA on the amount of Th retained on RP column.*
Conditions: 3 mM sodium n-octanesulphonate as IIR. Other conditions were same as in Fig.2.5.

2.3.3.3 Separation of Fission Products from Thorium

Dual gradient elution was employed to yield the separation of lanthanides from Th and U along with better resolution amongst lanthanides. This was achieved by employing concentration gradient of HIBA (pH 6.2) for separating individual lanthanides and for retaining Th and U onto the stationary phase. After their separation, low pH HIBA was introduced for the elution of Th and U. The optimized chromatographic conditions are given in Table 2.11.

Table 2.11: Optimized conditions for separation of lanthanides in presence of large amounts of Th

Time (min)	Concentration (M) of α-HIBA at pH 6.2	Concentration (M) of α-HIBA at pH 2.0
0	0.08	0
6	0.13	0
8	0.17	0.4
17	0.17	0.4

Other chromatographic conditions were same as in Fig. 2.6.

Simulated thorium samples containing fission products as per different burn-ups were injected in to the HPLC system under the optimized separation conditions. Figure 2.7 shows the chromatogram of lanthanides, U and Th from a simulated sample of thoria with 1atom% burn-up under the optimized gradient conditions as given in Table 2.11. Separation of lanthanides was completed before the matrix elements started eluting from 11 min and took further 5 min for their complete removal from the column. Hence, the complete chromatographic separation took 16 min for completion. The dual gradient elution yielded fast separation of lanthanides with sharp, symmetric peaks and with base-line resolution. Since Th was retained using high pH (6.2) in the early stage and then eluted strongly by drastic change in pH, it eluted out as a sharp peak in spite of its large amount (260 μg). As U is eluted after Th, the separation amongst them becomes difficult due to the large amount of Th and drastic eluting conditions.

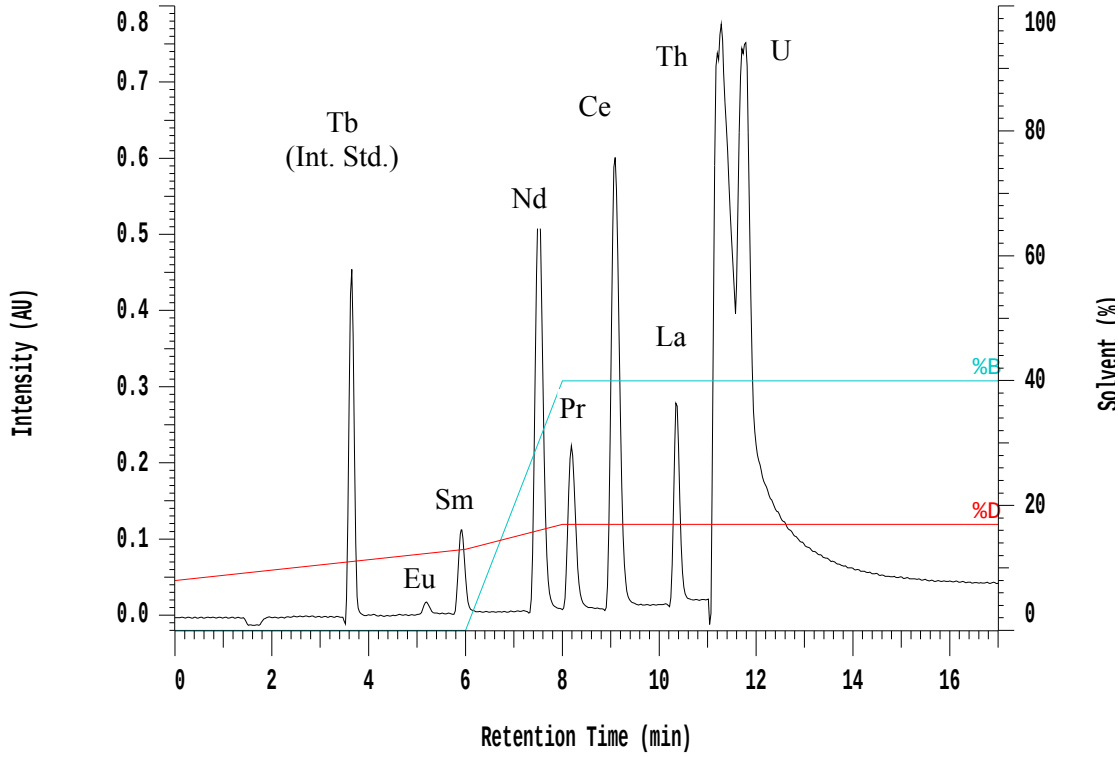

Figure 2.7: *Separation of lanthanides, Th and U in simulated 1 atom% burn-up solution using dual (concentration and pH) gradient. Elution conditions used are given in Table 2.11.*

Only La, Ce, Pr, Nd, Sm, and Eu were included in the mixture as the fission yields of other lanthanides are very low and hence are not possible to detect in the real life samples. Most of the other fission products do not form complex with Arsenazo (III) and hence, do not interfere with lanthanide determinations using photometric detection. This has also been confirmed by injecting 100 ppm each of Rb, Sr, Y, Zr, Nb, Mo, Ru, Rh, Pd, Cs, and Ba under the optimized conditions. The chromatogram obtained for all these non-rare-earth elements yielded no signal above the noise level until 12 min. i.e., in the region where lanthanides, Th and U are expected to elute. Table 2.12 gives the typical composition of dissolver solution of irradiated thoria sample with burn-up 1atom% fission calculated based on the yield of fission products.

Table 2.12: Chemical composition of dissolver solution of irradiated thoria sample

Element	Concentration (ppm)	Element	Concentration (ppm)
Rb	1.8	La	1.1
Sr	3.3	Ce	2.2
Y	1.8	Pr	1.12
Zr	8.5	Nd	3.0
Mo	5.3	Pm	0.3
Ru	2.8	Sm	0.2
Rh	0.4	Eu	0.03
Pd	0.1	Gd	0.003
Cs	3.3	Th	2600
Ba	1.0	U	38

Reference[124]

The concentrations of lanthanides added to form simulated Th sample with burn-ups 0.5, 1 and 2 atom% are given in Table 2.13. For all these samples, the amount of Th injected into the column was kept at 260 µg (below the maximum capacity).

Table 2.13: Concentrations of lanthanides, U &Th in simulated samples

Element	Concentration (ppm)		
	SS-I*	SS-I1*	SS-1II*
La	0.56	1.07	1.98
Ce	1.16	2.24	4.12
Pr	0.58	1.12	2.06
Nd	1.61	3.09	5.68
Sm	0.29	0.56	1.03
Eu	0.06	0.12	0.21
Th	2600	2600	2600
U	40	40	40
Tb[#]	0.80	0.80	0.80

** SS-I, II & III correspond, respectively, to simulated samples of thoria with burn-up of 0.5, 1 & 2 atom% fission.*

[#] used as internal standard.

2.3.3.4 Quantification of La and Nd

The detector response of lanthanides varies depending on the eluent and PCR flow rates, magnitude of pump pulsations, which may change from time to time. Though the short term repeatability was satisfactory, the precision among the data recorded over long durations (>5 hrs) worsened indicating the need of running fresh calibrations. This problem was circumvented by employing internal standard (Tb). Tb meets the conditions required for an internal standard for the quantification of lanthanides in burn-up sample [29]. Its fission yield is insignificant in the nuclear fission of U and Th based fuels [124]; it shows identical chromatographic behaviour as that of lanthanide fission products; and is well resolved from other fission products including Y during HPLC separation. Nd and La are used as the fission monitors for the burn-up determination of thoria based fuels. These two elements were chosen as the representatives of lanthanides for quantification. Table 2.14 shows the concentrations of La and Nd determined by using internal standard method.

Table 2.14: Quantification of La and Nd determined (in ppm) using internal standard

Element	**Amount**	**Sample**		
		SS-I*	**SS-I1***	**SS-1II***
La	Added	55.9	107.4	197.6
	Determined (without I.S.)	62.2±5.1	112.8±3.1	193.4±5.7
	Determined (with I.S.)	55.4±0.8	105.8±1.3	196.1±0.9
Nd	Added	160.7	308.8	568.3
	Determined (without I.S.)	171.8±5.8	323.3±3.1	556.2±5.3
	Determined (with I.S.)	159.6±1.4	312.2±0.7	560.9±0.9

** SS-I, II & III correspond, respectively, to simulated samples of thoria with burn-up of 0.5, 1 & 2 atom% fission.*

The three simulated samples were repeatedly analysed over a period of two weeks and during this period, the mobile phase and the PCR solution were changed three times. The overall precision for the determination of La and Nd concentrations by internal standard method was found to be better (< 2%) for all the three samples compared to the peak area precisions. The detection limit of the method was 3 ng for La. Since quantification is carried out using Tb as an internal standard and all lanthanide ions exhibit similar chemical properties, it is expected that similar precision and accuracy would be obtained for other lanthanides also. The method used is fast and cost effective as compared to classical ID-TIMS methodology. Since HPLC (which is not coupled to MS detector) does not give any information about the isotopic composition of the separated elements, ^{148}Nd cannot be used as a burn-up monitor in this approach. However, one could use total Nd as a burn-up monitor. No such difficulty arises for La since it is produced almost mono-isotopic (^{139}La) during fission.

2.3.3.5 Application of the Method for Irradiated Fuel Sample

The HPLC system was suitably positioned in a fume-hood for handling radioactive samples. The methodology for the separation was validated by employing simulated high level liquid waste solution (SHLLW) with composition equivalent to irradiated PHWR fuel with burn-up of ~0.7 atom%. Under the dual gradient elution condition, the lanthanides were well separated and were not interfered by the presence of other fission products. The experiment was repeated by introducing Th (200 ppm) and Pu (25 ppm) in the above SHLLW solution. In all the cases, the lanthanide peaks were not interfered by the presence of actinide ions. The sample was directly injected into the system after dilution.

Subsequently, the developed method was applied for the separation of lanthanide fission products from irradiated (Th,Pu)O_2 fuel sample. Figure 2.8 shows the chromatogram obtained

by injection of the dissolved fuel solution after reconstituting in the mobile phase. Apart from the other 5 lanthanides, the chromatogram also shows the base line separation of Pm, which does not exist naturally. As discussed earlier, concentrations of lanthanide fission products were determined based on their peak areas employing Tb as an internal standard. Concentration of Nd in the dissolver solution of irradiated fuel sample was found to be 1.6 µg/gm which was in agreement with that obtained by ID-TIMS method.

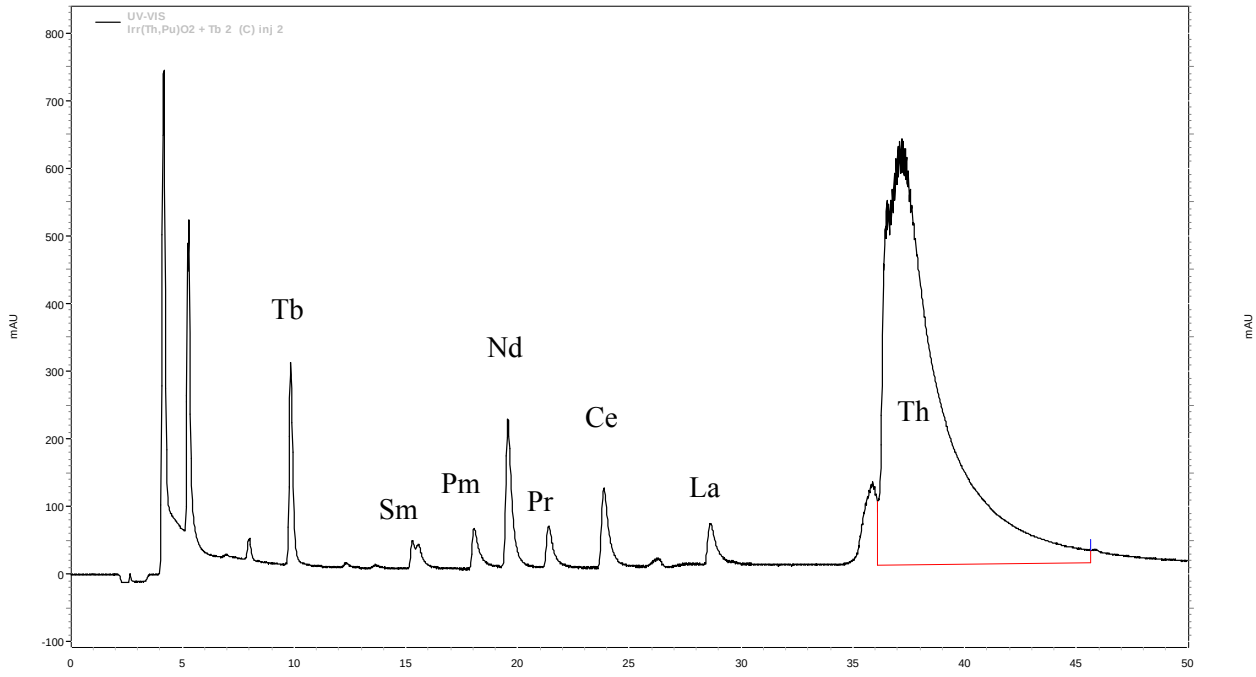

Figure 2.8: *Separation of lanthanides from the dissolved (Th,Pu)O_2 sample using dual gradient elution.*

2.4 Ligand exchange and Coupled Column Liquid Chromatography using Mandelic Acid for the Determination of Lanthanides in Thorium Matrix

2.4.1 Background

As mentioned in previous Sections, determination of low levels of lanthanides in thorium (Th) matrix is important for different applications in nuclear technology. In the front-end of fuel cycle, it is important to characterize Th for impurities such as Sm, Eu, Gd and Dy in view of their high thermal neutron absorption cross-sections [22,125]. In the back-end of the fuel cycle, the determination of lanthanides produced in the nuclear fission can be used as fission monitors for the experimental determination of burn-up, which is an important parameter to evaluate the performance of the fuel in a nuclear reactor [119]. Direct determination of trace levels of lanthanides in bulk of Th by the established analytical techniques are often restricted by spectral interference, suppression of analyte intensity, column overloading, possibility of masking the analyte peaks by the matrix element peaks etc. [126,127]. Thus it becomes essential for most of the analytical techniques to carry out the matrix separation before the actual determination of lanthanides. Common methods employed for the actinide matrix separation are solvent extraction, ion-exchange, precipitation etc [37,128]. Most of these off-line methods are time consuming and labour intensive. An LC method for the direct determination of lanthanides in irradiated thoria is reported in Section 2.3 of this Chapter [129]. This methodology is capable of determination of lanthanides in Th samples with Th/Ln amount ratios <10,000. The problem of column overloading restricts the application of this method to samples with larger amount ratios. A coupled column LC method for the determination of trace levels of lanthanides in Th employing mandelic acid as a chelating agent is presented in this Section. The fact that mandelic acid forms more hydrophobic complex with Th than that formed with α-HIBA implies the possibility of attaining higher Th loading capacities which in turn enhances the Th/Ln amount ratios.

Further, availability of an unmodified RP column exclusively for matrix element retention significantly enhances the limiting Th concentrations at which column overloading occurs.

2.4.2 Experimental

2.4.2.1 Instrumentation

The experimental set up used for the separation studies is shown in Fig. 2.9. A quaternary gradient pump and a photodiode array detector were used as mentioned in Section 2.2.2.1. The samples were injected using a Rheodyne injector (7725i) with 100 μL loop. 100 mm x 4.6 mm C_{18} monolith (Merck), 150 mm x 4.6 mm C_{18} particulate (Merck) and 250 mm x 2 mm bonded ion exchanger (Dionex) columns were used for carrying out the separation studies. The columns were coupled using a six way valve (Rheodyne) so that the first column can be switched in and out of the mobile phase stream.

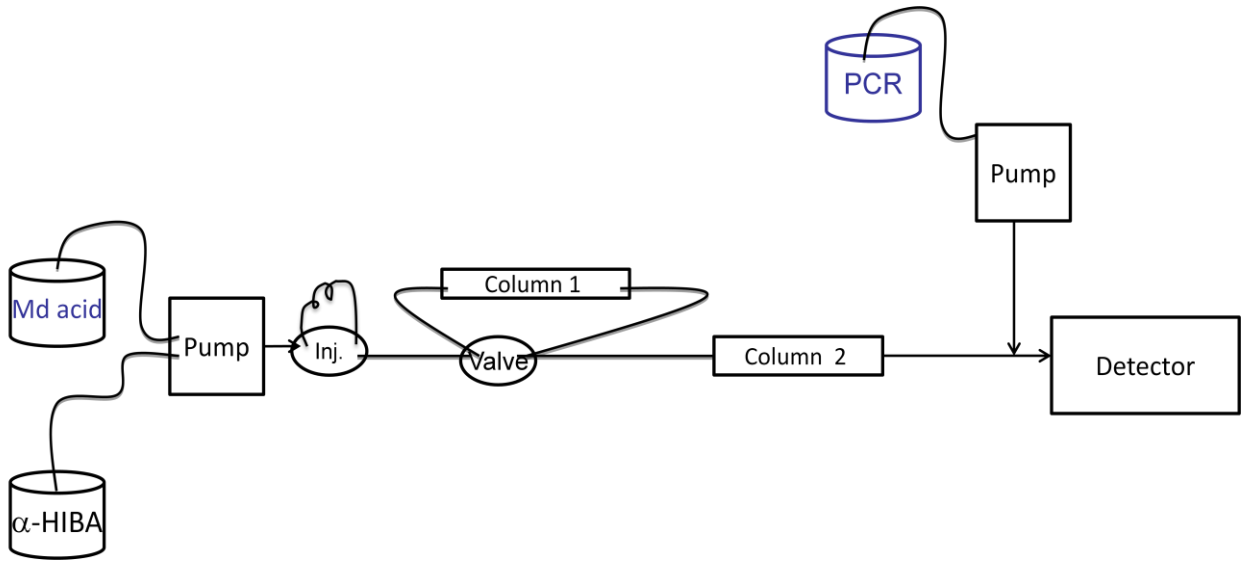

Figure 2.9: *Schematic diagram of the coupled column chromatographic set-up.*

2.4.2.3 Reagents

Mandelic acid (Merck) and α-HIBA (Lancaster) were used as the ligands and n-octadecylsulphonate (Alfa-Aesar) was used as the IIR in this work. Stock solutions of

lanthanides and Th as mentioned in Section 2.2.2.2 were used for synthetic samples. High-purity reagents such as HNO_3 (Merck) and NH_4OH (Merck) were used for pH adjustment and gradient grade MeOH (Merck) was used for mobile phase.

2.4.2.2 Procedure

The particulate RP column was modified by passing 1600 mL n-octadecylsulphonate ($2.5x10^{-4}$ M prepared in 30% of MeOH) followed by washing with 700 mL of water. Initially, the first (unmodified RP) column was switched into the mobile phase and after proper conditioning with mandelic acid, the sample was injected. The matrix Th was retained by the RP column while lanthanides move out as a group into the second column. At this time, the first column was by-passed from the flow stream using the six way valve. Mobile phase programming was adjusted (Table 2.13) in such a way that from this point onwards, HIBA gradient was launched to cause the individual separation of lanthanides. When the lanthanide separation was over, the first column was switched back into the flow stream and a combination of mandelic acid and MeOH was passed to elute Th from the first column.

2.4.3 Results and Discussion

2.4.3.1 Effect of Concentration and pH of Mandelic Acid

La and Lu were chosen as the representative elements for the lanthanides. Figure 2.10 shows the changes in the retention times of lanthanide and Th on an unmodified RP column as a function of concentration of mandelic acid. During this study, a pH of 3.5 was chosen for the mobile phase and an unmodified RP column was used as the stationary phase. Both La and Lu showed relatively less retention which decreased slightly with the increase in concentration of eluent. On the other hand, Th showed a significant retention onto the stationary phase at low concentrations of mandelic acid. A concentration of 0.2M of mandelic

acid was chosen for further studies as it gave good resolution without very long separation time.

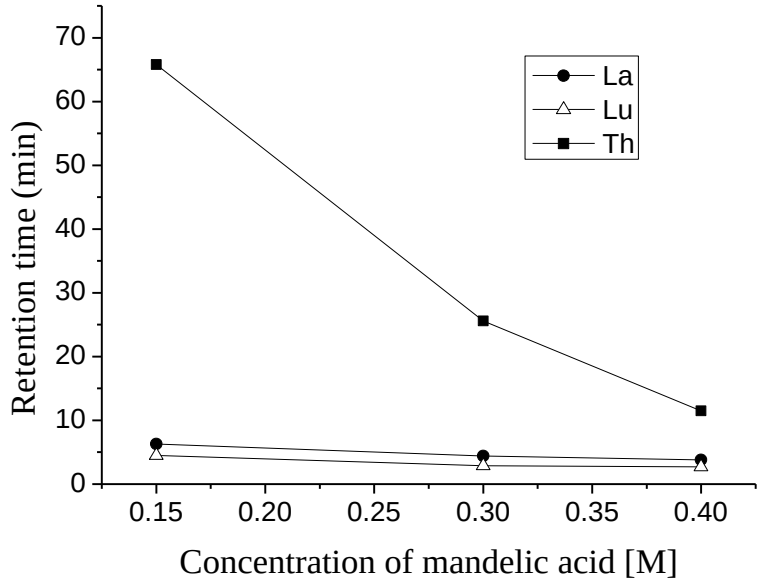

Figure 2.10: *Effect of concentration of mandelic acid on the retention of La, Lu and Th on a RP stationary phase.*

The influence of pH of the mobile phase on the retention of lanthanides and Th is shown in Fig 2.11. It is seen that the retentions of all the three ions increases with increase in pH of the mobile phase. This observation is in contrast with the trend exhibited by aliphatic hydroxycarboxylic acids (HIBA, lactic acid etc.) which show a decreasing trend with the rise in pH of the mobile phase. At high pH of the mobile phase, there is a marked increase in the retention of Th as compared to that of lanthanides. This is attributed to the increased hydrophobicity of Th-mandelate complex arising from the larger coordination number. Based on the present study, a pH of 4 was chosen as Th showed highest retention at this pH.

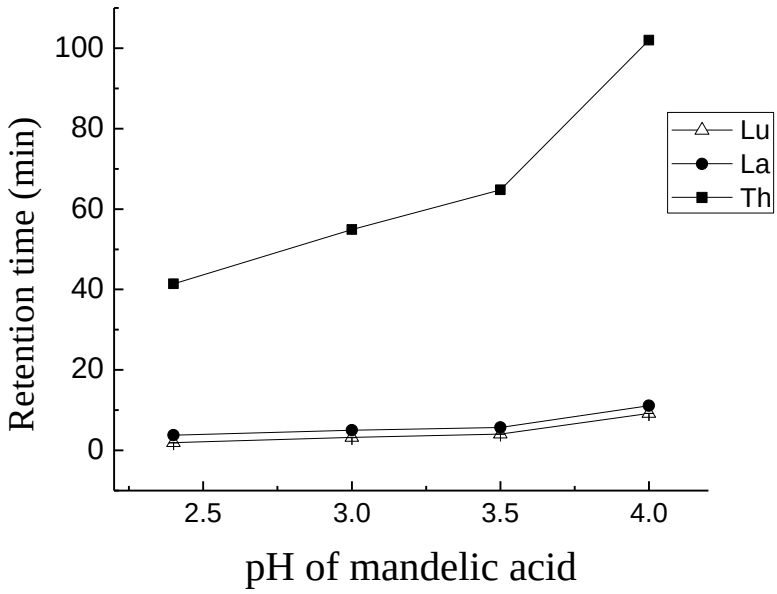

Figure 2.11: *Change in the retention of La, Lu and Th on RP stationary phase as a function of pH of the mobile phase.*

2.4.3.2 Mechanism of Retention of Metal Mandelates

With an objective of understanding the mechanism of adsorption of lanthanide ions onto RP phase, different electrolytes such as $NaNO_3$, $Ca(NO_3)_2$ and $Al(NO_3)_3$ were introduced into the mobile phase. Figure 2.12 shows the retention of lanthanides and Th as function of concentration of $NaNO_3$ in the mobile phase. If the adsorption of lanthanides and Th was taking place by the ion exchange mechanism offered by the mandelate anions sorbed onto the RP surface, then the increase in concentration of the competing cations should result in a decrease in their retentions. But as it is seen from Figure, the retention time of all the ions were unaffected by the presence of different concentrations of electrolytes in the mobile phase. Similar observations were obtained with the inclusion of other electrolytes such as $Ca(NO_3)_2$ and $Al(NO_3)_3$ in the mobile phase. The use of different electrolytes did not show any adverse effect on the retentions of lanthanide and Th indicating that sorption of

lanthanide-mandelate is taking place by hydrophobic interaction and not by ion exchange mechanism as reported earlier by other workers [130].

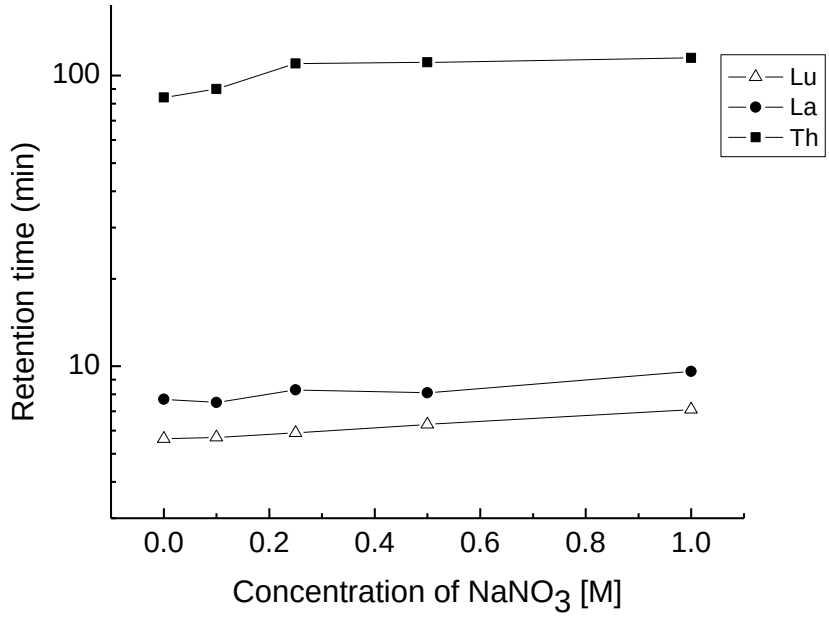

Figure 2.12: *Effect of concentration of $NaNO_3$ in mobile phase on the retention times of La, Lu and Th.*

It is seen that Th-mandelate retains very strongly on the RP stationary phase as compared to lanthanide complexes. The preferential retention of Th on to the RP stationary phase can be used for the on-line matrix removal under the coupled column configuration. Thorium-mandelate retains strongly whereas lanthanide-mandelates are eluted out of RP column into a second column connected in sequence.

As compared to HIBA, mandelic acid was found to be less efficient in separating the individual lanthanides. Though the initial separations were satisfactory with mandelic acid, the resolutions among lanthanide pairs deteriorated with time due to the dominance of chelation chromatography. HIBA being aliphatic acid does not show enough affinity for the RP stationary phase and thus offers consistently good efficiency for the separation of individual lanthanides. Thus the process of ligand exchange, mandelic acid ligand for matrix

separation and HIBA ligand for separation of lanthanides, was adopted for the effective utilization of the two chelating agents.

In the present case, dynamically modified columns cannot be used for the individual separation of lanthanides as it lowers the capacity of the first column to retain Th and also results in increased retention of lanthanides in the first column. Hence, for the individual separation of lanthanides, an RP column modified with n-octadecylsulphonate and a commercially available cation exchange column were compared under identical separation conditions. Figures 2.13(a) and (b) show the separation of a mixture of 14 lanthanides on a bonded cation exchanger and on a modified cation exchange stationary phase, respectively.

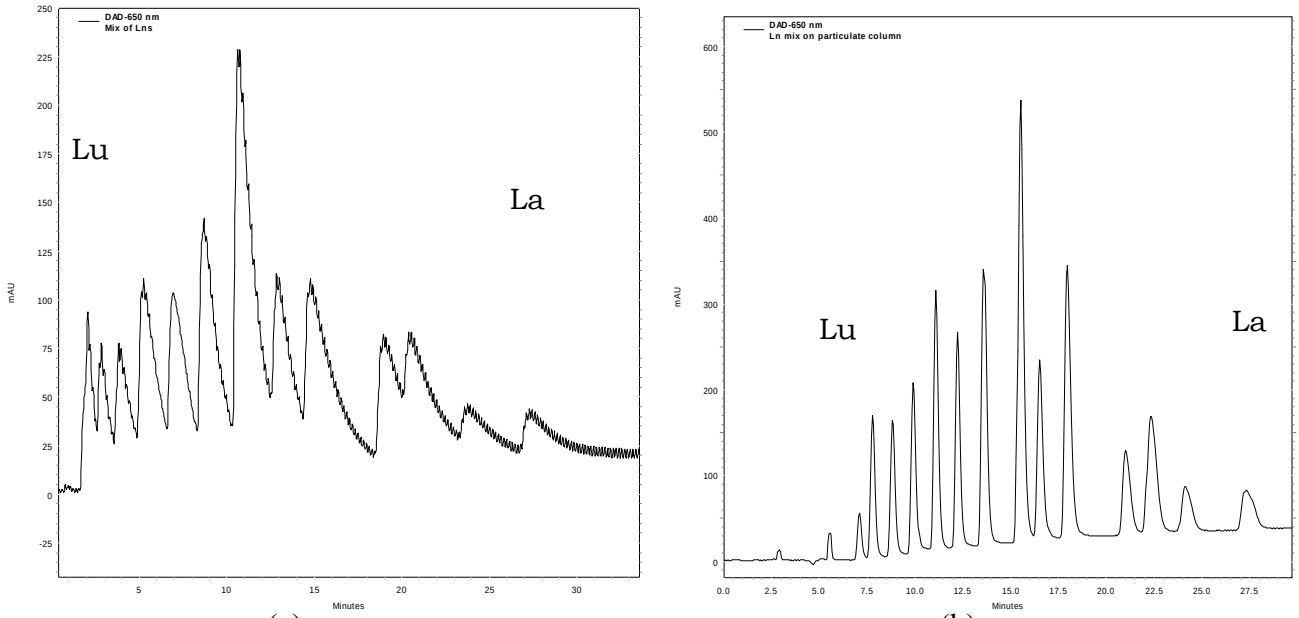

(a) (b)

Figures 2.13: *Separation of individual lanthnides using (a) bonded cation exchanger column and (b) RP column modified with C-18 sulphonate.*

Due to the excellent mass transfer effects, the modified column gave baseline separation of all the lanthanides with sharp peaks whereas the resolution was very poor and the peaks were quite broad in the case of the separation obtained using bonded phase ion exchanger. Thus the modified RP column was selected for coupling with the unmodified column for the separation of lanthanides. In addition, excellent stability of IIR modified column obviated the

need of a continuous supply of ion interaction reagent (IIR) in the mobile phase which otherwise would have degraded the thorium-retention capacity of the first RP column. Thus different mobile phase conditions were required for the retention of Th and individual separation of lanthanides. The optimized gradient conditions developed for matrix separation and individual separation by the coupled column strategy are shown in Table 2.15.

Table 2.15: Optimized gradient conditions for the coupled column separation

Time (min)	**(v/v)%**		
	α-HIBA (pH 6.0)	**Mandelic acid (pH 4.0)**	**Water (%)**
0	0	30.0	0
12	0	30	0
12.1	0	0	100
13	0	0	100
15	3	0	0
30	15	0	0

1 M each of mandelic acid and HIBA were used as the stock solutions in the reservoir.

After the separation of lanthanides was completed, Th adsorbed onto the first column was eluted by using a mobile phase consisting of 0.2 M mandelic acid and 30% (v/v) MeOH. Care must be taken that during the matrix elution step, the second column is isolated from the mobile phase stream as MeOH can strip the C18-sulphonate coated onto the RP surface. Absence of interference from the matrix element was confirmed by the injection of lanthanides (1 ppm each) and Th (10,000 ppm) under the identical separation conditions. Figures 2.14 (a) and (b) show the chromatograms obtained using mixture of lanthanides and Th matrix, respectively.

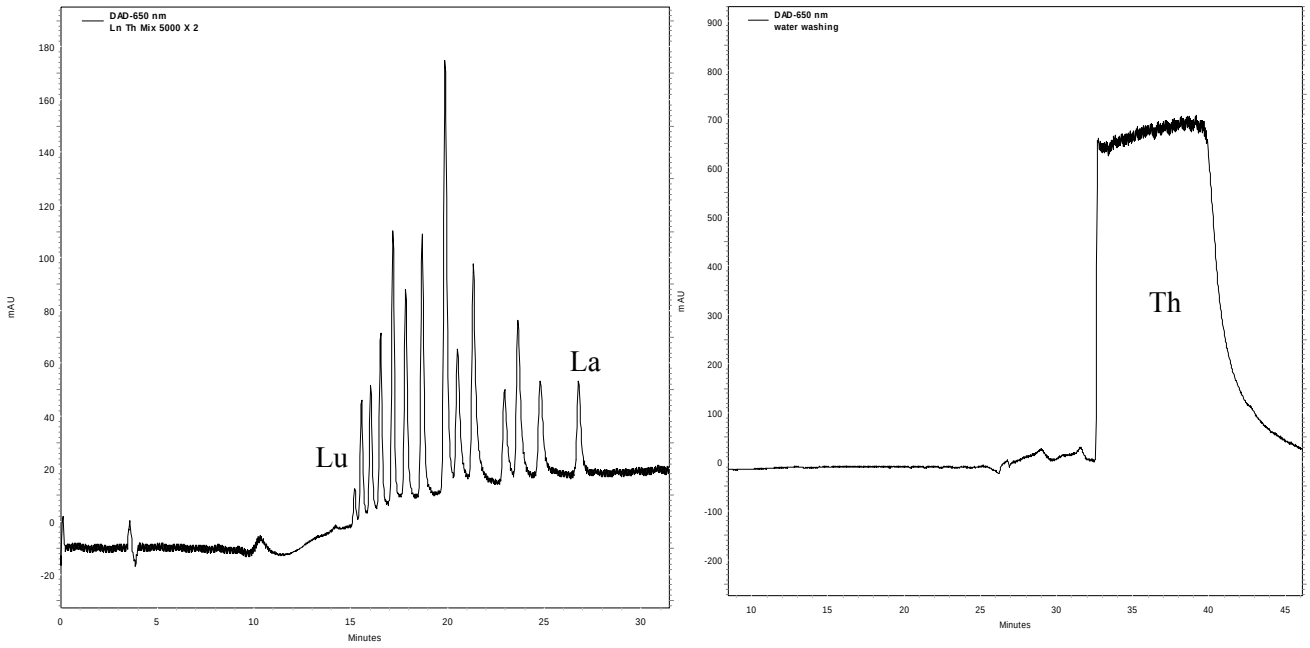

(a) (b)

Figure 2.14: *Chromatograms for the separation of lanthanides (1 ppm each) and Th (10,000 ppm) under identical elution conditions.*

The methodology is fast, avoids chances of contamination and sample loss and has been successfully employed to synthetic samples with Th/Ln amount ratios of up to 20,000. Table 2.16 presents the recovery of lanthanides determined by the above method with the expected values in a synthetic sample.

Table 2.16: Recovery of lanthanides added to Th

Element	Concentration (ppm)		
	Expected	Observed	Expected/ Observed
Lu	1.2	1.1	1.1
Yb	1.8	1.6	1.1
Tm	1.4	1.5	0.9
Er	1.5	1.4	1.1
Ho	1.8	1.7	1.1
Dy	1.1	1.2	0.9
Tb	1.1	1.0	1.1
Gd	1.8	1.9	0.9
Eu	1.5	1.6	0.9
Sm	1.1	1.1	1.0
Nd	1.2	1.4	0.9
Pr	1.1	1.0	1.1
Ce	1.1	1.0	1.1
La	1.2	1.1	1.1

2.4.4 Conclusions

The studies demonstrated the versatility and efficiency of IIC for the separation of lanthanides for different type of samples. The comparative study of C18-sulphonate and C20-sulphate as IIRs showed that C18-sulphonate provides higher resolutions for the lanthanide separation as compared to C20-sulphate. The increased resolution offered by C-18 sulphonate is believed to be due to its preferential uptake by the RP column containing similar number of carbon atoms in its bonded alkyl chain. C18-sulphonate was also found to exhibit excellent

adsorption stability and hence need not be added to mobile phase during the separation of lanthanides by HPLC. This reagent can be employed as a potential modifier for the separation of lanthanides in complex samples requiring high resolution. The absence of modifier (IIR) in the eluted fractions of lanthanides would be helpful for the TIMS determination of isotope ratios.

The developed dual gradient elution method offers an easy, cost effective method for the determination of burn-up of irradiated thoria samples. As the method involves no pre-separation step for the matrix elements from sample, it permits lesser exposure to radioactivity and less chances for sample loss during transfers. Since no preliminary separation procedure is involved, analysis is faster and is less prone to contamination. The method can be used as a quick substitute for mass spectrometric analysis of the burn-up determination with reasonable precision and accuracy using Tb as an internal standard. Since internal standard is used for quantification, it takes care of majority of the fluctuations and uncertainties during the sample handling. The developed methodology was applied for the separation and determination of lanthanide fission products in simulated as well as in irradiated fuel samples.

A ligand exchange column switching liquid chromatographic method was developed for the on-line matrix separation followed by individual separation of lanthanides. The experimental set-up is more complicated and takes longer separation times than single column approach. However, the possibility of using two columns with different characteristics in isolation has helped in utilizing their full potential and at the same time imparts flexibility to the operation. In the present study, a small monolith column (100 mm x 4.6 mm) with less capacity was used for the matrix isolation. It should be possible to handle samples with larger Th/Ln amount ratios by incorporating particulate columns with higher capacity and by suitable modifications of the gradient.

Chapter 3

Separation of Thorium and Uranium by HPLC

3.1. Introduction

Thorium (Th) and Uranium (U) are the two important actinide elements in the nuclear energy program. Their separation and determination in presence of each other has drawn much attention because of their importance in energy related applications and environmental concerns [131-133].The accurate determination of these two elements is often difficult due to interferences present in sample matrix. Conventional sample treatment methods such as column chromatography and solvent extraction which are used for circumventing the above problems are time consuming and complicated. Development of new methodologies for the separation and determination of Th and U is of considerable importance to thorium based nuclear fuel cycle [134,135]. Different methods such as extraction chromatography, solid-phase extraction (SPE), solvent extraction, ion exchange, precipitation etc. have been reported for the separation of U and Th in various matrices [131,134-140].HPLC methods are also reported for the separation and determination of Th and U in different matrices due to its ability to provide rapid and high performance separations [103,123,141]. HPLC using chelating agents as eluents combines selective complexation, separation and specific detection for the determination of Th and U [142].

This Chapter deals with the studies carried out for the separation of Th and U under following scenarios:

1) Separation of Th and U when present in similar proportions
2) Determination of U in presence of large amounts of Th
3) Understanding the mechanism of separation of Th and U when mandelic acid is used as an eluent.

3.2 Separation of Similar Proportions of Th and U (Th/U = 1 to 100)

3.2.1 Background

Th and U are naturally occurring actinide elements found at trace levels in the environment. U is widely distributed throughout earth's crust with trace amounts present in different rock types, natural waters including seawater. Th is also distributed in nature but relatively less widely than U. Estimated Th content in the earth's crust is about 2-3 times more than that of U. Exploitable deposits of Th and U result partly from the original inhomogeneities in earth's crust and partly from the interplay of erogenic and geochemical processes [149]. At the early stages of magma recrystallization, in reducing and alkaline environments, U(IV) compounds enter the rock forming minerals and form relatively high U concentration in granites. Both Th and U possess ionic radii and charges which prevent them from fitting comfortably into the lattices of any of the common major minerals of granite. However, they fit into some of the accessory minerals such as zircon, allanite etc. because U and Th in +4 state can substitute Zr in +4 state in zircon. In exogenous environments, tetravalent U compounds become unstable and change to hexavalent ones. It then leaches out of the near surface parts of the mineral. Due to the lack of multiple oxidation states, most of the Th bearing minerals are resistant to oxidation under exogenous conditions. Thus the concentrations of Th and U are used as the markers for indicating important geochemical cycles. Determination of natural radionuclides such as U and Th in soil samples is also important from the viewpoint of radiation protection.

This Section presents the development of an HPLC method based on the hydrophobic interaction of hydroxyisobutyric acid (HIBA) complexes of Th and U on the RP stationary phase. The chromatographic parameters such as pH of the eluent and the concentration of the eluent were studied to optimise the separation between the two elements. Presence of MeOH

in the mobile phase was found to improve the peak shape as well as sensitivity of the method for U determination.

3.2.2 Experimental

3.2.2.1 Instrumentation

The HPLC system used in this study was mentioned in detail in Section 2.2.2. A 150 mm x 4.6 mm C_{18}particulate (5 µm) column (Supecosil) was used as the stationary phase in the present work.

3.2.2.2 Reagents

HIBA (Fluka) was used as the eluent. Thorium nitrate and uranyl nitrate were used for preparing the stock solutions after standardization by complexometric titration and biamperometric method, respectively. Suprapure grades of HNO_3 and NH_4OH (Merck) were used for adjusting the pH of the mobile phase. MeOH (Gradient grade, Merck) was used for changing the polarity of the mobile phase.

3.2.2.3 Procedure

HIBA was dissolved in water and made to 1M. After adjusting the pH, the mobile phase was filtered through 0.45µm Millipore membrane filters. The mobile phase was pumped through the column until equilibrium condition was attained as indicated by the pH stability of the effluent.

3.2.3 Results and Discussion

3.2.3.1 Effect of Concentration of HIBA

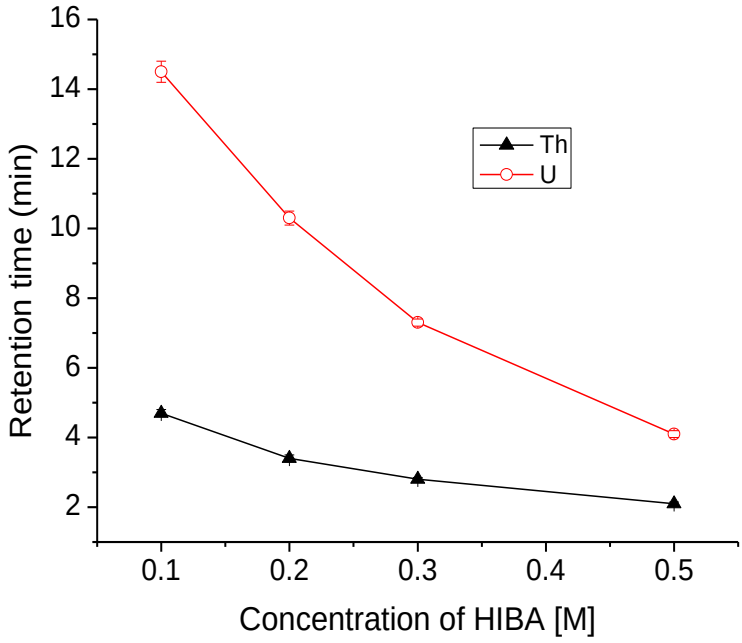

Figure 3.1: *Changes in the retention time of Th and U as a function of concentration of eluent.*
Chromatographic conditions: 4.6 mm x 150 mm C_{18} column using HIBA of pH 4.0.

Influence of the concentration of HIBA on the retention of Th and U is shown in Fig. 3.1. It is seen that the retention of both Th and U decreases steadily with the increase in the concentration of HIBA in the mobile phase. This trend is attributed to the increased formation of the metal-ligand complex at higher concentrations of the ligand. Also the fraction of the undissociated molecule responsible for the displacement of metal-HIBA complex from the stationary phase increases with the increase in concentration of the eluent. It is interesting to note that the retention of U at any given concentration of the ligand is greater than that of Th.

3.2.3.2 Effect of pH of Mobile Phase

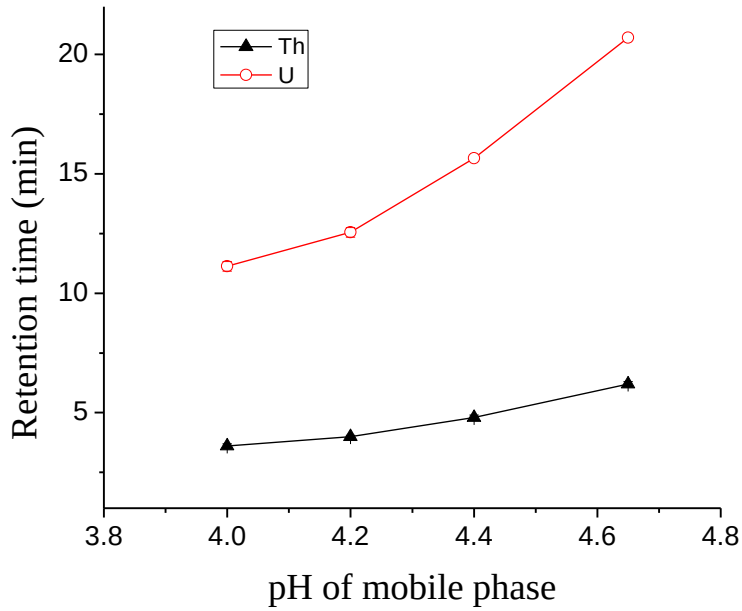

Figure 3.2: *Effect of pH of mobile phase on retention of Th and U. Chromatographic conditions: 4.6 mm x 150 mm C_{18} column using 0.25 M of HIBA.*

The effect of pH of the mobile phase on the retention times of Th and U on the RP stationary phase is shown in Fig. 3.2. During this study, the concentration of the eluent was fixed at 0.25 M. The complexation increases with increase in pH of the mobile phase and consequently, the proportion of the hydrophobic species responsible for the retention on the stationary phase increases. The percentage of the undissociated HIBA molecule which can compete with the RP stationary phase also decreases with the increase in pH. These factors result in an increase in the retention of both Th and U with the increase in pH of the eluent. In this case also, the retention of U was greater than that of Th at every pH studied. From the pH study, it was found that 0.25 M HIBA of pH 4 provides a good separation between Th and U within a reasonable run time.

3.2.3.3 Effect of Methanol

It was found that the peak shape as well as the response of U peak improves with the increase in the methanol content in the mobile phase. Figure 3.3 shows the increase in the peak response (peak height) of U with the increase in the percentage of methanol in the mobile phase.

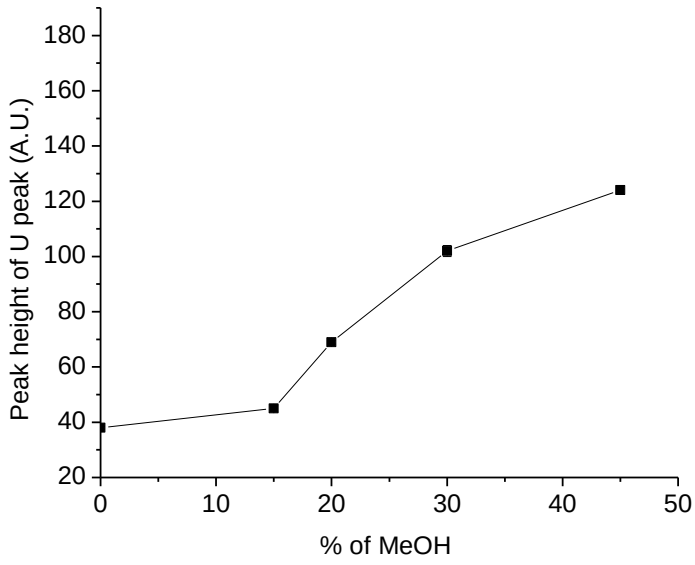

Figure 3.3: *Effect of methanol in the mobile phase on U peak response. Chromatographic conditions:4.6 mm x 150 mm C_{18} column;0.25 MHIBA of pH 4.0.*

Introduction of MeOH lowers the polarity of the mobile phase and thus helps in faster elution of the hydrophobic species such as Th and U complexes with HIBA. Introduction of MeOH results in increased number of theoretical plates which translates into improved peak shapes. Another advantage of inclusion of MeOH in the mobile phase is the decrease in the overall separation time. Hence, a concentration gradient of methanol and HIBA was selected for the separation of U and Th. Figure 3.4 shows the chromatographic separation of Th and U under optimized gradient conditions on the RP column. Under these conditions, separation between Th and U could be completed within 8 min with base line separation between them.

In the present case, U to Th amount ratio was ~70. The pulsations generated by the piston pump during delivery of post-column reagent restricted the quantitation limit of U to 20ng.

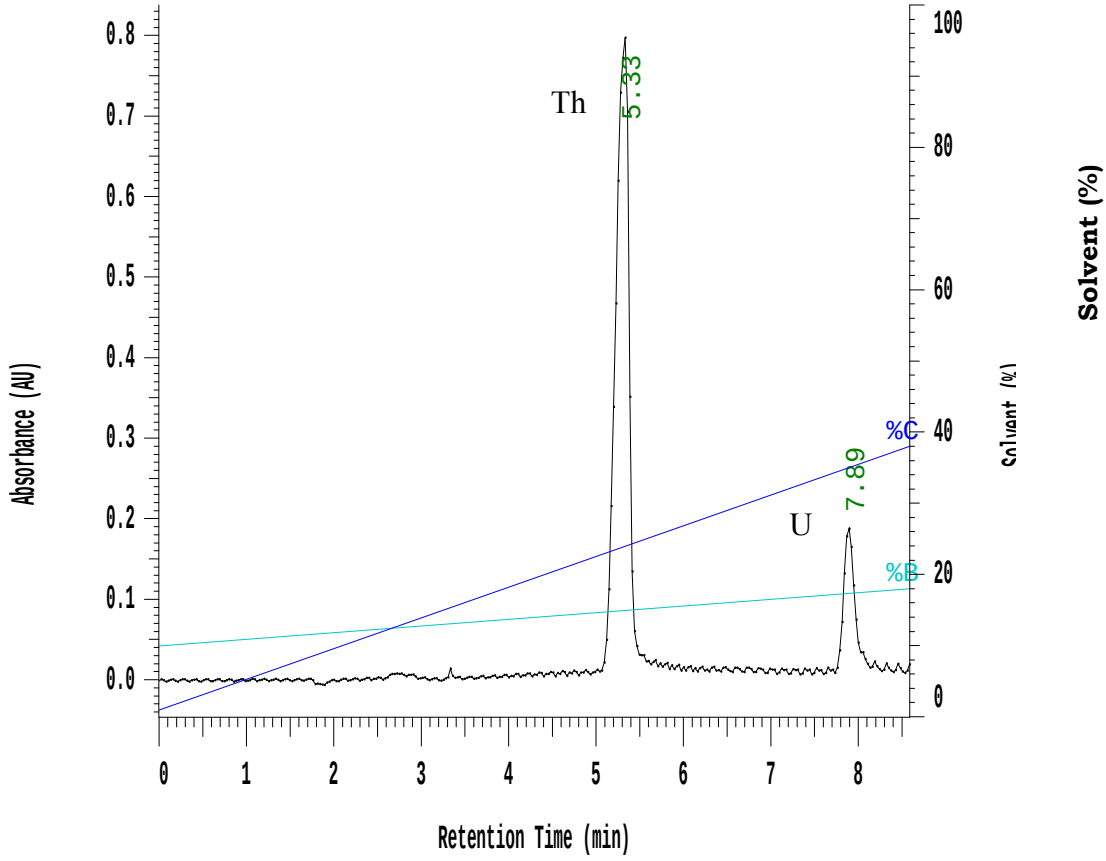

Figure 3.4: *Separation of Th and U using concentration gradient of HIBA and MeOH in the mobile phase.*
Chromatographic conditions: (B) 0.15 to 0.30M of HIBA (pH 4.0) and (C) 1 to 45 (v/v)% methanol in 10 min, Stationary phase: 4.6 mm x 150 mm C_{18} column.

Thus HIBA is found to be a suitable eluent for the separation of Th and U when these elements are present in proportions Th/U ≤ 100. The fact that HIBA is the most successful eluent for the individual separation of lanthanides also favours the selection of this eluent for the separation of Th and U in geological samples.

3.3 Determination of U in Presence of Large Amounts of Th

3.3.1 Background

Th occupies a unique place in Indian scenario due to its large resources and limited U deposits available in the country. Thus India has embarked upon the third stage of nuclear power program, based on Th-^{233}U fuel cycle (Advanced Heavy Water Reactor - AHWR), for the long term energy security of the country [22,113]. Though a number of HPLC methods have been developed and reported for the separation of U and Th, majority of these reports deal with samples containing nearly equal amounts of U and Th [103,123,135,141-144]. However, Th fuel cycle demands quantification of small amounts of U in presence of large amounts of Th. The mixed oxide of ThO_2 containing 4% $^{233}UO_2$is the proposed fuel for the AHWR [125] whereas in the irradiated fuel, Th/U amount ratio can range from 25 to 70 depending upon burn-up of the fuel [129]. Determination of U, often at low concentration levels, is also important to evaluate the performance of various separation processes in AHWR. For example, some process samples generated during the recovery of ^{233}U from irradiated Th contain trace amounts of U in Th [145]. The feed material (thorium sulphate) used for the production of nuclear grade ThO_2 is always associated with trace amounts of uranium (10-100µg/g) [146]. Due to similar chemistry, the separation and accurate determination of U in presence of a large excess of Th is a challenging task. The highest Th/U amount ratio reported for the HPLC analysis is 1000 and the method utilizes a RP column modified by amide coating [145]. As per this procedure and most of the other reported HPLC separation conditions involve the use of hydroxycarboxylic acids as eluents, wherein Th is eluted prior to U [109,129]. The small U peak appearing on the shoulder of large Th peak introduces errors for the determination of U based on the peak area or peak height measurements. Tailing of the preceding peak reduces the resolution and has a detrimental effect on the integration of the small peak of the analyte [65]. It has been well established that

the peak integration error becomes the dominating error source at low concentrations, e.g. at concentrations below the five-fold of the LOQ [147].

This Section reports the development of an HPLC method using mandelic acid as an eluent for the determination of U in samples with Th/U amount ratios as high as 100 000, without involving any pre-separation of the matrix element (Th). The parameters such as concentration and pH of the eluent were studied to optimize the separation conditions. The capacity of the stationary phase for the retention of Th was determined as a function of pH and percentage of MeOH in the mobile phase. The data obtained were used to optimize a separation methodology allowing elution of U prior to Th so that the accurate determination of the former can be carried out in presence of large amounts of Th. Use of different types of stationary phases viz. monolith and particulate columns provides flexibility to the method to cater to samples with wide range of Th/U ratios. Results on the quantitative determination of Th and U by the developed method are also discussed in this Section.

3.3.2 Experimental

3.3.2.1 Instrumentation

The HPLC system with post-column reaction set-up as described in Section 2.2.2.1 of Chapter 2 was used in the present study. C_{18} monolith RP columns with dimensions 50 mm × 4.6 mm and 100 mm × 4.6 mm (Chromolith, Merck) and a 150 mm x 4.6 mmC_{18} particulate RP column (Purospher STAR, Merck) were used as the stationary phases. Samples were injected into the column using a Rheodyne injector (Model 9725i) with a 100 μL sample loop. The signal from the detector was processed by EZChrom software package.

3.3.2.2 Reagents

Mandelic acid (Merck) was used as an eluent. Thorium and uranium stock solutions were prepared from thorium nitrate and uranyl nitrate, respectively, after the standardization procedure mentioned elsewhere [111,112].MeOH (Gradient grade, Merck) was used as the organic modifier for the mobile phase.

3.3.2.3 Procedure

Appropriate quantity of mandelic acid was dissolved in Milli-Q water to obtain solution with 0.5 M concentration. Mandelic acid solution was adjusted to the desired pH using NH_4OH and HNO_3. Post-column reagent was prepared using Arsenazo(III) as mentioned in Section 2.2.2.3.1 mL/min and 0.3 mL/min were the flow rates used for the mobile phase and PCR, respectively. Quantification was carried out based on the chromatographic peak area.

3.3.3 Results and Discussion

The parameters such as pH and concentration of the eluent were studied to optimise separation between Th and U on the RP column. Initial studies were carried out using a short column (50 mm x 4.6 mm) as this would require less volume of the mobile phase as well as shorten the chromatographic run time.

3.3.3.1 Effect of pH of Mandelic Acid

Figure 3.5 shows the changes in the retention times of Th and U on RP stationary phase as a function of pH of mandelic acid. 0.5 M mandelic acid solution was used for these studies so as to complete the elution of Th and U within a reasonable time, especially at higher pH conditions.

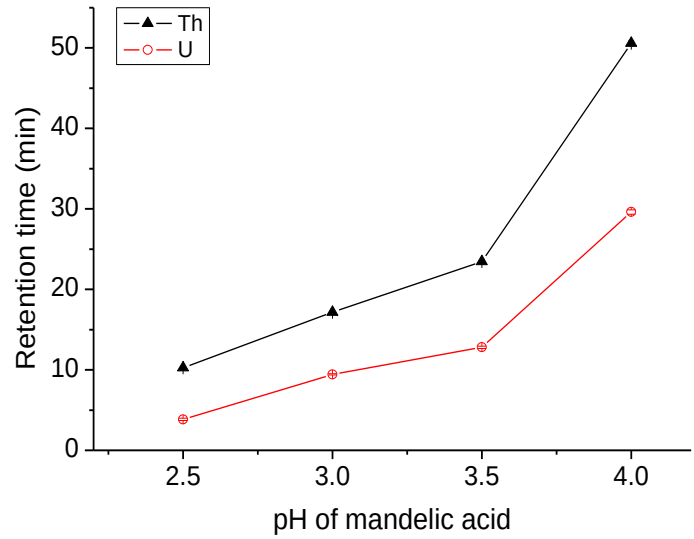

Figure 3.5: *Effect of pH of mandelic acid eluent on the retention time of Th and U. Chromatographic conditions: C_{18} (50 mm x 4.6 mm) monolith column; 0.5M mandelic acid.*

It was observed that the retention of both Th and U onto the C_{18} stationary phase increased with the increase in pH of mandelic acid. This is attributed partly to the increased ionisation of mandelic acid and the consequent increase in its complexation with Th and U at higher pH. The fact that the competition from the undissociated mandelic acid molecules for the reversed-phase sites decreases at higher pH, also contributes to the increased retention of mandelate complexes of Th and U. At pH ≥ 4.5, both Th and U could not be eluted from the column even after 100 min and thus the study was restricted up to pH 4.0. It is seen that the retention of Th on the stationary phase is greater than that of U at all the pH values employed (2.5 – 4.0). This pattern is different from those observed with other hydroxycarboxylic acids (e.g. α-hydroxyisobutyric acid, lactic acid, glycolic acid etc.) commonly employed for the separation of U and Th, where Th has a lower retention than U [109,129,145]. pH of 3.0 was chosen for further studies as it offered separation of Th and U with sufficient resolution within a reasonable time. Lower pH (≤ 2.5) was not considered as it is deleterious to the column

whereas higher pH (≥ 3.5) causes stronger retention of both Th and U and thus would require more time for elution.

3.3.3.2 Effect of Concentration of Mandelic Acid

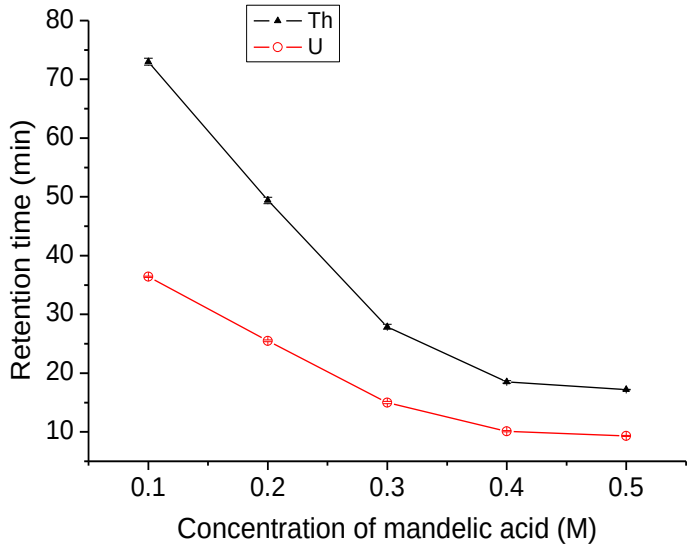

Figure 3.6: *Effect of concentration of mandelic acid on the retention of Th and U. Chromatographic conditions: mandelic acid (pH 3.0); other conditions same as in Fig.3.5.*

Figure 3.6 shows the effect of concentration of mandelic acid in the mobile phase (pH 3.0) on the retentions of Th and U onto the RP column. Retention of both Th and U was found to decrease with the increase in concentration of mandelic acid in the mobile phase. This was attributed to the increased displacement of metal-mandelate complexes from the stationary phase by the undissociated mandelic acid molecules. Higher the concentration of mandelic acid, more number of undissociated mandelic molecules would be available to compete for the RP stationary phase. The separation factor between Th and U was also found to decrease at higher concentrations of mandelic acid. Thus 0.2M solution of mandelic acid, which offers a good degree of separation between Th and U, was selected for further studies.

3.3.3.3 Effect of Methanol Content

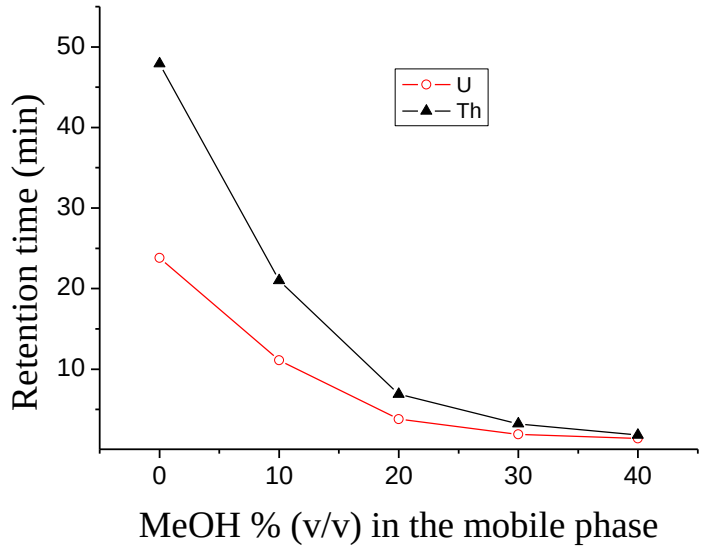

Figure 3.7: *Effect of methanol content on the retention behaviour of Th and U. Chromatographic conditions: 0.2M mandelic acid of pH 3.0; other conditions same as in Fig.3.5.*

Figure 3.7 shows the change in the retention behaviour of Th and U as a function of MeOH % (v/v) in the mobile phase. 0.2 M mandelic acid of pH 3.0 was used as an eluent in this study. Retention of both Th and U was found to decrease with increase in percentage of MeOH (v/v) in the mobile phase. Introduction of MeOH lowers the overall polarity of the mobile phase. The decrease in the retention times of Th and U with the increase in the MeOH content in the mobile phase is indicative of the hydrophobic nature of these metal-mandelate complexes. It may also be noted that Th-mandelate showed a significant reduction in its retention indicating a greater level of hydrophobicity as compared to U-mandelate. Introduction of MeOH was also found to improve the peak shapes of both Th and U and also helped in reducing the overall separation time. However, the separation between Th and U decreases significantly as a function of MeOH% (v/v) and hence 20% (v/v) of MeOH was chosen for carrying out further separation studies.

3.3.3.4 Separation of Th and U by Monolith Column

The data from the pH and eluent concentration studies were used for developing an HPLC method for the separation of Th and U on a C_{18} column using mandelic acid as the eluent. Mandelic acid concentration and pH were selected as 0.2 M and pH 3, respectively, for the mobile phase. A longer monolith column (100 mm x 4.6 mm) was employed for these studies in view of its higher capacity. 20% methanol (v/v) was found to be sufficient to improve the peak shapes of U and Th and to reduce the separation time from 50 min to 7 min. Figure 3.8 shows the chromatogram obtained for the separation of U and Th (Th/U amount ratio ~ 1) on an RP column using mandelic acid as the eluent. It is seen that the peaks are well separated and U is eluted prior to Th.

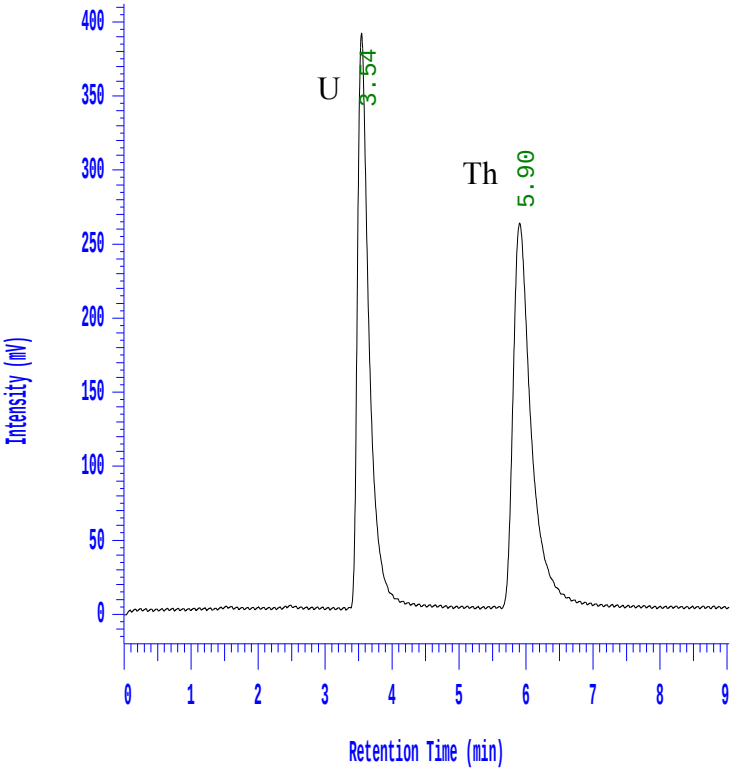

Figure 3.8: *Separation of Th and U (Th/U amount ratio = 1) on an RP column using mandelic acid as the eluent.*
Chromatographic conditions: C_{18} (100 mm x 4.6 mm) monolith column; 0.2 M mandelic acid of pH 3.0; 20% (v/v) MeOH.

3.3.3.5 Determination of Small Amounts of U in Presence of Large Amounts of Th

Mandelic acid is a promising eluent for the determination of U in presence of large amounts of Th as it causes the elution of U prior to Th with good resolution. Thus the applicability of the method for U determination depends on the amount of Th, which can be retained onto the RP column till U elution is completed. During these studies, it was found that the retention of thorium-mandelate complex onto the RP column is significantly influenced by the pH of the mobile phase and the MeOH content. Thus further experiments were carried out to determine the retention capacity of the column for Th by varying methanol content and pH of the mobile phase.

3.3.3.5.1 Effect of Methanol Content on the Th Retention Capacity

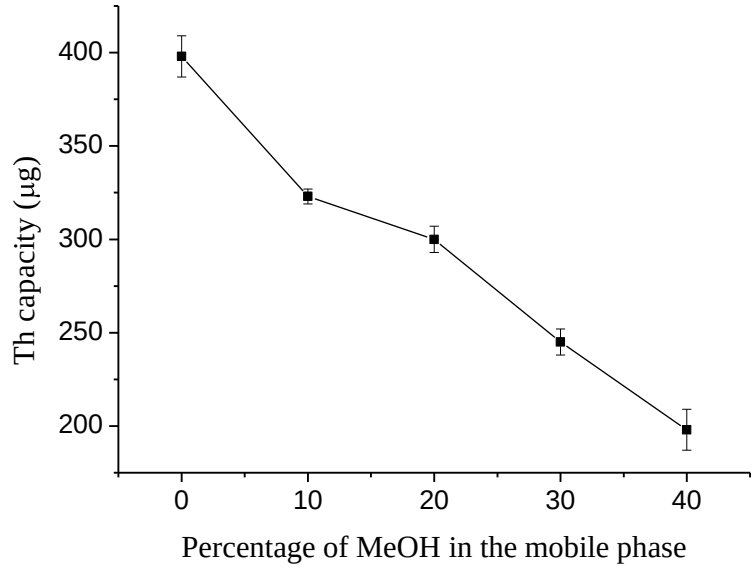

Figure 3.9*: Th retention capacity of stationary phase as a function of methanol content in the mobile phase.*
Chromatographic conditions: 0.2M mandelic acid (pH 3.0); 100 mm x 4.6 mm C_{18} *monolith column.*

Th retention capacity may be expressed as the maximum amount of Th which can be retained by the stationary phase until the complete elution of U (100 ng injected) occurs. At a given percentage of MeOH in the mobile phase, if the amount of Th injected is beyond this

limiting value, then retention time of Th peak would advance in such a way that it would interfere with the early eluting U peak. Figure 3.9 shows the changes in the Th capacity of the monolith RP column (100 mm x 4.6 mm) as a function of MeOH % (v/v) in the mobile phase. The pH of the mobile phase was 3.0 during this study. The retention capacity of the stationary phase for Th was found to decrease with the increasing percentage of methanol in the mobile phase due to increased non-polarity of the mobile phase. Under the conditions chosen (20% (v/v) MeOH) for the separation of U and Th, the retention capacity of the column was found to be 300 μg of Th.

3.3.3.5.2 Effect of pH of Mobile Phase on the Th Retention Capacity

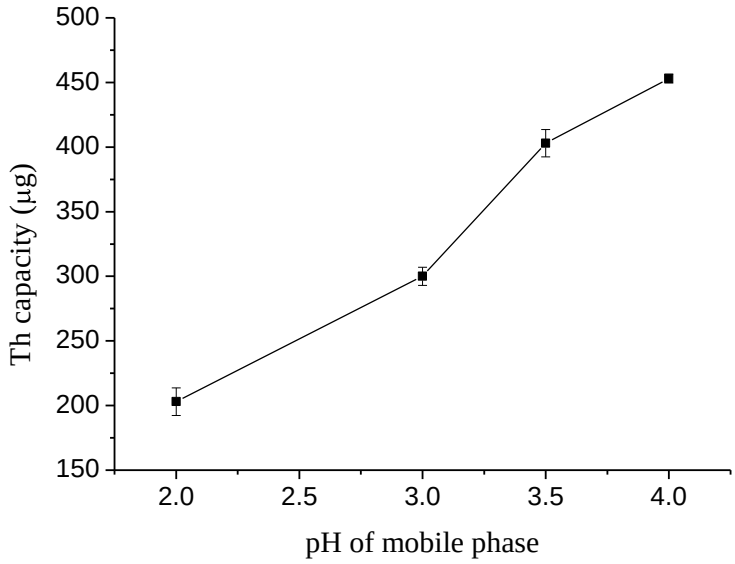

Figure 3.10: *Th retention capacity of monolith column as a function of pH of mobile phase. Chromatographic conditions: MeOH: 20 % (v/v); Other conditions same as in Fig. 3.9.*

Figure 3.10 shows the changes in the Th retention capacity of the monolith RP column as a function of pH of the mobile phase. Th retention capacity of the stationary phase increases with the increasing pH of the mobile phase. This is due to the increased retention of Th associated with the increased formation of hydrophobic thorium mandelate complex at higher pH, as indicated in Fig. 3.5. During this study, the methanol content in the mobile

phase was kept at 20% (v/v). Though the Th retention capacity under the chosen condition is ~ 300 μg, it can be improved by proper selection of pH of the mobile phase depending on the Th/U amount ratio in the samples.

3.3.3.5.3 Calibration Curves for U and Th

Since the ultimate aim of the present investigations was to develop an HPLC methodology for the determination of U and Th in thorium based nuclear fuel cycle, a stock solution was prepared with Th/U amount ratio 25. Aliquots were prepared by dilution in the concentration range of 0.9 - 40 μg mL^{-1} for U and 22 - 1200 μg mL^{-1} for Th. Figures 3.11 and 3.12 show the calibration curves obtained for U and Th, respectively, using several mixtures with the same Th/U amount ratio of 25. U showed good linearity in the concentration range of 0.9 – 40 μg mL^{-1}. Good correlation between peak area response and Th concentration in the injected solution was observed in the concentration range from 22 to 500 μg mL^{-1}. At higher concentration levels of Th, peak area response showed saturation trends. These calibration curves demonstrate that U and Th can be determined from a single chromatographic run as long as Th/U amount ratio is ≤ 25.

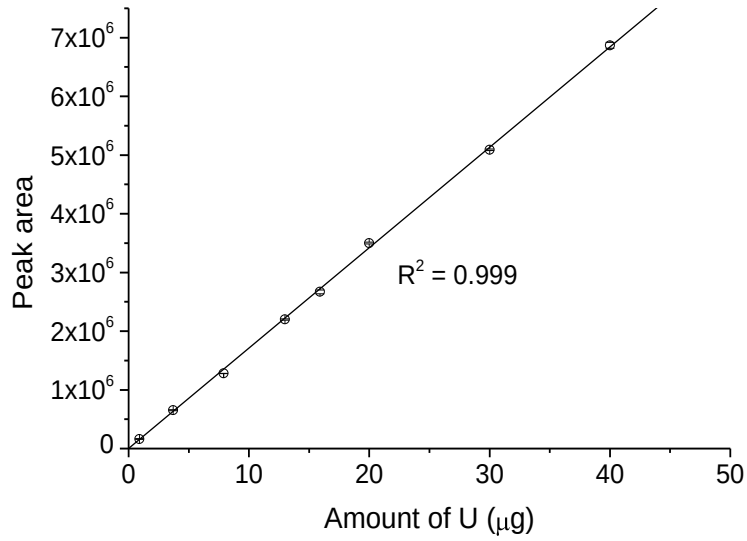

Figure 3.11: *Calibration curve for U in presence of Th (Th/U amount ratio 25). Chromatographic conditions: same as in Fig. 3.10.*

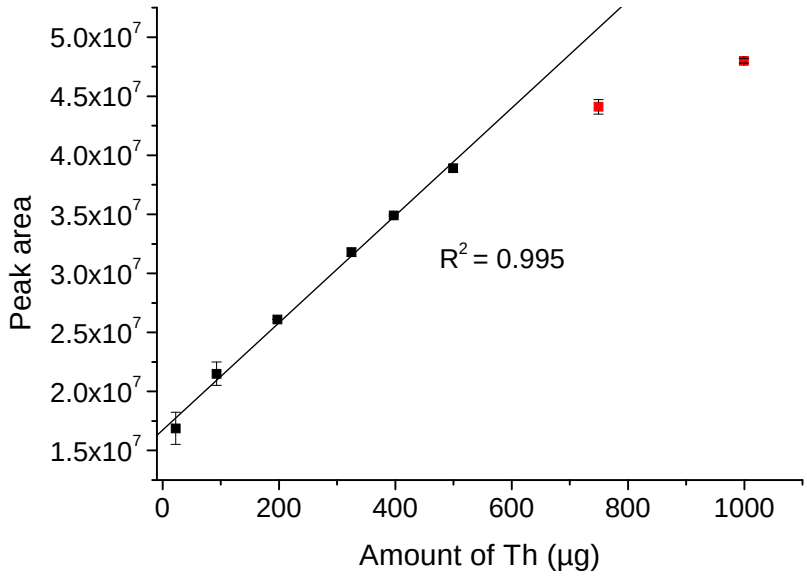

Figure 3.12: *Calibration curve for Th in presence of U (Th/U amount ratio 25). Chromatographic conditions: same as in Fig. 3.10.*

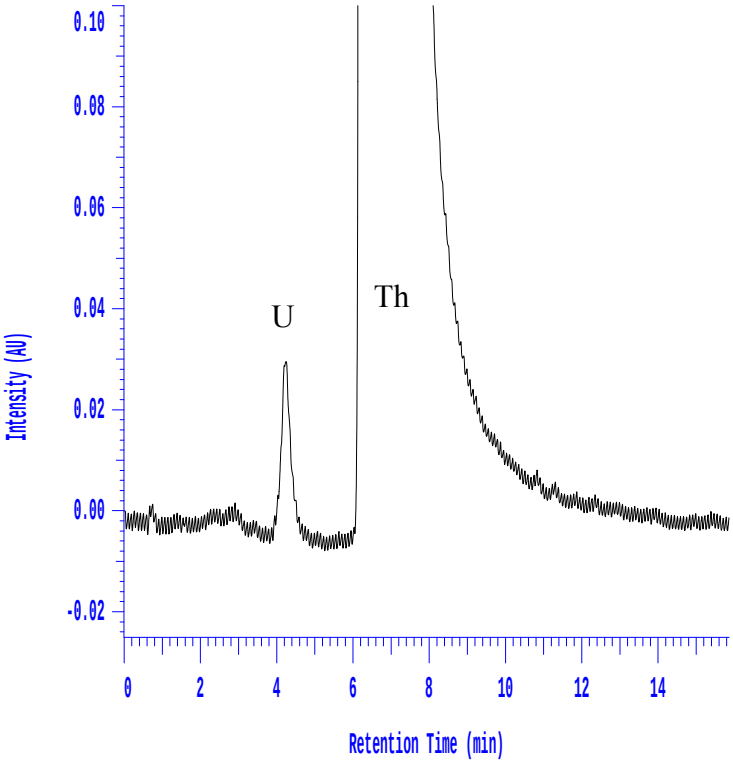

Figure 3.13: *Separation of U and Th in a mixture with Th/U amount ratio of 3000on a monolith RP column.*
Injected 100 µL of synthetic mixture containing Th: 3000 µg/g; U: 1 µg/g; Chromatographic conditions: same as in Fig. 3.10.

Th retention capacity experiments showed that under the optimised conditions for the separation, up to 300 µg of Th can be retained on the monolith RP column. Considering that the minimum amount of U going into the column is 0.1 µg, the method allows the determination of U in samples with Th/U amount ratios up to 3000 using the C_{18} monolith column as shown in Fig.3.13. The capacity for Th retention (300µg) is higher than that reported based on the modification of the column [145] with extractants. Th retention capacity obtained by the present method is significant, considering the smaller column dimensions (100 mm x 4.6 mm), porous nature of the monolith column and that the method does not involve any column modification step.

3.3.3.5.4 Separation of Th and U by Particulate Column

Use of monolith column offered the advantages such as low-pressure resistance (> 25 bar) and shorter separation time (> 15 min) under the optimized conditions. However, the Th retention capacity offered by the monolith column was not sufficient enough to determine U present at trace levels in Th. Hence a particulate RP column with dimensions 150 mm x 4.6 mm (5µm particle size) was employed for the separation of U and Th in the case of synthetic samples with Th/U amount ratios > 3000.

Multiple injections of the sample were required since the amount of U injected into the column (< 20 ng) in a single injection would be below the quantification level of the method for samples with Th/U amount ratios > 10 000. Synthetic samples with higher concentrations of Th could not be prepared as the samples started showing turbidity on standing over a period of time (1 hr to overnight) due to the precipitation of $Th(OH)_4$. Hence the concentration of Th^{4+} in the synthetic mixture solution was restricted to about 3000 µg/g. These solutions were prepared in 0.2 M mandelic acid and at pH 1.5. No turbidity was observed in the solution for a period of 24 hrs for the synthetic mixture.

The gradient condition was also modified to allow multiple injections of the sample during the same chromatographic run. Even a MeOH content of 30% (v/v) in the mobile phase did not cause any broadening or splitting of the U peak, after introducing the samples in as many as 16 repeated injections for a single chromatographic run.

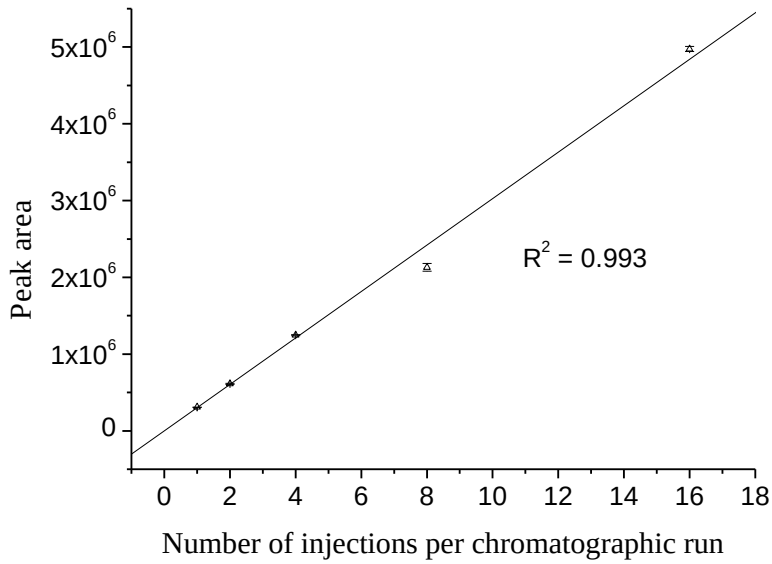

Figure 3.14: *Peak area response of U as a function of number of injections. Chromatographic conditions: particulate C_{18} RP column (150 mm x 4.6 mm). Mandelic acid: 0.2M, pH: 3.0; MeOH: increased from 30% (v/v) to 40% (v/v)in 35 min; Injection volume: 100 µL; U concentration: 0.51 µg/g.*

The possibility of introducing the sample into the column through multiple injections was checked by injecting different volumes of a U solution of known concentration (0.51 µg/g). Figure 3.14 shows the peak area response as a function of number of injections (100 µL each) during a chromatographic run. Good linearity was obtained between the number of injections and the peak area of U for 1 – 16 injections, provided the time gap between successive injections was maintained less than 30 sec. Even from 16 consecutive injections, U was found to elute as a sharp peak, well separated from Th peak.

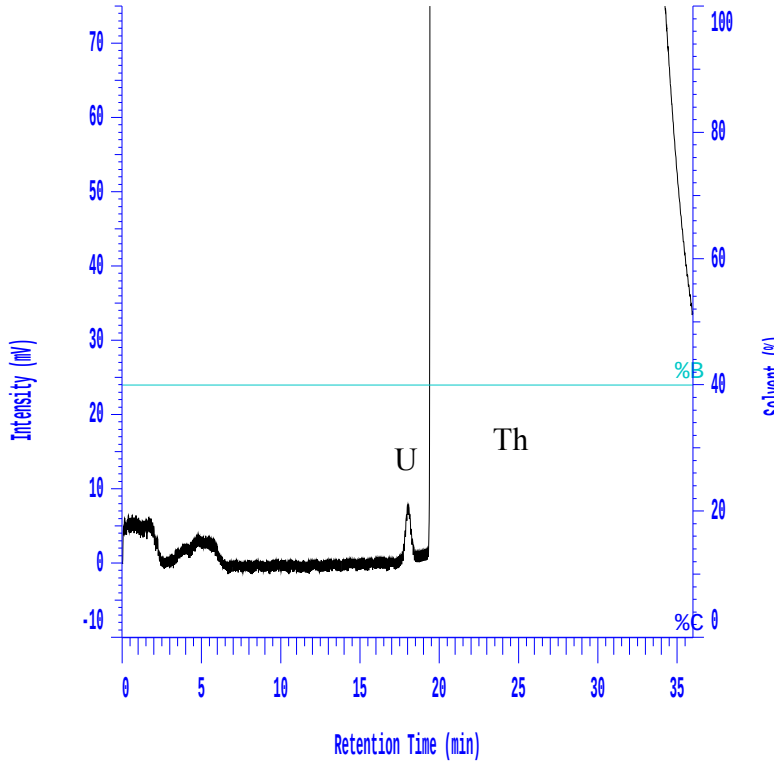

Figure 3.15: *Separation of U and Th in a mixture with Th/U amount ratio of 106479, on a particulate C_{18} RP column.*
Injected 12x100 µL of synthetic mixture; Th: 2268 µg/g; U: 0.021 µg/g;
Chromatographic conditions: same as in Fig. 3.14.

Figure 3.15 shows the chromatogram obtained by injecting a mixture with Th/U amount ratio 106300 using particulate RP column. U peak is separated from Th peak with a time gap of almost 1 min indicating that the determination of the former would not be interfered by the latter peak. Table 3.1 shows the concentration of U determined by the above method for different synthetic mixtures of Th and U. Concentration of U was determined from a calibration curve obtained by injecting standard solutions in the concentration range 0.21 - 0.55µg mL^{-1}. A good agreement was obtained between the added and the determined concentrations of U. The practical constraints of using the particulate column are the longer separation times (~35 min) and high back pressure during the chromatographic run (180 bar). Th retention capacity can be further scaled up by the proper choice of column size or by working at a higher pH, which would allow the analysis of samples with even higher Th/U amount ratios.

Table 3.1: Determination of U in synthetic mixtures with different Th/U amount ratios

Sr. No.	Synthetic sample concentration (µg/g)		Th/U amount ratio	No. of injections	U concentration determined (µg/g)	U expected/determined
	Th	U				
1	2753	0.504	5462	1	0.467 ± 2%	1.08
2	2825	0.291	9708	1	0.274 ± 3%	1.06
3	2290	0.114	20144	3	0.118 ± 2%	0.96
4	2963	0.059	50220	5	0.065 ± 5%	0.90
5	2268	0.021	106479	12	0.021 ± 5%	1.02

Chromatographic conditions: same as in Fig. 3.14.

3.4 Mechanism of Separation of Th and U using Mandelic Acid Eluent

3.4.1 Background

Hydroxycarboxylic acids are extensively used for the separation of Th and U by RP-HPLC. Use of mandelic acid (2-hydroxy-2-phenyl acetic acid) has been reported in the literature for the separation of U and Th in geological samples [103,142,148]. Retention behaviour of mandelate complexes of UO_2^{2+} and Th^{4+} ions has been compared with those of glycolic acid and HIBA by Hao *et al.* [148]. Use of mandelic acid has been investigated for studying the elution behaviour of transition elements, lanthanides and actinides by ion interaction chromatography [103]. When aliphatic derivatives of the hydroxycarboxylic acids such as glycolic acid, HIBA etc. are used as the eluent, the typical order of elution is Th followed by U [109,148]. It was observed that the elution order reverses when mandelic acid, which is an aromatic derivative of the hydroxycarboxylic acid, is used as the eluent. It was of interest to understand the factors responsible for the different behavior in the elution pattern as in both HIBA and mandelic acid, the functional groups are the same. This Section deals with the studies carried out to understand the mechanism of adsorption of the two metal-mandelate complexes onto the RP stationary phase.

3.4.2 Experimental

The instrumentation, reagents and procedure used in this study were given in Section 3.3.2. Sodium n-octanesulphonate monohydrate (Fluka) and tetra-n-butylammonium bromide (Merck) were used as ion interaction reagents (IIRs). The IIRs were dissolved in Milli-Q water to obtain solutions with 0.1 M concentration.

3.4.3 Results and Discussion

The adsorption of mandelate complexes of Th and U onto the RP stationary phase could be due to the hydrophobic interaction or due to the ion exchange mechanism offered by the mandelate ions adsorbed on to the hydrophobic stationary phase. To understand the mechanism of adsorption, two different IIRs viz. sodium *n*-octane sulphonate and tetra-*n*-butyl ammonium bromide were introduced independently into the mobile phase at varying concentrations and the corresponding changes in the retention times of Th and U were monitored.

3.4.3.1 Effect of Sodium n-Octane Sulphonate IIR

The hydrophobic anion, n-octane sulphonate, was introduced into the mobile phase at different concentrations ranging from 0 to 0.015M. Figure 3.16 shows the changes in the retention times of Th and U as a function of IIR concentration in the mobile phase. Introduction of n-octane sulphonate in the mobile phase results in the formation of cation exchange sites on the surface of the RP stationary phase. Thus if the adsorption of Th or U is based on cation exchange mechanism, then an increase in concentration of n-octane sulphonate is expected to increase the retention. As it is seen from the Figure, the retentions of both Th and U decrease with the increase in the concentration of the IIR in the mobile phase. This indicates that the adsorption of Th and U on the reversed-phase is due to hydrophobic interaction of the respective metal-mandelate complex with the C_{18} stationary phase, rather than cation exchange mechanism. The decrease in retention of Th and U is due to the competition by the hydrophobic moiety of the IIR. At concentrations higher than 0.01 M of the IIR in the mobile phase, the retentions of both Th and U are not affected appreciably, indicating that the stationary phase is almost saturated by the IIR. An increase in the concentration of IIR in the mobile phase led to a pronounced effect on the adsorption of Th

than that of U. This indicates a higher degree of hydrophobic character of thorium-mandelate complex as compared to uranyl-mandelate complex. This is also corroborated by the higher retention exhibited by Th compared to U during the pH as well as in concentration variation experiments shown in Fig. 3.5 and Fig. 3.6, respectively.

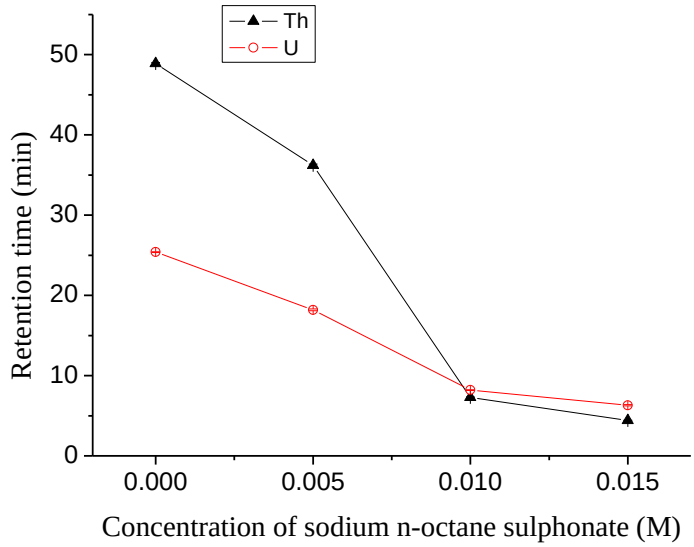

Figure 3.16: *Retention times of Th and U as a function of concentration of n-octane sulphonate.*
Chromatographic conditions: 0.2M mandelic acid (pH 3.0); C_{18} (50 mm x 4.6 mm) monolith column.

3.4.3.2 Effect of Tetra-n-butyl Ammonium Bromide IIR

The experiments discussed above involving the addition of hydrophobic anion (*n*-octane sulphonate) into the mobile phase, ruled out the possibility of adsorption of any positively charged species of Th or U onto the stationary phase. But the presence of negative charge on the adsorbed species can be identified by monitoring the change in the retention time of the species after introducing a hydrophobic cation at different concentrations. Table 3.2 shows the data on the retention of Th and U on the RP column at different concentrations of tetra-n-butylammonium bromide in the mobile phase. The retention time of thorium-mandelate complex decreases steadily with the increase in concentration of IIR similar to that

observed for the hydrophobic anion IIR (*n*-octane sulphonate). This was attributed to the competition of hydrophobic anion for the hydrophobic stationary phase. This observation also supports the strong hydrophobic character and charge neutrality of thorium-mandelate complex. At 0.005 M concentration of IIR, the decrease in the retention of Th was more significant using tetra-*n*-butyl ammonium bromide as compared to that with n-octane sulphonate. However, for higher concentrations of IIR (0.01 and 0.015 M), n-octane sulphonate is observed to have a prominent effect on the retention time of Th as compared to tetra-*n*-butyl ammonium bromide. The reason behind the differing pattern exhibited by the two IIRs is not known.

On the other hand, retention of U increases with increase in concentration of the cationic IIR indicating the anionic nature of uranyl-mandelate complex. The interaction was found to be so strong that at tetra-n-butyl ammonium bromide concentrations ≥ 0.007M, uranyl-mandelate could not be eluted even after 100 min using 0.2 M mandelic acid as the eluent. The experimental data support the predictions made by Hao *et al.* [147] that U forms anionic complex viz. uranyl-tris(mandelate) with mandelic acid. The experiment also clarifies the ambiguity regarding the retention of thorium-mandelate onto the RP column. Two possible mechanisms suggested by Hao *et al.*[147] for the elution of U followed by Th using mandelic acid eluent are: (a) Th(IV) co-ordination sphere is selectively hindered by the phenyl group of mandelic acid, so that no hydroxyl group could take part in the coordination, which may be possible in the case of glycolic acid and HIBA. Thus Th(IV)-tetra(mandelate) is a neutral species and exhibits stronger retention than uranyl-tris(mandelate), which is anionic in nature; (b) thorium mandelate complex may be associated with negative charge as in the case of HIBA but the strong hydrophobicity of the mandelate complex overshadows the effect of negative charge, so that the hydrophobic character of the complex is dominant.

Hence the retention order would be dependent on the number of ligands in the complex rather than charge on the complex.

If thorium-mandelate in solution is associated with hydroxyl group in the coordination sphere, its retention time should increase (similar to that of uranyl complex) with increase in concentration of cationic IIR in the mobile phase. As per data given in Table 3.2, retention of Th decreases with increase in concentration of cationic IIR suggesting the charge neutrality of thorium mandelate complex. Hence it is the first mechanism, which is responsible for the stronger adsorption of Th and this also explains elution of U prior to Th. This also supports the behaviour observed for the retentions of mandelate complexes of U and Th with the changes in the concentrations of different IIRs.

Table 3.2: Effect of concentration of tetra-n-butylammonium bromide on the retention time of Th and U on the RP column

Concentration of tetra-n-butylammonium bromide in the mobile phase (M)	Retention time (in minutes) for	
	U	Th
0	25.4 ± 0.1	49.0 ± 0.3
0.005	28.8 ± 0.2	30.1 ± 0.03
0.007	No elution*	13.5 ± 0.2
0.010	No elution*	13.1 ± 0.1
0.015	No elution*	12.5 ± 0.3
0.020	No elution*	11.1 ± 0.1

Chromatographic conditions: 0.2M mandelic acid (pH 3.0); C_{18} (50 mm x 4.6 mm) monolith column.

** No elution till 100 min.*

3.4.4 Conclusions

An HPLC method was initially developed for the separation of Th and U using HIBA as the eluent. The chromatographic parameters such as pH, concentration of eluent and MeOH content were optimized for the efficient separation of Th and U. This method is suitable for samples containing Th and U in similar proportions such as geological samples.

However, samples relevant to Th based nuclear fuel cycle would require determination of trace levels of U in presence of large amounts of Th. Hence, an LC method was developed for their separation using mandelic acid as the eluent. When mandelic acid was employed as the eluent, the elution order was found to be U followed by Th. The distinct elution pattern would allow reliable determination of U based on the chromatographic peak response in samples containing large amounts of Th. Use of C_{18} monolith column and C_{18} particulate column offers the flexibility to adopt this method for samples with different Th/U amount ratios; monolith column for Th/U amount ratios up to 3000 whereas particulate column could be used for Th/U ratios up to 100000. The method is based on a standard C_{18} RP column and no modification of the stationary phase is involved. Hence the proposed method is expected to be easier to adopt and more reproducible than those involving column modifications.

Detailed studies were carried out using different IIRs to understand the mechanism of adsorption of Th-mandelate and U-mandelate on the RP stationary phase. It was confirmed that on the RP stationary phase, Th is retained as neutral thorium mandelate complex whereas U is adsorbed as anionic uranyl-mandelate complex. The presence of these major species explains the distinct elution pattern observed when mandelic acid is used as an eluent.

Chapter 4

HPLC Methods for the Determination of Uranium in Seawater

4.1 Introduction

As the world's demand for U increases, materials which contain this element in low concentrations will have to be explored as potential sources. Seawater is thus considered as a possible source of U[149,150]. Concentration of U, present at ppb levels, in seawater varies with water salinity, depth, temperature etc [151]. Though concentration of U in seawater is low, the advantages of the dissolved state and almost inexhaustible quantities of uranium in seawater appear interesting for U recovery. Furthermore, U extracted from seawater qualifies as a green fuel, since the process leaves no mill tailings at the recovery site and U fission in nuclear reactor generates electrical energy without CO_2 emissions. Studies are being pursued by different research groups to explore the feasibility of recovering U from seawater in an economic way. These studies demand the availability of a method for determination of U at different stages of pre-concentration and separation. In addition, determining the fate of U in natural water systems including seawater is important for environmental monitoring [152]. However, U determination in seawater is a challenging task because of the high salt content, presence of bio-fouling agents and low ppb concentrations of the analyte. A variety of analytical techniques commonly employed for the determination of U at ppb levels are inductively coupled plasma–mass spectrometry [153-155], inductively coupled plasma-atomic emission spectroscopy [156], spectrophotometry [157], differential pulse polarography [158], solid state nuclear track detector [159], X-ray fluorescence [160], laser fluorimetry[161], radiometry[162,163] etc. Low U concentrations and large amounts of other dissolved species in seawater necessitate chemical separation of U prior to its determination by most of the above mentioned techniques. Commonly used separation procedures are precipitation [153], solid phase extraction [155,158,164], liquid-liquid extraction [160,163], ion-exchange [163], magnetic separation [165] and supercritical fluid extraction [166].

Only a few reports are available in the literature on the use of HPLC for the determination of U in natural water systems [123,143, 167-169].Most of these studies were performed using spiked samples containing significantly large amounts of U added externally. To the best of knowledge, there is no report available on the determination of U in actual seawater by HPLC method. This Chapter describes the development of two LC methods for the determination of U in seawater as well as processed seawater samples as given below:

1. Method using HIBA as the chelating agent for pre-concentration and determination of uranium in seawater.

2. Method for the determination of uranium in seawater and processed seawater samples using mandelic acid as a complexing agent.

4.2 HPLC Method using HIBA as the Chelating Agent for Pre-concentration and Determination of Uranium in Seawater

4.2.1 Background

A few studies are reported on the use of HIBA as the complexing agent for the liquid chromatographic determination of uranium. Cassidy *et al.* used HIBA for the determination of U in groundwater and simulated urine samples with a bonded-phase cation exchange stationary phase [167]. Kerr *et al.* also used HIBA for the selective pre-concentration of U on a reversed-phase (RP) column for U determination in groundwater samples [168]. These authors included a dynamic cationic modifier in the mobile phase along with HIBA to improve the peak shape during elution. Hao and Haddad studied the retention behaviour of HIBA complexes of Th and U with an objective to understand the mechanism of their elution pattern under reversed-phase conditions [123]. Hao *et al.* also compared glycolic acid, HIBA and mandelic acid for the on-line pre-concentration of Th and U [143]and observed poor recovery (40%)by HIBA. Subsequently, Shaw *et al*. reported the utilisation of chelation ion chromatography based on 2,6-pyridinedicarboxylic acid as the chelating agent for the determination of U in spiked seawater samples [169]. Majority of these studies were performed using spiked samples containing significantly large amounts of U added externally compared to the amount present in seawater.

The present work was undertaken with following objectives. The main aim was to develop an HPLC method using HIBA for the selective pre-concentration as well as determination of U in seawater employing the commonly used post-column reagent i.e. Arsenazo(III).Since this reagent is neither specific nor highly sensitive to U, optimized conditions were developed for the separation of U from other metal ions present in seawater as well as for its pre-concentration. The combination of HIBA as ligand and C_{18} as stationary

phase satisfied the requirements of pre-concentration step [143]. Experimental parameters were optimized for quantitative recovery and fast elution with a good peak shape for quantification. Seawater samples were analysed by the optimized method and the results obtained were substantiated by an independent analytical methodology viz. isotope dilution-TIMS.

4.2.2 Experimental

4.2.2.1 Instrumentation

The HPLC system mentioned in Section 2.2.2 was used in the present study. Rheodyne injector with 20 μL and a custom made 2.4 mL sample loops was connected to the system. 50 mm x 4.6 mm monolith C_{18} column (Merck) was used as the stationary phase. An isocratic pump with all SS contact parts (Waters Corporation) was used as the concentrator pump for delivering the sample solution through the column. FinniganMAT-261 (Thermo Electron) thermal ionization mass spectrometer equipped with multi-Faraday cup detection system was employed for isotope dilution experiments.

4.2.2.2 Reagents

Milli-Q water was used for all the dissolutions and dilutions. HIBA (Lancaster) was used as the chelating agent. Suprapure grade reagents such as HNO_3, NH_4OH (Merck) were used for sample treatment. Gradient grade MeOH (Merck) was used as the organic modifier for the mobile phase. Arsenazo (III) (Fluka) was used as the post-column reagent. NaCl, KCl, $Mg(NO_3)_2$, $Ca(NO_3)_2$and $Sr(NO_3)_2$(Thomas Baker) were used for preparing simulated seawater. Tributyl phosphate (TBP) and dodecane (S.D. Fine Chemicals) were used for the solvent extraction of U. The seawater samples were received from the Desalination Division of BARC.

4.2.2.3 Procedure

The glass-wares used were cleaned by immersing them in 7 M HNO_3 overnight and then boiling in 3 M HNO_3. 0.5 M of HIBA was prepared in water, adjusted to the desired pH using NH_4OH and $HNO_3$and was filtered through 0.45 μm Millipore membrane filters. Using the salts of Na^+, K^+, Mg^{2+}, $Ca^{2+}$and Sr^{2+} simulated seawater was prepared as per the composition given in Table 4.1. Concentration of uranium in uranyl nitrate stock solution was determined as mentioned elsewhere employing biamperometric method [112]. 15% (v/v) solution of TBP was prepared by mixing appropriate volumes of TBP and dodecane. The seawater sample was acidified to pH 2-3 using HNO_3 and was heated to boiling for 15 minutes. The solution was cooled to room temperature and was filtered through 0.45 μm filters. The filtered solution was made-up to known volume and was divided into two portions; one for HPLC analysis and the other for ID-TIMS analysis.

Table 4.1: Composition of simulated seawater sample

Element	Concentration (μg g^{-1})
Sodium	10,500
Magnesium	1350
Potassium	380
Calcium	400
Strontium	113

Ref. [170,171]

HPLC Procedure: In the portion used for HPLC experiments, 0.025 M HIBA was added and the pH of the solution was adjusted to 6 – 7. The C_{18}column was conditioned with 10 mL of 0.025 M HIBA solution of pH 6-7 using HPLC pump. The conditioned column was

disconnected from the system and was connected to the concentrator pump as shown in Fig. 4.1. A known quantity (25 – 50 mL) of the treated seawater was passed through the column at a flow rate of 1.5 mL min^{-1}. The effluents from the column were collected and weighed to determine the exact amount of sample passed though the column. The loaded column was then connected again with the HPLC system and washing was done with 10 mL of 0.025 M HIBA solution of pH 6-7 to remove the salts. The adsorbed U was eluted from the column by using (HIBA+MeOH) gradient given in Table 4.2. The experiments for determining the blank with 0.025 M HIBA of pH 6-7 was performed before and after the sample analysis under identical conditions. Quantification of U was based on the area of peak from chromatogram.

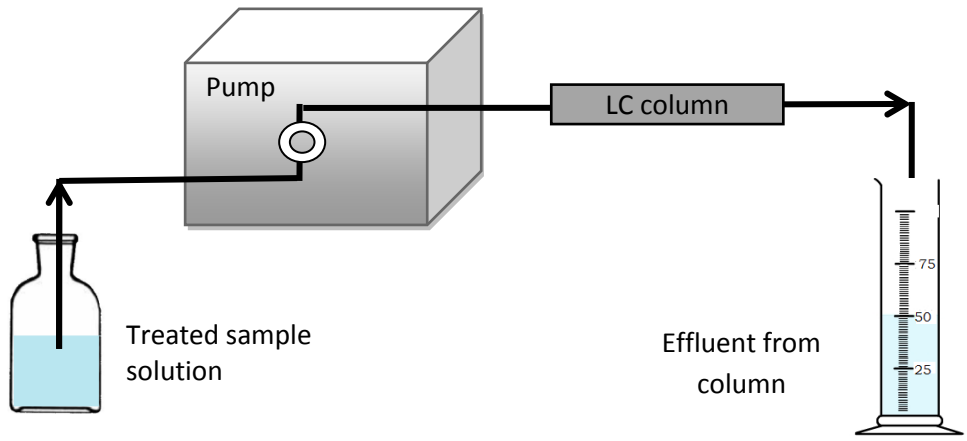

Figure 4.1: *Schematic diagram of the preconcentration set-up.*

Table 4.2: Optimized gradient condition for the elution of U

Time (min)	HIBA(pH 6 – 7) [M]	HIBA (pH 2.5) [M]	MeOH (v/v)%
0.0	0.025	0	0
2.0	0.025	0	0
2.5	0.025	0.2	35
10	0.025	0.2	35

ID-TIMS Procedure: The fraction for ID-TIMS analysis was mixed with a known amount of pre-calibrated ^{233}U spike. The mixture was treated with 8 M HNO_3 and evaporated to near dryness. The treatment with 8 M HNO_3 was repeated three times to ensure proper isotopic exchange between sample and the spike isotopes. The spiked mixture was then dried and dissolved in 8 M HNO_3 to carry out the solvent extraction of U using an equal volume of 15% TBP solution. This extraction procedure was repeated three times and the 8 M HNO_3 aqueous phase was discarded. U was stripped from the organic phase by back-extracting successively four times with 0.01 M HNO_3. The aqueous phase was collected and was evaporated to dryness. The residue was dissolved in 1 M HNO_3 for loading onto the sample filament of a double Rhenium filament assembly for TIMS analysis. The sample and the ionization filaments were heated to temperatures corresponding to heating currents of 2.2A and 6A, respectively. The mean value of $^{233}U/^{238}U$ atom ratio was determined by taking run summary from three blocks, each block consisting of 10 to 12 scans.

4.2.3 Results and Discussion

HIBA was selected for the pre-concentration of U since previous studies had shown showed that uranyl-HIBA complex exhibits strong retention on RP column due to the hydrophobic nature of this complex [109]. A monolith column was selected for the present study as it offers the advantage of low back-pressure and fast separation.

4.2.3.1 Optimization of Parameters for U Pre-concentration

Uranyl ion is known to form various complexes with HIBA such as $UO_2(HIBA)^+$; $UO_2(HIBA)_2$; $UO_2(HIBA)_3^-$ etc. It is reported that the composition of the different complex species changes as a function of concentration of HIBA and pH of the medium[123]. Though the influence of concentration of HIBA on the retention of U was studied earlier with an

objective of separation, now the aim is its quantitative recovery. The effect of concentration of HIBA on the retention of U was studied at a pH of 3 and the results are shown in Fig.4.2. It is seen that the retention of U decreases with the increase in concentration of HIBA in the mobile phase. Since the retention of U is significant even at 0.5MHIBA, this concentration was selected for studying the effect of pH.

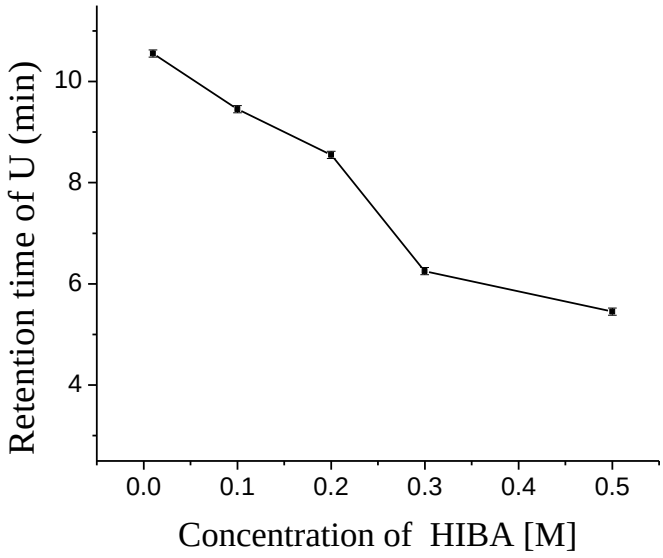

Figure 4.2: *Effect of concentration HIBA on the retention of U. Chromatographic conditions: C_{18} (50 mm × 4.6 mm) monolith column; mobile phase: HIBA of pH 3.0.*

It is well established that uranyl ion forms stable complex with HIBA in the pH range 2 to 8 with a complex formation constant value of 6.6 (log β_3) at pH 4.0 for $UO_2(HIBA)_3^-$ [172]. In the pH range 2 to 4, HIBA shows dominant bidentate coordination via oxygen atoms of carboxylic acid group and at pH≥ 5 an enhancement of chelation occurs due to the involvement of –OH group of the ligand in the complexation. Therefore, we performed the studies by varying the pH of HIBA between 2 to 6. Figure 4.3 shows the effect of pH of the mobile phase on the retention of U. In this Fig., retention time of U is compared with that of La since the latter does not form any hydrophobic complex with HIBA. It is seen that increase in pH increases the retention of U significantly whereas there is no effect on La. When pH 6

HIBA was used, U could not be eluted even with a mobile phase solution equal to 80 times the column volume. This was attributed to (i) the hydrophobic nature of the uranyl-HIBA complex and (ii) the increased complexation of U due to increased fraction of ionized HIBA at higher pH.

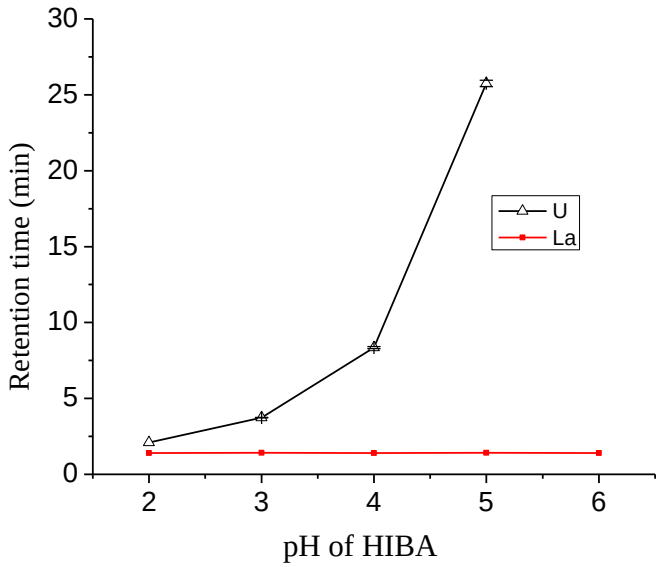

Figure 4.3: *Effect of pH of HIBA on the retention of U and La. Chromatographic conditions: 0.5 M HIBA; other conditions same as in Figure 4.2.*

These studies demonstrate that U can be pre-concentrated on the RP column with HIBA at high pH of 6 to 7 and can be eluted using HIBA at pH 2.5.At low pH, U exists as uranyl ion (UO_2^{2+}) and would have no preference for the RP column.

4.2.3.2 Optimization of Parameters for U Separation

Figure 4.4 (a) shows the chromatogram obtained for injection of 20 µL of aqueous solution containing 10 ppm of U. Elution was carried out isocratically using 0.2 M HIBA of pH 2.5. The chromatogram shows two closely eluting peaks. The peak height of the second peak decreased with sample dilution with no effect on the first peak which was found to depend on the volume of the condition solution passed and sample solution injected. Thus the

second peak was identified to be that of U. The first peak was also seen during the blank experiments and probably corresponds to the elution of HIBA sorbed onto the stationary phase during conditioning, loading and washing stages. Since the two peaks were eluting quite closely, studies were performed to improve the resolution between the two peaks.

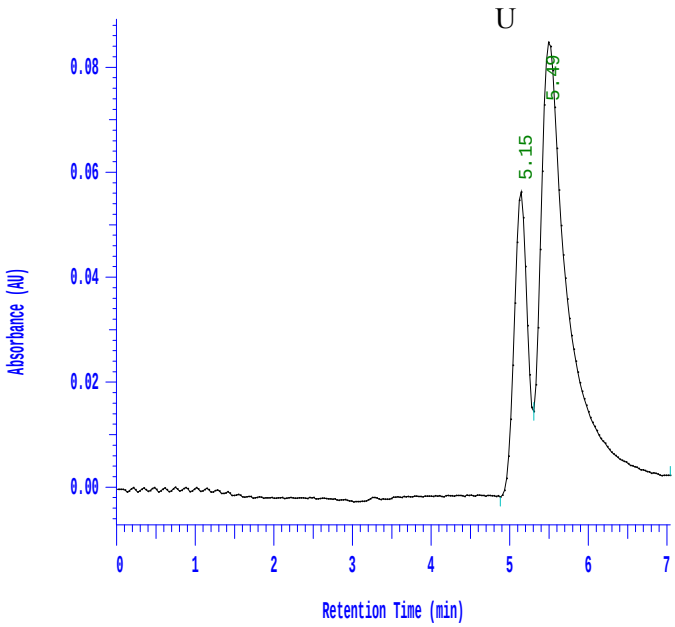

Figure 4.4(a): *Chromatogram of isocratic separation of U.*
Chromatographic conditions: 0.2 M HIBA of pH 2.5;injected 10 µg g^{-1} of U through 20 µL loop; other conditions same as in Fig.4.2.

It was observed during previous studies that the peak shape and the response of U peak improve with the increase in the methanol content in the mobile phase (Section 3.2.3.3). Hence, a concentration gradient of methanol and HIBA as given in Table 4.2 was selected for the separation of U. Figure 4.4 (b) shows the chromatographic separation of U under optimized gradient conditions.

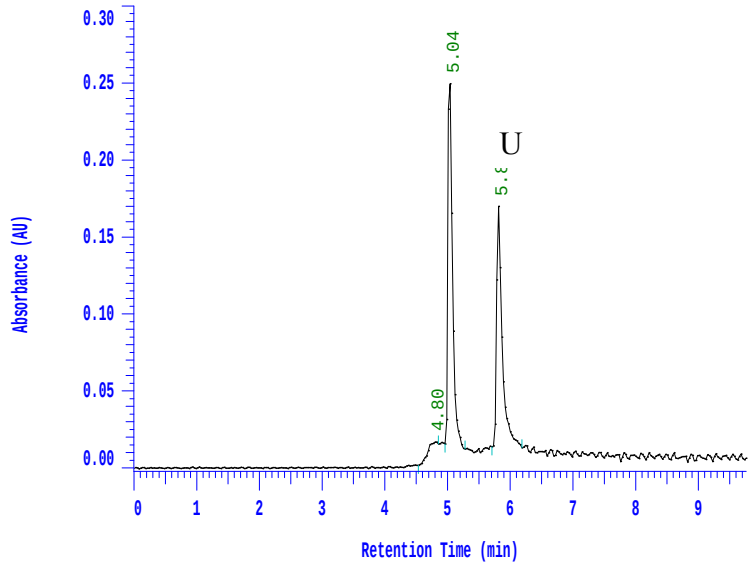

Figure 4.4(b): *Separation of U under the optimized gradient condition. Chromatographic conditions: mobile phase as per Table 4.2; other conditions same as in Fig. 4.4 (a).*

4.2.3.3 Pre-concentration Studies

Since a larger volume of the seawater sample needs to be injected for pre-concentration of U, efforts were made to introduce the sample into the column using one of the inlets of quaternary gradient pump. This has the advantage of accurate sample delivery and ease of operation by programming all the steps to be executed in sequence. However, no elution peak for U could be seen using this procedure. A detailed examination revealed that during sample loading step, U gets adsorbed onto the walls of PTFE tubing used as solvent inlets and, therefore, does not reach the RP column. This was checked by flushing the inlet tubing with pH 2.5HIBA as shown in Fig. 4.5.This is in sharp contrast to a report published in literature which employed the hydrophobic interaction of uranyl complexes as basis of enrichment [123]. This approach resulted in significant loss of U (> 80% for 50 mL solution with 100 ppb of U) during the on-line pre-concentration.

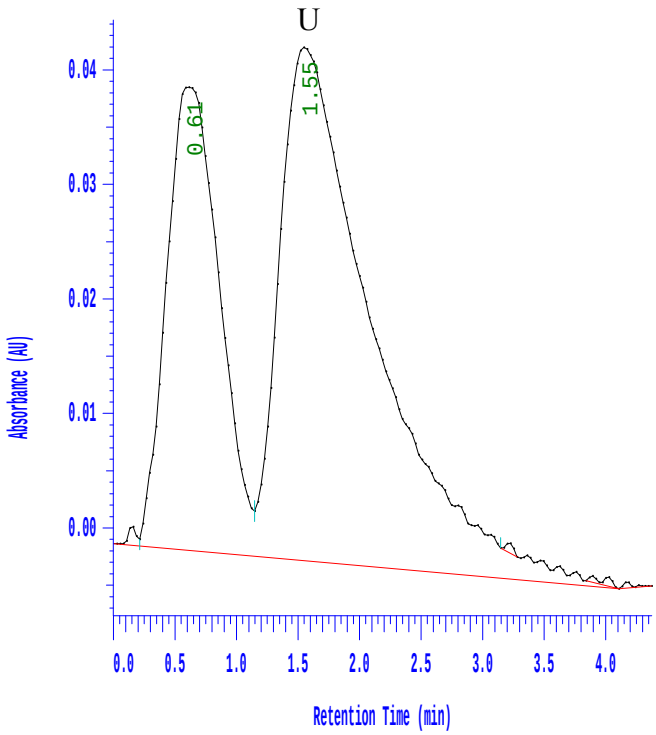

Figure 4.5: *Chromatogram of elution of U adsorbed onto the PTFE tubing. Loading condition: 50 mL of 100 ppb U in 0.025 M HIBA passed through the PTFE tubing; Elution condition: 0.2 M HIBA of pH 2.5.*

To overcome the poor recovery problem, 20µL loop of the Rheodyne injector was replaced with a custom-made 2.4 mL loop. Initially, the sample solution was repeatedly injected manually onto the column with intermediate flushing with conditioning solution and elution with the (HIBA + MeOH) gradient. Though the method offered linear response for aqueous samples with U amounts ranging from 10 ppb to 1000 ppb, it was abandoned for further studies due to the fact that multiple injection procedure is laborious. In addition, injection loop needs to be flushed with sample solution of at least 3 times the loop volume to ensure reproducible results [173]. In view of the consumption of large volume of sample and the difficulty associated with the manual injection, multiple manual injections was not followed.

A high-pressure pump with all stainless tubing connection was, therefore, used as a concentrator pump for delivering the sample into the column. Sample was prepared in 0.025M HIBA and a definite quantity of the sample was fed through the column after

adjusting the pH to 6-7. The effluent from the column was collected and weighed to determine the actual amount of the sample solution passed through the column. The column is then connected to the HPLC system for U separation. Under the optimized conditions, most of the interfering metal ions (10 ppm of each of V, Ni, Ti, Mo) were not retained on the column. The separation of U was then carried out using (MeOH + pH 2.5HIBA) gradient and the chromatographic run was completed in 6 min. This arrangement was found to give satisfactory recovery of U.

4.2.3.4 Studies with Simulated Samples

Simulated seawater sample containing 10 ppb of U was prepared and 50 mL of this solution was fed to the column at different flow rates. The effect of sample loading flow rate on the recovery was studied by loading at 0.5mL min^{-1} to 2.5 mL min^{-1}. Figure 4.6 shows the effect of flow rate on the recovery of U by the RP column. It is seen that recovery of U remains independent of flow rate in the range 0.5 to 1.5mL min^{-1} and at higher flow rates there was a steady loss on the amount of U retained by the column. Hence, a flow rate of 1.5mL min^{-1} was chosen for carrying out the sample loading studies. Recovery of U was found to be 94±5% for 50 mL of 5 ppb of U in simulated seawater sample. Linearity studies were carried out using simulated seawater sample. 50 mL of solutions containing U in the range 1 to 50 ppb were analysed by the developed procedure. Figure 4.7 shows the linearity observed for the peak area response as a function of U concentration from 1 to 30 ppb and the regression coefficient (R^2) obtained was 0.998. Detection limit of U in simulated seawater was found to be 0.2 ppb employing 100 mL of sample with a S/N ratio of 3 [174]. Intra-day precision of the developed method was evaluated by analyzing ten replicates of simulated seawater sample containing 10 ppb of U and was found to be 7%.

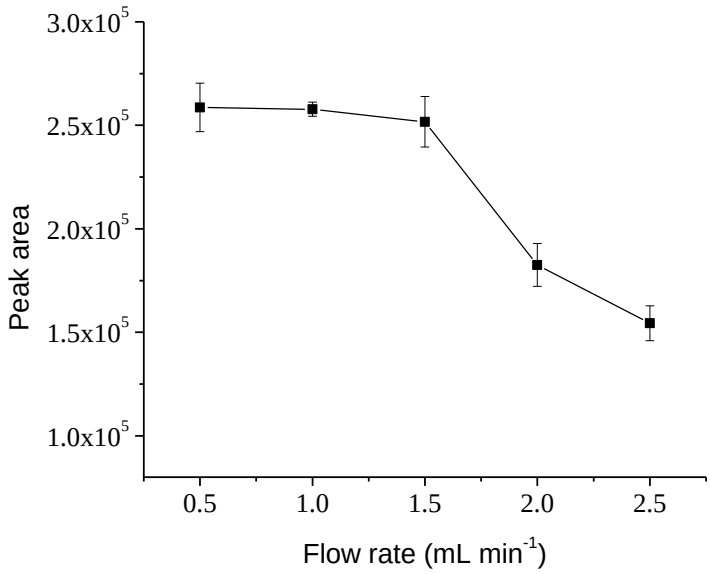

Figure 4.6: *Recovery of U as function of loading flow rate. Chromatographic conditions: 50 mL of 10 ppb U in simulated seawater solution containing 0.025 M HIBA and pH 6 – 7 was passed through the pre-conditioned 50 mm x 4.6 mm column. After washing with 10 mL of 0.025 M HIBA, elution was carried out as per the conditions given in Table 4.2.*

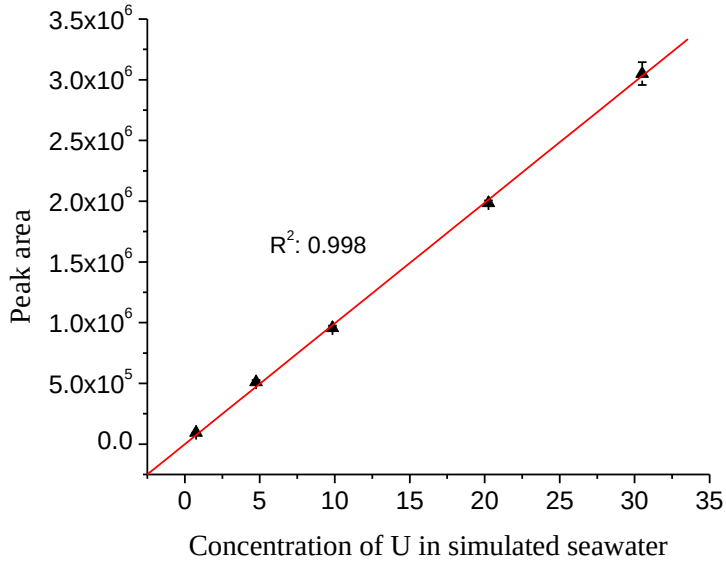

Figure 4.7: *Peak area of U as function of its concentration in simulated seawater. Chromatographic conditions: Sample passed through the column at 1.5mL min^{-1}. Other conditions same as in Figure 4.6.*

4.2.3.5 Analysis of Seawater Samples

In seawater U exists in the hexavalent state and anionic uranyl-carbonato complexes, $[UO_2(CO_3)_2]^{2-}$ and $[UO_2(CO_3)_3]^{4-}$govern the chemical behavior of U in solution under

seawater conditions [175]. Acidification of seawater samples results in the destabilization of the carbonato species and the formation of uranyl-hydroxo or uranyl-aquo complexes. Hence the seawater samples were acidified with HNO_3 to pH 2-3 and boiled for 15 min to ensure complete dissociation of the carbonato complexes. pH of the treated samples was then adjusted to 6 – 7 and the HPLC analysis was performed as per the procedure discussed above. 25-50 mL of this treated sample was used for pre-concentration. Three seawater samples were analysed for U concentration by the above developed method. In the case of the samples obtained after the concentration of seawater by Reverse Osmosis (RO1 & RO2), the samples were diluted to twice the original volume to take care of the excessive salt content of the solution. Figure 4.8 shows the chromatogram obtained for one of the seawater samples. The concentration of U in seawater was determined by standard addition method in HPLC. The results obtained by HPLC and ID-TIMS are given in Table 4.3. ID-TIMS method was applied only to three seawater samples viz. SW-1, SW-2 and SW-3. It is seen that within the measurement uncertainty, the results compare well between the two methods.

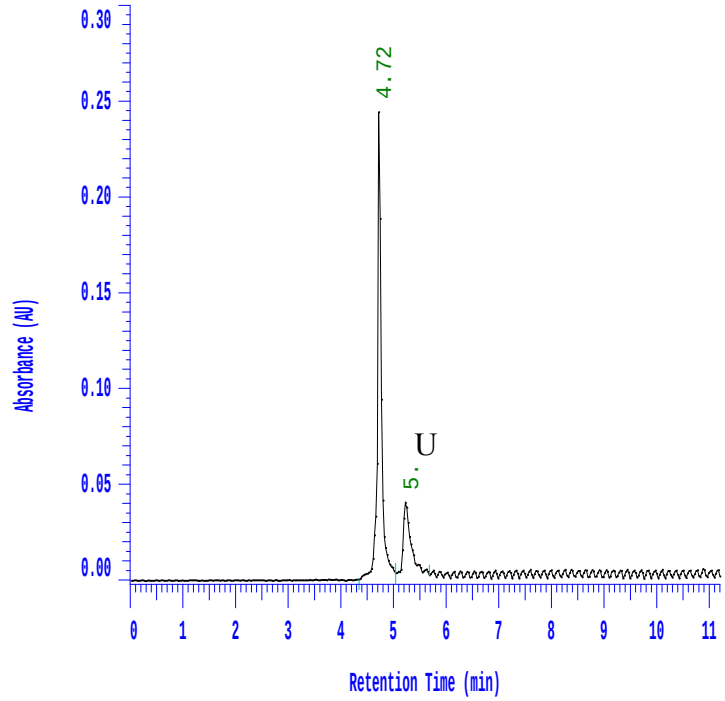

Figure 4.8: *Chromatogram obtained for a seawater sample. Chromatographic conditions: same as in Fig. 4.7.*

Table 4.3: Concentration of U in seawater determined by HPLC and ID-TIMS

Sample code	U Concentration (ng g^{-1})	
	HPLC*	**ID-TIMS#**
SW-1	3.2 ± 9%	3.4±7%
SW-2	3.4 ± 5%	3.2 ± 6%
SW-3	13.0 ± 7%	12.2 ± 5%
RO-1	5.3 ± 2%	-
RO-2	4.5± 3%	-

Chromatographic conditions: same as given in Figure4.7.
**Concentration determined by standard addition method.*
#*Mean of three determinations.*

Thus the method based on the chelation of U by HIBA at pH 6-7 and its preferential adsorption on a RP column offers a simple approach for the quantitative preconcentration of U in seawater. A gradient of 2.5 pH HIBA and MeOH was used for elution of adsorbed U from the column. No interference was observed from other metal ions viz. V, Ni, Ti and Mo.

4.3 Liquid Chromatographic Method for the Determination of Uranium in Seawater and Process Samples using Mandelic Acid as a Complexing Agent

4.3.1 Background

As discussed earlier, recovery of U from seawater is proposed as an option for increasing its availability to meet the future energy requirements. Hence recovery of uranium from seawater has gained importance in recent years and different processes are in the development stage for recovering U in an economic way [176,177]. This requires methodologies to determine U at different stages of recovery process as well as in the starting material.

Section 4.2 described about the development of an LC method for U determination in seawater using HIBA as a chelating agent [178]. This method required the use of HIBA of pH 6-7 for the effective pre-concentration of U onto the RP column. However, when determining U in processed samples containing high levels of Fe, this method was found to be unsuitable due to the clogging of the pre-concentration column by the precipitate formed in the feed solution. Process samples were collected from various stages of uranium recovery from seawater. Stripping of U from various organic based adsorbents previously immersed in sea was carried out in a vessel in 1-2 M HCl medium. The elute contains vanadium (0.06-0.8 µg/mL) and U (0.09-0.9 µg/mL) along with Fe [179]. The source of Fe could be due to the leaching from the steel vessels used for the acidic stripping of U in the recovery step. It is also reported that RP based methods lose the resolution capacity in the presence of a high concentration of Fe (III) and thus separation of uranium is affected [169]. Previously reported methods were found unsuitable for adoption of processed samples due to the presence of large amounts of Fe, inadequate detection limits, and the difficulty in adapting to RP based systems. The objectives of the work presented in this Section are (i) good separation between U and Fe

(III) so that accurate determination of U based on its chromatographic peak area is achievable, (ii) possibility to introduce the samples at pH ≤ 4.0 so that formation of turbidity is avoided, and (iii) offer quantitative recovery of U during the pre-concentration procedure.

Use of mandelic acid as a chelating agent for U was explored for the determination of U in seawater and processed samples. Though both HIBA and mandelic acid are hydroxycarboxylic acids, latter being more hydrophobic offers stronger retentions for U complex on the RP stationary phase and thus provides better recovery of U at relatively lower pH which is essential to minimize the hydrolysis of F(III). The developed methodology was found to offer good recovery of U. This method was validated by comparing the values with those obtained from isotope dilution–thermal ionisation mass spectrometry.

4.3.2 Experimental

4.3.2.1 Instrumentation

The HPLC system mentioned in Section 2.2.2 was used in the present study. Pre-concentration set-up and the thermal ionisation mass spectrometer used in the present study are already mentioned in Section 4.2.2.1. Rheodyne injector with 100 μL sample loops was used with the HPLC system. Monolith C_{18} columns(Merck) with dimensions 50 mm x 4.6 mm and 100 mm x 4.6 mm and a C_{18} particulate RP column (150mm × 4.6mm, 5 μm; Merck)were used as the stationary phases.

4.3.2.2 Reagents

Milli-Q water was used for all the dissolutions and dilutions. HIBA (Lancaster) and mandelic acid (Merck) were used as the chelating agents. Tetrabutylammonium bromide (Fluka) was used as the ion interaction reagent. Other reagents such as HNO_3, NH_4OH were used for sample treatment and MeOH was used as the organic modifier for the mobile phase.

NaCl, KCl, $MgCl_2$, $Ca(NO_3)_2$ and $SrCl_2$ (Thomas Baker) were used for preparing simulated seawater. U stock solution was prepared from uranyl nitrate after the standardization procedure mentioned elsewhere [112]. ^{233}U was used as the spike for the isotope dilution method. Uranium and Tetravalent Actinides - UTEVA resin (Eichrom Technologies Inc.) was used for the purification of U for the mass spectrometric analysis. The seawater samples and process samples were received from the Desalination Division of BARC.

4.3.2.3 Procedure

The procedure for preconcentration of U in seawater was almost similar to that reported in Section 4.2.2.3. Appropriate quantities of HIBA and mandelic acid were dissolved in water to prepare 0.5 M solutions. Different solutions were adjusted to the desired pH using NH_4OH and $HNO_3$and were filtered through 0.45 μm Millipore membrane filters. Simulated seawater was prepared as per Section 4.2.2.3. The seawater and processed water samples were treated and filtered as mentioned in Section 4.2.2.3. The filtered solution was made-up to known volume and was divided into two portions; one for HPLC analysis and the other for ID-TIMS analysis.

*HPLC Procedure:*0.075 M mandelic acid was added to the treated sample and the pH of the solution was adjusted to 4.0. The different steps involved in the HPLC analysis are summarized in Table 4.4. Blank was determined with 0.075 M mandelic acid of pH 4.0 before and after the sample analysis under identical conditions. Quantification of U was based on the area of peak from the chromatogram.

Table 4.4: Sequence of operations involved in the HPLC analysis of seawater/processed samples

Step	Mobile phase	Stationary phase	Flow rate (mL/min)	Volume (mL)	Remark
Conditioning	0.075 M mandelic acid of pH 4.0	100 mm x 4.6 mm C_{18} monolith column	1	10	Column connected to HPLC pump
Loading	Sample prepared in 0.075 M mandelic acid and pH 4.0	100 mm x 4.6 mm C_{18} monolith column	1-7	5-30	Column connected to S.S. pump
Washing	0.075 M mandelic acid of pH 4.0	100 mm x 4.6 mm C_{18} monolith column	1	10	Column connected to HPLC system
Elution	Gradient as given in Table 4.5	100 mm x 4.6 mm C_{18} monolith column and 150 mm x 4.6 mm C_{18} particulate column connected in series, in the same direction	1	20	Column connected to HPLC system

ID-TIMS Procedure: The fraction for mass spectrometric analysis was mixed with a known amount of pre-calibrated ^{233}U spike followed by treatment with 8 M HNO_3 as mentioned in Section 4.2.2.3. Purification of the U fraction was carried out using UTEVA resin as per the reported procedure [180]. The spiked mixture was evaporated, dissolved in 3 M HNO_3 and loaded onto UTEVA resin taken in a glass column (4 mm ID). Washing of the matrix elements was carried out with 3 M HNO_3. Finally, U was eluted by 0.05 M ammonium oxalate solution. The eluate was evaporated to dryness and the residue was dissolved in 1 M HNO_3 for loading onto the sample filament of a double rhenium filament assembly for TIMS analysis. The sample and the ionization filaments were heated to temperatures corresponding to heating currents of 2.2A and 6A, respectively. The mean value of $^{233}U/^{238}U$ atom ratio was determined by taking run summary from three blocks, each block consisting of 10–12 scans.

4.3.3 Results and Discussion

The possible interferences of matrix elements are iron and vanadium in process samples. It has been shown in the previous part of this Chapter that vanadium does not interfere under the RP conditions employing hydroxycarboxylic acids as eluent and hence it was not considered in the present study. Matrix elements in seawater such as Na, K, Mg, Ca and Sr do not retain under present RP-conditions. Though Arsenazo(III) is a chromogenic reagent specific for lanthanides and actinides, many other elements including Fe are also known to form coloured complexes with it, albeit with less molar absorbtivity[181]. It was found that the molar absorbtivity of Fe(III)-Arsenazo(III) was 446 M^{-1} dm^3 cm^{-1} at 650 nm, at which U elution was monitored.

4.3.3.1 Fe and U Separation study

4.3.3.1.1 Separation of Fe and U on a Modified RP Column

One of the outcomes of the studies presented in Chapter 3 is that the predominant species responsible for the retention of uranyl-mandelate is anionic in nature and its adsorption onto the RP stationary phase increases in presence of a cationic ion interaction reagent (IIR) [182]. No information was available on the retention behaviour of Fe under the similar conditions. Hence retention of Fe and U were compared on a RP column dynamically modified with tetrabutylammonium bromide as the IIR. Figure 4.9 shows the changes in the retention time of Fe and U as a function of concentration of IIR in the mobile phase. It is seen that the presence of IIR does not influence the retention of Fe and a fairly long retention (~ 23 min) is observed. It can be seen from the Figure that the separation between Fe and U is sufficiently high at IIR concentration of 0.02M. However, from practical point of view, it will not be attractive to use a cationically modified column for pre-concentration purpose, as separation takes a very long time and peak shape is broad. Nevertheless, this study

demonstrated that the kind of interaction of Fe and U with the RP stationary phase is different and thus it was decided to study the effect of concentration of mandelic acid and MeOH content on the retention of Fe and U.

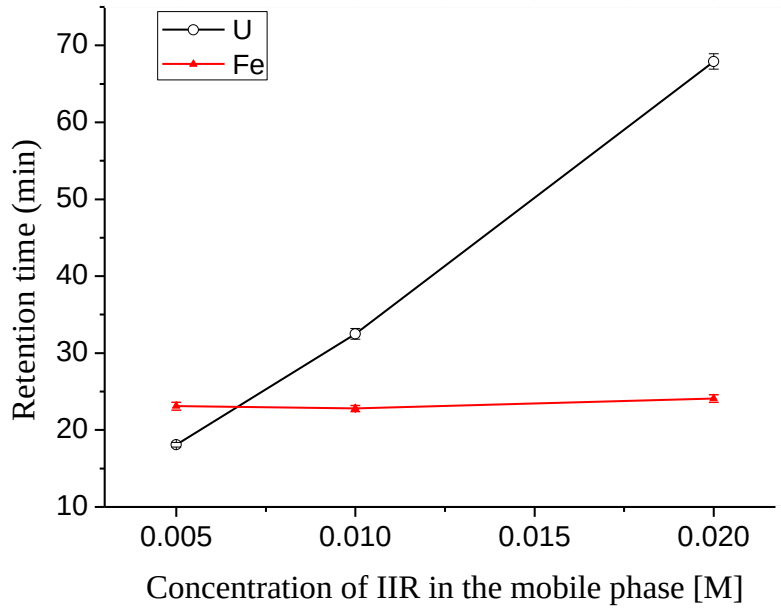

Figure 4.9*: Effect of concentration of tetrabutylammonium bromide on the retention of Fe and U.*
Chromatographic conditions: C_{18}(50 mm × 4.6 mm) monolith column; 0.2 M mandelic acid (pH 2.5).

4.3.3.1.2 Effect of Concentration of Mandelic Acid on the Retention of Fe and U

Figure 4.10 shows the effect of concentration of mandelic acid in the mobile phase (pH 2.5) on the retention of Fe and U using a 5 cm RP column. During this study 20% MeOH (v/v) was included in the mobile phase. Retention of both Fe and U show similar pattern with the change in the mandelic acid concentration in the mobile phase. In the absence of mandelic acid, both the ions elute out in the solvent front. As the concentration of mandelic acid is increased from 0 to 0.1 M, the adsorption of both the ions increases due to the formation of hydrophobic mandelate complex. However, as the concentration of mandelic acid is increased further, the competition for the stationary phase from the undissociated mandelic acid molecules (due to pH 2.5) becomes significant and retention of both the ions decreases. Thus

0.1 M mandelic acid was used in the mobile phase for further separation studies as it offers a good degree of resolution between Fe and U.

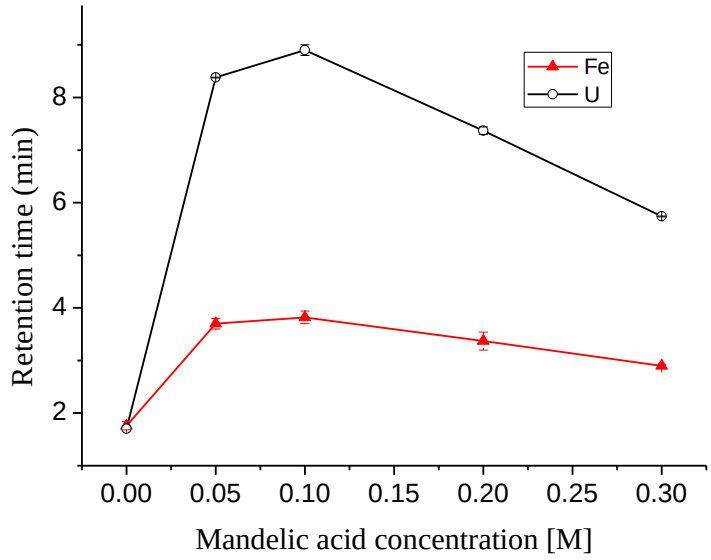

Figure 4.10: *Effect of concentration of mandelic acid on the retention of Fe and U. Chromatographic conditions: 20% (v/v) MeOH; other conditions same as in Fig. 4.9.*

4.3.3.1.3 Effect of Methanol Content on the Retention of Fe and U

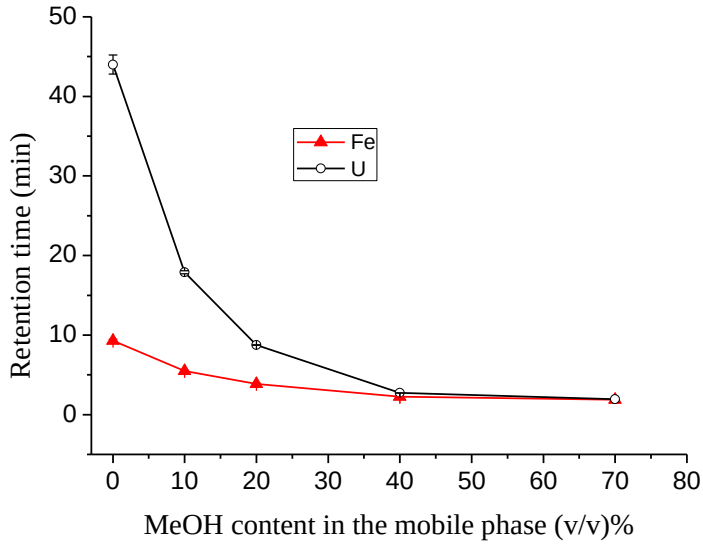

Figure 4.11: *Effect of methanol content on the retention of Fe and U. Chromatographic conditions:0.1 M mandelic acid; rest of the conditions same as in Fig. 4.9.*

Figure 4.11 shows the effect of retention of Fe and U on a RP column as a function of MeOH % (v/v) in the mobile phase. 0.1 M mandelic acid of pH 2.5 was used as eluent. With the increase in MeOH content in the mobile phase retention of both Fe and U decreases, with a drastic reduction in the retention time of U. These studies suggests that the use of a gradient system consisting of gradually increasing mandelic acid (pH 2.5) concentration and then a midway increase in MeOH content should be appropriate for improving the peak shape of U and also for improving its separation from Fe (III). The gradient conditions thus optimised for the separation of U employing a C_{18} column are given in Table 4.5. In view of increasing the separation of U peak from Fe peak and also to maximize the Fe loading, a particulate column was coupled with the monolith column while carrying out the analytical separation.

Table 4.5: Optimised gradient condition for the separation of U

Time (min)	pH 4.0 mandelic acid [M]	pH 2.5 mandelic acid [M]	% MeOH (v/v)
0	0.075	0	0
3	0	0.18	15
19	0	0.18	35

Stationary phase: combination of 100 mm x 4.6 mm monolith C_{18} column and 150 mm x 4.6 mm C_{18} particulate column.

4.3.3.2 Preconcentration Study

Since the present method employs mandelic acid which forms complexes with uranyl ion with greater degrees of hydrophobicity as compared to those formed with HIBA, operating parameters such as pH of mobile phase, concentration of chelating agent, sample-loading flow rate, volume of the sample solution and trace metal elution etc. needed optimization. As the SS pump used for the sample loading did not have a timer-control, the volume of the sample solution passed through the pre-concentrator was determined by weighing the effluent. First of all, selection of suitable elution conditions was required to evaluate the effect of all the parameters affecting the recovery of U by the C_{18} column.

4.3.3.2.1 Suitability of Eluent

It was reported by Hao *et al*. that mandelic acid is not a suitable ligand for the elution of U from a C_{18} column because of the very poor chromatographic efficiency [143]. Therefore, a ligand exchange approach by incorporating HIBA as the eluting ligand for the separation step was used in their work. Retention time of U on a 100 mm x 4.6 mm monolith C_{18} column was determined employing different eluents such as 0.2 MHIBA (pH 2.5), 0.2 M mandelic acid (pH 2.5), MeOH (20 v/v%) and combinations of (mandelic acid + MeOH) and (HIBA + MeOH). Table 4.6 shows a comparison of the retention time of U on the monolith RP column by employing different mobile phases. Retention time of U was found to be 4.4 and 22.4 min using HIBA and mandelic acid (both 0.2 M and pH 2.5), respectively. Eluents containing HIBA show better efficiency than that containing mandelic acid due to the higher thermodynamic stabilities and the faster kinetics of the HIBA complexes. However, the presence of MeOH in the mandelic acid eluent drastically reduces the retention time of U (also seen in Fig. 4.11) and can become comparable to that obtained with HIBA. It was also seen that when only MeOH was used in the mobile phase, no elution occurred till 35 min, indicating that MeOH alone is not an efficient eluent for U.

Table 4.6: Comparison of elution of U from RP column using different eluents

Mobile phase	Retention time of U (min)
0.2 M HIBA of pH 2.5 + 20 (v/v)% MeOH	1.98 ± 0.01
0.2 M mandelic acid of pH 2.5 + 20 (v/v)% MeOH	2.76 ± 0.06
0.2 M HIBA of pH 2.5	4.37 ± 0.05
0.2 M mandelic acid of pH 2.5	22.44 ± 0.09
20 (v/v)% MeOH	No elution till 35 min

Stationary phase: 100 mm x 4.6 mm monolith C_{18} column.

Hence the combination of mandelic acid and MeOH is advantageous for efficient elution apart from its ability to provide good separation between Fe and U. This implies that

the use of ligand exchange is not essential and the use of HIBA was, therefore, not explored for the separation of Fe and U. MeOH included in the mobile phase during the elution stage also improves the peak shape of U and thus increases its sensitivity. Thus, combination of mandelic acid (pH 2.5) and MeOH was used as the eluent for optimizing parameters influencing the pre-concentration of U. These studies were carried out using U solution prepared in simulated seawater.

4.3.3.2.2 Effect of Concentration of Mandelic Acid on the Recovery of U

Figure 4.12 shows the peak area (per gm of U solution passed through the concentrator column) as a function of mandelic acid used for the loading of U onto concentrator column. Mandelic acid of pH 6.0 was used in this study as at pH ≥ 6.0, HIBA showed highest recovery of U. Concentrator column conditioning, loading, and washing were carried out with mandelic acid of the given concentration. Elution was carried out by using the combination of mandelic acid (pH 2.5) and MeOH. The recovery was found to be satisfactory when mandelic acid concentration was > 0.05M. Thus 0.075 M of mandelic acid was chosen for carrying out further pre-concentration studies.

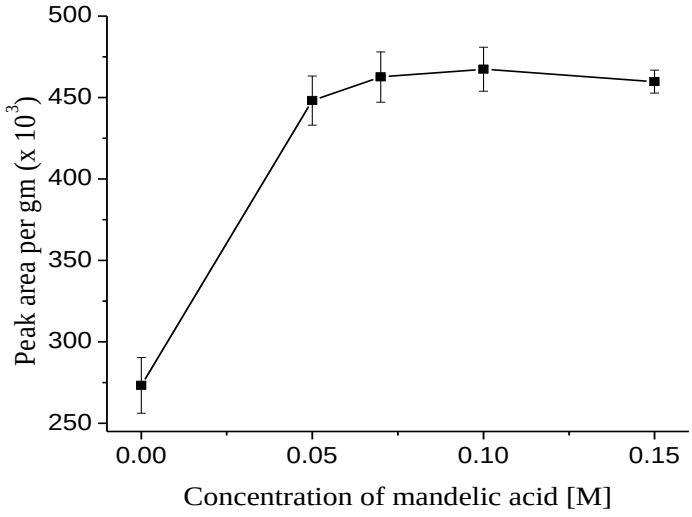

Figure 4.12: *Effect of concentration of mandelic acid on the recovery of U. Chromatographic conditions:10 mL of 75 ppb U prepared in simulated seawater containing given concentration of mandelic acid was passed through the concentrator column during loading step.*

4.3.3.2.3 Effect of pH of Mandelic Acid on the Recovery of U

The effect of pH of the conditioning and loading solutions on the recovery of U by the RP column is shown in Fig. 4.13. The study was carried out employing 50 mm x 4.6 mm monolith column. The column conditioning, U loading and washing were carried out using 10 mL of 0.075 M mandelic acid of a given pH in the range 2 – 6. When pH of the solution was < 4, U was removed from the column during the washing stage itself. Good recovery was obtained with mandelic acid solutions of pH 4 - 6. The increased dissociation of mandelic acid at higher pH levels helps in stronger complexation and thus the retention increases. The strong hydrophobic nature of mandelic acid complex enables the better retention and hence recovery at relatively lower pH as compared to HIBA. Thus pH 4.0 was chosen for carrying out further studies. Lower pH is preferred as it would minimize the hydrolysis of other metal ions present in processed seawater samples and prevent the formation of turbidity. Though it is a practice to include a small percentage of MeOH(1-5%) in the loading solution to wet the surface of the RP concentrator, it was not followed in the present study since the presence of MeOH adversely affects the breakthrough volume of uranyl-mandelate.

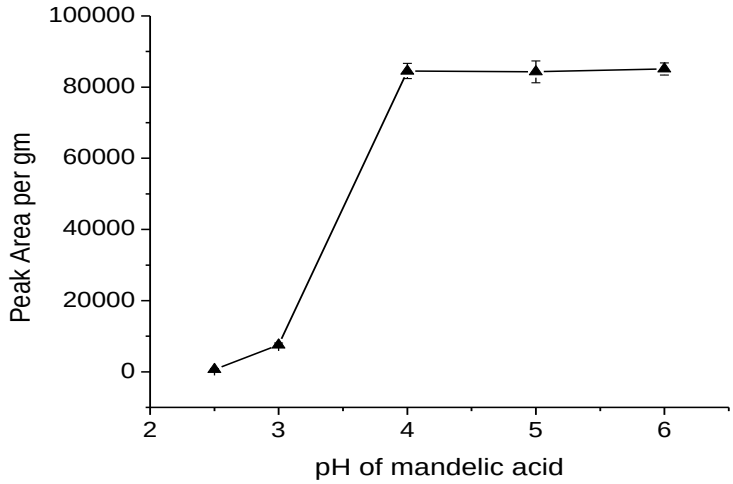

Figure 4.13*: Effect of pH of mandelic acid on the recovery of U.*
Chromatographic conditions:10 mL of 0.075 M mandelic acid of a given pH was used for conditioning, sample loading and washing of the concentrator column; 15 ppb U prepared in simulated seawater containing 0.075 M mandelic acid was passed through the concentrator column at a flow rate of 1 mL/min.

4.3.3.2.4 Effect of Amount of the Sample Solution

This study was carried out to determine the maximum amount (volume) of the sample solution that can be passed through the column without affecting the quantitative recovery of U. This study was initially carried out employing a 50 mm x 4.6 mm column as the concentrator. The previously conditioned column was connected to the off-line pump and different volumes of simulated seawater containing U were passed through the column. The column was then subjected to washing followed by elution as discussed previously. The shape and area of U peak were examined over a range of 1 mL to 100 mL of simulated seawater containing 10 ppb of U at a flow rate of 1 mL/min. Though a linear relationship was observed between the U peak area and the loading volume up to 100 mL, it was found that the peak showed considerable broadening for volumes ≥ 50mL. For example, the peak width was 1.6 min for 50 mL and was increased to 4.2 min for 100 mL. This observation indicates that though the concentrator column quantitatively retains U within the volume range studied, there is a definite spreading of the analyte taking place due to the self-elution by the loading/washing solution. This can have two deleterious effects: (i) restricting the detection limit of the method as low-level concentration of the analyte would demand the passage of a large volume of the samples, and (ii) probability for interference in view of the excessive broadening. Hence, it was decided to use a monolith column of larger dimension (100 mm x 4.6 mm) for pre-concentration and to introduce a particulate column for carrying out the separation. Table 4.7 shows the comparison of the U peak area as well as peak width obtained for the passage of different amounts of U solution through the two different concentrator columns. It is seen that the peak area obtained using the combination of 100 mm x 4.6 mm monolith column for the concentration and 150 mm x 4.6 mm particulate column for the separation yielded better peak shape and a linear response was obtained for the sample

solution amount up to 200 mL. This also indicates that in the case of 100 mm x 4.6 mm monolith concentrator, breakthrough volume for uranyl-mandelate is greater than 200 mL.

Table 4.7: Comparison of the data on the response of U using two different stationary phases for concentration and separation

50 mm x 4.6 mm monolith column as concentrator column and 100 mm x 4.6 mm monolith as separation column				**100 mm x 4.6 mm monolith column as concentrator column and 150 mm x 4.6 mm particulate as separation column**			
Amount of solution (gm)	Peak area	Area/gm	Peak width (min)	Amount of solution (gm)	Peak area	Area/gm	Peak width (min)
1.0045	68784	68476	1.3	0.9677	66792	69021	1.5
4.895	326409	66682	1.3	5.1083	330982	64793	1.6
25.0589	1676809	66915	1.5	25.098	1653834	65895	1.6
53.1483	3358753	63196	1.8	49.0583	3123911	63678	1.7
100.072	6189352	61849	4.3	94.911	6360941	67020	1.9
-	-	-	-	203.86	1.4E+07	68033	2.3
Average area/gm		65424±4%		Average area/gm		66407±3%	

Concentration of U: 10 ppb in simulated seawater solution.
Elution conditions as per Table 4.5.

In most of the reported methods, elution of the analyte from the concentrator is done by back flushing i.e. the sample loading is carried out in one direction and the elution is performed in the opposite direction [143,168]. It was decided to examine whether the back flushing of uranium-mandelate from the concentrator column helps in improving the peak shape. Chromatograms were recorded using a 50 mm x 4.6 mm monolith column as the concentrator and a 100 mm x 4.6 mm monolith as the analytical column. The pre-conditioned column was loaded with 50 mL of 5 ppb U prepared in simulated seawater containing 0.075 M mandelic acid and pH 4.0. In the first set of experiments, sample loading, column washing (10 mL) and elution were performed in the same direction of the flow. Figure 4.14(a) shows the chromatogram obtained under the forward flush conditions. Figure 4.14(b) shows the chromatogram obtained by carrying out the experiment in the same way except the elution

was carried out in the opposite direction of the sample loading. As is seen, forward flushing yields sharper peaks as compared to back flushing and hence this configuration of concentrator and analytical columns was used for further studies. Comparison of retention time and peak shape of chromatograms (a) and (b) indicates that the diffusion of the analyte band must be occurring to a certain extent within the concentrator during the sample loading and washing stages for the entire range of injection volume studied.

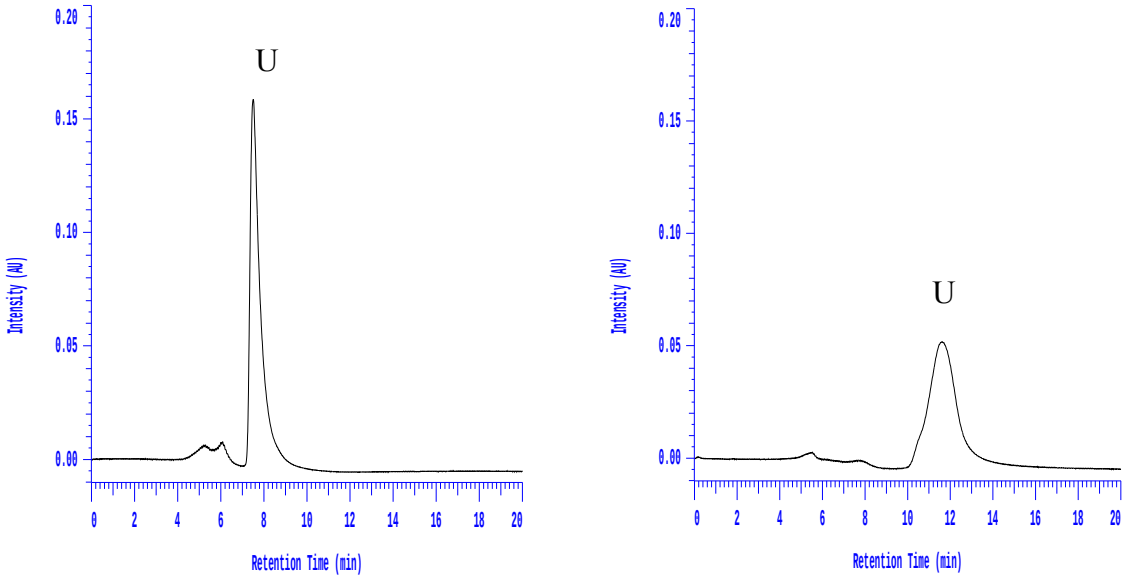

(a) **(b)**

Figures 4.14: *Chromatograms obtained by the elution of concentrator column (a) in the forward and (b) in the reverse directions.*
Chromatographic conditions: concentrator column 50 mm x 4.6 mm monolith column and 100 mm x 4.6 mm monolith as analytical column. Conditioning and washing of the column with 0.075 M mandelic acid pH 4.0; loaded 50 gm of 5 ppb U prepared in simulated seawater containing 0.075 M mandelic acid and pH 4; elution as per the gradient in Table 4.5.

4.3.3.2.5 Effect of Sample Loading Flow Rate on the Recovery of U

A 100 mm x 4.6 mm C_{18} monolith column was used for carrying out pre-concentration whereas a combination of this monolith column and a 150 mm x 4.6 mm C_{18} particulate column was used for the separation of the retained species. Due to its high porosity, monolith column offered the advantage of low pressure operation even at high sample loading flow rates (< 90 bar at 7 mL/min). Use of particulate column with its high capacity ensured good

separation between U and Fe even when the latter is present at a higher proportion. Thus the use of monolith column in combination with particulate column shortens the overall analysis time, ensures the complete transfer of analytes to the separating column and better efficiency for separation. The conditioned monolith column was connected to pre-concentration pump. Approximately 10 mL of uranyl solution (5 ppb) prepared in simulated seawater containing 0.075 M of mandelic acid and pH adjusted to 4.0 was passed through the column at different flow rates in the range 0.5 mL/min to 7.7 mL/min. After the loading process, washing and elution of the column was done as described previously. Uranyl peak area/gm of sample solution passed was determined as a function of flow rate of the loading solution. Figure 4.15 shows the response of uranyl peak area/gm of sample solution passed as a function of flow rate of the loading solution. It is seen that the sample loading flow rate does not affect the retention of uranyl-mandelate on the stationary phase up to 7.7 mL/min, which was the maximum flow rate possible with the concentration pump. The combination of C_{18} monolith column with high permeability as a concentrator and mandelic acid as a ligand forming strong hydrophobic complex with U resulted in a pre-concentration system offering flexibility of sample loading rate depending upon the concentration and volume of the sample solution.

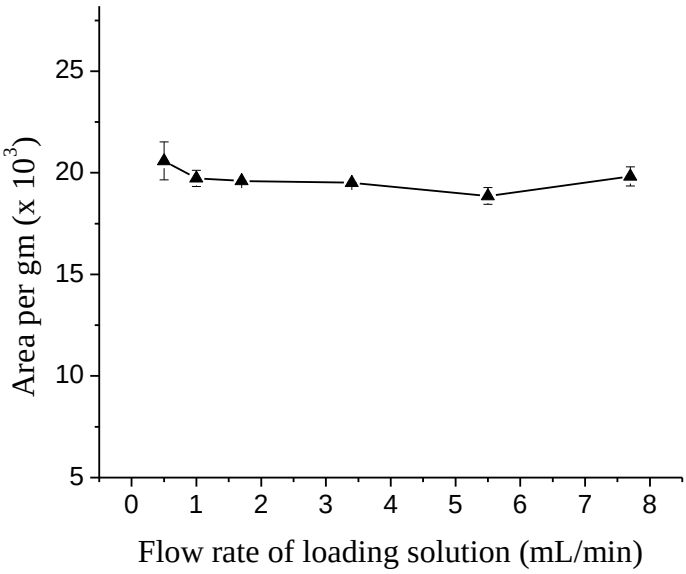

Figure 4.15: *Effect sample loading flow rate on the recovery of U. Chromatographic conditions:100 mm x 4.6 mm monolith column was used as concentrator column, a combination the monolith column and 150 mm x 4.6 mm particulate column was used for the separation. Other conditions same as Fig. 4.14.*

4.3.3.3 Linearity and Reproducibility of the Method

The method optimised for the determination of U in seawater and processed samples based on the above set of experiments is summarized in Table 4.4. Linearity of the method with respect to the concentration of uranyl solution was examined by loading 10-25 mL of simulated seawater samples containing uranyl ion in the concentration range 0.5 ppb to 1000 ppb at a flow rate of 3 mL/min. Rest of the procedure was same as described in Table 4.4. Figure 4.16 shows the U peak area per gm of the simulated seawater solution passed through the concentrator column as a function of concentration of U in the sample solution. A linear relationship between the peak area/gm of sample solution for U concentration was observed from 0.5 ppb to 500 ppb with a regression coefficient r^2=0.999. However, the response was saturated at concentrations above 500 ppb of U. Simulated seawater solution containing 5 ppb of U was repeatedly analysed (n=12) as per the above method over a period of two days and

the reproducibility (%RSD) on the U peak area/gm of sample solution was found to be 3.6%. The detection limit of the method was found to be 0.2 ppb of U using 30 mL of simulated seawater passed through the pre-concentrator and considering the S/N of 3.

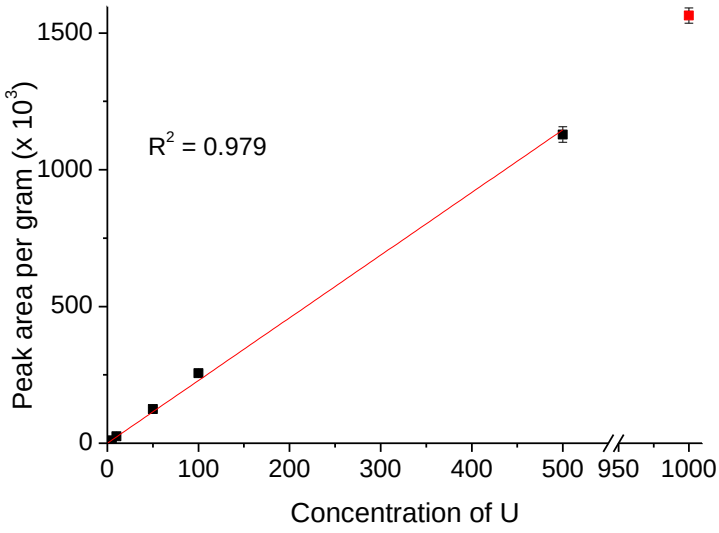

Figure 4.16*: Peak area/gm of U as function of its concentration in simulated seawater. Chromatographic conditions as per the Table 4.4.*

The quantitative recovery of U by the optimized method was also verified. 100 ppb of U solution prepared in simulated seawater solution was injected directly through the 100 µL loop connected to the Rheodyne injector and the chromatogram was recorded by running the elution gradient. Subsequently, multiple injections were given through the same 100 µL loop before carrying out the elution. Later on the conditioned concentrator column was mounted onto the pre-concentration pump and known amounts of uranyl solutions were passed through the column followed by washing as mentioned previously. The loaded pre-concentrator column was then connected to the HPLC system and elution was performed. The area/mL obtained for the U peak under different injection/loading conditions are compared in Table 4.8. It is seen that the method offers quantitative recovery for U from simulated seawater solution.

Table 4.8: Comparison of peak area/mL obtained for U under different injection/loading conditions

Mode of sample introduction	Injected volume	Peak area	Area/mL
Direct injection using Rheodyne	100 µL	64890	648900
	2x 100 µL	129038	645190
	5 x 100 µL	320517	641034
	15 x 100 µL	965698	643799
Off-line pre-concentration pump	3.8 mL	2453576	645678
	7.9 mL	5134080	649884
	16.0 mL	10532784	658299

Concentration of U: 100 ppb in simulated seawater solution.
Elution condition as per Table 4.5.

4.3.3.4 Effect of Fe on the Recovery of U

One of the objectives of this work was to determine U in processed samples containing larger proportions of Fe. Thus studies were carried out to find out the effect on recovery/quantification of U by including varying proportions of Fe and U in the simulated seawater containing 0.075 M mandelic acid and pH 4.0. Fe to U amount ratio in the simulated sample was varied from 0 to 3000. The concentration of U was maintained at 10 ppb in all the cases and about 10 mL of the sample solution was passed through the column. The column conditioning, washing and elution were performed as described previously. Figure 4.17 shows the chromatogram showing the separation of a simulated seawater sample containing Fe and U in the proportion 3000:1. It is seen that U peak area is not affected by the presence of Fe in the sample up to a Fe/U amount ratio of 3000. Further, there was enough time difference (~ 1 min) between Fe and U peaks to assure the unbiased determination of U.

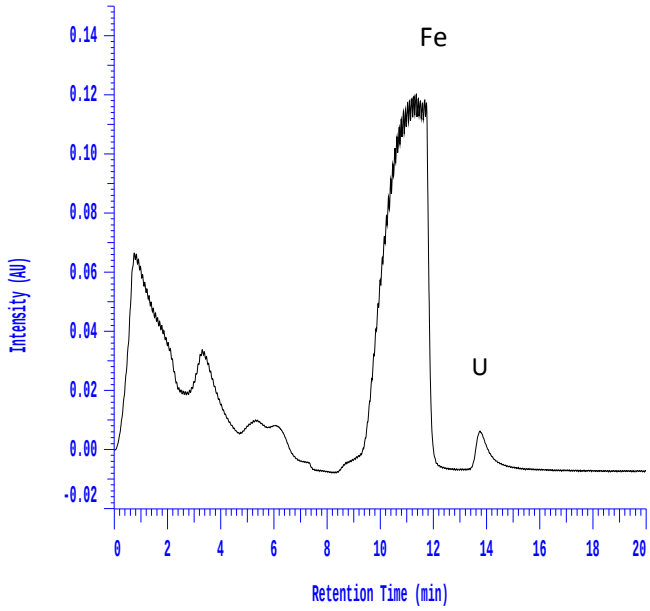

Figure 4.17: *Chromatogram of a simulated seawater sample containing Fe and U in the proportion 1:3000.*
Chromatographic conditions: concentrator column: 50 mm x 4.6 mm, rest of the conditions same as in Table 4.4.

4.3.3.5 Analysis of Seawater Samples

The treated seawater samples were mixed with the required quantity of mandelic acid and pH of the solution was adjusted to 4.0. The HPLC analysis was performed as per the procedure discussed in Table 4.4. Two seawater samples (SW) and two processed samples (PSW) were analysed for U concentration by the developed method. The processed sample was 40 times diluted before passing through the concentrator column. Figures 4.18 (a) and (b) show the typical chromatograms obtained for the seawater sample and processed sample, respectively. As it is seen, U peak is well separated from Fe peak in the case of process sample. Concentration of U in seawater was determined by standard addition method employing HPLC. The results obtained by HPLC and ID-TIMS are given in Table 4.9. It is seen that within the measurement uncertainty, the results compare well by the two methods.

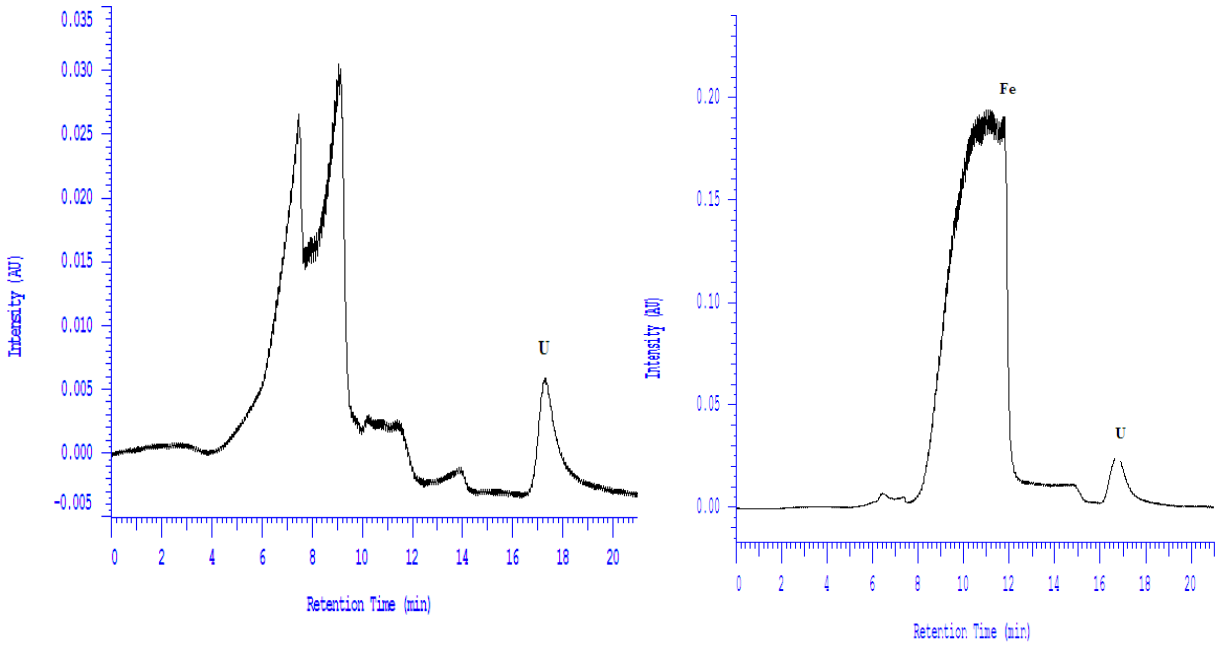

(a) **(b)**

Figures 4.18: *Chromatograms obtained for (a) seawater sample and (b) processed sample.*

Table 4.9: Concentration of U in seawater and processed samples obtained by HPLC and ID-TIMS

Sample code	U Concentration (ng/g)	
	HPLC*	ID-TIMS#
SW-1	3.1 ± 8%	3.2 ± 6%
SW-2	13.5 ± 7%	12.2 ± 5%
PSW-3	769 ± 3%	767 ± 2%
PSW-4	6.9 ± 6%	7.8 ± 5%

**Concentration determined by standard addition method*

#Mean of three determinations

Thus the pre-concentration method using mandelic acid as the chelating agent allows carrying out the quantitative recovery of U at lower pH conditions and thus made the method adaptable for processed seawater sample containing larger amounts of Fe. The combination of optimised gradient condition as well as the choice of the stationary phase helped to obtain good separation between Fe and U peaks. As a result, the LC method based on mandelic acid

as the chelating agent yielded a wider dynamic range and more ruggedness as compared to the one based on HIBA.

4.4 Conclusions

Two LC methods, one based on HIBA and the other based on mandelic acid as the chelating agents, were developed for the ultra-trace level determination of U in seawater. The methods involve preconcentration followed by analytical separation. The pre-concentration method based on the chelation of U by HIBA at pH 6-7 and its preferential adsorption on a RP column offers a simple approach for the quantification of U in seawater. Low pH HIBA and MeOH were used for elution of adsorbed U from the column. In this method, the same column was used for the pre-concentration and separation of U. The methodology was applied for the determination of U present at ppb levels in seawater. However, this methodology could not be used for the determination of U in processed seawater samples due to the presence of large amounts of Fe.

In the second method based on mandelic acid, a monolith column and a combination of monolith and particulate column was used for the preconcentration and separation, respectively. The pre-concentration method for U is robust in terms of flow rate, volume of sample and offers tolerance to pH up to 4. Hence the method offers excellent recovery of U from seawater and process samples containing large amounts of iron. Elution conditions were optimized by studying the concentration of mandelic acid, MeOH content in the mobile phase etc. to provide good separation of U and Fe. The optimized LC separation offers quantification of U in presence of Fe up to an amount ratio of 3,000. The approach offers quantitative pre-concentration of uranium in the concentration range of 0.5 to 500 ppb. This methodology was applied for the determination of U in seawater and process samples.

Both the methodologies were validated by simulated samples as well as by comparing the results obtained on seawater samples by HPLC and ID-TIMS. No interference was observed in both the methods from other metal ions viz. V, Ni, Ti, Mo and other major ions such as Na, K, Mg, and Ca. the developed LC methods presents economically viable way for the U determination in seawater.

Chapter 5

ESI-MS Studies on Uranyl Complex with α-Hydroxyisobutyric Acid and Mandelic Acid

5.1. Introduction

Research on complexation of U is of interest in nuclear technology as well as in environmental science. Speciation studies of U are important to understand its solution chemistry which is a decisive factor in nuclear fuel reprocessing, waste handling, mobility and fate in the geologic subsurface [183].Speciation data of U are essential to predict its behavior in fuel reprocessing and also to develop the flow sheet for reprocessing of the spent nuclear fuels by solvent extraction process [184,185]. The potential impact of the release of radionuclide to the environment is influenced by the speciation characteristics of the element [186-188].A few studies on actinide complexation reported in the literature have provided better understanding of the interactions of complexing agents present in the environment [189-192].

It is established that the migration of radionuclides in the environment is greatly influenced by the complexing agents especially, humic substances due to their ubiquitous presence in the environment and large number of functionalities[193-196].Since humic substances are very complex and their exact structures are not accessible, it is suggested that simple compounds such as lactic acid, alpha hydroxyisobutyric acid (HIBA) and salicylic acid that mimic the main functionalities can be used as model compounds to understand their binding characteristics[197-199].Derivatives of hydroxycarboxylic acids are also used for the decontamination of radionuclides such as U from different surfaces [200].Hydroxycarboxylic acids are also used as eluents for the separation of lanthanides and actinides by liquid chromatography (LC)[97,129,201]. HIBA is also used as a chelating agent in capillary electrophoresis (CE) for improving the separation of lanthanides [38,43,44]. Studying the nature of different species of the metal-eluent complexes is, therefore, important from the point of view of designing better chromatographic as well as CE conditions for their separation.

Electrospray ionization mass spectrometry (ESI-MS) is emerging as a useful tool for studying the metal speciation in solution [202]. The measurement of chemical species in solution by ESI-MS has several potential merits such as high sensitivity, specificity, speed and the ability to determine stoichiometry. Studies have shown that there exists a fairly good agreement between the solution phase equilibrium and gas phase ion abundances[203-205]. Reports are available in the literature on the ESI-MS studies on the interactions of uranyl ion (UO_2^{2+}) with different ligands. Stipdonk *et al.* investigated the collision induced dissociation pathways of UO_2^{2+} complex with water and methanol [206].Pasilis and Pemberton reported the speciation dependence of UO_2^{2+}- citrate system on the pH of the medium [192]. Stepper *et al.* reported the general trend in the hydrolysis of uranyl species by the direct ESI-MS measurement of sample solutions [207]. However, the chemical species observed by ESI-MS may include species produced through ionization, ion extraction processes and solvent evaporation[208].

This Chapter deals with the characterization of UO_2^{2+}complex formed with the hydroxycarboxylic ligands viz. HIBA and mandelic acid using ESI-MS. The speciation data of the complex formed between $UO_2^{2+}$and the ligand can assist in designing optimum conditions for different separations. For example, it was seen in Chapter 3 that the liquid chromatographic elution pattern of U and Th reverses when mandelic acid was used as an eluent instead of HIBA[182].

Initially, ESI-MS was used to characterize the different uncomplexed uranyl species after optimizing the experimental parameters. Later, the technique was employed to follow the speciation of uranyl-HIBA complex as well as uranyl-mandelate complex in water-methanol medium. One of the objectives of the present study was to identify the suitable mobile phase conditions for acquiring the ESI-MS spectra of uncomplexed uranyl and uranyl-HIBA complex systems. The work also focuses on the optimisation of experimental conditions to

reflect a reasonable approximation to the true solution conditions. The overall trend in the complexation was studied as a function of ligand-to-metal ratio. The complexation study of uranyl-mandelic acid system was also performed the same manner. The ESI-MS studies of uranyl-hydroxycarboxylate system carried out in this Chapter can be summarized as follows:

1. Studies on uncomplexed uranyl system to optimize the experimental conditions

2. Speciation studies on the uranyl-HIBA system

3. Speciation studies of uranyl-mandelic acid system

5.2 Experimental

5.2.1 Instrumentation

An electrospray mass spectrometer with Quadruple-Time-of-Flight analyzer (model micrOToFQ-II, Bruker Daltonik GmbH) was used for the studies. Compass Isotope Pattern software (Bruker Daltonik GmbH) was used to obtain theoretically predicted spectra. Compass Data Analysis software (Bruker Daltonik GmbH) was used to process the data obtained in the MS as well as in MS/MS modes. Samples taken in a 500 µL syringe were introduced into the ESI-MS system using a syringe pump (Nemesys, Cetrol GmbH). pH measurements were done using a PHAN pH meter with a glass electrode (Labindia, Mumbai).

The atmospheric pressure ionization interface settings such as lens voltage and quadrupole voltage were initially optimized for maximum ion transmission by using the sodium formate tune mix. Capillary potentials of -4500 V and +3800 V were employed for the measurements performed in the positive ion mode and in the negative ion mode, respectively. An end-plate off-set voltage of -500 V was employed during these studies. High purity argon was used as a collision gas for MS/MS. Nitrogen was used as an auxiliary gas as well as the sheath gas. The following ESI conditions were routinely employed: capillary temperature, 180 °C; sheath gas-flow rate, 4 L/min and the auxiliary gas pressure, 0.3 bar. The sample solutions were introduced into the electrospray at a flow rate of 3 µL/min.

5.2.2 Reagents

Uranyl nitrate hexahydrate (BDH), α-hydroxyisobutyric acid (Sigma-Aldrich) and mandelic acid (Merck) were used as received. Water purified by Milli-Q system (Millipore, Bengaluru, India) and methanol, isopropyl alcohol, acetone, acetonitrile and dichloromethane (Sigma-Aldrich) were used for the dilutions and also to prepare the mobile phase for sample

introduction into ESI. High purity $HClO_4$, HNO_3, NaOH and NH_4OH (Merck, Mumbai, India) were used for adjusting the ionic strength and pH. NaH_2PO_4, Na_2HPO_4, CH_3COOH and CH_3COONa (Merck, Mumbai, India) were used for preparing the buffers needed for pH meter calibration. Sodium formate (Sigma-Aldrich) prepared in methanol was used for mass calibration of the instrument.

5.2.3 Procedure

Stock solution of uranyl nitrate (10^{-2} M) was prepared by dissolving uranyl nitrate hexahydrate in water. 0.1 M each of HIBA and mandelic acid solution was also prepared in water. Solutions for the ESI experiments were prepared by mixing the aqueous stock solutions with methanol and water such that the composition of the resultant solutions ranged from 10% to 100% of methanol by volume. Solutions of uranyl nitrate ($5x10^{-6}$ M) and the ligand were mixed on volume basis to obtain the required proportion of ligand-to-metal ratio. After the introduction of a given sample into the ESI-MS system, the nebulizer was taken out and cleaned by manually injecting a solution of 10^{-4} M HNO_3 in methanol. While measuring pH of the electrospraying solutions prepared in methanol-water mixture, correction was applied for the presence of methanol following the method reported by Canals *et al.*[209].

5.3 Results and Discussion

5.3.1 ESI-MS Studies on Uncomplexed Uranyl Ion

5.3.1.1 Need of Electrolyte

Figure5.1(a) presents the ESI-MS spectrum obtained from a $5x10^{-6}$ M solution of uranyl nitrate in methanol in the positive ion mode. Initially, 100% methanol was used as the mobile phase in view of its good ESI response. The uranyl species observed were: $[UO_2(CH_3O)]^+$ *m/z* 301.06; $[UO_2(CH_3OH)(OH)]^+$ *m/z*319.06;

$[UO_2(CH_3OH)(CH_3O)]^+$ *m/z*333.08; $[UO_2(CH_3OH)(H_2O)(OH)]^+$ *m/z*337.07; $[UO_2(CH_3OH)(H_2O)_2(OH)]^+$ *m/z*355.09 and $[UO_2(H_2O)(CH_3OH)_2(OH)]^+$ *m/z*369.09. No doubly charged uranyl species were observed in the spectrum, though a peak corresponding to bare UO_2^+ ion with *m/z* 270.04 was seen with low intensity (~ 4% w.r.t. the base peak). The total ion current (TIC) was found to be highly fluctuating with time and the peak corresponding to $[UO_2(CH_3O)]^+$ was found to be partially masked by an impurity peak observed at *m/z* 301.15. When different concentrations of uranyl nitrate were introduced, the ESI-MS response of the uranyl species was not in proportion to the concentration of $UO_2(NO_3)_2$ present in the sample solution. This was attributed to the fact that the sensitivity and dynamic range achievable in ESI is greatly influenced by the ionisation process which in turn is dependent on ionic strength, ionisation efficiency and pH of the medium[210].

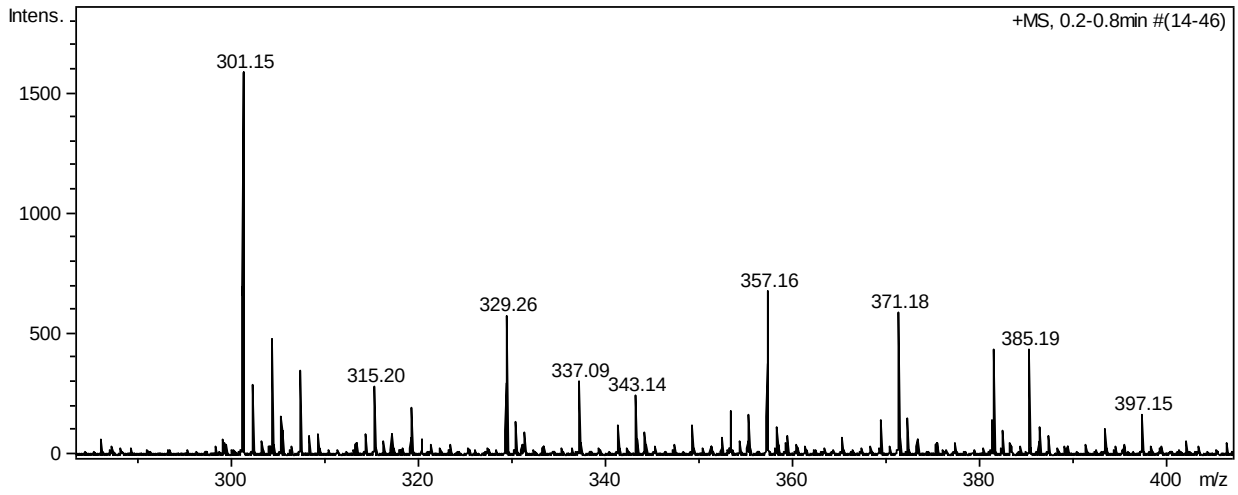

Figure 5.1(a): *ESI MS spectrum of 5x10^{-6} M $UO_2(NO_3)_2$ in MeOH, in positive ion mode.*

The abrupt change in the ESI-MS spectra obtained with higher concentrations of uranyl nitrate is due to the increase in the ionic strength of the medium. The importance of a medium which does not modify the speciation by complexation and allows for fixing the ionic strength in ESI was highlighted by Moulin *et al.*[211]. The two electrolytes, viz. perchloric acid and sodium perchlorate were added separately in the mobile phase in view of their non-complexing nature, for improving the signal stability in ESI. Data shown in Table 5.1

demonstrate the influence of concentration of two different electrolytes on the ion intensities of two representative uranyl species, $[UO_2(CH_3O)]^+$ and $[UO_2(CH_3OH)(OH)]^+$.

Table 5.1: Effect of electrolyte on the ESI response of UO_2 species

Electrolyte used	Intensity (counts per second)	
	$[UO_2(CH_3O)]^+$ ***m/z* 301.06**	**$[UO_2(CH_3OH)(OH)]^+$** ***m/z*319.06**
No electrolyte	635 ± 162	1623 ± 39
10^{-6} M $HClO_4$	38674 ± 5674	10837 ± 1460
10^{-5} M $HClO_4$	222850 ± 12162	61435 ± 3701
10^{-4} M $HClO_4$	146072 ± 313	33764 ± 204
10^{-6} M $NaClO_4$	199509 ± 3649	47733 ± 1703
10^{-5} M $NaClO_4$	258281 ± 2695	65203 ± 1187
10^{-4} M $NaClO_4$	128341 ± 456	29846 ± 34

$5x10^{-6}$ M $UO_2(NO_3)_2$ in MeOH in the positive ion mode.

It can be seen that the ESI intensities of both the species increase when either of the electrolytes was present in the mobile phase in the concentration range 10^{-6}M to 10^{-5} M and better response was obtained with $NaClO_4$ as compared to that with $HClO_4$. TIC was observed to become more stable with the introduction of these electrolytes and the ESI-MS response of the species increased in proportion to the added concentration of the uranyl salt in sample solution. The linear ESI response was obtained over a narrow range of $3x10^{-7}$ M to $7x10^{-6}$ M of uranyl nitrate concentration. The mass spectra looked cleaner without any potential impurity causing isobaric interference at the *m/z* of uranyl species of interest. The improved ESI response of uranyl species was attributed to the enhanced conductivity of the sample solution. Further, buffered ionic strength in the solution allows ESI response to be in proportion to the added concentration of uranyl nitrate in the sample solution. It was observed that the UO_2 species form complexes with ClO_4^- at concentrations $\geq 10^{-4}$ M for both the

electrolytes. A large number of peaks with specific isotopic patterns started appearing probably due to the perchlorate clusters when higher ($\geq 10^{-4}$ M) concentration of the electrolyte was employed.

Since $HClO_4$ is a strong acid, it can alter the pH of the medium at different concentrations of the electrolyte. The resultant change in pH would also affect the degree of dissociation of hydroxycarboxylic acid ligands due to the common ion effect and this can alter its complexation with uranyl ion. Thus 10^{-5} M $NaClO_4$ was selected as an electrolyte for all the experiments and Fig. 5.1(b) shows the mass spectrum obtained for $5x10^{-6}$ M uranyl nitrate prepared in 10^{-5} M $NaClO_4$ and CH_3OH.

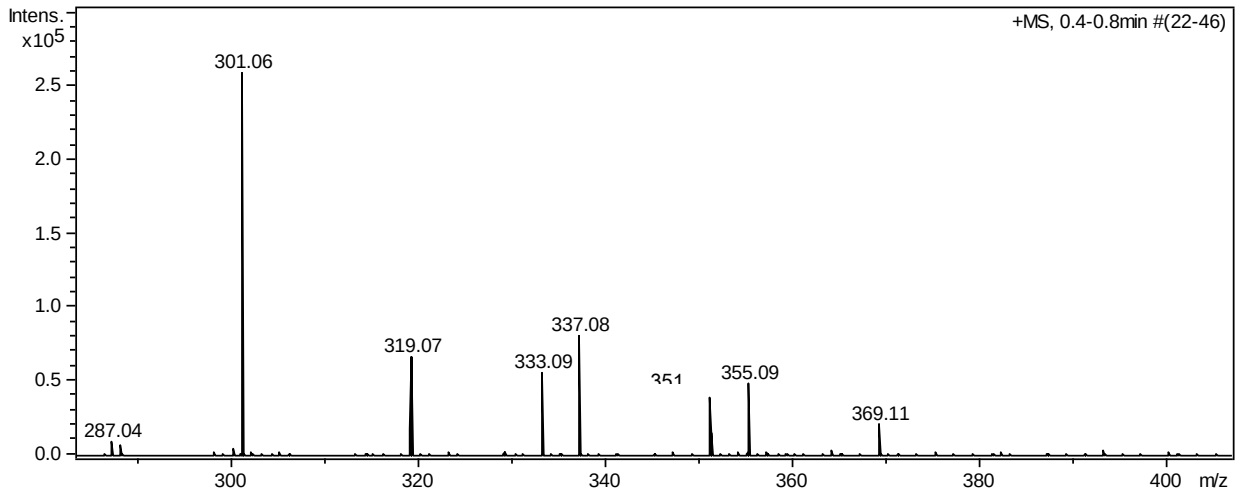

Figure 5.1(b): *ESI MS spectrum of $5x10^{-6}$ M $UO_2(NO_3)_2$ in MeOH and 10^{-5} M $NaClO_4$ added as electrolyte.*

While characterizing the solution equilibrium, it is desirable that ESI produces ions which are representative of the solution phase. Water as a medium is considered to be a better representative of actual sample solutions expected in the environmental conditions. However, ESI response of all the species was extremely poor in 100% water due to its high surface tension. Hence methanol was added in the mobile phase in view of its electrospray compatibility [85]. Other reasons favouring the selection of methanol were (i) its dipolar moment (1.71 D) being similar to that of water (1.85 D) and (ii) its use as a modifier in the

mobile phase for the LC separation of U and Th [129,182,212]. In order to identify the optimum composition of the mobile phase for the ESI investigations, the influence of solution composition on the ESI-MS spectra of uranyl ion was, therefore, studied.

5.3.1.2 Effect of Solution Composition

Mass spectra were recorded with $5x10^{-6}$ M $UO_2(NO_3)_2$ and 10^{-5} M $NaClO_4$ in different proportions of water, ranging from 0% to 90% (v/v), in the mobile phase. Table 5.2 shows the distribution of different species of uranyl ion at various water-methanol compositions in the mobile phase. Different species of uranyl ion coordinated with water, alcohol and nitrate ligands were observed. The general formulae for most of the ions observed can be represented as $[UO_2(OH)S_n]^+$, $[UO_2(CH_3O)S_n]^+$ and $[UO_2(NO_3)S_n]^+$, where S denotes H_2O or CH_3OH. The value of n was found to vary from 0 to 3 and the maximum coordination number of uranyl ion was found to be 4, which is in agreement with the previously reported ESI-MS work on uranyl-aqua complex system[213,214]. It may be added that, in the aqueous solution, UO_2^{2+} coordinated by five H_2O ligands in the inner solvation sphere forms the most stable configuration[189,190,215].

Some of the major species observed in the mass spectra were $[UO_2(OH)]^+$, $[UO_2(CH_3O)]^+$,$[UO_2(H_2O)(OH)]^+$, $[UO_2(CH_3OH)(OH)]^+$, $[UO_2(H_2O)_2(OH)]^+$, $[UO_2(CH_3OH)(CH_3O)]^+$, $[UO_2(CH_3OH)_2(OH)]^+$ and $[UO_2(CH_3OH)(H_2O)_2(OH)]^+$. It may be noted that none of the major species contained $(NO_3)^-$ ligand. The species in which uranyl ion coordinated to the less number of ligands accounted for the maximum number of abundant ions in the spectra. The higher nucleophilicity of OH^- and CH_3O^- species might be a factor for the high abundance of low coordinated uranyl species.

Table 5.2: Distribution of uranyl species in methanol-water system in positive ion mode

Species	*m/z*	Relative intensities with respect to base peak				
		100% MeOH	**90% MeOH + 10% H_2O**	**75% MeOH + 25% H_2O**	**50% MeOH + 50% H_2O**	**10% MeOH + 90% H_2O**
$[UO_2]^+$	270.04	4.0±0.2	3.9±0.4	3.8±0.3	6.0±0.6	6.7±0.5
$[UO_2(OH)]^+$	287.04	4.6±0.4	4.6±0.2	3.2±0.2	35.5±0.5	28.1±0.7
$[UO_2(H_2O]^+$	288.05	2.3±0.1	2.2±0.2	2.1±0.2	3.0±0.2	5.2±0.3
$[UO_2(CH_3O)]^+$	301.07	100	100	100	100	100
$[UO_2(H_2O)(OH)]^+$	305.05	1.1±0.1	1.2±0.1	1.0±0.1	10.6±0.2	10.0±0.5
$[UO_2(CH_3OH)(OH)]^+$	319.06	28.6±0.4	27.7±0.5	27.8±0.3	32.7±0.4	33.4±0.7
$[UO_2(CH_3OH)(H_2O)]^+$	320.07	0.4±0.1	0.4±0.1	0.4±0.1	0.6±0.1	1.3±0.2
$[UO_2(H_2O)_2(OH)]^+$	323.06	0.8±0.1	0.9±0.1	0.8±0.1	7.6±0.3	7.3±0.5
$[UO_2(NO_3)]^+$	332.03	0.2±0.1	0.2±0.1	0.2±0.1	0.4±0.1	2.3±0.2
$[UO_2(CH_3OH)(CH_3O)]^+$	333.08	14.9±0.3	21.0±0.7	30.8±0.5	11.1±0.4	15.2±0.6
$[UO_2(CH_3OH)_2]^+$	334.09	0.5±0.1	0.7±0.1	0.9±0.1	0.6±0.1	1.0±0.2
$[UO_2(CH_3OH)(OH)(H_2O)]^+$	337.07	28.7±0.4	29.3±0.5	30.9±0.3	38.4±0.3	43.6±0.8
$[UO_2(H_2O)_3(OH)]^+$	341.07	0.5±0.1	0.6±0.1	0.6±0.1	4.3±0.2	4.4±0.4
$[UO_2(NO_3)(H_2O)]^+$	350.04	-	-	-	-	-
$[UO_2(CH_3OH)_2(OH)]^+$	351.09	10.7±0.2	15.7±0.5	23.6±0.8	10.0±0.3	14.9±0.2
$[UO_2(CH_3OH)(OH)(H_2O)_2]^+$	355.09	16.2±0.3	17.5±0.4	19.5±0.5	26.9±0.8	30.5±0.7
$[UO_2(NO_3)(CH_3OH)]^+$	364.05	1.4±0.1	1.9±0.1	2.5±0.1	1.3±0.1	1.9±0.2
$[UO_2(OH)(H_2O)(CH_3OH)_2]^+$	369.11	6.0±0.2	9.1±0.3	14.3±0.2	6.8±0.3	13.0±0.2
$[UO_2(CH_3OH)(OH)(H_2O)_3]^+$	373.10	0.4±0.1	0.6±0.1	0.5±0.1	0.6±0.1	1.6±0.2
$[UO_2(NO_3)(H_2O)(CH_3OH)]^+$	382.08	1.2±0.1	1.8±0.1	2.2±0.1	1.4±0.2	2.0±0.2
$UO_2(NO_3)(H_2O)_3]^+$	386.06	-	-	-	-	-
$[UO_2(CH_3OH)(OH)(H_2O)_4]^+$	391.11	0.4±0.1	0.7±0.1	0.8±0.1	0.9±0.1	2.6±0.2
$[UO_2(NO_3)(H_2O)_2(CH_3OH)]^+$	400.08	1.0±0.1	1.5±0.1	1.8±0.2	1.3±0.1	1.8±0.2

Solutions contained $5x10^{-6}$ M $UO_2(NO_3)_2$ and 10^{-5} M $NaClO_4$
Capillary voltage: 4500 V; dry gas temperature: 180 ºC

As expected, the relative abundances of uranyl species containing either H_2O or CH_3OH ligand increased with increase in the percentage of the respective solvent in the mobile phase. The change in the pattern of the major species in the mass spectra as a function of methanol-water composition is an indicative of the fact that the solution equilibrium is represented in the gas phase. Further, the pH of the solution was found to change from 5.6 for 10% MeOH medium to 7.3 for 100% MeOH medium. This change in the pH would also be contributing to the difference in the distribution of major uranyl species observed in the ESI-mass spectra.

Though the relative intensities of the major species changed when the mobile phase composition was changed over a wide range, there seems to be a preference of uranyl ion for the CH_3OH ligand as compared to H_2O. This may be attributed to the fact that the gas phase basicity of methanol is marginally higher than that of water [216]. Many studies have pointed to the importance of analyte basicity as a source of selectivity in ESI-MS leading to improved response [213,217,218]. In order to validate this point in the present study, the distribution pattern of various uranyl species as a function of the composition of the mobile phase was studied using different solvents such as dichloromethane, isopropyl alcohol and acetone. In all the cases, methanol was used as the reference solvent and its proportion in the mobile phase was changed from 90% to 10% (v/v). In the case of methanol-isopropyl alcohol and methanol-acetone systems, the major peaks were those containing either isopropyl alcohol or acetone and the base peaks corresponded to $[UO_2(C_3H_9O)(NO_3)]^+$ *m/z* 452.14 and $[UO_2(C_3H_6O)(OH)]^+$ *m/z* 461.17, respectively. The gas phase basicities of both isopropyl alcohol and acetone are higher than that of methanol and this corroborates the distribution pattern observed in the ESI- mass spectra [213,219].

It is seen from Table 5.2 that there was no significant deviation in the intensity distribution patterns of the major species with mobile phase containing 90% and 50% water.

Since water is more nucleophilic than methanol in the liquid phase, it is expected that when >50% water is present in the mobile phase, uranyl ion would be mostly surrounded by water molecules in its inner-sphere coordination in the liquid phase [220]. Thus mobile phase composition of 1:1 water-methanol was chosen for further studies with ESI-MS in view of its improved overall response.

5.3.1.3 Effect of Solute Concentration

The peak corresponding to $UO_2(CH_3O)]^+$ was found to be the base peak when methanol content in the mobile phase was in the range of 10% to 100%. This pattern is in contrast to the observation made by Stipdonk *et al*., who reported $[UO_2(CH_3OH)_3(NO)_3)]^+$*m/z* 428.11 as the most abundant species in the mass spectrum obtained in 1:1 water-methanol mobile phase[206]. The progressive dominance of $–NO_3$containing species with increase in the concentration of $UO_2(NO_3)_2$ in aqueous medium used for electrospraying was also reported by Tsierkezo *et al.*[221]. Hence the dependence of the distribution of different uranyl species on the concentration of $UO_2(NO_3)_2$ was studied in the concentration range $1x10^{-6}$ M to $1x10^{-3}$ M and the data are presented in Table 5.3. The pH of the solution was found to decrease with increase in the uranyl nitrate concentration. For example, the pH values obtained for $1x10^{-6}$ M, $1x10^{-5}$ M, $1x10^{-4}$ M and $1x10^{-3}$ M uranyl nitrate in 1:1 water-methanol medium were 7.1, 5.4, 4.2 and 3.3, respectively. It was observed that with the increase in the concentration of $UO_2(NO_3)_2$, there is a steady decrease of (OH) and (CH_3O) containing uranyl species and a corresponding increase in the abundances of (NO_3)containing uranyl species. Tsierkezos *et al.* attributed this increased preference for the (NO_3) ligands to the decrease in the pH of the solution with the increase in concentration of uranyl nitrate[221]. However, in all the concentrations of uranyl nitrate studied, $[UO_2(CH_3O)]^+$ *m/z* 301.06 continued to be the base peak.

Table 5.3:Distribution of species at different concentrations of uranyl nitrate in mobile phase

Species	*m/z*	Relative intensities of the peaks at different concentrations of uranyl nitrate (M)			
		$1x10^{-6}$	$1x10^{-5}$	$1x10^{-4}$	$1x10^{-3}$
$[UO_2]^+$	270.04	6.6±0.1	5.6±0.1	5.2±0.1	4.2±0.1
$[UO_2(OH)]^+$	287.04	27.5±0.7	26.6±0.7	17.1±0.1	5.3±0.1
$[UO_2(CH_3O)]^+$	301.06	100	100	100	100
$[UO_2(H_2O)(OH)]^+$	305.05	6.7±0.2	6.3±0.1	3.9±0.1	1.1±0.1
$[UO_2(CH_3OH)(OH)]^+$	319.07	36.6±0.3	33.7±0.2	32.6±0.1	29.6±0.1
$[UO_2(H_2O)_2(OH)]^+$	323.06	5.2±0.3	5.2±0.1	2.9±0.1	1.1±0.1
$[UO_2(NO_3)]^+$	332.03	0.6±0.1	0.6±0.1	1.0±0.1	2.6±0.1
$[UO_2(CH_3OH)(CH_3O)]^+$	333.08	15.1±0.3	11.3±0.1	12.7±0.2	14.4±0.1
$[UO_2(CH_3OH)(H_2O)(OH)]^+$	337.08	39.2±0.6	37.9±0.5	35.4±0.1	30.4±0.4
$[UO_2(H_2O)_3(OH)]^+$	341.07	3.5±0.2	3.4±0.2	1.8±0.1	0.7±0.1
$[UO_2(H_2O)(NO_3)]^+$	350.04	0.4±0.1	0.6±0.1	0.9±0.1	1.7±0.1
$[UO_2(CH_3OH)_2(OH)]^+$	351.09	11.6±0.2	9.6±0.1	8.3±0.1	7.8±0.2
$[UO_2(CH_3OH)(H_2O)_2(OH)]^+$	355.09	28.8±0.4	27.9±0.6	21.9±0.1	17.1±0.1
$[UO_2(CH_3OH)(NO_3)]^+$	364.05	2.2±0.1	3.0±0.1	5.5±0.1	22.8±0.3
$[UO_2(H_2O)_2(NO_3)]^+$	368.05	0.5±0.1	0.7±0.1	0.9±0.1	1.7±0.1
$[UO_2(CH_3OH)_2(H_2O)(OH)]^+$	369.11	7.8±0.2	6.1±0.1	5.6±0.1	5.1±0.1
$[UO_2(CH_3OH)(H_2O)(NO_3)]^+$	382.06	2.1±0.1	2.4±0.1	4.6±0.1	15.7±0.2
$[UO_2(H_2O)_3(NO_3)]^+$	386.06	0.4±0.1	1.0±0.1	1.3±0.1	2.4±0.1
$[UO_2(CH_3OH)_2(NO_3)]^+$	396.08	0	0.3±0.1	0.7±0.1	3.8±0.1
$[UO_2(CH_3OH)(H_2O)_2(NO_3)]^+$	400.07	2.6±0.1	3.3±0.1	5.8±0.1	20.0±0.2
$[UO_2(CH_3OH)_2(H_2O)(NO_3)]^+$	414.09	0	0.4±0.1	0.7±0.1	3.2±0.1
$[UO_2(CH_3OH)_3(NO_3)]^+$	428.11	0	0	0	0.02
$[(UO_{2)2}(NO_3)_3)]^+$	726.048	0	0	0.5±0.1	2.8±0.1
$[(UO_{2)2}(NO_3)_3(H_2O)]^+$	744.06	0	0	0.5±0.1	2.5±0.1
$[(UO_{2)2}(NO_3)_3(CH_3OH)]^+$	758.07	0	0.3±0.1	1.3±0.1	10.2±0.2
$[(UO_{2)2}(NO_3)_3(H_2O)_2]^+$	762.07	0	0	0.4±0.1	2.6±0.1
$[(UO_{2)2}(NO_3)_{3(}H_2OH)(H_2O)]^+$	776.09	0	0.3±0.1	1.2±0.1	9.3±0.1
$[(UO_{2)2}(NO_3)_3(H_2O)_3]^+$	780.08	0	0.3±0.1	1.3±0.1	7.9±0.1
$[(UO_{2)2}(NO_3)_3(H_2O)_2(CH_3OH)]^+$	794.09	0	0.3±0.1	2.4±0.1	18.0±0.1
$[(UO_{2)2}(NO_3)_3(H_2O)(CH_3OH)_2]^+$	808.12	0	0	0.10±0.01	1.0±0.1

$UO_2(NO_3)_2$ solution prepared in mobile phase containing 10^{-5} M $NaClO_4$ and 1:1 methanol-water; capillary voltage : 4500 V; dry gas temperature: 180^oC.

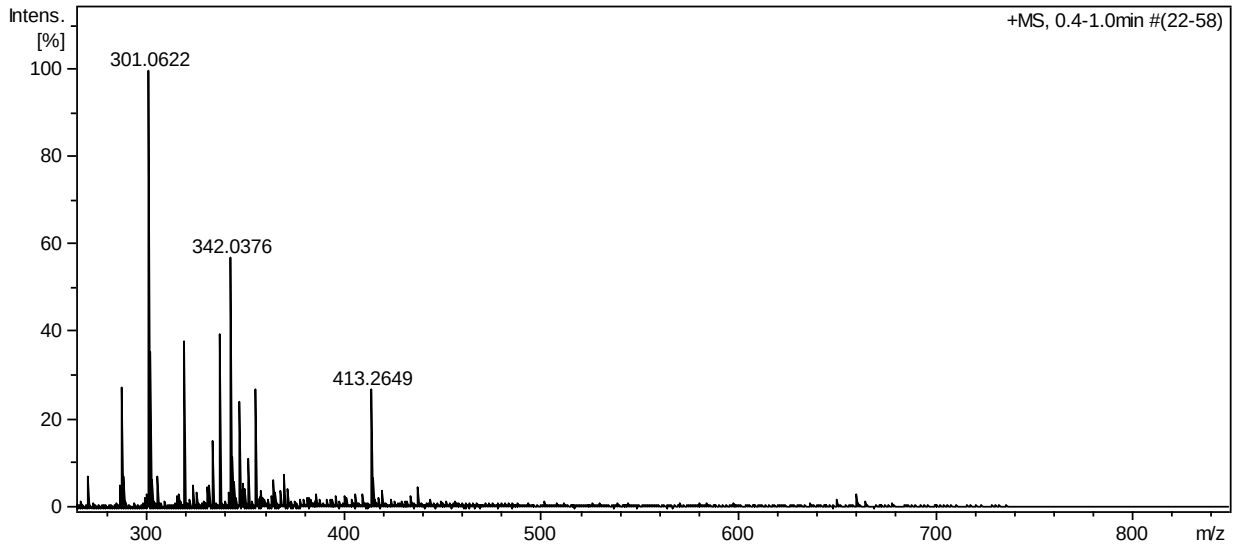

(a)

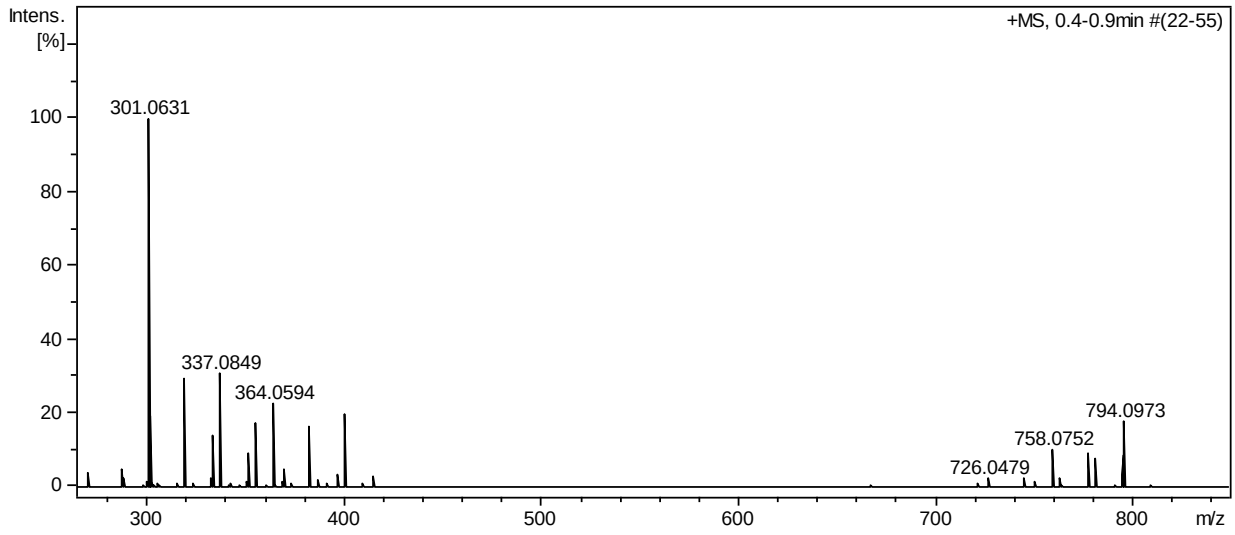

(b)

Figures5.2: *Positive mode ESI-MS spectra of uranyl nitrate solution prepared in mobile phase containing 10^{-5} M $NaClO_4$ and 1:1 methanol-water (a) 10^{-6} M $UO_2(NO_3)_2$ and (b) 10^{-3} M $UO_2(NO_3)_2$.*

It may be noted that even at 10^{-3} M concentration of $UO_2(NO_3)_2$, the intensity of peak at *m/z* 428.11 was only ≤0.02% with respect to the base peak. But there was a substantial increase in the abundance of other (NO_3) containing species with the increase in concentration of uranyl nitrate. For example, the relative intensities of the species: $[UO_2(CH_3OH)(NO_3)]^+$ *m/z* 364.05, $UO_2(CH_3OH)(H_2O)(NO_3)]^+$ *m/z* 382.06 and

$[UO_2(CH_3OH)(H_2O)_2(NO_3)]^+$ *m/z* 400.07 were 29%, 16% and 20% at 10^{-3} M uranyl nitrate concentration. At $UO_2(NO_3)_2$ concentrations $\geq 10^{-4}$ M, binuclear uranyl nitrate species with a general formula, $[(UO_2)(NO_3)_3(S)_n]^+$ (where 'S' denotes CH_3OH or H_2O and 'n' changed from 0 to 3) started to appear in the spectra. The maximum concentration of $UO_2(NO_3)_2$ employed for this study was limited to 10^{-3} M to safeguard the detector. Figures 5.2 (a) and 5.2 (b) show the mass spectra obtained by electrospraying solutions containing $UO_2(NO_3)_2$ at concentrations 10^{-6} M and 10^{-3} M, respectively, in 1:1 water-methanol medium.

5.3.2 Complexation of Uranyl Ion with α-Hydroxyisobutyric Acid

It is reported that HIBA coordinates with uranyl ion via oxygen atoms of carboxylic acid group in the pH range of 2 to 4 [123,172]. At pH ≥ 5, enhancement of complexation occurs due to the involvement of –OH group of the ligand in the complexation. In the pH range used in the present study (4.7 to 6.4), the carboxylic acid group is appreciably dissociated and both the carboxyl group and hydroxyl group can involve in the complexation with uranyl ion [123].With HIBA, uranyl ion forms various complexes which are cationic or anionic in nature and hence mass spectra were acquired in both the positive and the negative ion modes. Figures 5.3(a) and 5.3(b) show the mass spectra obtained in the positive and the negative ion modes, respectively, for a solution containing $5x10^{-6}$ M of $UO_2(NO_3)$ and $1x10^{-4}$ M of HIBA and 10^{-5} M $NaClO_4$ in 1:1 water-methanol mobile phase. pH of this solution was found to be 6.4, which indicates almost complete deprotonation of the ligand and an enhanced complexation with the uranyl ion. The dependence of the distribution of different uranyl-HIBA species on the pH of the medium was also reported by Raju *et al*.[135].

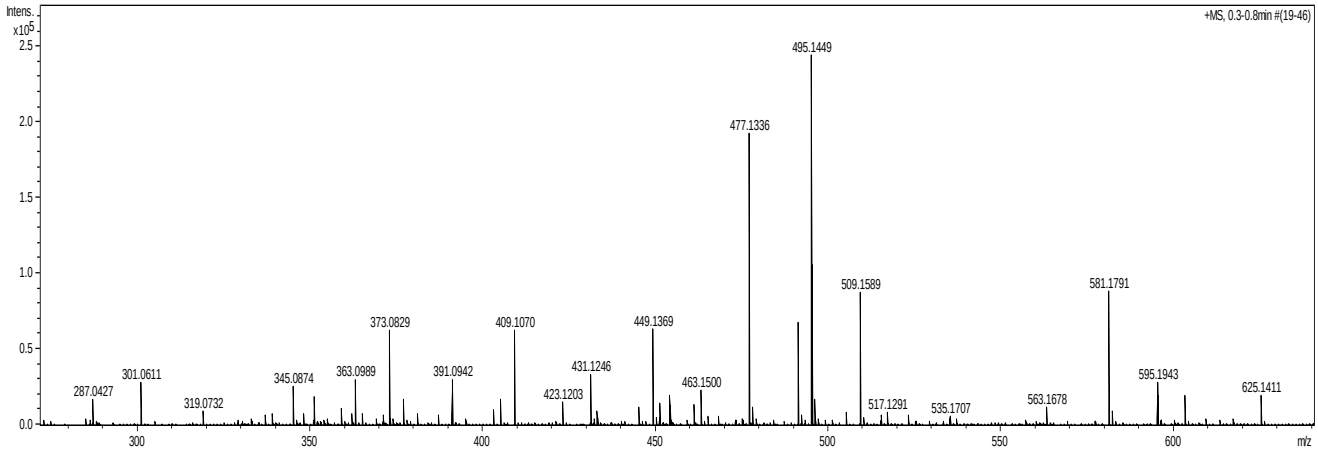

(a)

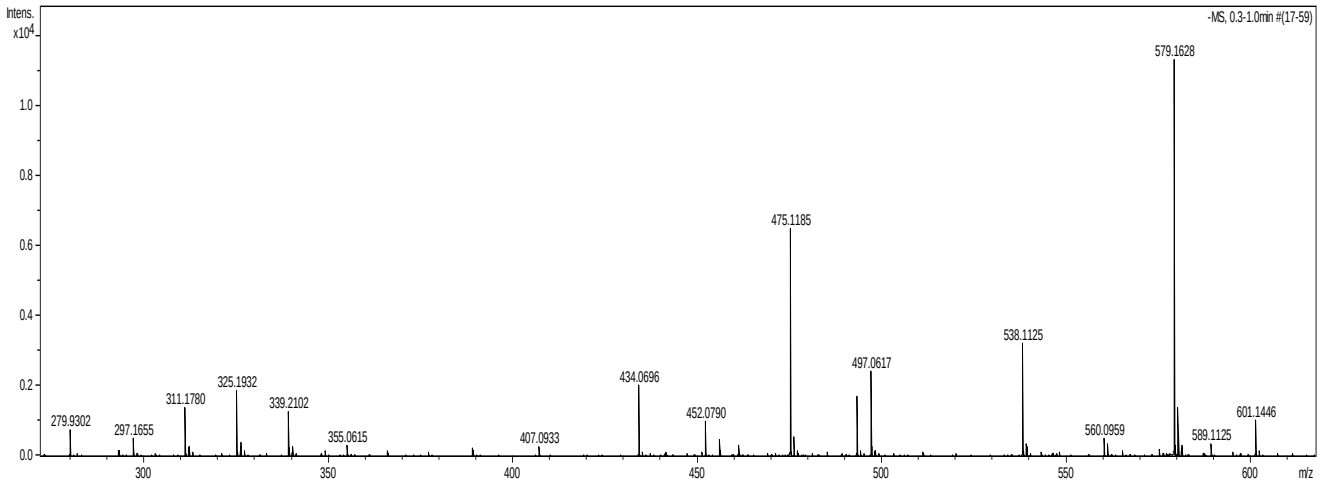

(b)

Figure 5.3: *ESI-MS spectra of UO_2 – HIBA system in (a) positive mode and (b) negative mode.*
Conditions: $5x10^{-6}$ M $UO_2(NO_3)_2$ mixed with 10^{-4} M HIBA in 1:1 methanol-water mobile phase containing 10^{-5} M $NaClO_4$.

5.3.2.1 Positive Ion Mode

Deprotonation of α-hydroxyisobutyric acid may be represented by the following schematics:

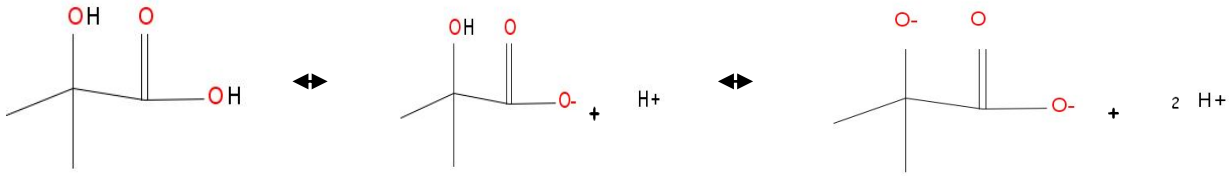

HIBA IBA (IBA-H)

Uranyl complexation by HIBA to form the species observed in the positive ion mode can be represented by following reactions:

$UO_2^{2+} + HIBA = [UO_2(IBA)]^+ + H^+$ --- Eq (1)

$UO_2^{2+} + 2\ HIBA = [UO_2(HIBA)(IBA)]^+ + H^+$ --- Eq (2)

$UO_2^{2+} + 3\ HIBA = [UO_2(HIBA)_2(IBA)]^+ + H^+$ --- Eq (3)

Major species identified in the mass spectra obtained in the positive and the negative ion modes are presented in Tables 5.4(a) and 5.4(b), respectively. Identification of the peaks was done by matching with the theoretically predicted isotopic pattern as well as by accurate mass matching.

Table 5.4(a): Uranyl-HIBA species observed in the positive ion mode

Species	**Type**	***m/z***	**Intensity* obtained using ligand-to-metal ratio**	
			10	**20**
$[UO_2(C_4H_8O_3)]^+$	M-H	373.08	25.5	13.7
$[UO_2(C_4H_8O_3)(H_2O)]^+$		391.09	12.4	6.2
$[UO_2(C_4H_8O_3)(CH_3OH)]^+$		405.11	7.2	3.5
$[UO_2(C_4H_8O_3)(H_2O)_2]^+$		409.10	25.4	12.0
$[UO_2(C_4H_8O_3)(H_2O)(CH_3OH)]^+$		423.11	6.2	3.3
$[UO_2(C_4H_8O_3)_2]^+$		477.13	76.2	85.8
$[UO_2(C_4H_8O_3)_2(H_2O)]^+$		495.14	100	100
$[UO_2(C_4H_8O_3)_2(CH_3OH)]^+$		509.15	35.5	42.1
$[UO_2(C_4H_8O_3)_3]^+$		581.17	35.8	46.0

** Relative intensity with respect to the base peak*

Table 5.4(b): Uranyl-HIBA species observed in the negative ion mode

Species	Type	*m/z*	Intensity* obtained using ligand-to-metal ratio	
			10	**20**
$[UO_2(C_4H_7O_3)(OH)]^-$	M-H	389.07	2.3	1.5
$[UO_2(C_4H_7O_3)(H_2O)(OH)]^-$		407.10	2.4	1.7
$[UO_2(C_4H_7O_3)(NO_3)]^-$		434.06	22	19.1
$[UO_2(C_4H_7O_3)_2]^-$		475.11	57.5	69.5
$[UO_2(C_4H_7O_3)_2(H_2O)]^-$		493.12	15.2	23.0
$[UO_2(C_4H_8O_3)(NO_3)(OH)]^-$		452.07	10.2	10.8
$[UO_2(C_4H_8O_3)(NO_3)_2]^-$		497.06	21.4	21.5
$[UO_2(C_4H_7O_3)_2(NO_3)]^-$	M	538.11	15.1	21.1
$[UO_2(C_4H_7O_3)_3]^-$		579.16	100	100

** Relative intensity with respect to the base peak*
$5x10^{-6}$ M $UO_2(NO_3)_2$ and 10^{-5} M $NaClO_4$ prepared in 1:1 methanol-mobile phase

As discussed in Section 5.3.1.2, in the case of uranyl nitrate dissolved in water-methanol mixture, the solvated uranyl species was having a maximum coordination number of 4 and the major species were those containing methanol in the coordination sphere. It is seen from Table 5.4(a) that uranyl-HIBA complexes also undergo solvation with H_2O or CH_3OH molecules. However, the maximum number of ligands observed around the uranyl ion is only 3. Even in the case of ML_1(where 'M' represents UO_2^{2+} and 'L' represents HIBA) type complexes, the maximum number of solvent molecules involved in coordination was found to be 2. Similarly, there was no peak observed in the spectra suggesting the solvation complexation of the species ML_3. This indicates that at least one of the HIBA molecules bonded to uranyl ion is in bidentate coordination. The typical intensities of different uranyl-HIBA species obtained from the MS spectra using solutions containing uranium and the

ligand in ratios 1:10 and 1:20 are also listed in Table 5.4(a). It is interesting to note that in the case of solvated uranyl-HIBA complexes, H_2O containing species were more abundant than those containing CH_3OH. For example, the species $[UO_2(C_4H_8O_3)(H_2O)_2]^+$ *m/z* 409.10 was observed with a noticeable intensity whereas the analogous CH_3OH containing species $[UO_2(C_4H_8O_3)(CH_3OH)_2]^+$ with expected *m/z* 437.13 was not seen across any of the ligand-to-metal ratios used. This is in contrast to the pattern observed with only uranyl ion in water-methanol mixture. It is presumed that in the solution phase, H-bonding must be existing between the HIBA and the water molecules coordinated to uranyl ion. This interaction may be restricting the replacement of coordinated water molecules by methanol in the gas phase and this leads to the dominance of the water containing species in the mass spectra.

5.3.2.2 Negative Ion Mode

In the case of ions observed under the negative ion mode of operation, complexation can be represented by following reactions:

$$UO_2^{2+} + HIBA + X^- = [UO_2(IBA\text{-}H)X]^- + 2H^+ \quad \text{--- Eq (4)}$$

$$UO_2^{2+} + 2HIBA = [UO_2(IBA\text{-}H)(IBA)]^- + 3H^+ \quad \text{--- Eq (5)}$$

$$UO_2^{2+} + 2HIBA + X^- = [UO_2(IBA)_2X)]^- + 2H^+ \quad \text{--- Eq (6)}$$

$$UO_2^{2+} + 3HIBA = [UO_2(IBA)_3)]^- + 3H^+ \quad \text{--- Eq (7)}$$

where, 'X' represents -OH, $-OCH_3$ or $-NO_3$

From the different uranyl-HIBA species listed in Table 5.4(b), it is seen that the maximum number of ligands available for coordination with uranyl ion is 3. NO_3^- containing uranyl complex species were found to be more abundant than those containing OH^-. This can be explained on the basis of higher basicity of OH^- ligand resulting in a decreased Lewis

acidity of the metal ion as compared to the case where uranyl ion complexed to NO_3^-. Unlike in the positive ion mode, no peak corresponding to CH_3OH containing uranyl species was observed in the negative ion mode. The fact that CH_3OH ligand is not helpful in dispersing the negative charge of the anionic metal complex could be a reason for the absence of CH_3OH bearing species in the negative ion mode. Non-existence of solvated ions in the negative mode was also observed in the ESI-MS studies on platinum-benzoylthiourea complex species in the acetonitrile medium[222].

The observation of ML_1 type complexes in the negative ion mode shows deprotonation of the hydroxyl group present in the HIBA. The species observed in the mass spectra in support to this argument were $[UO_2(C_4H_7O_3)(OH)]^-$ and$[UO_2(C_4H_7O_3)(NO_3)]^-$. The dissociation of HIBA was also discussed by Moll *et al.* in their UV-Vis spectrometry studies and the authors proposed that the deprotonation of OH group must be taking place at higher pH conditions[172].

5.3.2.3 Selection of ESI Parameters

It is seen from Tables 5.4(a) &5.4(b) that the most dominating species in the positive and the negative ion modes correspond to $[UO_2(C_4H_8O_3)_2(H_2O)]^+$ (M-H type ion) and $[UO_2(C_4H_7O_3)_3]^-$, respectively. Also there is a marked difference in the distribution of other species observed in the two modes. For instance, at a ligand-to-metal ratio of 10, ML_1 and ML_2 type species accounted for about 24% and 65% of the total uranyl-HIBA species in the positive ion mode whereas in the negative ion mode, they contributed to only 11% and 49%, respectively. Initially, it was felt that the inherent easiness in the formation of positive ions by ML_1 type of species and negative ions by ML_3 type species is responsible for the differences in the distribution pattern in the two modes, as described by eqs. (1) to (7). But it is also likely that ions of uranyl species undergo some changes during their transition from the solution

phase to gas phase. Desolvation and ion extraction processes in the ESI interface might contribute to the production of ions which may not be originally present in the solution phase[208,217]. The instrumental parameters are, therefore, likely to influence the intensity distribution of different species observed in the positive and the negative ion modes. Hence it was of interest to study the influence of electrospray ion generation, desolvation and ion transfer parameters on the ESI-MS spectra of uranyl ion. The fragmentation of a given ionic species is dependent on the dry gas temperature and capillary voltage used for the ESI process. Hence, the effects of capillary voltage and dry gas temperature on the ion intensities of important uranyl species were monitored in view of minimizing the fragmentation process. Typical sample solution used for the optimization studies consisted of $5x10^{-6}$ M $UO_2(NO_3)_2$, $5x10^{-5}$ M HIBA and 10^{-5} M $NaClO_4$ in 1:1 water-methanol mixture.

5.3.2.3.1 Capillary Voltage

The effect of capillary voltage on the intensities of different uranyl species was studied in the positive and in the negative ion modes. Capillary voltage was changed from -2500V to -5000 V and from 2500 V to 4000 V in the positive and the negative ion modes, respectively. Figures 5.4(a) &5.4(b) show the effect of change in capillary voltage on the fractional intensities of different uranyl species formed in the positive and the negative modes, respectively. In the positive ion mode, $[UO_2(C_4H_8O_3)_2(H_2O)]^+$ *m/z* 495.14 was found to be the most abundant species at all the capillary voltages employed. The intensities of species viz. $[UO_2(C_4H_8O_3)_2(H_2O)]^+$ and $[UO_2(C_4H_8O_3)(H_2O)]^+$ *m/z* 391.09 showed slight decreasing trend with the increase in the capillary voltage indicating that they are susceptible to fragmentation. A proportional increase in the fractional intensities of $[UO_2(C_4H_8O_3)_2]^+$*m/z* 477.13 (M-H type ion) and $[UO_2(C_4H_7O_3)]^+$*m/z* 373.08 was observed. There was no apparent change in the fractional intensity of $[UO_2(C_4H_8O_3)_3]^+$*m/z* 581.17 (M-H type ion) across the voltage range studied, indicating absence of any production or dissociation routes in the gas phase for this

species. There was a nominal increase in the intensities of $[UO_2(CH_3O)]^+$ *m/z* 301.06 and $[UO_2]^+$ *m/z* 270.04 owing to the marginal dissociation of the uranyl complexes at high capillary voltages. Further, there was no significant increase in the peak intensity of $[UO_2(C_4H_8O_3)_2(CH_3OH)]^+$ *m/z* 509.15 (M-H type ion) confirming no replacement of H_2O by CH_3OH in the gas phase.

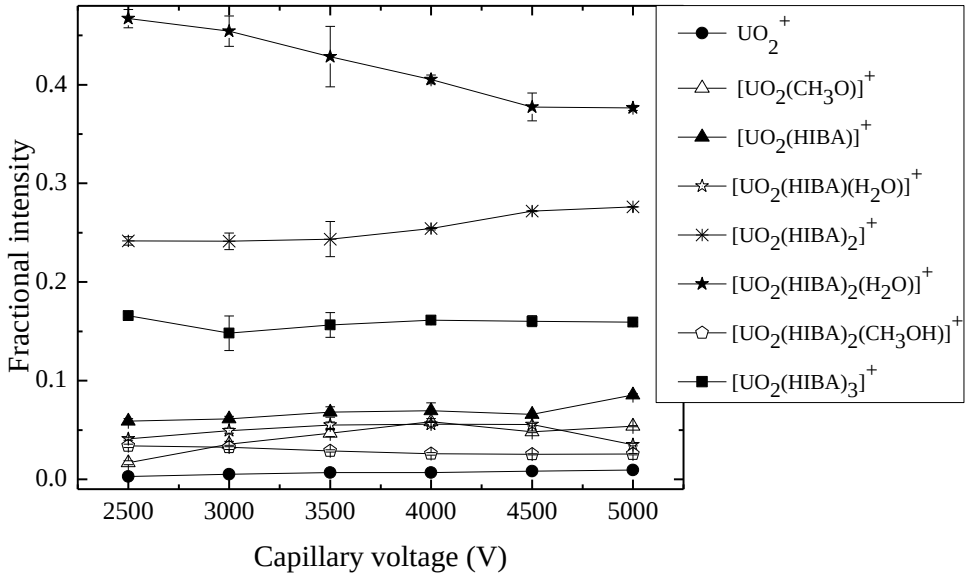

(a)

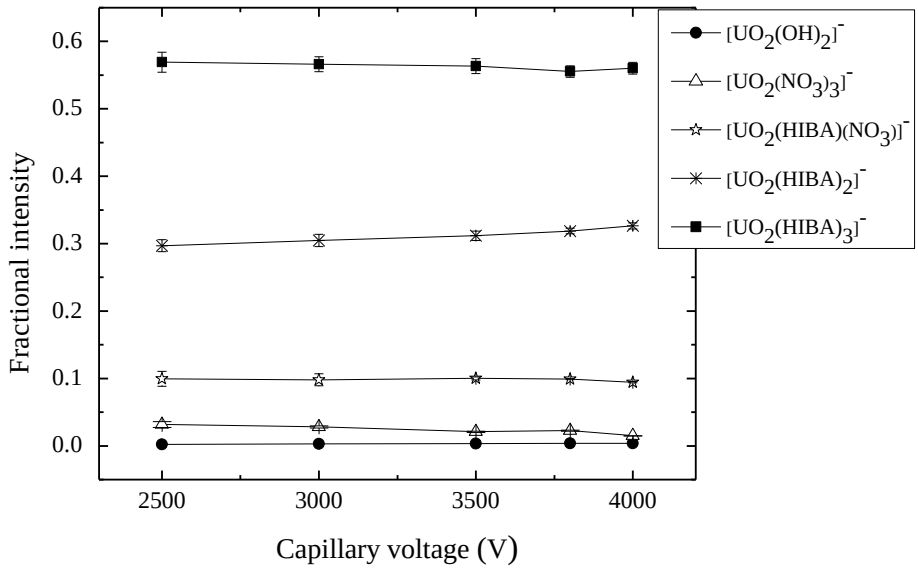

(b)

Figures 5.4: *Changes in the fractional intensities of uranyl species as a function of capillary voltage in (a) the positive ion mode and (b) the negative mode.*

In the negative ion mode, $[(UO_2(C_4H_7O_3)_3]^-$ *m/z* 579 was found to be the most abundant species at all the capillary voltages applied. Similar to the observations in the positive ion mode, $[(UO_2(C_4H_7O_3)_3]^-$ ion did not show any noticeable change in the intensity with the change in the capillary voltage. Intensity of $[(UO_2(C_4H_7O_3)_2]^-$ *m/z* 475 (M-H type ion) showed a slight increasing trend possibly due to the dissociation of $[(UO_2(C_4H_7O_3)_2(NO_3)]^-$ *m/z* 538.11. Intensity of the uncomplexed uranyl species, represented by $[(UO_2(NO_3)_3]^-$ *m/z* 456.01 also showed a decreasing trend indicative of fragmentation at higher capillary voltages. It was seen that in both the modes, the intensities of all the uranyl species increased steadily with the increase in the capillary voltage. Considering the sensitivity of ESI response and robustness of the species, -4000 V and 3500 V were chosen as the capillary voltages for the subsequent studies in the positive and the negative ion modes, respectively.

5.3.2.3.2 Dry Gas Temperature

Increasing the dry gas temperature improves the desolvation process but may also lead to the decomposition of thermally labile ions. Dependence of different uranyl species ions detected in the positive mode on the dry gas temperature of the ESI system is represented in Figure 5.5.During this study, dry gas heater temperature was increased from 90 ºC to 250 ºC. However, the actual temperature of the dry gas would be much lower than that of the heater. Since the instrument set-up allows the monitoring of the heater temperature, this parameter was used as it would show the relative change in the intensities of the different uranyl-HIBA species as a function of temperature. It was found that there was no significant change in the fractional intensity of uranyl species with the increase in dry gas temperature. Throughout the dry gas temperature studied, the peak corresponding to $[UO_2(C_4H_8O_3)_2(H_2O)]^+$ continued to be the most abundant, followed by $[UO_2(C_4H_8O_3)_2]^+$ and $[UO_2(C_4H_8O_3)_3]^+$. Though most of the uranyl species of interest showed fairly good thermal stability, a dry gas heater temperature of 150^0C to 180^0C was found to be optimum in view of the ESI-MS response.

Similarly, influence of dry gas temperature on the intensity distribution of uranyl species was studied in the negative ion mode. In this case also, the uranyl-HIBA species were found to be quite stable and the best ESI response was noted in the 150^{0}C to 180 ^{0}C temperature range. A reduction in the overall sensitivity was observed at temperatures above and below the selected range.

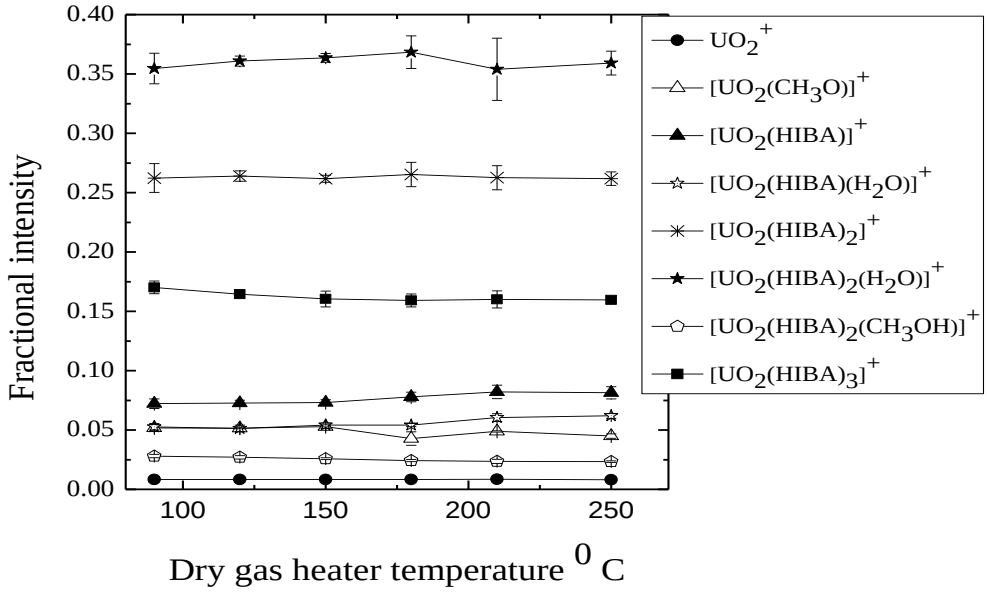

Figure 5.5: *Changes in the fractional intensity of uranyl species as a function of dry gas temperature in the positive mode.*

The studies on the capillary voltage and dry gas temperature showed that though these parameters significantly affect the relative intensities of most of the uranyl species, the distribution of species is not affected. Hence ion extraction parameters such as, in-source collision induced dissociation energy, quadrupole ion energy, collision cell energy and end-plate off set voltage were also investigated for their influence in the fragmentation of the species in the gas phase.

5.3.2.3.3 In-source CID Energy

In ESI-MS, cone voltage is often used to observe the change in the distribution of ion intensity as a result of in-source fragmentation of the molecular ion. Since the ESI-MS system used in the present study was equipped with funnels in place of cones, a parameter equivalent to cone voltage known as 'in-source collision induced dissociation' (ISCID) was changed to monitor the distribution of ion intensity. Figure 5.6 shows the relative ion intensities of important uranyl species as a function ISCID in the positive ion mode.

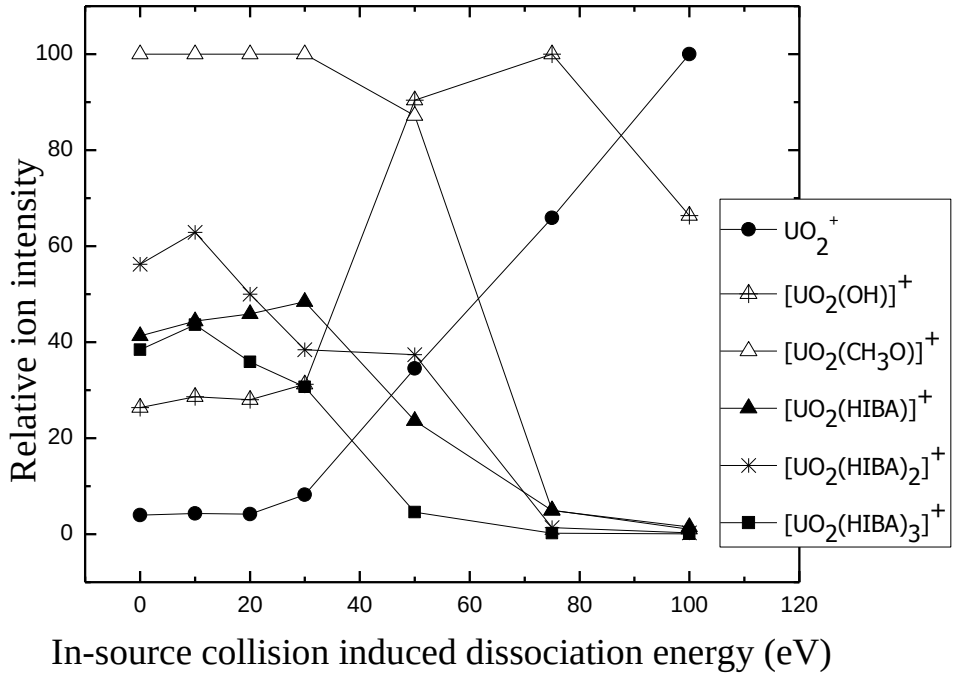

Figure 5.6: *Changes in the relative intensities of uranyl species as a function of in-source collision induced dissociation energy in the positive ion mode.*

It is seen that the uranyl-HIBA complex species show stability in the ISCID energy range of 0 to 10 eV only. As the energy increases beyond 10 eV, the complex species start dissociating with ML_3 showing greater degree of fragmentation. The species $[UO_2(CH_3O)]^+$ was found to be the base peak when the ISCID energy was less than 50 eV. At ISCID energies exceeding 50 eV, only the uranyl ion species such as UO_2^+, $[UO_2(OH)]^+$ were seen as the

major species due to the severity of the fragmentation. This study demonstrated that all the uranyl-HIBA species are relatively fragile to the CID process occurring in the ion source. Based on this experiment, an ISCID energy of 5 eV was selected for rest of the studies.

5.3.2.3.4 Quadrupole Ion Energy

Figure 5.7 shows the distribution of fractional intensities of the major uranyl species as a function of quadrupole ion energy. A capillary voltage of -4000 V and an end-plate offset voltage of -500 V were employed for the optimization of transfer parameters in the positive ion mode. Collision energy of 5 eV was used while optimizing the quadrupole ion energy. To make the interpretation simpler, the behavior of some of the less important uranyl species is not presented in the Figure.

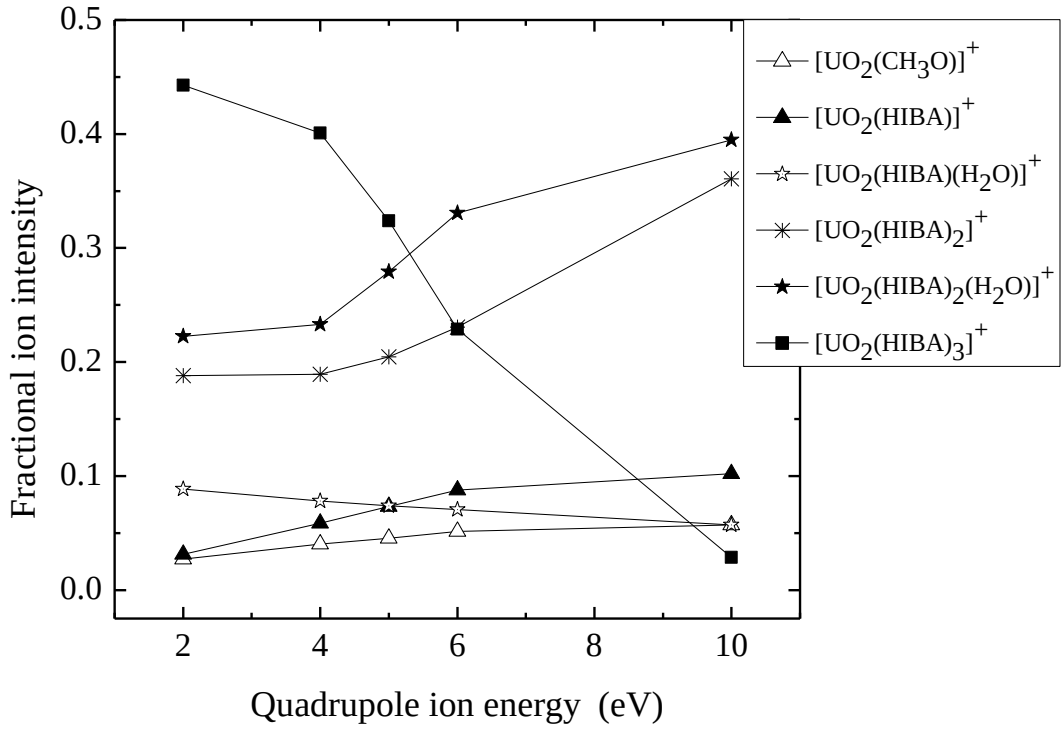

Figure 5.7: *Distribution of uranyl species as a function of quadrupole ion energy in the positive ion mode.*

It is seen that with the increase in the quadrupole ion energy, the fractional intensity of $[UO_2(HIBA)_3]^+$ decreases sharply. Proportionately, there is increase in the intensities of$[UO_2(HIBA)_2(H_2O)]^+$ and $[UO_2(HIBA)_2]^+$ indicating their formation by the fragmentation of $[UO_2(HIBA)_3]^+$. Also there is an increase in the intensity of the unbound uranyl species $[UO_2(CH_3O)]^+$. Intensities of other unbound uranyl species such as $[UO_2(OH)]^+$ and UO_2^+also followed the increasing trend (not shown in the Fig.) indicative of multiple pathways for the fragmentation of bulkier species. It was also noticed that the fractional intensity of the adduct species $[(UO_2(HIBA\text{-}H)_2)_2H]^+$*m/z* 953.24, increased steadily with the increase in the applied voltage. At quadrupole ion energies below 5 eV, $[UO_2(HIBA)_3]^+$was seen as the most intense peak. At higher values of quadrupole energy, the species $[UO_2(HIBA)_2(H_2O)]^+$ and $[UO_2(HIBA)_2]^+$ were observed as the most intense peaks. Based on the behavior of ions, a quadrupole ion energy of 4 eV was chosen for further studies.

5.3.2.3.5 Collision Cell Energy

Figure 5.8 shows changes in the fractional intensities of the major uranyl species with the change in collision cell energy. Various transfer parameters fixed for studying the influence of collision cell energy were the same as those employed for the quadrupole ion energy. Though fractional intensity pattern obtained was found to be similar to that observed in the case of quadrupole ion energy, the influence of the collision cell energy appeared to be more significant. This could be due to the fact a higher residual gas pressure is maintained in the collision cell (10^{-3} mbar) as compared to quadrupole (10^{-5} mbar) for facilitating the ion cooling and focusing. The species $[UO_2(HIBA)_2(H_2O)]^+$ was found to undergo fragmentation at collision cell energies > 6 eV. $[UO_2(HIBA)_3]^+$,$[UO_2(HIBA)_2(H_2O)]^+$ and $[UO_2(HIBA)_2]^+$ were observed as the most abundant species when the collision cell energies were ≤ 2 eV, 3 to 6 eV and > 6 eV, respectively.

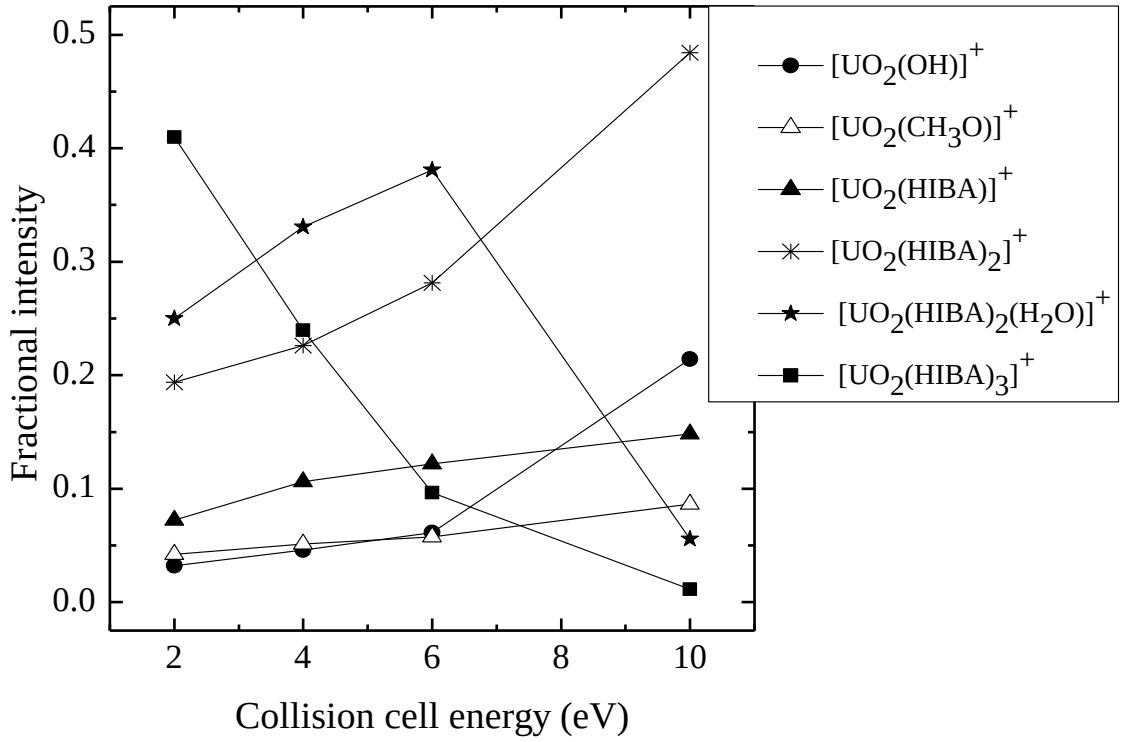

Figure 5.8: *Distribution of uranyl species as a function of collision cell energy in the positive ion mode.*

In general, it is seen that the low values of collision cell energy and quadrupole ion energy are preferred from the point of minimizing the fragmentations. However, a certain minimum value of potentials need be applied for effective transfer of ions through these devices. Thus an energy of 2eV was selected for the collision cell with a view to minimizing the fragmentation of the major species viz. $[UO_2(HIBA)_3]^+$. Similar experiment was carried out in the negative ion mode and the optimum collision cell energy was found to be 4 eV.

5.3.2.3.6 End-plate Offset Voltage

Figure 5.9 shows the effect of end-plate offset voltage on fractional intensities of different uranyl species in the positive mode. End-plate offset is the difference in the voltage applied to the end-plate with respect to the glass capillary.

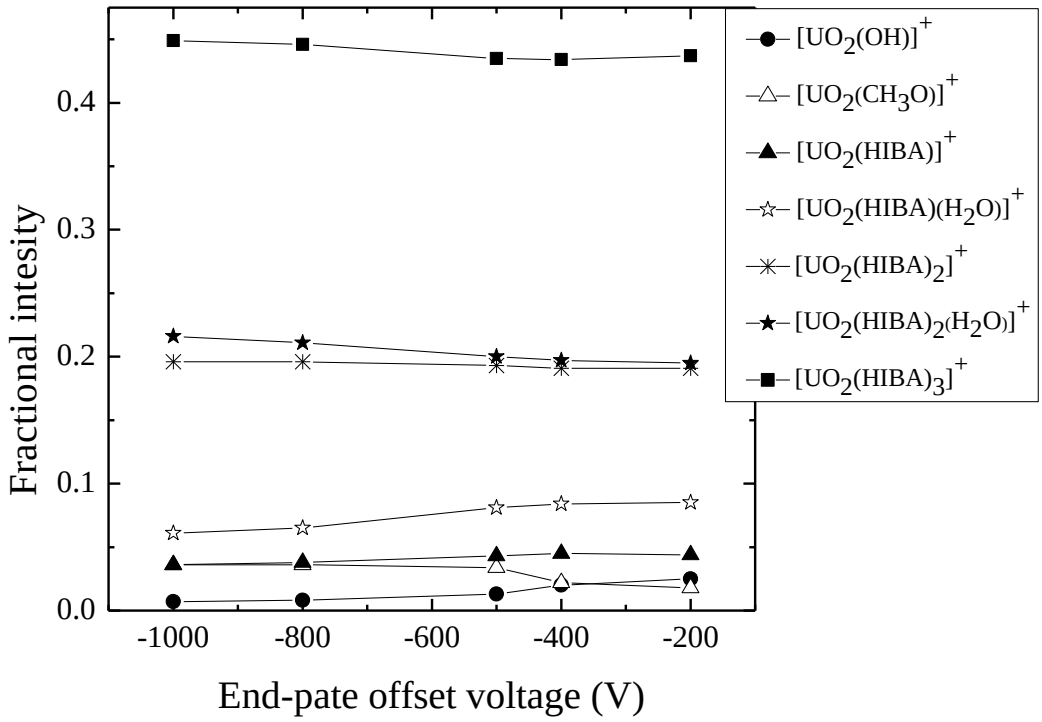

Figure 5.9: *Effect of end-plate offset voltage on the distribution of uranyl species in the positive mode.*

The effect of end-plate offset voltage on fractional intensities of different uranyl species was studied in the positive ion mode and in the negative ion mode. The studies were carried out using a capillary voltage of -4000 V. As the off-set value is lesser, the voltage applied to the end-plate becomes higher and this improves the transmission of ions through the orifice of the end-plate. However, application of a higher potential might lead to fragmentation of some of the fragile species present in the nebulizer spray. Fractional intensities of all the bulkier species $[UO_2\text{-}(HIBA)_2]^+$, $[UO_2\text{-}(HIBA)_2(H_2O)]^+$ and $[UO_2\text{-}(HIBA)_3]^+$ showed a slight decreasing trend with resultant increase in the fractional intensities of the fragments such as $[UO_2(OH)]^+$, $[UO_2\text{-}(HIBA)]^+$ and $[UO_2\text{-}(HIBA)(H_2O)]^+$. In view of maintaining a balance between the transmission efficiency and fragmentation, -800 V was chosen as the end-plate offset voltage in both the positive and the negative ion modes for the subsequent experiments. However, it is not clear why the species$[UO_2\text{-}(HIBA)_3]^+$, which was

moderately robust under end-plate offset voltage and capillary voltage studies, underwent severe fragmentation when collision cell energy and quadrupole ion energy were increased.

5.3.2.4 Effect of Ligand-to-Metal Ratio

After optimizing the transfer parameters, the complexation reaction between uranyl ion and HIBA was followed as a function of the ligand-to-metal ratio in order to monitor the overall trend in complexation. Figure 5.10(a) shows the changes in the fractional intensities of different uranyl species as a function of ligand-to-metal ratio in the positive ion mode.

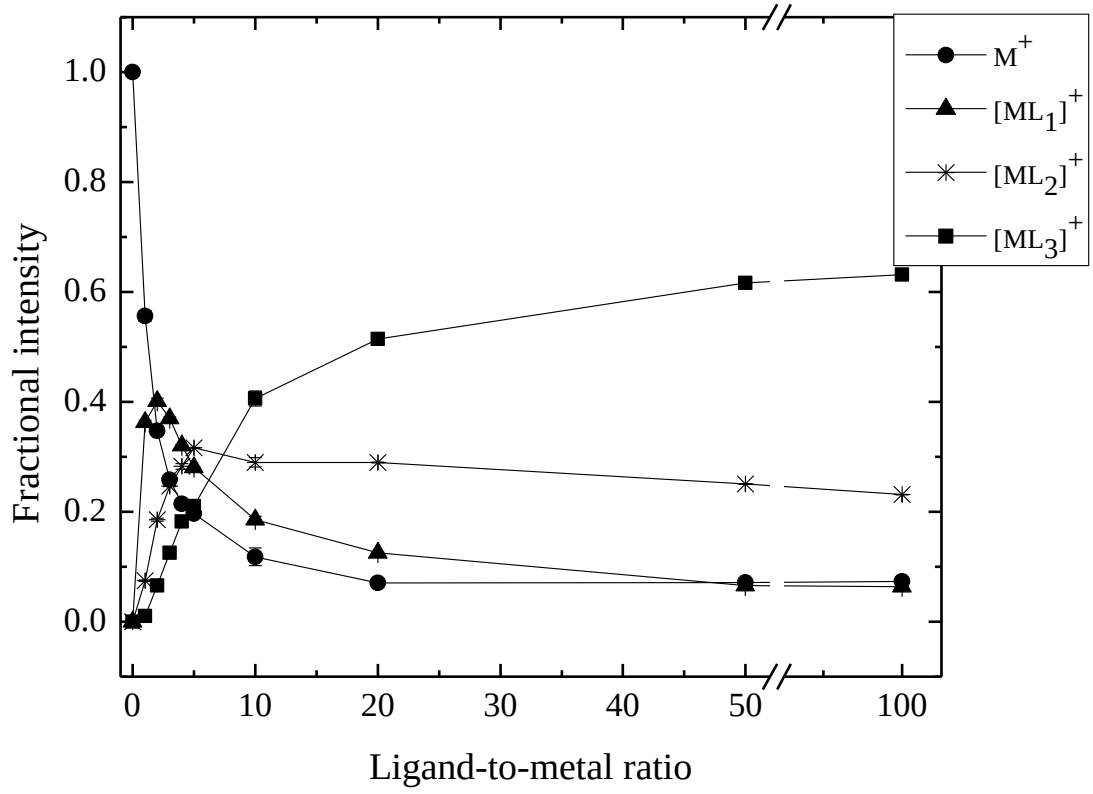

Figure 5.10(a): *Distribution of uranyl-HIBA complex species as a function of ligand-to-metal ratio in positive ion mode.*
$5x10^{-6}$ M $UO_2(NO_3)_2$ solution in H_2O:MeOH (1:1 v/v). ESI parameters employed: dry gas temperature: 180 °C, capillary voltage: -4000 V; end-plate offset voltage: -800V; quadrupole ion energy: 4 eV and collision cell energy: 2 eV.

Concentration of uranyl ion for this set of experiments was fixed at $5x10^{-6}$ M in 1:1 water-methanol mixture containing 10^{-5} M $NaClO_4$.Uranyl nitrate and HIBA solutions were mixed on volume basis to give the complex solution with the required ligand-to-metal ratios in the range 0 to 100. pH of the resultant solution used for the ESI-MS work was found to be in the range of 6.4 to 4.7 for ligand-to-metal ratio from 1 to 100. After acquiring the spectrum for each ligand-to-metal ratio, nebulizer was cleaned to ensure low background before proceeding with the next sample. Memory effect was more acute in the negative ion mode and long time cleaning with dilute solutions of EDTA or HNO_3 was necessary to bring down the background to satisfactory levels. However, manual cleaning of the nebulizer offered a very fast cleaning.

This distribution plot was arrived at assuming that the ion current in the gas phase quantitatively represents the solution equilibrium[223]. The response of the unbound uranyl species was obtained by summing up the fractional intensities of all the free uranyl species. Similarly, responses of ML_n were obtained by summing up the fractional intensities of all the species associated with UO_2-$(HIBA)_n$. Thus factional intensity of ML_1 complex was obtained by adding the individual fractional intensities of $[UO_2(C_4H_7O_3)]^+$, $[UO_2(C_4H_7O_3)(H_2O)]^+$, $[UO_2(C_4H_7O_3)(CH_3OH)]^+$, $[UO_2(C_4H_7O_3)(H_2O)_2]^+$ and $[UO_2(C_4H_7O_3)(H_2O)(CH_3OH)]^+$. The changes in the distribution of the different species with the increase in the ligand-to-metal ratio clearly indicate the progress of complexation reaction. As is seen from the Figure, the species corresponding to uncomplexed uranyl species decreased drastically with the increase in the proportion of HIBA in the mixture. The response of ML_1complex was found to increase, reached a maximum (at ligand-to-metal ratio = 2) and then decreased with further increase in the ligand-to-metal ratio. The ML_2 complexes were found to be predominant species at ligand-to-metal ratio of 5. ML_3 was found to be the most prominent species at the ligand-to-metal ratio ≥ 10.

Similarly, the distribution of different uranyl species as a function of ligand-to-metal ratio was studied in the negative ion mode and the results are presented in Figure 5.10(b). The species distribution obtained in the negative ion mode is similar to that obtained in the positive ion mode.

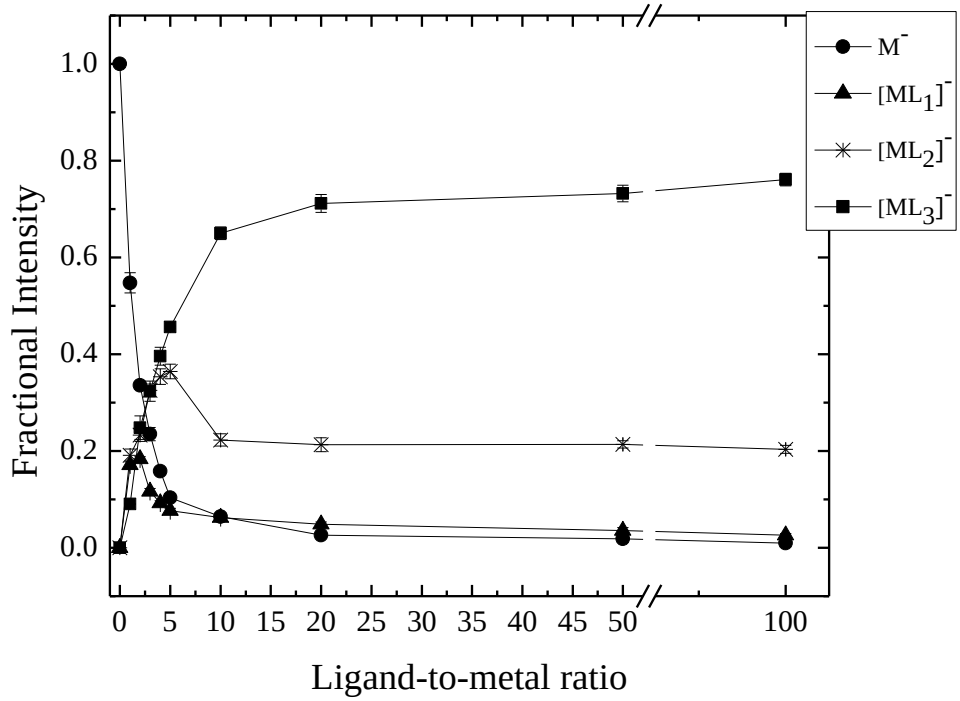

Figure 5.10(b): *Distribution of uranyl-HIBA complex species as a function of ligand-to-metal ratio in the negative ion mode.*
ESI parameters employed: dry gas temperature: 180 °C, capillary voltage: 3500 V, end-plate offset voltage : -800 V, quadrupole ion energy: 4 eV and collision cell energy : 4 eV.

It is seen that ML_3 is of the highest intensity in the negative ion mode e.g. ML_3 becomes the base peak at ligand-to-metal ratio as low as 5 in contrast to ligand-to-metal ratio of 10 in the positive ion mode. This is attributed to the relative ease for ML_3 species to form the negative ions as compared to ML_1 and ML_2 species. Similarly, the task of maintaining positive charge becomes difficult for ML_3 species due to the presence of three carboxylate groups in the complex and a working pH of 4.7 to 6.4. Studies on the influence of the experimental parameters such as sample type and mobile phase composition on the ESI

spectra are reported elsewhere [224]. Intensities of most of the uranyl species were slightly affected as the transmission parameters were kept at low energy values in both the modes. Complexing constants of uranyl-HIBA system are reported as log β_1 =3.2, logβ_2 = 5.1 and logβ_3 = 6.6 at pH 4.0 and this is indicative of the fact that the proportions of the ML_1, $ML_2$and ML_3 species in the solution are dependent on the ligand-to-metal ratio [172].

5.3.3 Complexation of Uranyl Ion with Mandelic Acid

Mandelic acid (α-hydroxyl phenyl acetic acid, $C_8H_8O_3$) is known to form hydrophobic complexes with Th& U and is a suitable ligand for their selective pre-concentration. Uranyl ion forms various complexes with mandelic acid and these can be cationic or anionic in nature and hence mass spectra were acquired in both the positive and the negative modes. Figure 5.11(a) shows the mass spectrum obtained by introducing 10^{-6}M $UO_2(NO_3)_2$ and 10^{-5} M mandelic acid in 1:1 methanol-water medium in the positive ion mode containing 10^{-5} M $NaClO_4$. Solution composition was chosen based on the work carried out on uranyl-HIBA system [225].

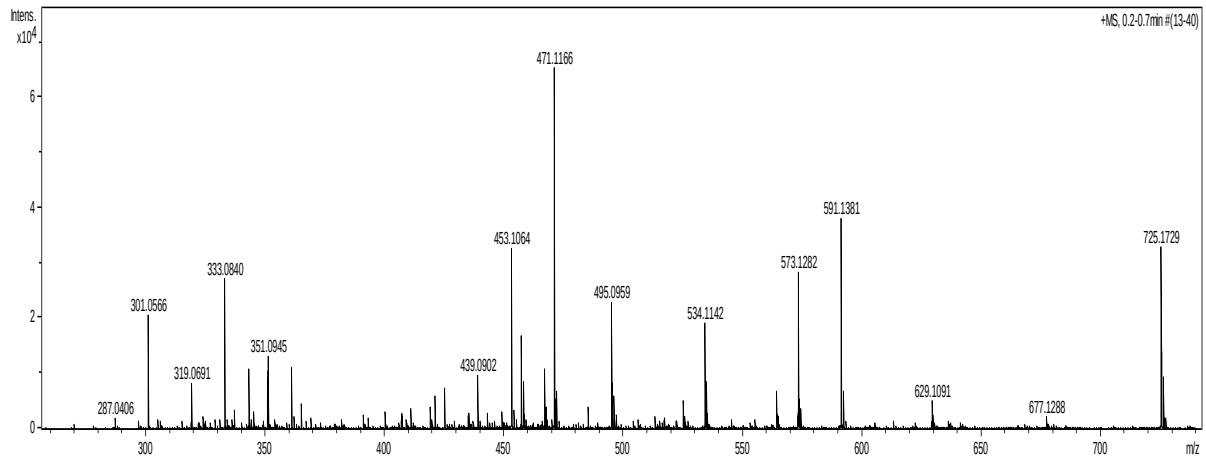

Figure 5.11(a): *ESI-MS spectrum of uranyl-mandelic acid system in the positive ion mode. $5x10^{-6}$ M $UO_2(NO_3)_2$ and 10^{-5} M mandelic acid in H_2O:MeOH (1:1 v/v).*

Different species identified in the mass spectrum are listed in Table 5.5(a).In the case of mandelic acid also, the maximum number of ligands observed around the UO_2^{2+} ion is only 3. Even in the case of ML_1 type complexes, the maximum number of solvent molecules involved in coordination was found to be 2. In the positive ion mode, the species $[UO_2(C_8H_8O_3)(CH_3OH)(H_2O)]^+$, at *m/z* 471.1, was the most intense peak. This is in contrast to the observation in uranyl-HIBA system where methanol containing species were the least abundant.

Table 5.5(a): Uranyl-mandelic acid species observed in the positive ion mode

Species	Type	*m/z*	Relative intensity*
$[UO_2(C_8H_8O_3)]^+$	M-H	421.1	9.5
$[UO_2(C_8H8O_3)(CH_3OH)]^+$		453.1	50.2
$[UO_2(C_8H_8O_3)(CH_3OH)(H_2O)]^+$		471.1	100
$[(UO_2)_2(C_8H_8O_3)_4]^{2+}$		573.1	43.7
$[(UO_2)(C_8H8O_3)_2(H_2O)]^+$		591.1	58.5
$[UO_2(C_8H_8O_3)_3]^+$		725.1	49.7

** Relative intensity with respect to the base peak at m/z 471.1*

Figure 5.11(b) shows the mass spectrum obtained for the uranyl-mandelic acid in the negative ion mode. The important species observed in the spectrum are listed in Table 5.5(b). In the negative ion mode also, the maximum number of ligands available for coordination with uranyl ion was found to be 3. Similar to the uranyl-HIBA system, the most intense peak in the negative ion mode was found to be of ML_3 species.

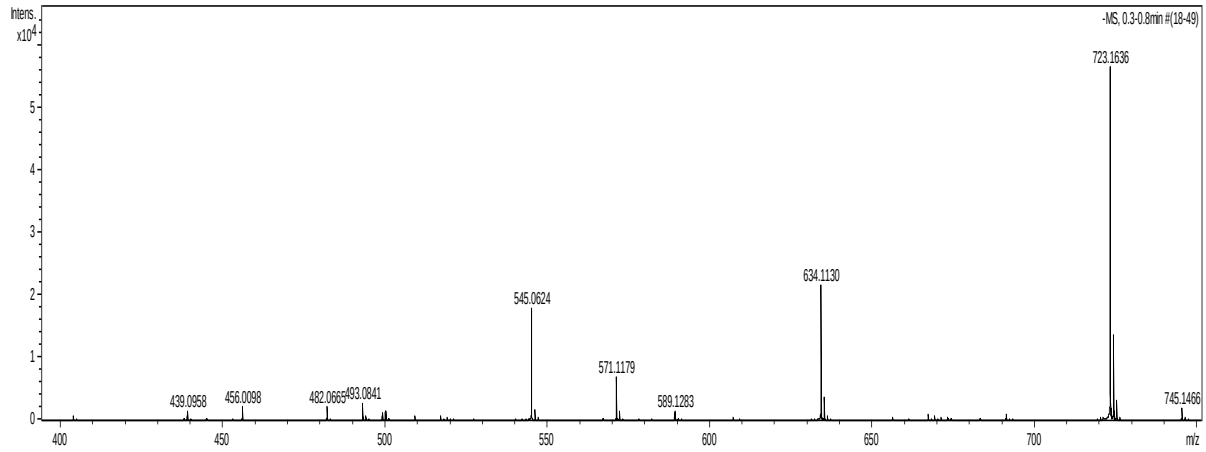

Figure 5.11(b): *ESI-MS spectrum of uranyl-mandelic acid system in the negative ion mode. $5x10^{-6}$ M $UO_2(NO_3)_2$ and 10^{-5} M mandelic acid in H_2O:MeOH (1:1 v/v).*

Table 5.5(b): Uranyl-mandelic acid species observed in the negative ion mode

Species	Type	*m/z*	Relative intensity*
$[UO_2(NO_3)_3]^-$	M-H	456.1	3.8
$[UO_2(C_8H_7O_3)(NO_3)]^-$	M-H	482.1	4.2
$[UO_2(C_8H_7O_3)(NO_3)(OH)]^-$	M	500.1	2.3
$[UO_2(C_8H_7O_3)(NO_3)_2]^-$	M	545.1	31.7
$[UO_2(C_8H_7O_3)_2]^-$	M-H	571.1	12.9
$[UO_2(C_8H_7O_3)_2(OH)]^-$	M	589.1	2.8
$[UO_2(C_8H_7O_3)_2(NO_3)]^-$	M	634.1	38.6
$[UO_2(C_8H_7O_3)_3]^-$	M	723.1	100

** Relative intensity with respect to the base peak at m/z 723.1*

Another interesting observation was the appearance of doubly positive dimeric species $[(UO_2)_2(C_8H_8O_3)_4]^{2+}$*m/z* 573.1, under soft ionization conditions. This is in contrast to the pattern observed with uranyl-HIBA system in water-methanol mixture, where no doubly charged species was observed. This dimeric species was found to convert into the monomeric species, $[(UO_2)(C_8H_8O_3)_2]^{2+}$*m/z* 573.1at high energy collision dissociation conditions

(collision cell energy > 30 eV). Though the dimer and monomer species appear at the same *m/z* value they could be distinguished based on the different isotopic patterns shown in Figures 5.12 (a) and 5.12(b). The monomeric product obtained is analogous to one of the prominent species, $[UO_2(C_4H_8O_3)_2]^+$,observed with uranyl-HIBA system. The formation of the dimeric species was favoured by the increase in concentration of uranyl-mandelate complex in the solution and decrease in the nebulizer gas flow rate.

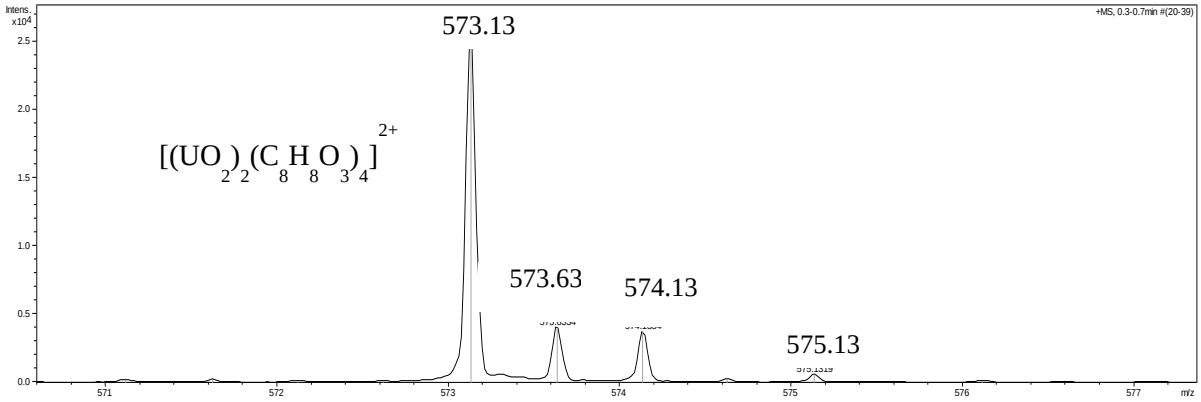

Figure 5.12(a): *ESI-MS spectrum of the dimericuranyl-mandelic acid species* $[(UO_2)_2(C_8H_8O_3)_4]^{2+}$.
$5x10^{-6}$ M $UO_2(NO_3)_2$ and $5x10^{-5}$ M mandelic acid in H_2O:MeOH (1:1 v/v), collision cell energy : 5 eV.

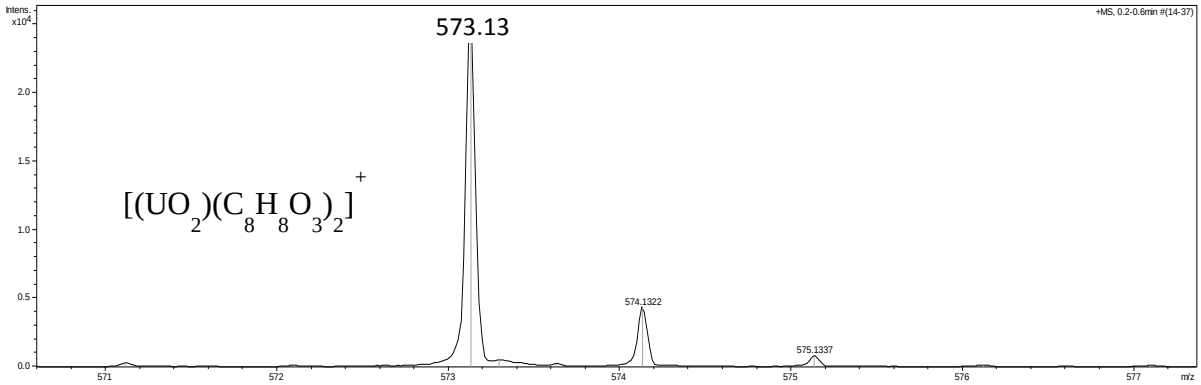

Figure 5.12(b): *ESI-MS spectrum of the monomeric uranyl-mandelic acid species* $[(UO_2)(C_8H_8O_3)_2]^+$.
$5x10^{-6}$ M $UO_2(NO_3)_2$ and $5x10^{-5}$ M mandelic acid in H_2O:MeOH (1:1 v/v), collision cell energy : 40 eV.

5.3.3.1 Effect of Electrospray Ionisation and Transfer Parameters

Figure 5.13shows the changes in the intensities of different uranyl-mandelate species in the positive ion mode as a function of dry gas temperature. The ion intensities are expected to increase with increase in temperature due to the efficient solvent drying. However, the increase in temperature can also result in the thermal dissociation of fragile species. Thus the intensities of the species viz. $[UO_2(C_8H_8O_3)_3]^+$at *m/z* 421.1 is seen to increase with increase in temperature. However, the ion $[UO_2(C_8H_8O_3)(CH_3OH)(H_2O)]^+$at *m/z*471.1 showed a steady decrease in intensity with the increase in temperature. The optimum dry gas temperature chosen for the subsequent experiments was 150^{o}C.

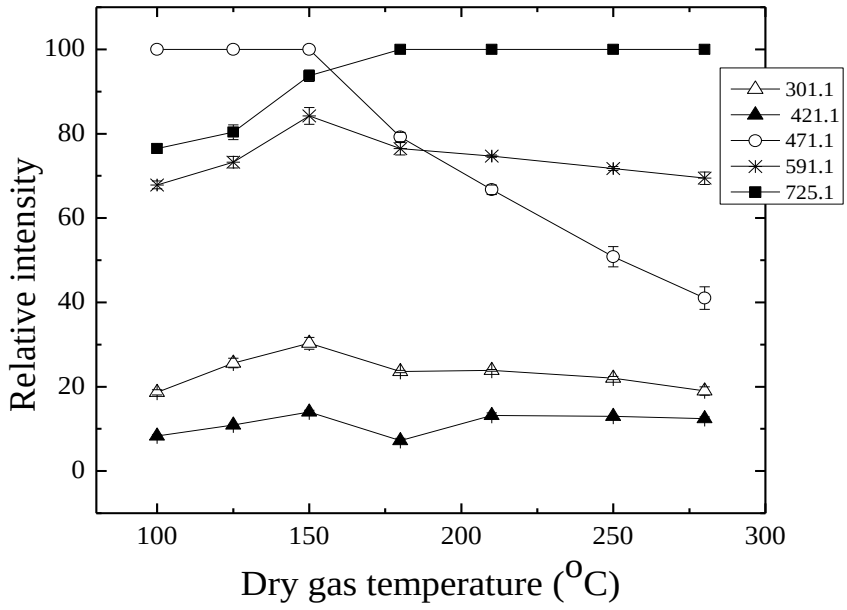

Figure 5.13: *Changes in the intensities of uranyl-mandelate species as a function of dry gas temperature in the positive ion mode.*

Changes in the intensities of different uranyl-mandelate species as a function of in-source collision induced dissociation energy (ISCID) are shown in Fig.5.14. Increase in the energy would lead to increased acceleration of the ionic species leading to more energetic collisions. However, collisions to a greater extent may lead to fragmentation of the species

concerned. It is seen from the Figure that the ESI responses of ML_2 and ML_3 remained the same whereas the ML_1 solvated species with methanol showed decrease in intensity. Interestingly, dimeric species $[(UO_2)_2(C_8H_8O_3)_4]^{2+}$ was found to be stable till the ISCID energy of 30 eV and at the 40 eV, dimeric species converted into the monomeric, as confirmed from isotopic pattern.

Similarly the distribution of different uranyl-mandelate species was studied as a function of collision energy.$[UO_2(C_8H_8O_3)(CH_3OH)(H_2O)]^+$*m/z* 471.1 and $[UO_2(C_8H_8O_3)_3]^+$ at *m/z* 725.1 were found to show drastic decrease in intensities with increase in the collision energy. However, $[(UO_2)(C_8H_8O_3)_2(H_2O)]^+$was found to be stable till the collision energy of 10 eV and further increase in collision energy led to fragmentation of this species.

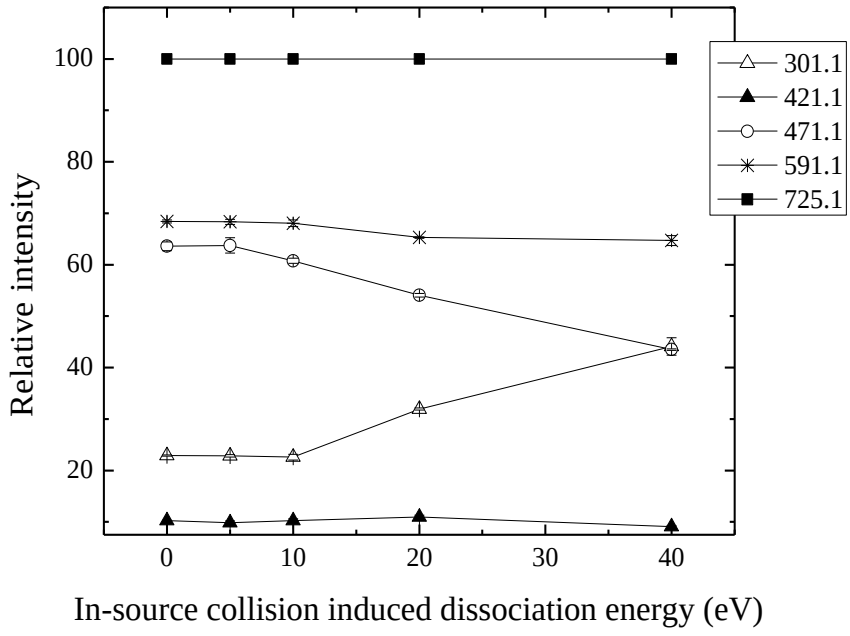

Figure 5.14: *Changes in the intensities of uranyl-mandelate species as a function of in-source collision induced dissociation energy in the positive ion mode.*

5.3.4 Conclusions

ESI-MS was used to identify different species of uranyl complex with HIBA and mandelic acid in methanol-water medium. A detailed study on the influence of the mobile

phase composition and concentrations of the electrolyte and uranyl salt on the distribution of major uranyl species was carried out. These studies were helpful to obtain sensitive and representative ESI-MS spectra. ESI-MS spectra were acquired in both the positive and the negative ion modes to obtain a complete picture of the complexation. Major uranyl-hydroxycarboxylic acid species observed in the positive and the negative ion modes were identified. The effects of electrospray as well as transfer parameters on the distribution of important species were investigated and optimized conditions were employed for obtaining information about the solution phase equilibrium. Though HIBA and mandelic acid showed more or less similar patterns in their complexation with uranyl ion, some of the distinct behaviors of mandelic acid were the formation of prominent methanol containing species and doubly charged adduct species under soft ESI conditions. ESI-MS was employed for following the overall trend in the complexation between uranyl ion and HIBA ligand. The methodology is attractive for uranyl-hydroxycarboxylic acid complex speciation studies in view of its sensitivity and ability to identify and monitor a large number of complexed and uncomplexed species.

References

1. L. Perna, F. Bocci, L.A. Heras, J. De Pablo and M. Betti. Studies on simultaneous separation and determination of lanthanides and actinides by ion chromatography inductively coupled plasma mass spectrometry combined with isotope dilution mass spectrometry. *J. Anal. At. Spectrom.*, 2002,17, 1166 - 1171.

2. I.G. Leopold, N. Kivel, J.K. Waldis, B. Wernli. Characterization of nuclear fuels by ICP mass-spectrometric techniques. *Anal. Bioanal. Chem.* (2008) 390, 503 - 510.

3. J.M.B. Moreno, J.M.G. Alonso, J.I.P. Arbore, G. Nicolaou, L. Koch. Characterization of spent nuclear fuels by ion chromatography-inductively coupled plasma mass spectrometry. *J. Anal. At. Spectrom.* 11 (1996) 929 - 935.

4. R. Kautenburger and H.P. Beck. Influence of geochemical parameters on the sorption and desorption behaviour of europium and gadolinium onto kaolinite. *J. Environ. Monit.*, 2010,12, 1295 - 1301.

5. S. Sahijpal, K. K. Marhas and J. N. Goswami. Determination of rare earth and refractory trace element abundances in early solar system objects by ion microprobe. Proc. Indian Acad. Sci. (Earth Planet. Sci.), 112 (2003) 485 - 498.

6. G. Han, Y. Xu, Z. Tang and G. Zhang. Rare Earth Element Patterns in the Karst Terrains of Guizhou Province, China: Implication for Water/Particle Interaction. Aquat. Geochem., 2009, 15, 457 - 484.

7. N. L. Misra, S. Dhara, A. Das, G. S. Lodha, S. K. Aggarwal and I. Varga. Trace determination of uranium in fertilizer samples by total reflection X-ray fluorescence. Pramana- *J. Phys.*, 76 (2011) 357 - 360.

8. Nomenclature of Inorganic Chemistry, 2nd Edition, IUPAC Commission on the Nomenclature of Inorganic Chemistry, London, Butterworths, 1970

9. K. A. Gschneidner Jr. and L. Eyring, Handbook on the Physics and Chemistry of Rare Earths, Vol. 11, Chapter 11, Elsevier publishers, 1988.

10. J.S. Fritz. Recent developments in the separation of inorganic and small organic ions by capillary electrophoresis. J. Chromatogr. A 2000, 884, 261 - 275.

11. G.T.Seaborg, G.J. Bushey, A. Klingsberg (Eds.), *Kirk-Othmer Encyclopedia of Chemical Technology*, 3rd Ed.,Vol. 1, John Wiley and Sons, New York 1978, pp. 456 - 488.

12. S.G. Lee, D.H. Lee, Y. Kim, B.G. Chae, W.Y. Kim and N.C. Woo. *Appl. Geochem.* 2003, 18, 135 - 143.

13. D. L. Clark. The Chemical Complexities of Plutonium. Los Alamos Science (2000) 26, 364 - 381.

14. Katz, J. J., G. T. Seaborg, and L. R. Morss, Eds. 1986. The Chemistry of the Actinide Elements. London: Chapman and Hall.

15. R.D. Shannon. Revised effective ionic radii in halides and chalcogenides. *Acta Cryst.* A32 (1976), 751 - 767.

16. R. G. Pearson. Hard and soft acids and bases. J. Am. Chem. Soc., 1963, 85, 3533 - 3539.

17. British Geological Survey Natural Environmental Research Council. (2010). Rare Earth Elements.http://www.bgs.ac.uk/downloads/start.cfm?id=1638

18. T. Prasada Rao, V. M. Biju. Trace Determination of Lanthanides in Metallurgical, Environmental and Geological Samples. Critical Reviews in Analytical Chemistry, 30 (2000)179 - 220

19. M. L. Grossbeck, J.P.A. Renier, and R.T. Bigelow. Development of Improved Burnable Poisons for Commercial Nuclear Power Reactors (2003). http://www.osti.gov/bridge/servlets/purl/820689-RdjHch/native/820689.pdf

20. T. Kitada, K. Shimozato, K. Ieyama, H. Okochi and A. Ymamoto. Analysis of Sample Worth for Dy_2O_3, Ho_2O_3, Er_2O_3 and Tm_2O_3 Measured at KUCA by MVP with Recent Version of ENDF and JENDL. Progress in Nuclear Science and Technology, 2 (2011) 330-333.

21. M. Humphries. Rare Earth Elements: The Global Supply Chain. (2011)http://www.fas.org/sgp/crs/natsec/R41347.pdf].

22. K. Anantharaman, V. Shivakumar and D. Saha. Utilisation of thorium in reactors. Journal of Nuclear Materials 383 (2008) 119 - 121.

23. S. K. Sahoo, M. Hosoda, S. Kamagata, A. Sorimachi, T. Ishikawa, S. Tokonami and S. Uchida. Thorium, Uranium and Rare Earth Elements Concentration in Weathered Japanese Soil Samples. Progress in Nuclear Science and Technology, 1, (2011) 416 - 419.

24. B. Zawisza, K. Pytlakowska, B. Feist, M. Polowniak, A. Kita and R. Sitko. Determination of rare earth elements by spectroscopic techniques: a review. J. Anal. At. Spectrom., 26 (2011) 2373 - 2390.

25. Standard Specification for Nuclear-Grade, Sinterable Uranium Dioxide Powder. ASTM C753 − 04 (Reapproved 2009).

26. S.K. Aggarwal, P.G. Jaison, V.M. Telmore, P.S. Khodade, R.V. Shah, R. Govindan, V.L. Sant and P.M. Shah, Determination of burn-up of irradiated PHWR fuel samples from KAPS-1 by mass spectrometry, (BARC Report) BARC/2007/E/020 (2007).

27. J.S. Kim, Y.S. Jeon, S.D. Park, B.C. Song, S.H. Han and J.G. Kim. Dissolution and burn-up determination of irradiated U-Zr alloy nuclear fuel by chemical methods. Nuclear Engineering and Technology, 38 (2006) 301 - 310.

28. Atom percent fission in uranium and plutonium fuel (Neodymium-148 method). ASTM Standard Method ANSI/ASTM E 321-96 (1996).

29. N. Sivaraman, S. Subramaniam, T. G. Srinivasan, P. R. Vasudeva Rao. Burn-up measurements on nuclear reactor fuels using high performance liquid chromatography. Journal of Radioanalytical and Nuclear Chemistry. 2002, 253, 35 - 40.

30. P. Henderson and C. T. Williams, Application of intrinsic Ge detectors to the instrumental neutron activation analysis for rare earth elements in rocks and minerals. J. Radioanal. Chem., 67,1981,445 - 452.

31. R.S. Dybczynski, E. Czerska, B. Danko, K. Kulisa and Z. Samczynski, Comparison of performance of INAA, RNAA and ion chromatography for the determination of individual lanthanides, *Applied Radiation and Isotopes* 68 (2010) 23 - 27.

32. S. Durani, M. Krishnakumar and Satyanarayana. Solid phase separation and ICP-OES/ICP-MS determination of rare earth impurities in nuclear grade uranium oxide. J. Radioanal. Nucl. Chem 294 (2012) 215 - 220.

33. A.J.R. Kent, B. Jacobsen, D.W. Peate, T.E. Waight and J.A. Baker. Isotope Dilution MC-ICP-MS Rare Earth Element Analysis of Geochemical Reference Materials NIST SRM 610, NIST SRM 612, NIST SRM 614, BHVO-2G, BHVO-2, BCR-2G, JB-2, WS-E, W-2, AGV-1 and AGV-2. Geostandards and Geoanalytical Research, 28 (2004) 417 - 429.

34. R. G. Fernandez, J. I. G. Alonso. Separation of rare earth elements by anion-exchange chromatography using ethylenediaminetetraacetic acid as mobile phase. Journal of Chromatography A, 1180 (2008) 59 - 65.

35. C. Pin, J.F.S. Zalduegui, Sequential separation of light rare-earth elements, thorium and uranium by miniaturized extraction chromatography: Application to isotopic analyses of silicate rocks. Anal. Chim. Acta 339 (1997) 79 - 89.

36. J.M. Schwantes, R.S. Rundberg, W.A. Taylor and D.J. Vieira. Rapid, high-purity, lanthanide separations using HPLC. Journal of Alloys and Compounds 418 (2006) 189 - 194.

37. W. R. Pedreira, J. E. S. Sarkis, C. Rodrigues, I. A. Tomiyoshi, C.A. Q. da Silva, A. Abrao. Determination of trace amounts of rare earth elements in highly pure praseodymium oxide by double focusing inductively coupled plasma mass spectrometry and high-performance liquid chromatography. Journal of Alloys and Compounds 323 (2001) 49 – 52.

38. P. Janos. Analytical separations of lanthanides and actinides by capillary electrophoresis. Electrophoresis 24 (2003) 1982 -1992.

39 D. I. Ryabchikov and V. A. Ryabukhin, Analytical Chemistry of Yttrium and the Lanthanide Elements, Ann Arbor- Humphrey Science Publishers, London, 1970.

40. S. P. Sinha, Complexes of Rare-Earths, Pergamon Press, Oxford London, 1st Edition, 1966.

41. M. Hansen, F. Ojala, D. Kifle, N. Borg, B. Nilsson. Optimization of preparative chromatographic separation of multiple rare earth elements. *J. Chromatogr. A* 1218 (2011) 9155 - 9161.

42. I. Billard, A. Ouadi, C. Gaillard. Liquid–liquid extraction of actinides, lanthanides, and fission products by use of ionic liquids: from discovery to understanding. Analytical and Bioanalytical Chemistry 400 (2011)1555 - 1566.

43. M. Macka, P. Nesterenko, P. Andersson, P. R. Haddad. Separation of uranium(VI) and lanthanides by capillaryelectrophoresis using on-capillary complexation with arsenazo III. *J. Chromatogr. A*, 803 (1998) 279 - 290

44. S.P. Verma, R. Garcıa, E. Santoyo, A. Aparicio. Improved capillary electrophoresis method for measuring rare-earth elements in synthetic geochemical standards. *J. Chromatogr. A* 884 (2000) 317 - 328.

45. Y. Lin, H. Wu, N. G. Smart, C. M. Wai. Studies on in-situ chelation/supercritical fluid extraction of lanthanides and actinides using a radiotracer technique. Separation Science and Technology, 36, (2001) 1149 - 1162.

46. M. Kumar, Recent Trends in Chromatographic Procedures for Separation and Determination of Rare Earth Elements -A Review, *Analyst*, 119 (1994) 2013 - 2024.

47. K.L. Nash and M.P. Jensen. Analytical-scale separations of the lanthanides: A review of techniques and fundamentals. *Sep. Sci. Technol.*36 (2001)1257 - 1282.

48. D.A. Skoog and J.J Leary. Principles of Instrumental Analysis (1992) 4th Edn. Saunders College Publishing: Fort Worth.

49. C.Y. Liu, N.M. Lee and T.H. Wang. Chelation ion chromatography as a technique for trace elemental analysis in complex matrix samples. *Analytica Chimica Acta* 337 (1997) 173 - 182.

50. Z. Varga, R. Katona, Z. Stefánka, M. Wallenius, K. Mayer and A. Nicholl. Determination of rare-earth elements in uranium-bearing materials by inductively coupled plasma mass spectrometry. *Talanta* 80 (2010)1744 - 1749.

51. P.N. Nesterenko, P. Jones. Isocratic separation of lanthanides and yttrium by high-performance chelation ion chromatography on iminodiacetic acid bonded to silica. *J. Chromatogr. A*, 804 (1998) 223 - 231.

52. W. Yantasee, G.E. Fryxell, R.S. Addleman, R.J. Wiacek, V. Koonsiripaiboon, K. Pattamakomsan, V. Sukwarotwat J. Xu and K.N. Raymond. Selective removal of lanthanides from natural waters, acidic streams and dialysate. Journal of Hazardous Materials 168 (2009) 1233 -1238.

53. R. M. Cassidy, S. Elchuk, N. L. Elliot, L. W. Green, C. H. Knight and B. M. Recoskie, Dynamic ion exchange chromatography for the determination of number of fissions in uranium dioxide fuels. *Anal. Chem.,* 58, (1986) 1181 -1186.

54. K.L. Nash and M.P. Jensen. Analytical separations of the lanthanides: basic chemistry and methods. Handbook on the Physics and Chemistry of Rare Earths 28 (2000) 311 - 371.

55. E. Santoyo, M. Guevara and S.P. Verma. Determination of lanthanides in international geochemical reference materials by reversed-phase high-performance liquid chromatography using error propagation theory to estimate total analysis uncertainties. *J. Chromatogr. A*, 1118 (2006) 73 - 81.

56. K. Robards, S. Clarke and E. Patsalides. Advances in the analytical chromatography of the lanthanides. A review. *Analyst* 113 (1988) 1757 - 1779.

57. M.S. Tswett, Tr. Protok. Varshav. Obshch. Estestvoistpyt., Otd. Biol., 14 (1905) 20. On the new Category of Adsorption Phenomena and their Applications in Biochemical Analysis, Reprinted and Translated in G. Hesse and H. Weil, "Michael Tswett's erste chromatographische Schrift," Woelm, Eschwegen, 1954.

58. M.S. Tswett, T.P. Varshav and O. Estestvoistpyt. On the new Category of Adsorption Phenomena and their Applications in Biochemical Analysis. *Otd. Biol.,* 14 (1905) 20 .

59. A.P.J. Martin and R.L.M. Synge. A new form of chromatogram employing two liquid phases. Biochem. J. 35 (1941) 1358 - 1368.

60. B.H. Ketelle and G.E. Boyd. The exchange adsorption of ions from aqueous solutions by organic zeolites; the separation of the yttrium group rare earths. *J. Am. Chem. Soc.* 69 (1947) 2800 - 2812.

61. J. N. Story and J. S. Fritz. Forced-flow chromatography of the lanthanides with continuous in-stream detection. *Talanta,* 21 (1974) 892 - 894.

62. P. Dufek, M. Vobecky, J. Holik and J. Valasek. Separation of some rare earths and transplutonium elements by high-performance liquid chromatography on Ostion cation exchanger. J Chromatogr 435 (1988) 249 -252.

63. R. P. W. Scott. Contemporary liquid chromatography. Wiley, New York, 1976.

64. L.R. Snyder, J.J. Kirkland and J.W. Dolan. Introduction to Modern Liquid Chromatography. 3rd Edn. (2009), John Wiley and Sons, New Jersy.

65. V.R. Meyer. Practical High-Performance Liquid Chromatography. 5th Edn. (2010), John Wiley and Sons, West Sussex, UK.

66. http://www.sigmaaldrich.com/analytical-chromatography/hplc/learning-center/chromatographic-selectivity.html

67. R.P. W. Scott . Liquid Chromatography. Chrom-Ed Book Series Principles and Practice of Chromatography (2003).

68. A.M. Siouffi. Silica gel-based monoliths prepared by the sol–gel method: facts and figures. *J. Chromatogr. A,* 1000 (2003) 801 - 818.

69. C. F. Poole. The Essence of Chromatography. 1st Edition, (2003) Elsevier Science B.V., Amsterdam, The Netherlands.

70. R.P.W. Scott. Chromatographic Detectors: Design, Function, and Operation, Marcel Dekker, 1996, New York.

71. K. Macek, Z. Deyl, J. Janak. Liquid Column Chromatography: A Survey of Modern Techniques and Applications. Elsevier Scientific Publishing Co. (1975) Amsterdam, The Netherlands.

72. R. Schoftner, W. Buchberger and H.Malissa. Determination of quaternary alkylammonium compounds by capillary zone electrophoresis and indirect UV detection as a real alternative to ion chromatography with suppressed conductivity detection. *J. Chromatogr. A*, 920 (2001) 333 - 344.

73. I.D. Wilson, U.A.Th. Brinkman. Hyphenation and hypernation: The practice and prospects of multiple hyphenation. *J. Chromatogr. A*, 1000 (2003) 325 - 356.

74. A. P. Snyder. Electrospray: A Popular Ionization Technique for Mass Spectrometry. Chapter 1, ACS Symposium Series, 619 (1996) 1 - 20.

75. A. El-Aneed, A. Cohen and J. Banoub. Mass Spectrometry, Review of the Basics: Electrospray, MALDI, and Commonly Used Mass Analyzers. *Applied Spectroscopy Reviews*, 44 (2009) 210 – 230.

76. I.V. Chernushevich. Duty cycle improvement for a quadrupole–time-of-flight mass spectrometer and its use for precursor ion scans Eur. J. Mass Spectrom. 6 (2000) 471 – 479.

77. R.N. Zare, F.M.Fernandez, and J.R. Kimmel. Hadamard Transform Time-of-Flight Mass Spectrometry: More Signal, More of the Time. Angew. Chem. Int. Ed . 4 (2003) 30 – 35.

78. G.L. Glish and R.W. Vachet. The basics of mass spectrometry in the twentyfirst century. Nature Reviews 2 (2003) 140 - 150.

79. J. N Louris, R.G. Cooks, J.E.P. Syka, P.E. Kelley, G.C. Stafford, and J.F.J. Todd. Instrumentation, Applications and Energy Deposition in Quadrupole Ion Trap MS/MS Spectrometry. *Analytical Chemistry* 59 (1987)1677 - 1685.

80. A.G. Marshall and C.L. Hendrickson. High-Resolution Mass Spectrometers. *Annual Review of Analytical Chemistry.* 1 (2008) 579 - 599.

81. P.S.H. Wong and R.G. Cooks. Ion Trap Mass Spectrometry. http://www.currentseparations.com/issues/16-3/cs16-3c.pdf

82. M. Guilhaus, D. Selby and V. Mlynsk, Orthogonal acceleration time-of-flight mass spectrometry, *Mass Spectrometry Reviews* 19 (2000) 65 - 107.

83. D. Alamelu, Ph. D (Science) Thesis, University of Mumbai (2009).

84. P. Kebarle and M. Peschke, On the mechanisms by which the charged droplets produced by electrospray lead to gas phase ions, *Analytica Chimica Acta* 406 (2000) 11 - 35.

85. N.B. Cech and C.G. Enke, Practical implications of some recent studies in electrospray ionization fundamentals, *Mass Spectrometry Reviews* 20 (2001) 362 - 387.

86. J.B. Fenn, M. Mann, C.K. Meng, S.F Wong and C.M. Whitehouse, Electrospray ionization for mass spectrometry of large biomolecules, Science, 246 (1989) 64-71.

87. P. Kebarle and U.H. Verkerk, Electrospray: from ions in solution to ions in the gas phase, what we know now. *Mass Spectrometry Reviews*, 28 (2009) 898 - 917.

88. I.V. Chernushevich, A. V. Loboda, B. A. Thomson. An introduction to quadrupole–time-of-flight mass spectrometry, J. Mass Spectrom. 36 (2001)849 - 865.

89. J.L. Wiza, Microchannel plate detectors, *Nuclear Instruments and Methods*. 162 (1979) 587 - 601.

90. F. Albarede and B. Beard, Analytical methods for non-traditional isotopes, *Reviews in Mineralogy & Geochemistry*, 55 (2004)113 - 152.

91. A. Al-Shawi and R. Dahl, Determination of lanthanides in magnesium alloys by ion chromatography. *Anal. Chim. Acta*333(1996) 23 – 30.

92. R. Saraswati, Simultaneous determination of transition and rare earth metal ions in Nd-Fe-B Material by high performance ion chromatography using post-column chelation technique. *J. Liq. Chromatgr*. 16 (1993) 4095 - 4105.

93. H. Stray and S.A. Dahlgren, A combined classical ion-exchange and HPIC procedure for the separation of Nd and Sm for isotopic analysis of geological samples. *Chem. Geol*. 125 (1995) 233 -238.

94. R. Bros, J. Carpena, V. Sere and A. Beltritti, Occurrence of Pu and fissiogenic REE in hydrothermal apatites from the Fossil Nuclear Reactor 16 at Oklo (Gabon). *Radiochim. Acta* 74 (1996) 277 - 282.

95. S. Rollin, Z. Kopajtic, B. Wernli and B. Magyar, Determination of lanthanides and actinides in uranium materials by high performance liquid chromatography with inductively coupled plasma mass spectrometric detection, *J. Chromatogr. A*, 739 (1996) 139 -149.

96. M.R. Buchmeiser, G. Seeber and R. Tessadri, Quantification of lanthanides in rocks using succinic acid-derivatized sorbents for on-line SPE-RP-ion-pair HPLC, *Anal. Chem.* 72 (2000) 2595 - 2602.

97. P. Deepika, N. Sivaraman, K.N. Sabharwal, T.G. Srinivasan and P.R.V. Rao, Separation of lanthanides and actinides on a bistriazinyl pyridine coated reverse phase column, *Radiochimica Acta* 99 (2011) 325 - 334.

98. S.P. Verma and E. Santoyo, High-performance liquid and ion chromatography: Separation and quantification analytical techniques for rare earth elements, *Geostandards and Geoanalytical Research*. 31 (2007) 161 - 184.

99. N.M. Raut, P.G. Jaison and S.K. Aggarwal, Comparative evaluation of three α-hydroxycarboxylic acids for the separation of lanthanides by dynamically modified reversed-phase high-performance liquid chromatography.*J. Chromatogr. A*959 (2002) 163-172.

100. R.M. Cassidy and S. Elchuk, Dynamically coated columns for the separation of metal ions and anions by ion chromatography. *Anal. Chem.* 54 (1982)1558 - 1563.

101. N. Sivaraman, R. Kumar, S. Subramaniam and P.R. V. Rao, Separation of lanthanides using ion-interaction chromatography with HDEHP coated columns, *J. Radioanal. Nucl. Chem.*252 (2002) 491 - 495.

102. K. Joe, Y.S. Jeon, J.S. Kim, S.H. Han, J.G. Kim and W.H. Kim, Separation of burn-up monitors in spent nuclear fuel samples by liquid chromatography, *Bull. Korean Chem. Soc.* 26 (2005) 569 - 574.

103. S. Elchuk, K. I. Burns, R. M. Cassidy and C. A. Lucy, Reversed-phase separation of transition metals, lanthanides and actinides by elution with mandelic acid, *J. Chromatogr*. 558 (1991) 197 - 207.

104. L. E. Vera-Avila and E. Camacho, RP-IPC with a lactic acid modified eluent for separation and determination of lanthanide ions, *J. Liq. Chromatogr.* 15 (1992) 835 - 850.

105. V.T. Hamilton, W.D. Spall, B.F. Smith and E.J. Peterson, Quantitative analysis of thorium in plutonium using reversed-phase liquid chromatography and spectrophotometric detection, *J. Chromatogr.* 469(1989)369 - 377.

106. R. M. Cassidy, S. Elchuk, L.W. Green, C. H. Knight, F.C. Miller and B.M. Recoskie, Liquid chromatographic determination of the number of fissions in uranium/aluminium nuclear fuels, J. Radioanal. Nucl. Chem. 139 (1990) 55 - 64.

107. T. Cecchi. Ion Pairing Chromatography. Critical Reviews in Analytical Chemistry 38 (2008) 161 - 213.

108. N.L. Elliot, L.W. Green, B.M. Recoskie and R.M Cassidy, Mass spectrometric determination of lanthanum in nuclear fuels, *Anal. Chem.* 58 (1986) 1178 - 1181.

109. N.M. Raut, P.G. Jaison and S.K. Aggarwal, Separation and determination of lanthanides, thorium and uranium using a dual gradient in reversed-phase liquid chromatography, *J. Chromatogr. A* 1052 (2004)131 - 136.

110. N.M Raut, P.G. Jaison and S.K. Aggarwal, Proceedings of 9th ISMAS Workshop on Mass Spectrometry (9th ISMAS-WS 2000) held in Goa during December 12-16, 2000, p.144, RS-6.

111. K. Chander, S.P. Hasilkar, A.V. Jadhav and H.C. Jain, A titrimetric method for the sequential determination of thorium and uranium, *J. Radioanal. Nucl. Chem.* 174 (1993) 127 - 132.

112. M. Xavier, P. R. Nair, K. V. Lohithakshan, S. G. Marathe and H. C. Jain, Determination of uranium in the presence of iron and plutonium by Ti(III) reduction and biamperometric titration, *J. Radioanal. Nucl. Chem.* 148 (1991) 251 - 256.

113. R.K Sinha and A. Kakodkar, Design and development of the AHWR-the Indian thorium fuelled innovative nuclear reactor, Nuclear Engineering and Design 236 (2006) 683 - 700.

114. R.K Sinha, Advanced nuclear reactor systems - An Indian perspective, Energy Procedia 7 (2011) 34 - 50.

115. S.F. Boulyga and J.S. Becker, Isotopic analysis of uranium and plutonium using ICP-MS and estimation of burn-up of spent uranium in contaminated environmental samples, *J. Anal. At. Spectrom.*,17 (2002)1143 - 1147.

116. S. Burger, L.R. Riciputi, D.A. Bostick, S. Turgeon, E.H. McBay and M. Lavelle, Isotope ratio analysis of actinides, fission products, and geolocators by high-efficiency multi-collector thermal ionization mass spectrometry, *International Journal of Mass Spectrometry* 286 (2009) 70 - 82.

117. V. P. Mironov, J. L. Matusevich, V. P. Kudrjashov, P. I. Ananich, V. V. Zhuravkov, S. F. Boulyga and J. S. Becker, Determination of uranium concentration and burn-up of irradiated reactor fuel in contaminated areas in Belarus using uranium isotopic ratios in soil samples, *Radiochimica Acta* 93 (2005) 781 - 784.

118. S. Koyama, M. Osaka, T. Sekine, K. Morozumi, T. Namekawa and M. Itoh, Measurement of Burnup in FBR MOX Fuel Irradiated to High Burnup, *J. Nucl. Sci. Tech*. 40 (2003) 998 - 1013.

119. H. Knight, R. M.Cassidy, B.M.Recoskie and L.W.Green, Dynamic ion exchange chromatography for determination of number of fissions in thorium-uranium dioxide fuels, *Anal. Chem.* 56 (1984) 474 - 478.

120. M.E.Meek and B.F.Rider, Compilation of fission product yields, NEDO-12154-1 (1974).

121. E.H. Borai and A.S. Mady, Separation and quantification of ^{238}U, ^{232}Th and rare earths in monazite samples by ion chromatography coupled with on-line flow scintillation detector, *Applied Radiation and Isotopes* 57 (2002) 463 - 469.

122. A. Datta, N. Sivaraman, T.G. Srinivasan and P.R.V. Rao, Rapid separation of lanthanides and actinides on small particle based reverse phase supports, Radiochimica Acta 98 (2010) 277-285.

123. H. Fuping, P.R. Haddad, P.E. Jackson and J. Carnevale, Studies on the retention behaviour of α-hydroxyisobutyric acid complexes of thorium(IV) and uranyl ion in reversed-phase high-performance liquid chromatography, *J. Chromatogr*. 640 (1993) 187 - 194.

124. A.C. Wahl, Nuclear-charge distribution and delayed-neutron yields for thermal-neutron-induced fission of ^{235}U, ^{233}U, and ^{239}Pu and for spontaneous fission of ^{252}Cf, *Atomic Data and Nuclear Data Tables* 39 (1988) 1 - 156.

125. T.R.G. Kutty, M.R. Nair, P. Sengupta, U. Basak, Arun Kumar and H.S. Kamath, Characterization of (Th,U)O2 fuel pellets made by impregnation technique, *Journal of Nuclear Materials* 374 (2008) 9 - 19.

126. A.S. Amin and T.Y. Mohammed, Simultaneous spectrophotometric determination of thorium and rare earth metals with pyrimidine azo dyes and cetylpyridinium chloride, *Talanta* 54 (2001) 611 - 620.

127. A. Premadas and C.R. Khorge, Solvent extraction separation of heavy rare earth elements from light rare earth elements and thorium: ICP-AES determination of REEs and yttrium in monazite mineral, *Atomic Spectroscopy* 27 (2006) 170 - 177.

128. A.A. Argekar, M.J. Kulkarni, J.N. Mathur and A.G. Page, Chemical separation and ICP–AES determination of 22 metallic elements in U and Pu matrices using cyanex-923extractant and studies on stripping of U and Pu, *Talanta* 56 (2002) 591 - 601.

129. P.G. Jaison, Narendra M. Raut and S.K. Aggarwal, Direct determination of lanthanides in simulated irradiated thoria fuels using reversed-phase high-performance liquid chromatography, *Journal of Chromatography A*, 1122 (2006) 47 - 53.

130. C.A. Lucy, L. Gureli and S. Elchuk, Determination of trace lanthanide impurities in nuclear grade uranium by coupled-column liquid chromatography, *Anal. Chem*.65 (1993) 3320 - 3325.

131. S. Seyhan, M. Merdivan, and N. Demirel, Use of o-phenylene dioxydiacetic acid impregnated in Amberlite XAD resin for separation and preconcentration of uranium(VI) and thorium(IV), *Journal of Hazardous Materials* 152 (2008) 79 - 84.

132. S.R. Yousefi, S.J. Ahmadi, F. Shemirani, M.R. Jamali and M.S. Niasari, Simultaneous extraction and preconcentration of uranium and thorium in aqueous samples by new modified mesoporous silica prior to inductively coupled plasma optical emission spectrometry determination, *Talanta* 80 (2009) 212 - 217.

133. D. Das, M. Dutta, M.L. Cervera and M. de la Guardia, Recent advances in on-line solid-phase pre-concentration for inductively-coupled plasma techniques for determination of mineral elements, *Trends in Analytical Chemistry* 33 (2012) 35 - 45.

134. S. Jeyakumar, V.G. Mishra, M.K. Das, V.V. Raut, R.M. Sawant and K.L. Ramakumar, Separation behavior of U(VI) and Th(IV) on a cation exchange column using 2,6-pyridine dicarboxylic acid as a complexing agent and its application for the rapid separation and determination of U and Th by ion chromatography, *Journal of Separation Science* 34 (2011) 609 - 616.

135. Ch.S.K. Raju, M.S. Subramanian, N. Sivaraman, T.G. Srinivasan and P.R. V. Rao, Retention studies on uranium, thorium and lanthanides with amide modified reverse phase support and its applications, *Journal of Chromatography A* 1156 (2007)340-347.

136. E.P. Horwitz and D.R. McAlister, The recovery of trace thorium from large quantities of uranium, Solvent Extraction and Ion Exchange 27 (2009) 474–488.

137. T.L. Tsai, C.C. Lin, T.C. Chu, Micro-column solid phase extraction to determine uranium and thorium in environmental sample *Appl. Radiat. Isot.,* 66 (2008), p. 1097 - 1103.

138. V. G. Torgov, M. G. Demidova, A. I. Saprykin, I. V. Nikolaeva and E. P. Chebykin, Extraction preconcentration of uranium and thorium traces in the analysis of bottom sediments by inductively coupled plasma mass spectrometry, *J. Anal. Chem*. 57 (2002) 303 - 309.

139. G. Koulouris, B. Slowikowski, R. Pilvio, T. Bostrom, M. Bichel, Pre-concentration of actinoids from waters: A comparison of various sorbents, *Appl. Radiat. Isot*. 53 (2000) 279-287.

140. Coordination and separation studies of the uranyl ion with iso-butyramide basedligands: Synthesis and structures of $[UO_2(NO_3)_2(^iC_3H_7CON\{^iC_4H_9\}_2)_2]$ and $[UO_2(C_6H_5COCHCOC_6H_5)_2(^iC_3H_7CON\{^iC_3H_7\}_2)][UO_2(NO_3)_2(^iC_3H_7CON\{iC_4H_9\}_2)_2]$ and $[UO_2(C_6H_5COCHCOC_6H_5)_2(^iC_3H_7CON\{^iC_3H_7\}_2)]$, S. Kannan, S.B. Deb, J.S. Gamare, M.G.B. Drew, *Polyhedron* 27 (2008) 2557 - 2562.

141. D. J. Barkley, L. A. Bennett, J. R. Charbonneau, L. A. Pokrajac, Applications of high-performance ion chromatography in the mineral processing industry, *J. Chromatogr*. 606 (1992) 195 - 201.

142. F. Hao, B. Paull and P.R. Haddad, Determination of thorium and uranyl in nitrophosphate solution by on-line matrix-elimination reversed-phase chromatography, *Chromatographia* 42 (1996) 690 - 696.

143. F. Hao, B. Paull and P.R. Haddad, Determination of trace levels of thorium(IV) and uranyl by reversed-phase chromatography with on-line preconcentration and ligand exchange, *Journal of Chromatography A* 749 (1996) 103 - 113.

144. R. Unsworth, J. M. Cook, S. J. Hill, Determination of uranium and thorium in natural waters with a high matrix concentration using solid-phase extraction inductively coupled plasma mass spectrometry, *Anal. Chim. Acta* 442 (2001) 141 - 146.

145. V. Vidyalakshmi, M.S. Subramanian, N. Sivaraman, T.G. Srinivasan and P.R.V. Rao, Retention behaviour of uranium and thorium and their determination on an amide-coated reverse phase column by HPLC, *J. Liq. Chromatogr. Related Technol*., 27 (2004) 2269 - 2291.

146. A. Abrao, A. A. de Freitas and F.M.S. de Carvalho, Preparation of highly pure thorium nitrate via thorium sulfate and thorium,peroxide, *J. Alloys and Compounds* 323 (2001) 53 - 56.

147. F. Hao, B. Paull and P.R. Haddad, Retention behaviour of thorium(IV) and uranyl on a reversed-phase column with glycolate and mandelate as eluents, *Journal of Chromatography A* 739 (1996) 151 - 161.

148. N. Clavier, R. Podor and N. Dacheux, Crystal chemistry of the monazite structure, *Journal of the European Ceramic Society*, 31 (2011) 941 - 976.

149. http://www.world-nuclear.org/info/inf75.html

150. http://www.jaea.go.jp/jaeri/english/ff/ff43/topics.html

151. R. Djogic, I. Pizeta and M. Brancia, Electrochemical determination of dissolved uranium in krka river estuary, *Wat. Res.* 35 (2001)1915 - 1920.

152. Z. Tosheva, K. Stoyanova and L. Nikolchev, Comparison of different methods for uranium determination in water, *J. Environ. Radioact.* 72 (2004) 47 - 55.

153. S.H. Leea, P.P. Povineca, E. Wysea and M.A.C. Hotchkis, Ultra-low-level determination of ^{236}U in IAEA marine reference materials by ICPMS and AMS, *Appl. Radiat. Isot.* 66 (2008) 823 - 828.

154. J. Zheng, M. Yamada, T. Aono and M. Kusakabe, Vertical distribution of uranium concentrations and $^{235}U/^{238}U$ atom ratios in the coastal water off Aomori, Japan: A survey prior to the operation of a nuclear fuel reprocessing facility. *J. Radioanal. Nucl. Chem*. 270 (2006) 669 - 675.

155. S. Hirata, T. Kajiya, N. Takano, M. Aihara, K. Honda, O. Shikino and E. Nakayama, Determination of trace metals in seawater by on-line column preconcentration inductively coupled plasma mass spectrometry using metal alkoxide glass immobilized 8-quinolinol, *Anal. Chim. Acta* 499 (2003)157 -165.

156. K. Oshita, K.Seo, A. Sabarudin, M. Oshima, T. Takayanagi and S. Motomizu, Synthesis of chitosan resin possessing a phenylarsonic acid moiety for collection/concentration of uranium and its determination by ICP-AES, *Anal. Bioanal. Chem.* 390 (2008)1927 - 1932.

157. C. Jie, L. Zaijun and L. Ming. Spectrophotometric determination of ultra trace uranium(VI) in seawater after extractive preconcentration with ionic liquid and dimethylphenylazosalicylfluorone, *Int. J. Environ. Anal. Chem.* 88 (2008) 583 - 590.

158. Dj. Dojozan, M.H. Pournaghi-Azar and J. Toutounchi-Asr, Preconcentration of trace uranium from seawater with solid phase extraction followed by differential pulse polarographic determination in chloroform eluate, *Talanta* 46 (1998)123 - 128.

159. P.C. Kalsi, P.D. Sawant, A. Ramaswami and V.K. Manchanda, Track etching characteristics of polyester track detector and its application to uranium estimation in seawater samples, J. Radioanal. Nucl. Chem. 273 (2007) 473 - 477.

160. N.L. Misra, S. Dhara and K.D. Singh Mudher, Uranium determination in seawater by total reflection X-ray fluorescence spectrometry, *Spectrochim. Acta Part B* 61 (2006)1166 - 1169.

161. S.A. Kumar, N.S. Shenoy, S. Pandey, S. Sounderajan and G. Venkateswaran, Direct determination of uranium in seawater by laser fluorimetry, *Talanta* 77 (2008) 422 - 426.

162. S. Antoniou, C. Costa and I. Pashalidis, Alpha-radiometry of seawater by liquid scintillation counting, *J. Radioanal. Nucl. Chem*. 270 (2006)593 - 596.

163. I. Pashalidis and H. Tsertos, Radiometric determination of uranium in natural waters after enrichment and separation by cation-exchange and liquid-liquid extraction, *J. Radioanal. Nucl. Chem.* 260 (2004) 439 - 442.

164. M. Kazeraninejad, A.M.H. Shabani, S. Dadfarnia and S.H. Ahmadi, Solid phase extraction of trace amounts of uranium(VI) from water samples using 8-hydroxyquinoline immobilized on surfactant-coated alumina, *Journal of Analytical Chemistry* 66 (2011) 373 - 377.

165. A. Rezaei, H. Khani, M. Masteri-Farahani, M.K.A. Rofouei, A novel extraction and preconcentration of ultra-trace levels of uranium ions in natural water samples using functionalized magnetic-nanoparticles prior to their determination by inductively coupled plasma-optical emission spectrometry, *Analytical Methods* (2012) 4107 - 4114.

166. Y.K. Agrawal, Selective supercritical fluid extraction of uranium(VI) using n-phenyl-(1,2-methano-fullerene C60)61-formohydroxamic acid and simultaneous on-line determination by inductively-coupled plasma-mass spectrometry (ICP-MS), *Fullerenes, Nanotubes, Carbon Nanostruct.* 14 (2006) 621 - 639.

167. R.M. Cassidy and S. Elchuk, Chromatography of uranium on high-performance ion exchangers, *Int. J. Environ. Anal. Chem.* 10 (1981) 287- 294.

168. A. Kerr, W. Kupferschmidt and M. Attas, Determination of uranium in natural groundwaters using high-performance liquid chromatography, *Anal. Chem*. 60 (1988) 2729 - 2733.

169. M. J. Shaw, S. J. Hill, R. Jones and R. N. Nesterenko, Determination of uranium in environmental matrices by chelation ion chromatography using a high-performance substrate dynamically modified with 2,6-pyridinedicarboxylic acid, *Chromatographia* 51 (2000) 695 - 700.

170. Ref: http://www.seafriends.org.nz/oceano/seawater.htm

171. http://www.oceanplasma.org/documents/chemistry.html

172. H. Moll, G. Geipel, T. Reich, G. Bernhard, T. Fanghanel and I. Grenthe, Uranyl(VI) complexes with alpha-substituted carboxylic acids in aqueous solution, *Radiochim. Acta* 91 (2003)11 - 20.

173. M. Laikhtman and J.S. Rohrer, Determination of fluorochemical surfactants in acid etch baths by ion chromatography with on-line matrix elimination, *J. Chromatogr. A* 822 (1998)321–325.

174. P. Jones, Major sensitivity improvements in ion chromatography determinations involving post-column spectrophotometric reaction detectors through elimination of pump noise using adual wavelength monitoring procedure, *Analyst* 125 (2000) 803 - 806.

175. R. M. Dunk, R. A. Mills and W. J. Jenkins, A re-evaluation of the oceanic uranium budget for the Holocene, *Chem. Geol.* 190 (2002) 45 - 67.

176. A.F. Reguillon, G. Lebuzit, J. Foos, A. Guy, M. Draye and M. Lemaire, Selective concentration of uranium from seawater by nanofiltration, *Ind. Eng. Chem. Res.* 42 (2003) 5900 - 5904.

177. H. Sodaye, S. Nisan, C. Poletiko, S. Prabhakar and P.K. Tewari, Extraction of uranium from the concentrated brine rejected by integrated nuclear desalination plants, *Desal.* 235 (2009) 9 - 32.

178. P.G. Jaison, V.M. Telmore, Pranaw Kumar and S.K. Aggarwal, A reversed-phase liquid chromatography method using α-hydroxy isobutyric acid for pre-concentration and determination of uranium in seawater, *J. Chromatogr. Sci*. 49 (2011)72 - 78.

179. A.K. Saxena, Experiments for recovery of uranium from seawater by harnessing tidal energy, BARC News Letter Issue 249 (2004) 226 - 232.

180. M.L. Godoy, J.M. Godoy, R. Kowsmann, G.M. dos Santos and R.P. da Cruz, ^{234}U and ^{230}Th determination by FIA-ICP-MS and application to uranium-series disequilibrium in marine samples. *J. Environ. Radioact*. 88 (2006) 109 - 117.

181. S. B. Savvin, Analytical applications of Arsenazo (III): The mechanism of complex formation between Arsenazo (III) and certain elements. Talanta, 11 (1964) 7 - 19.

182. P. G. Jaison, V. M. Telmore, Pranaw Kumar and S. K. Aggarwal, Reversed-phase liquid chromatography using mandelic acid as an eluent for the determination of uranium in presence of large amounts of thorium, *J. Chromatogr. A* 1216 (2009)1383 - 1389.

183. M. Luo, B. Hu, X. Zhang, D. Peng, H. Chen, L. Zhang and Y. Huan, Extractive electrospray ionization mass spectrometry for sensitive detection of uranyl species in natural water samples, *Anal. Chem.* 82 (2010) 282 - 289.

184. C. Moulin, P. Decambox, V. Moulin and J. G. Decaillon, Uranium speciation in solution by time-resolved laser-induced fluorescence, *Anal. Chem.*67 (1995) 348 - 353.

185. D. Orlander, Nuclear fuels – Present and future, *J. Nucl. Mater.* 289 (2009) 1 - 22.

186. P. Ivanov, T. Griffiths, N. D. Bryan, G. Bozhikov and S. Dmitriev, The effect of humic acid on uranyl sorption onto bentonite at trace uranium levels, *J Environ Monit.*14 (2012) 2968 - 2975.

187. C. Lomenech, R. Drot and R. Simoni. Speciation of uranium(VI) at the solid/solution interface: sorption modeling on zirconium silicate and zirconium oxide, *Radiochim. Acta* 91 (2003) 453- 462.

188. V. M. H. Geckeis, E. G. Robles, A. Loida, C. Bube and B. Kienzler, Radionuclide behaviour in the near-field of a geological repository for spent nuclear fuel, *Radiochim Acta* 100 (2012) 699 - 713.

189. C. Moulin, B. Amekraz, S. Colette, D. Doizi, C. Jacopin, C. Lamouroux and G. Plancque, Electrospray mass spectrometry for actinides and lanthanide speciation, *J. Alloys Compd*. 402 (2006) 1242 - 1245.

190. M. R. Vanengelen, E. K. Field, R. Gerlach, B. D. Lee, W.A. Apel and B. M. Peyton. UO_2^{2+} speciation determines uranium toxicity and bioaccumulation in an environmental Pseudomonas sp. isolate. *Environ. Toxicol. Chem*. 29 (2010) 763 - 769.

191. T. Vercouter, P. Vitorge, B. Amekraz and C. Moulin, Stoichiometries and thermodynamic stabilities for aqueous sulfate complexes of U(VI), *Inorg. Chem.*47 (2008) 2180 - 2189.

192. S. P. Pasilis and J. E. Pemberton, Speciation and coordination chemistry of uranyl(VI)-citrate complexes in aqueous solution, *Inorg. Chem.*42 (2003) 6793 - 6800.

193. G. R. Choppin, Actinide speciation in the environment, *J. Radioanal. Nucl. Chem.* 273 (2007) 695 - 703.

194. S. Gin, N. Godon, J. P. Mestre, E. Y. Vernaz and D. Beaufort. Experimental investigation of aqueous corrosion of R7T7 nuclear glass at 90 °C in the presence of organic-species. *Appl. Geochem.* 9 (1994) 255- 269.

195. S. Sachs and G. Bernhard, Influence of humic acids on the actinide migration in the environment: suitable humic acid model substances and their application in the studies with uranium – a review, *J. Radioanal. Nucl. Chem.* 290 (2011) 17 - 29.

196. A. Dube, R. Zbytniewski, T. Kowalkowski, E. Cukrowska and B. Buszewski, Adsorption and migration of heavy metals in soil, *Polish J. Environ. Stud.* 10 (2001) 1 - 10.

197. A. Barkleit, M. Acker and G. Bernhard, Europium(III) complexation with salicylic acid at elevated temperatures, *Inorg. Chim. Acta* 394 (2013) 535 - 541.

198. A. S. Kar, B. S. Tomar, S. V. Godbole and V. K. Manchanda, Time resolved fluorescence spectroscopy and modeling of Eu(III) sorption by silica in presence and absence of alpha hydroxy isobutyric acid, *Colloids Surf. A Physicochem. Eng. Asp*. 378 (2011) 44 - 49.

199. A. Jain, M. Mohapatra, S. V. Godbole and B. S. Tomar, Time resolved fluorescence spectroscopy of Eu(III) complexation with α-hydroxy isobutyric acid, *Spectrochim. Acta A* 71 (2008) 1007 - 1010.

200. A. J. Francis, C. J. Dodge, J. A. Mc Donald and G. P. Halad, Decontamination of uranium-contaminated steel surfaces by hydroxycarboxylic acid with uranium recovery, *Environ. Sci. Technol.* 39 (2005) 5015 - 5021.

201. G. R. Choppin, B. G. Harvey and S. G. Thompson, A new eluant for the separation of the actinide elements , *J. Inorg. Nucl. Chem*. 2 (1956) 66 - 68.

202. T. Oikawa, T. Urabe, S. Kawano and M. Tanaka, Basic study of lanthanide nitrate species in solution by electrospray ionization mass spectrometry, *J. Solution Chem*. 40 (2011) 1094 - 1107.

203. R. S. R. Andrew, M. G. Ikonomou, J. A. J. Thompson and K. J. Orians, Determination of dissolved metal species by electrospray ionization mass spectrometry, *Anal. Chem.*70 (1998) 2225 - 2235.

204. H. Wang and G. R. Agnes, Kinetically labile equilibrium shifts induced by the electrospray process, *Anal. Chem.*71 (1999) 4166 -4172.

205. P. Delangle, C. Husson, C. Lebrun, J. Pecaut and P. J. A. Vottero, Solid state and solution studies of lanthanide(III) complexes of cyclohexanetriols: models of the coordination sites found in sugars, *Inorg. Chem.*40 (2001) 2953 - 2962.

206. M. Van Stipdonk, V. Anbalagan, W. Chien, G. Gresham, G. Groenewold and D. Hanna, Elucidation of the collision induced dissociation pathways of water and alcohol coordinated complexes containing the uranyl cation, *J. Am. Soc. Mass Spectrom.*14 (2003) 1205 - 1214.

207. M. Steppert, C. Walther, M. Fuss and S. Buchner, On the polymerization of hexavalent uranium: An electrospray mass spectrometry study, *Rapid Commun. Mass Spectrom.* 26 (2012) 583 - 591.

208. C. Lamouroux, S. Rateau and C. Moulin. Use of electrospray ionization mass spectrometry for the study of Ln(III) complexation and extraction speciation with calixarene-CMPO in the fuel partitioning concept, *Rapid Commun. Mass Spectrom*. 20 (2006) 2041- 2052.

209. I. Canals, F. Z. Oumada, M. Roses and E. Bosch, Retention of ionizable compounds on HPLC. 6. pH measurements with the glass electrode in methanol–water mixtures, *J. Chromatogr. A*,911 (2001) 191 - 202.

210. K. Tang, J. S. Page and R. D. Smith, Charge competition and the linear dynamic range of detection in electrospray ionization mass spectrometry, *J. Am. Soc. Mass Spectrom*. 15 (2004) 1416 - 1423.

211. C. Moulin, N. Charron, G. Plancque and H. Virelizier, Speciation of uranium by electrospray ionization mass spectrometry: comparison with time-resolved laser-induced fluorescence, *Appl. Spectrosc.* 54 (2000) 843 - 848.

212. D.R. Lide, CRC Handbook of Chemistry and Physics, *87*th Ed, Taylor and Francis, BocaRaton, FL, 2007. http:/www.hbcpnetbase.com

213. M. J. Van Stipdonk, W. Chien, V. Anbalagan and K. Bulleigh, Gas-phase complexes containing the uranyl ion and acetone, *J. Phys. Chem. A* 108 (2004) 10448 - 10457.

214. S. Spencer, L. Gagliardi, N. C. Handy, A. G. Ioannou, C. K. Skylaris, A. Willetts and A. M. Simper, The Hydration of UO_2^{2+} and PuO_2^{2+}, *J. Phys. Chem. A* 103 (1999) 1831 - 1837.

215. P. J. Hay, R. L. Martin and G. Schreckenbach, Theoretical studies of the properties and solution chemistry of AnO_2^{2+} and AnO_2^{+} aquo complexes for An = U, Np, and Pu, *J. Phys. Chem. A* 104 (2000) 6259 - 6270.

216. J. L. William, Modern Inorganic Chemistry, *2*nd Edn. New York: McGraw-Hill (1991).

217. B. M. Ehrmann, T. Henriksen and N. B. Cech, Relative importance of basicity in the gas phase and in solution for determining selectivity in electrospray ionization mass spectrometry, *J. Am. Soc. Mass Spectrom.*,19 (2008) 719 - 728.

218. M. G. Ikonomou, A. T. Blades and P. Kebarle, Investigations of the electrospray interface for liquid chromatography/mass spectrometry, *Anal. Chem*. 62 (1990) 957 - 967.

219. L. L. Jessome and D. A. Volmer, Ion Suppression: A Major Concern in Mass Spectrometry, *LCGC*. 24 (2006) 498 - 510.

220. F. Tanaka, Y. Kawasaki and S. Yamashita, Preferential solvation of the europium(III) ion in water–non-aqueous solvent mixtures. A luminescence lifetime study, *J. Chem. Soc., Faraday Trans*. 84 (1988) 1083 - 1090.

221. N. G. Tsierkezos, J. Roithova, D. Schroder, M. Oncak and P. Slavicek, Can electrospray mass spectrometry quantitatively probe speciation? Hydrolysis of uranyl nitrate studied by gas-phase methods, *Inorg. Chem.* 48 (2009) 6287 - 6296.

222. P. Kumar, P. G. Jaison, M. Sundararajan, V. M. Telmore, S. K. Ghosh and S. K. Aggarwal, Speciation studies of platinum-benzoylthiourea in acetonitrile using electrospray ionization mass spectrometry and density functional theory, *Rapid Commun. Mass Spectrom.* 27 (2013) 947 - 954.

223. S. Colette, B. Amekraz, C. Madic, L. Berthon, G. Cote and C. Moulin, Use of electrospray mass spectrometry (ESI-MS) for the study of europium(III) complexation with bis(dialkyltriazinyl) pyridines and its implications in the design of new extracting agents, *Inorg. Chem.* 41 (2002) 7031 - 7041.

224. C. L. Crawford, G. A. Fugate, P. R. Cable-Dunlap, N. A. Wall, W. F. Siems and H. H. Hill, The novel analysis of uranyl compounds by electrospray-ion mobility-mass spectrometry, *Int. J. Mass Spectrom.*, 333 (2013) 21 - 26.

225. P.G. Jaison, P. Kumar, V. M. Telmore and S. K. Aggarwal, Electrospray ionization mass spectrometric studies on uranyl complex with α-hydroxyisobutyric acid in water-methanol medium, *Rapid Commun. Mass Spectrom.27 (2013)* 1105 - 1118.